University of Windsor
Scholarship at UWindsor

Electronic Theses and Dissertations

1995

Metalated macrocyclic receptors.

James Edward. Kickham
University of Windsor

Follow this and additional works at: http://scholar.uwindsor.ca/etd

Recommended Citation
Kickham, James Edward., "Metalated macrocyclic receptors." (1995). *Electronic Theses and Dissertations.* Paper 2712.

This online database contains the full-text of PhD dissertations and Masters' theses of University of Windsor students from 1954 forward. These documents are made available for personal study and research purposes only, in accordance with the Canadian Copyright Act and the Creative Commons license—CC BY-NC-ND (Attribution, Non-Commercial, No Derivative Works). Under this license, works must always be attributed to the copyright holder (original author), cannot be used for any commercial purposes, and may not be altered. Any other use would require the permission of the copyright holder. Students may inquire about withdrawing their dissertation and/or thesis from this database. For additional inquiries, please contact the repository administrator via email (scholarship@uwindsor.ca) or by telephone at 519-253-3000ext. 3208.

National Library of Canada
Acquisitions and Bibliographic Services Branch
395 Wellington Street
Ottawa, Ontario
K1A 0N4

Bibliothèque nationale du Canada
Direction des acquisitions et des services bibliographiques
395, rue Wellington
Ottawa (Ontario)
K1A 0N4

Your file Votre référence

Our file Notre référence

NOTICE

The quality of this microform is heavily dependent upon the quality of the original thesis submitted for microfilming. Every effort has been made to ensure the highest quality of reproduction possible.

If pages are missing, contact the university which granted the degree.

Some pages may have indistinct print especially if the original pages were typed with a poor typewriter ribbon or if the university sent us an inferior photocopy.

Reproduction in full or in part of this microform is governed by the Canadian Copyright Act, R.S.C. 1970, c. C-30, and subsequent amendments.

AVIS

La qualité de cette microforme dépend grandement de la qualité de la thèse soumise au microfilmage. Nous avons tout fait pour assurer une qualité supérieure de reproduction.

S'il manque des pages, veuillez communiquer avec l'université qui a conféré le grade.

La qualité d'impression de certaines pages peut laisser à désirer, surtout si les pages originales ont été dactylographiées à l'aide d'un ruban usé ou si l'université nous a fait parvenir une photocopie de qualité inférieure.

La reproduction, même partielle, de cette microforme est soumise à la Loi canadienne sur le droit d'auteur, SRC 1970, c. C-30, et ses amendements subséquents.

Canada

Metalated Macrocyclic Receptors

By James E. Kickham

A Dissertation
Submitted to the Faculty of Graduate Studies and Research
Through the Department of Chemistry and Biochemistry
in Partial Fulfillment of the Requirements for
the Degree of Doctor of Philosophy at the
University of Windsor

Windsor, Ontario, Canada

1994

© 1994 James E. Kickham

National Library
of Canada

Acquisitions and
Bibliographic Services Branch

395 Wellington Street
Ottawa, Ontario
K1A 0N4

Bibliothèque nationale
du Canada

Direction des acquisitions et
des services bibliographiques

395, rue Wellington
Ottawa (Ontario)
K1A 0N4

Your file Votre référence

Our file Notre référence

THE AUTHOR HAS GRANTED AN IRREVOCABLE NON-EXCLUSIVE LICENCE ALLOWING THE NATIONAL LIBRARY OF CANADA TO REPRODUCE, LOAN, DISTRIBUTE OR SELL COPIES OF HIS/HER THESIS BY ANY MEANS AND IN ANY FORM OR FORMAT, MAKING THIS THESIS AVAILABLE TO INTERESTED PERSONS.

L'AUTEUR A ACCORDE UNE LICENCE IRREVOCABLE ET NON EXCLUSIVE PERMETTANT A LA BIBLIOTHEQUE NATIONALE DU CANADA DE REPRODUIRE, PRETER, DISTRIBUER OU VENDRE DES COPIES DE SA THESE DE QUELQUE MANIERE ET SOUS QUELQUE FORME QUE CE SOIT POUR METTRE DES EXEMPLAIRES DE CETTE THESE A LA DISPOSITICN DES PERSONNE INTERESSEES.

THE AUTHOR RETAINS OWNERSHIP OF THE COPYRIGHT IN HIS/HER THESIS. NEITHER THE THESIS NOR SUBSTANTIAL EXTRACTS FROM IT MAY BE PRINTED OR OTHERWISE REPRODUCED WITHOUT HIS/HER PERMISSION.

L'AUTEUR CONSERVE LA PROPRIETE DU DROIT D'AUTEUR QUI PROTEGE SA THESE. NI LA THESE NI DES EXTRAITS SUBSTANTIELS DE CELLE-CI NE DOIVENT ETRE IMPRIMES OU AUTREMENT REPRODUITS SANS SON AUTORISATION.

ISBN 0-612-01458-4

Canada

Abstract

The dissertation describes the incorporation of a stable organopalladium fragment into several macrocyclic structures, in which three of four palladium coordination sites are permanently occupied by an S_2C ligand "bracket". The remaining metal site is filled by a more labile donor, and is used for binding ancillary ligands (substrates) such as phosphines, *o*-aminopyridine, DNA nucleobases and hydrazine derivatives.

Chapter 2 describes the synthesis, oxidative addition, and coordination chemistry of [Pt(TT[11]MC)][BF_4] (4), [Pd(TT[11]MC)][BF_4], (8) and [Pd(*pr*-TOMB-1)][BF_4] (14), in which one donor (E=S,O) is displaced by stronger ancillary ligands, as confirmed by X-ray structural data as well as ^1H and $^{13}C\{^1H\}$ NMR spectroscopy.

Chapters 3 describes the synthesis of several *metalated macrocyclic receptors*, [Pd(CH_3CN)(TOMB-0)][BF_4] (21), [Pd(CH_3CN)(TOMB-1)][CF_3SO_3], (23) [Pd(CH_3CN)(TOMB-3)][BF_4], (25) and [Pd(CH_3CN)(TOMB-5)][BF_4], (26), containing an easily displaced ancillary acetonitrile ligand and polyether arrays for first- and second-sphere interactions with substrates. The receptors were characterized by ^1H NMR spectroscopy and X-ray crystallography.

Chapter 4 describes competition experiments of 21, 23, and 25 for pyridine and *o*-aminopyridine in which it was found that an increase in the number of oxygen atoms increases selectivity for *o*-aminopyridine. In extraction experiments performed in acetonitrile with the DNA nucleobases, only 21 was found to extract adenine in any appreciable amount, and 25 exhibits *molecular recognition* for

cytosine, over adenine and guanine. The nature of the first- and second sphere interactions was determined by X-ray crystallography

Chapter 5 describes the optimization of simultaneous first- and second-sphere interactions using primary amines and hydrazine derivatives as substrates, with 25 and 26 as receptors. Receptor 25 was found to be selective for *n*-butylamine over N-methylbutylamine. Both receptors exhibit remarkable interactions with hydrazine derivatives, forming 4 point and 7 point interactions between the hydrazinium cation and 25 and 26 respectively, as determined by X-ray crystallography.

Chapter 6 describes the development of a new receptor, incorporating a ferrocene moiety for additional characterization of receptor-substrate interactions. Metalation of the macrocycle proved to be difficult due to reduction of the palladium starting material by the ferrocene moiety.

This work is dedicated to my grandparents-
all 5 of them.
I hope someday you'll all get to read this.

Acknowledgements

First and foremost many, many thanks go to my boss, Steve Loeb. Steve is the kind of boss that every grad student should have. He's got a lot of ideas, but allows you to try your own. He's busy, but always finds time to talk about a problem you have. He's the boss, but he's your friend too. Thanks, Steve.

Thanks go to Shannon Murphy for synthesizing and crystallizing compounds 27, 36, 37. I would also like to thank Mike Fuerth. Mike gets thanked a lot in theses and dissertations, because he does a lot. I would also like to thank Jim Green for many helpful organic chemistry discussions, and Jerry Vriesacker and Dave Hill.

Next I would like to thank my Mom and Dad. Although it may not always seem like it, I do appreciate your interest and support, and it *was/is* needed. It was also nice of you to let me freeload over my last four months in Windsor. You're welcome to come and freeload on me anytime (soon?).

Throughout my graduate career there were people who made life bearable and fun; people whom I thankfully call 'friends'. These people are: Brian Atkins, Rick Barron, Kathy Baynton, Bob Berno, Martyn Brown, *Juncal DeSaja*, Hilary Jenkins, Andy Kickham, Barry Klassen, Craig Noren, Wania Moreira, Tim Nadasdi, Rhona Samuels, George Shimizu, and Mike Tonkin.

Finally I would like to thank the crew of the Enterprise-D, Van Halen, Rush, O.V., Upper Canada, Sleeman, Canadian, Formosa, etc...

Table of Contents

Abstract iii

Dedication v

Acknowledgements vi

Table of Contents vii

List of Figures xiv

List of Tables xx

List of Abbreviations xxiv

Chapter 1 1

1.1 Historical Background 2
1.2 Crown Thioethers 5
(i) Synthesis 5
(ii) Ligand Conformation 6
(iii) Bonding of Thioethers 8
1.3 Second-Sphere Coordination 10
(i) Concept 10
(ii) Second-Sphere Coordination 11
(iii) Simultaneous First-and Second Sphere Coordination 14
1.4 Molecular Recognition 16
1.5 Scope of the Thesis 19
(i) Summary 20
(ii) Trivial naming

Chapter 2 22

2.1 Introduction 23
(i) Thought Process 23
(ii) Literature Background 25
2.2 Experimental 28
General Comments 28
(i) Preparation of 4-Thiaheptane-1,7-diol, (1) 29
(ii) Preparation of 4-Thiaheptane-1,7-dithiol, (2) 29
(iii) Preparation of 2,6,10-Trithia[11]-m-Cyclophane, TT[11]MC, (3), Method A 30
(iv) Preparation of 2,6,10-Trithia[11]-m-Cyclophane, TT[11]MC, (3), Method B 30

(v) Preparation of [Pt(TT[11]MC)][BF_4], (4) 31
(vi) Preparation of [Pt(PPh_2Me)(TT[11]MC)][BF_4], (5) 31
(vii) Reactions of [Pt(TT[11]MC)][BF_4] with CO, H_2 and C_2H_2 32
(viii) Reactions of [Pt(PPh_2Me)(TT[11]MC)][BF_4] with CH_3I, PPh_3 and DMAD 32
(ix) Preparation of [PtI_2(TT[11]MC)][BF_4], (6) 33
(x) Preparation of [$PtCl_2$(TT[11]MC)][BF_4], (7) 33
(xi) Preparation of [Pd(TT[11]MC)][BF_4], (8) 34
(xii) Preparation of [Pd(PPh_2Me)(TT[11]MC)][BF_4], (9) 34
(xiii) Preparation of [$PdCl_2$(TT[11]MC)][BF_4], (10) 35
(xiv) Attempted oxidation of [Pt(TT[11]MC)][BF_4] 35
(xv) Metallation of [$PdCl_2$(TT[11]MC)] 36
(xvi) Preparation of 4-oxaheptane-1,7-diol, (11) 36
(xvii) Preparation of 4-oxaheptane-1,7-dithiol, (12) 36
(xviii) Preparation of 6-oxa-2,10-dithia[11]-*m*-cyclophane, (*pr*-TOMB-1), (13) 37
(xix) Preparation of [Pd(*pr*-TOMB-1)][BF_4], (14) 37
(xx) Preparation of [Pd(PPh_2Me)(*pr*-TOMB-1)][BF_4], (15) 38

2.3 X-Ray Diffraction Data Collection, Solution, and Refinement 38
(i) General Procedures 38
(ii) Structure Determination of TT[11]MC (3), [Pt(TT[11]MC)][BF_4] (4), [Pt(PPh_2Me)(TT[11]MC)]$^+$ [BF_4], (5), [PdI_2(PPh_2Me)(TT[11]MC)][BF_4], (6) 39
(iii) Structure Detemination of 6-oxa-2,10-dithia[11]*m*-cyclophane, *pr*-TOMB-1, (13) 40
(iv) Structure Detemination of [Pd(*pr*-TOMB-1)][BF_4], (14) 40

2.4 Results and Discussion 41
(i) Synthesis and Characterization of TT[11]MC, (3) 41
(ii) Crystal Structure of TT[11]MC, (3) 43
(iii) Formation of [Pt(TT[11]MC)][BF_4], (4) 46
(iv) Crystal Structure of [Pt(TT[11]MC)][BF_4], (4) 47
(v) Substitution Chemistry of [Pt(TT[11]MC)][BF_4], (4); Preparation of [Pt(PPh_2Me)(TT[11]MC)][BF_4], (5) 49
(vi) Crystal Structure of [Pt(PPh_2Me)(TT[11]MC)]$^+$ [BF_4], (5) 50
(vii) Oxidation Reactions of [Pt(TT[11]MC)][BF_4]; Preparation of [PtI_2(TT[11]MC)][BF_4] (6), and [$PtCl_2$(TT[11]MC)][BF_4], (7) 52
(viii) Crystal Structure of [PtI_2(TT[11]MC)][BF_4], (6) 52
(ix) Formation of [Pd(TT[11]MC[BF_4], (8) 54
(x) Comparison of [Pt(TT[11]MC)][BF_4], (4) and [Pd(TT[11]MC)][BF_4], (8) 57
(xi) Reaction Chemistry of [Pd(TT[11]MC)][BF_4], (4)58
(xii) Preparation of 6-oxa-2,10-dithia[11]-m-cyclophane, (*pr*-TOMB-1), (13) 60

(xiii) Crystal Structure of 6-oxa-2,10-dithia[11]-m-cyclophane, (*pr*-TOMB-1), (13) 62
(xiv) Preparation of [Pd(*pr*-TOMB-1)][BF_4], (14). 64
(xv) Crystal Structure of [Pd(*pr*-TOMB-1)][BF_4], (14) 64
(xvi) Preparation of [Pd(PPh_2Me)(*pr*-TOMB-1)][BF4], (15) 66
2.5 Conclusion 68

Chapter 3 70

3.1 Introduction 71
(i) Thought Process 71
(ii) Background Literature 73
3.2 Experimental 77
General Comments 77
(i) Preparation of 2,14-Dithia[15]-m-cyclophane, (TOMB-0), (16) 77
(ii) Preparation of 5-Oxa-2,8-dithia[9]-m-cyclophane, (TOMB-1), (17) 78
(iii) Preparation of 5,8,11-Trioxa-2,14-dithia[15]-m-cyclophane, (TOMB-3), (18). 79
(iv) Preparation of 1,17-dichloro-3,6,9,12,15-pentaoxaheptadecane, (19) 79
(v) Preparation of 5,8,11,14,17-pentaoxa-2,20-dithia [21]*m*-cyclophane, (TOMB-5), (20) 80
(vi) Preparation of [Pd(TOMB-0)(CH_3CN)][BF4], (21) 81
(vii) Preparation of [Pd(TOMB-1)(CH_3CN)][BF_4], (22) 81
(viii) Preparation of [Pd(TOMB-1)(CH_3CN)][CF_3SO_3], (23) 81
(ix) Preparation of [Pd(TOMB-3)Cl], (24) 82
(x) Preparation of [Pd(TOMB-3)(CH_3CN)][BF_4], (25) 82
(xi) Preparation of [Pd(TOMB-5)(CH_3CN)][BF_4], (26) 82
(xii) Preparation of [Pd(CH_3CN)(TOMB-P4)][BF_4], (27) 83
3.3 X-Ray Diffraction Data Collection, Solution, and Refinement. 83
(i) General Procedures 83
(ii) Structure Determination of 5,8,11-trioxa-2,14-dithia[15]-*m*-cyclophane, TOMB-3, (18) 83
(iii) Structure Determination of [Pd(CH_3CN)(TOMB-0)]$^+$ [BF_4], (21) 84
(iv) Strucuture Determination of [Pd(CH_3CN)(TOMB-1)]$^+$ [CF_3SO_3], (23) 85
(v) Strucuture Determination of [Pd(TOMB-3)Cl], (24) 85
(vi) Strucuture Determination of [Pd(CH_3CN)(TOMB-3)]$^+$ [BF_4], (25) 86
(vii) Structure Determination of [Pd(CH_3CN)(TOMB-P4)]$^+$ [BF_4], (27) 87
3.4 Results and Discussion 88
(i) Synthesis of the ligands TOMB-0,1,3,5 88

(ii) Crystal Structure of TOMB-3, (18) 90
(iii) Metalation Reactions of the Ligands TOMB-0 (16), TOMB-1 (17), TOMB-3 (18), and TOMB-5 (20) 92
(iv) NMR Spectroscopy of $[Pd(TOMB\text{-}X)(CH_3CN)]^+$ Cations (X=0,1,3,5) 94
(v) Crystal Structure of $[Pd(TOMB\text{-}0)(CH_3CN)][BF4]$, (21) 97
(vi) Crystal Structure of $[Pd(TOMB\text{-}1)(CH_3CN)][CF_3SO_3]$, (23) 99
(vii) Crystal Structure of [Pd(TOMB-3)Cl], (24) 101
(viii) Crystal Structure of $[Pd(TOMB\text{-}3)(CH_3CN)][BF_4]$, (25) 103
(ix) Crystal Structure of $[Pd(CH_3CN)(TOMB\text{-}P4)][BF_4]$, (27) 105
(x) Comparitive Structural Analysis for the $[Pd(TOMB\text{-}0)]^+$ (21), $[Pd(TOMB\text{-}1)]^+$ (23), $[Pd(TOMB\text{-}3)]^+$ (25) cations 107

3.5 Conclusion 108

Chapter 4 109

4.1 Introduction 110
(i) Thought Process 110
(ii) Background Literature 111
4.2 Experimental 115
General Comments 115
(i) Preparation of Receptor-Substrate Complexes 115
(ii) Preparation of $[Pd(PYR)(TOMB\text{-}0)][BF_4]$, (28) 116
(iii) Preparation of $[Pd(OAP)(TOMB\text{-}0)][BF_4]$, (29) 116
(iv) Preparation of $[Pd(PYR)(TOMB\text{-}1)][CF_3SO_3]$, (30) 116
(v) Preparation of $[Pd(OAP)(TOMB\text{-}1)][CF_3SO_3]$, (31) 117
(vi) Preparation of $[Pd(PYR)(TOMB\text{-}3][BF_4]$, (32) 117
(vii) Preparation of $[Pd(OAP)(TOMB\text{-}3)][BF_4]$, (33) 117
(viii) Preparation of $[Pd(PIC)(TOMB\text{-}3)][BF_4]$, (34) 118
(ix) Preparation of $[Pd(CYT)(TOMB\text{-}3)][BF_4]$, (35) 118
(x) Nucleobase Extractions 119
(xi) Competition Reactions 119
(xii) Syntheses not performed by the author 119
4.3 X-Ray Diffraction Data Collection, Solution, and Refinement. 120
(i) General Procedures 120
(ii) Strucuture Determination of $[Pd(OAP)(TOMB\text{-}1)][BF_4]$, (31) 120
(iii) Strucuture Determination of $[Pd(PYR)(TOMB\text{-}3)][BF_4]$, (32) 121
(iv) Strucuture Determination of $[Pd(PIC)(TOMB\text{-}3)][BF_4]$, (34) 122
(v) Strucuture Determination of $[Pd(CYT)(TOMB\text{-}3)][BF_4]$, (35)

(vi) Strucuture Determination of [Pd(PAP)(TOMB-P4)][BF_4], (36) 123
(vii) Strucuture Determination of [Pd(PAP)(TOMB-M4)][BF4], (37) 123
4.4 Results and Discussion 124
(i) Formation and NMR spectroscopy of Receptor-Substrate Complexes 123
(ii) Crystal Structure of [Pd(OAP)(TOMB-1)][BF_4], (30) 126
(iii) Crystal Structure of [Pd(PYR)(TOMB-3)][BF_4], (31) 128
(iv) Crystal Structure of [Pd(PIC)(TOMB-3)][BF_4], (33) 130
(v) Comparitive Structural Analysis of the Receptor-Substrate Complexes [Pd(OAP)(TOMB-1)][BF_4] (30), [Pd(PYR)(TOMB-3)][BF_4].$CHCl_3$, (31), and [Pd(PIC)(TOMB-3)][BF_4] (33) 132
(vi) Crystal Structure of [Pd(PAP)(TOMB-P4)][BF_4], (35) 133
(vii) Crystal Structure of [Pd(PAP)(TOMB-M4)][BF_4], (36) 135
(viii) Selectivity Experiment on [Pd(CH_3CN)(TOMB-X)]$^+$ (X=0,1,3) for o-aminopyridine (OAP) and pyridine (PYR) 137
(ix) Molecular Recognition of Biological Nucleobases 139
(x) Crystal Structure of [Pd(CYT)(TOMB-3)][BF_4], (34). 143
4.5 Conclusion 146

Chapter 5 148

5.1 Introduction 149
(i) Thought Process 149
(ii) Background Literature 150
5.2 Experimental 154
General Comments 154
(i) Preparation of [Pd(NH_3)(TOMB-$_3$)][BF_4], (38) 154
(ii) Preparation of [Pd(NH_2-n-Bu)(TOMB-3)][BF_4], (39) 155
(iii) Preparation of [Pd(NH(Me)-n-Bu)(TOMB-3)][BF_4], (40) 155
(iv) Attempted Preparation of [Pd(NMe_2-n-Bu)(TOMB-3)]$^+$ [BF_4] 156
(v) Preparation of [Pd(ALL)(TOMB-3)][BF_4], (41) 156
(vi) Preparation of [Pd(H_2O)(TOMB-5)][BF_4], (42) 156
(vii) Preparation of [Pd(NH_2NH_2)(TOMB-3)][BF_4], (43) 157
(viii) Preparation of [Pd(NH_2NH_2)(TOMB-3)][BF_4], (43) 157
(ix) Preparation of [Pd(NH_2NH_3)(TOMB-3)][CF_3SO_3]$_2$, (45) 157
(x) Preparation of [Pd(NH_2NH_3)(TOMB-5)][BF_4]$_2$, (46) 158
(xi) Preparation of [PdAg(H_2O)(TOMB-3)(CF_3SO_3)]$^+$ [CF_3SO_3], (47) 158

5.3 X-Ray Diffraction Data Collection, Solution, and Refinement. 159
(i) General Procedures 159
(ii) Strucuture Determination of [Pd(NH_3)(TOMB-3)][BF_4], (38) 159
(iii) Strucuture Determination of [Pd(H_20)(TOMB-5)][BF_4], (42) 160
(iv) Strucuture Determination of [Pd(NH_2NH_2)(TOMB-3)]$^+$ [BF_4], (43) 160
(v) Strucuture Determination of [Pd(NH_2NH_3)(TOMB-3)]$^{2+}$ [CF_3SO_3]$_2$, (45) 161
(vi) Strucuture Determination of [Pd(NH_2NH_3)(TOMB-5)] [BF_4]$_2$, (46) 162
(vii) Structure Determination of [PdAg(H_2O)(TOMB-3)-(CF_3SO_3)][CF_3SO_3], (47). 163
5.4 Results and Discussion 163
(i) Reaction of [Pd(CH_3CN)(TOMB-3)][BF_4] with ammonia 163
(ii) Crystal Structure of [Pd(NH_3)(TOMB-3)][BF_4], (38) 165
(iii) Reaction of [Pd(CH_3CN)(TOMB-3)][BF_4] with Amines: Formation of [Pd(NH_2-*n*-Bu)(TOMB-3)][BF_4] (39) and [Pd(NH)(Me)-*n*-Bu)(TOMB-3)][BF_4] (40) 167
(iv) Competition of NH_2-*n*-Bu and NH(Me)-*n*-Bu for [Pd(CH_3CN)(TOMB-3)][BF_4] 168
(v) Reaction of Allylamine with [Pd(CH_3CN)(TOMB-3)]$^+$ [BF_4]: Formation of [Pd(NH_2-CH_2CH=CH_2)(TOMB-3)] [BF_4], (41) 169
(vi) Crystal Structure of [Pd(H_2O)(TOMB-5)][BF_4], (42) 170
(vii) Reaction of [Pd(CH_3CN)(TOMB-3)][BF_4] and [Pd(CH_3CN)(TOMB-5)][BF_4] with Hydrazine: Formation of [Pd(NH_2NH_2)(TOMB-3)][BF_4], (43) and [Pd(NH_2NH_2)(TOMB-5)][BF_4], (44) 173
(viii) Crystal Structure of [Pd(NH_2NH_2)(TOMB-3)]$^+$ [BF_4], (43) 174
(ix) Reaction of [Pd(CH_3CN)(TOMB-3)][BF_4] and [Pd(CH_3CN)(TOMB-5)][BF_4] with the Hydrazinium cation: Formation of [Pd(NH_2NH_3)(TOMB-3)][CF_3SO_3]$_2$, (45) and Pd(NH_2NH_3)(TOMB-5)][BF_4]$_2$, (46) 176
(x) Crystal Structure of [Pd(NH_2NH_3)(TOMB-3)]$^{2+}$ [CF_3SO_3]$_2$, (45) 177
(xi) Crystal Structure of [Pd(NH_2NH_3)(TOMB-5)][BF_4]$_2$, (46) 179
(xii) Comparative Structural Analysis for the [Pd(NH_2NH_3)(TOMB-3)]$^{2+}$ (45) and [Pd(NH_2NH_3)(TOMB-5)]$^{2+}$ (46) dications 181
(xiii) Interaction of $AgCF_3SO_3$ with [Pd(CH_3CN)(TOMB-3)]$^+$ 182

[BF_4]: Formation and Crystal Structure of [$PdAg(H_2O)(TOMB\text{-}3)(CF_3SO_3)][CF_3SO_3]$,(47)
5.5 Conclusion 186

Chapter 6 188

6.1 Introduction 189
(i) Thought Process 189
(ii) Background Literature 190
6.2 Experimental. 193
General Comments. 193
(i) Preparation of 1,1'-Dibromoferrocene, (48) 194
(ii) Preparation of 1,1'-diacetoxyferrocene, (49) 194
(iii) Preparation of 1,1'-bis(2-chloroethoxy)ferrocene, (50) 195
(iv) Preparation of 1,1'-bis(5-chloro-3-oxapentoxy)-ferrocene, (51) 196
(v) Preparation of 5,9-dioxa-2,12-dithia-6,8-ferrocenyl[13]-*m*-cyclophane, (TOMB-F2) (52) 196
(vi) Attempted preparation of 2,18-dithia-5,8,12,15-tetraoxa-9,11-ferrocenyl[19]-*m*-cyclophane, (TOMB-F4) (53) 197
6.3 X-Ray Diffraction Data Collection, Solution, and Refinement. 198
(i) General Procedures 198
(ii) Structure Determination of 5,9-dioxa-2,12-dithia-6,8-ferrocenyl[13]-*m*-cyclophane, (TOMB-F2) (52) 198
6.4 Results and Discussion 199
(i) Synthesis of TOMB-F2, (52) 199
(ii) Crystal Structure of TOMB-F2 (52) 200
(iii) Attempted Preparation of TOMB-F4 (53) 203
(iv) Attempted Metalation of TOMB-F2; Oxidation of Ferrocene 205
6.5 Conclusion 207

Appendix A Supplimentary Material for X-ray Structural Determinations 209

References 294

Curriculum Vitae 305

List of Figures

Figure 1.1	Dibenzo-18-Crown-6, first isolated and identified by Pedersen.	2
Figure 1.2	Na^+ acts as a template in the cyclization of 15-Crown-5.	3
Figure 1.3	Lehn's [2.2.2]-cryptand and [3.2.2$_S$]-cryptand.	4
Figure 1.4	a) Cram's optically active binaphtho-20-crown-6. b) One of Cram's hemispherand molecules.	4
Figure 1.5	*Gauche* and *anti* placements at C-C-E-C bonds.	6
Figure 1.6	Crystal structures of 12-S-4, 15-S-5 and 18-S-6. Note that all C-S linkages in 12-S-4 and 18-S-6 and 8 of 10 in 15-S-5 are gauche.	7
Figure 1.7	Metal-thioether bonding assuming sp^3 hybridization at sulfur. σ-and π-donation to M, and π-back donation to S.	8
Figure 1.8	Copper(II) complexes of 14-S-4, and it's open chain analogue.	9
Figure 1.9	Schematic diagram of 18-crown-6 in the second sphere of M.	11
Figure 1.10	Crystal structure of [{*cis*-[$PtCl_2(NH_3)_2$]·dma}$_2$·(18-crown-6)].	12
Figure 1.11	Crystal structure of [{$Rh(COD)(NH_3)_2$}·(dibenzo-30-crown-10)].	13
Figure 1.12	Crystal structure of [{Pt(2,2'-bipyridine)$(NH_3)_2$}·(dinaphtho-30-crown-10)].	14
Figure 1.13	Crystal structure of macropolycyclic complex of [$Rh(COD)(NH_3)_2$].	14
Figure 1.14	Crystal structures of Alcock's Rh (I) complexes with a) water and b) ethanol interacting in the first- and second-sphere of the metal atom.	15
Figure 1.15	Schematic diagram of geometric complimentarity between a receptor and a substrate.	16
Figure 1.16	Schematic diagram of a) [2.2]paracyclophane and b) 15,15,36,36-tetramethyl-1,8,22,29-tetraoxa[8.1.8.1]-paracyclophane.	17
Figure 1.17	a) Hamilton's receptor-substrate complex of barbitol with 6 hydrogen-bonds. b) Crystal structure of Whitlock's receptor-substrate complex with π-hydrogen-bonds.	18
Figure 1.18	Rebek's self replicating system utilizing hydrogen-bonding and π–π stacking interactions for recognition.	19
Figure 1.19	Macrocyclic TOMB ligands studied in this dissertation.	21
Figure 2.1	Crystal Structure of Pd(TT[9]MC)Cl_2. The Pd atom is closer to C1-H than to S3.	23
Figure 2.2	a) Four fused 5-membered chelate rings in metalated TT[9]MC prevent its formation. b) Propylene linkages form two 6-membered chelate rings, lowering strain on TT[11]MC.	24
Figure 2.3	Placement of the donor atoms in TT[11]MC and *pr*-TOMB-1.	25

Figure 2.4	Crystal Structure of 2-(phenylmagnesio)-1,3-xylylene-18-crown-5.	25
Figure 2.5	a) Crystal Structure of *trans*-[2,6-(dimethyl-2,13-diazatetradecanediyl)-phenyl-*N*-*N'*]platinum(II) iodide.	26
Figure 2.6	Crystal structure of [PdCl(SCS)].	28
Scheme 2.1	These two routes can both be used to synthesize TT[11]MC.	42
Figure 2.7	TT[11]MC with heteroatom numbering scheme consistent with crystal structure and NMR discussion.	43
Figure 2.8	Perspective ORTEP drawing of TT[11]MC (3) showing the atom numbering scheme with 30% thermal ellipsoids.	44
Figure 2.9	Metalation Reaction for formation of [Pt(TT[11]MC)][BF_4].	46
Figure 2.10	Perspective ORTEP drawing of the [Pt(TT[11]MC)]$^+$ (4) cation showing the atom numbering scheme with 30% thermal ellipsoids.	48
Figure 2.11	Perspective ORTEP drawing of the [Pt(PPh_2Me)(TT[11]MC)]$^+$ (5) cation showing the atom numbering scheme with 30% thermal ellipsoids.	51
Figure 2.12	Perspective ORTEP drawing of the [PtI_2(TT[11]MC)]$^+$ (6) cation showing the atom numbering scheme with 30% thermal ellipsoids.	53
Figure 2.13	Sulfur coordination renders adjacent benzylic H-atoms inequivalent resulting in AB splitting pattern.	56
Scheme 2.2	Process of formation of [Pd(TT[11]MC)][BF_4].	57
Figure 2.14	Crystal Structure of the [Pd(TT[11]MC)]$^+$ cation.	57
Figure 2.15	$^{13}C\{^1H\}$ NMR spectrum of [Pt(PPh_2Me)(TT[11]MC)][BF_4] at 298 K in CD_3CN with inset diagram of the cation.	59
Scheme 2.3	Preparation of 4-oxa-1,7-heptanedithiol.	61
Figure 2.16	Perspective ORTEP drawing of *pr*-TOMB-1 (13) showing the atom numbering scheme with 30% thermal ellipsoids.	63
Figure 2.17	Perspective ORTEP drawing of the [Pd(*pr*-TOMB-1)]$^+$ (14) cation showing the atom numbering scheme with 30% thermal ellipsoids.	65
Figure 3.1	Schematic diagrams of the four [Pd(CH_3CN)(TOMB-0)]$^+$, [Pd(CH_3CN)(TOMB-1)]$^+$, [Pd(CH_3CN)(TOMB-3)]$^+$ and [Pd(CH_3CN)(TOMB-5)]$^+$ cationic receptors.	72
Figure 3.2	Structure of tetrakis-(μ-acetoxylato)dirhodium (II).	73
Figure 3.3	Ogoshi's porphyrin receptor containing coordination site and hydrogen bond donors.	74
Figure 3.4	Kimura's Zn(II)-cyclen receptor with pendant arm acridine group and N-H hydrogens for secondary interactions with substrates.	74
Figure 3.5	Reinhoudt's receptor molecule with a Ni(II) centre as the Lewis acid and polyether chains as hydrogen-bond acceptors.	75
Figure 3.6	Lehn's cryptand containing soft and hard donor sets.	75

Figure 3.7	a) General form of ligands synthesized in the Vogtle lab. b) TOMB-1 and c) TOMB-3.	76
Figure 3.8	Loeb's receptor molecule containing a metal centre, hydrogen-bond acceptors and π-stacking units.	76
Scheme 3.1	Preparation of TOMB ligands by two methods.	88
Figure 3.9	^{1}H NMR spectrum of 5,8,11-Trioxa-2,14-dithia[15]-*m*-cyclophane, (TOMB-3).	89
Figure 3.10	Perspective ORTEP drawing of TOMB-3 (18) showing the atom numbering scheme with 30% thermal ellipsoids.	91
Figure 3.11	Typical Preparation of a [Pd(TOMB-X)(CH_3CN)][BF_4] complex.	93
Figure 3.12	^{1}H NMR Spectra of a) [Pd(TOMB-0)(CH_3CN)]$^+$ (21) ($CDCl_3$), b) [Pd(TOMB-1)(CH_3CN)]$^+$ (23) (CD_3CN), c) [Pd(TOMB-3)(CH_3CN)]$^+$ (25) ($CDCl_3$), d) [Pd(TOMB-5)(CH_3CN)]$^+$ (26) ($CDCl_3$).	95
Figure 3.13	Schematic diagram of the aliphatic chain 'flipping' from one side of the aromatic ring to the other in the [Pd(TOMB-3)(CH_3CN)]$^+$ (25) cation.	96
Figure 3.14	Low temperature (213 K) ^{1}H NMR spectrum of the [Pd(TOMB-3)(CH_3CN)]$^+$ cation in $CDCl_3$ showing the CH_3CN. At low temperature free and complexed acetonitrile appear.	96
Figure 3.15	Perspective ORTEP drawing of [Pd(CH_3CN)(TOMB-0)]$^+$ cation (21) showing the atom numbering scheme with 30% thermal ellipsoids.	98
Figure 3.16	Perspective ORTEP drawing of [Pd(TOMB-1)(CH_3CN)]$^+$ cation (23) showing the atom numbering scheme with 30% thermal ellipsoids.	100
Figure 3.17	Perspective ORTEP drawing of [Pd(TOMB-3)Cl] (24) showing the atom numbering scheme with 30% thermal ellipsoids.	102
Figure 3.18	Perspective ORTEP drawing of [Pd(CH_3CN)(TOMB-3)]$^+$ cation (25) showing the atom numbering scheme with 30% thermal ellipsoids.	104
Figure 3.19	Perspective ORTEP drawing of [Pd(CH_3CN)(TOMB-P4)]$^+$ cation (35) showing the atom numbering scheme with 30% thermal ellipsoids.	106
Figure 4.1	Structures of pyridine and *o*-aminopyridine.	110
Figure 4.2	Structure of the four biological nucleobases in DNA.	111
Figure 4.3	Crystal structure of uranyl containing receptor-urea complex.	112
Figure 4.4	Simultaneous first- and second sphere coordination of the methyl ester of leucine by bis(2-hydroxynaphthyl)porphyrins.	112
Figure 4.5	Zn(II) cyclen receptor binding 1-methylthymine *via* first-sphere coordination and second-sphere hydrogen-bonding and π-stacking.	113

Figure 4.6	Crystal structure of tetrakis-(μ-acetamido)dirhodium(II) dimer complexing theophylline in first and second sphere.	114
Figure 4.7	Crystal Structure of guanine coordinating to palladium in the first sphere and hydrogen bonding and π-stacking in the second sphere of the palladium.	114
Figure 4.8	Comparison of the ^{1}H NMR spectra of the $[Pd(OAP)(TOMB-0)]^+$ (top), $[Pd(OAP)(TOMB-1)]^+$ (middle) and $[Pd(OAP)(TOMB-3)]^+$ (bottom) cations.	125
Figure 4.9	Perspective ORTEP drawing of the $[Pd(OAP)(TOMB-1)]^+$ cation (30) showing the atom numbering scheme with 30% thermal ellipsoids.	127
Figure 4.10	Perspective ORTEP drawing of the $[Pd(PYR)(TOMB-3)]^+$ cation (31) showing the atom numbering scheme with 30% thermal ellipsoids.	129
Figure 4.11	Perspective ORTEP drawing of $[Pd(PIC)(TOMB-3)]^+$ cation (33) showing the atom numbering scheme with 30% thermal ellipsoids.	131
Figure 4.12	Perspective ORTEP drawing of $[Pd(PAP)(TOMB-P4)]^+$ cation (35) showing the atom numbering scheme with 30% thermal ellipsoids.	134
Figure 4.13	Perspective ORTEP drawing of $[Pd(PAP)(TOMB-M4)]^+$ cation (36) showing the atom numbering scheme with 30% thermal ellipsoids.	136
Figure 4.14	^{1}H NMR spectrum a 1:1:1 mixture of $[Pd(CH_3CN)(TOMB-3)]^+$ $[BF_4]$, OAP and PYR in $CDCl_3$ at 253 K.	137
Figure 4.15	OAP:PYR ratio for each receptor at various temperatures. More ether oxygen atoms in a receptor results in a higher OAP:PYR ratio	139
Figure 4.16	Plots of percent extraction of solid nucleobase (cytosine C, adenine A, guanine G, thymine T) into a solution of PdTX.	140
Figure 4.17	^{1}H NMR spectrum of $[Pd(CYT)(TOMB-3)]^+$ (CD_3CN). Free and hydrogen-bonded N-H protons are observed at 6.71 and 7.28 ppm.	141
Figure 4.18	Three types of binding modes possible for adenine.	142
Figure 4.19	Perspective ORTEP drawing of $[Pd(CYT)(TOMB-3)]^+$ cation (34) showing the atom numbering scheme with 30% thermal ellipsoids.	144
Figure 5.1	Schematic diagram of simultaneous primary and secondary coordination of amines. X=NH_2 or NH_3^+.	150
Figure 5.2	Schematic diagram and crystal structure of the 2'-carboxy-1',3'-xylyl-18-crown-5-(*t*-butylamine) complex.	150
Figure 5.3	a) Schematic diagram of Fe(III) 'receptor' complex. b) Crystal structure of hydrogen-bonded Fe(III)-Zn(II) 'receptor-substrate' complex.	151
Figure 5.4	Crystal structure of $\{[Cu(NH_3)_4(H_2O)][PF_6]_2\text{-}(C_{12}H_{24}O_6)\}_n$.	151

Figure 5.5	a) Crystal structure of Reetz's substrate-receptor complex. b) Crystal structure of Stoddart's $[(Rh(COD)(NH_3))_2N_2O_4][PF_6]_2$ complex.	152
Figure 5.6	Crystal structure of the complex of Ag^+ with a *cis*-stilbene.	153
Figure 5.7	a) Schematic diagram of $[PtAg(C_6H_3(2,6\text{-}Me_2NCH_2)_2)\text{-}(RNCHNR')Br]$ complex stabilized by a bridging ligand. R=*p*-tolyl, R'=alkyl. b) Crystal Structure of $Pt((CH_3\text{-}C_6H_3(2,6\text{-}Me_2NCH_2)_2)\text{-}(o\text{-tolyl})][I]$.	153
Figure 5.8	^1H NMR spectrum of $[Pd(NH_3)(TOMB\text{-}3)][BF_4]$ in $CDCl_3$ at 298 K.	163
Figure 5.9	^1H NMR spectrum of $[Pd(NH_3)(TOMB\text{-}3)][BF_4]$ in $CDCl_3$ at 218 K.	164
Figure 5.10	Perspective ORTEP drawing of the $[Pd(NH_3)(TOMB\text{-}3)]^+$ cation (38) showing the atom numbering scheme with 20% thermal ellipsoids.	166
Figure 5.11	^1H NMR spectra of $[Pd(NH_2\text{-}n\text{-}Bu)(TOMB\text{-}3)][BF_4]$ (39) (top) and $[Pd(NH(Me)\text{-}n\text{-}Bu)(TOMB\text{-}3)][BF_4]$ (40) (bottom) at 298K in $CDCl_3$.	168
Figure 5.12	^1H NMR spectrum of 1:1:1 competition between NH_2-*n*-Bu and NH(Me)-*n*-Bu for $[Pd(CH_3CN)(TOMB\text{-}3)][BF_4]$ in $CDCl_3$ at 298 K.	169
Figure 5.13	Intended geometry of organometallic receptor-substrate complex.	170
Figure 5.14	Perspective ORTEP drawing of the $[Pd(H_2O)(TOMB\text{-}5)]^+$ cation (42) showing the atom numbering scheme with 30% thermal ellipsoids.	171
Figure 5.15	^1H NMR spectrum of $[Pd(NH_2NH_2)(TOMB\text{-}3)][BF_4]$ in $CDCl_3$ at 298K.	173
Figure 5.16	Perspective ORTEP drawing of the $[Pd(NH_2NH_2)(TOMB\text{-}3)]^+$ cation (43) showing the atom numbering scheme with 30% thermal ellipsoids.	175
Figure 5.17	Perspective ORTEP drawing of the $[Pd(NH_2NH_3)\text{-}(TOMB\text{-}3)]^{2+}$ dication (45) showing the atom numbering scheme with 30% thermal ellipsoids.	178
Figure 5.18	Perspective ORTEP drawing of the $[Pd(NH_2NH_3)(TOMB\text{-}5)]^{2+}$ dication (46) showing the atom numbering scheme with 30% thermal ellipsoids.	180
Figure 5.19	Schematic diagram of the interaction of Ag^+ with $[Pd(TOMB\text{-}3)]^+$	182
Figure 5.20	Perspective ORTEP drawing of $[PdAg(H_2O)(TOMB\text{-}3)\text{-}(CF_3SO_3)]^+$, (47) showing the atom numbering scheme with 30% thermal ellipsoids.	183
Figure 5.21	^1H NMR spectrum of interaction between $AgCF_3SO_3$ and $[Pd(CH_3CN)(TOMB\text{-}3)][BF_4]$ in $CDCl_3$ at 298 K.	185
Figure 6.1	Schematic drawing of ligand TOMB-F2, containing ferrocene.	189

Figure 6.2	A primary amine hydrogen-bonding with the receptor induces a change in ferrocene moiety redox potential.	190
Figure 6.3	Selection of 'ferrocenophanes' initially reported by Biernat and Wilczewski.	191
Figure 6.4	Selected macrocycles containing ferrocene synthesized by Beer's group.	191
Figure 6.5	Cryptand molecules containing ferrocene.	192
Figure 6.6	Spontaneous reduction of Cu(II) by ferrocene.	192
Figure 6.7	Crystal Structure of [Pd(1,5,9-trithia[9](1,1')-ferrocenophane)][BF_4]$_2$.	193
Figure 6.8	Preparation of TOMB-F2 from 1,1'-bis(2-chloroethoxy)-ferrocene and *meta*-xylene-α,α'-dithiol.	199
Figure 6.9	^{1}H NMR spectrum of TOMB-F2 in $CDCl_3$.	200
Figure 6.10	Perspective ORTEP drawing of TOMB-F2 (52) showing the atom numbering scheme with 30% thermal ellipsoids.	201
Figure 6.11	Intended preparation of TOMB-F4.	204
Figure 6.12	Actual product formed during preparation of TOMB-F4.	204
Scheme 6.1	The redox potential for 2 ferrocene + Pd^{2+} is positive; the reaction is spontaneous.	206
Figure 6.13	Redox reaction between TOMB-F2 and [Pd(CH_3CN)$_4$]$^{2+}$.	207
Figure 6.14	Proposed method of metalation of TOMB-F2.	208

List of Tables

Table 2.1	Torsional Angles about Sulfur Atoms in TT[11]MC.	45
Table 2.2	$^{13}C\{^1H\}$ NMR Chemical Shifts for TT[11]MC, $[Pt(TT[11]MC)]^+$ and $[Pt(PPh_2Me)(TT[11]MC)]^+$.	50
Table 2.3	Comparison of some X-ray structural parameters for $[Pt(TT[11]MC][BF_4]$ and $[Pd(TT[11]MC][BF_4]$.	58
Table 3.1	$^{13}C\{^1H\}$ NMR assignments ($CDCl_3$) for TOMB-X (X=0,1,3,5).	89
Table 3.2	Selected Torsional Angles for TOMB-3, (18).	92
Table 4.1	Results of variable temperature NMR selectivity experiment listing OAP:PYR ratios and percentage of OAP bound by the receptor.	138
Table 4.2	Comparison of Bond Angles around palladium for the four $[Pd(L)(TOMB-3)]^+$ complexes.	145
Table 6.1	Torsional angles around sulfur and oxygen atoms for TOMB-F2	203
Table A1.1	Summary of Crystal Data, Intensity Collection and Structure Refinement for *pr*-TOMB-1, (13).	210
Table A1.2	Positional parameters and β(eq) for *pr*-TOMB-1, (13).	211
Table A1.3	Intramolecular Distances (Å) Involving the Nonhydrogen Atoms for *pr*-TOMB-1, (13).	211
Table A1.4	Intramolecular Bond Angles Involving the Nonhydrogen Atoms for *pr*-TOMB-1, (13).	211
Table A1.5	Torsional Angles for *pr*-TOMB-1, (13).	212
Table A2.1	Summary of Crystal Data, Intensity Collection, and Structure Refinement for $[Pd(pr\text{-TOMB-1})][BF_4]$, (14).	213
Table A2.2	Positional Parameters and β(eq) for $[Pd(pr\text{-TOMB-1})][BF_4]$, (14).	214
Table A2.3	Intramolecular Distances (Å) Involving the Nonhydrogen Atoms for $[Pd(pr\text{-TOMB-1})][BF_4]$, (14).	215
Table A2.4	Intramolecular Bond Angles Involving the Nonhydrogen Atoms for $[Pd(pr\text{-TOMB-1})][BF_4]$, (14).	216
Table A3.1	Summary of Crystal Data, Intensity Collection and Structure Refinement for TOMB-3, (18).	217
Table A3.2	Positional parameters and β(eq) for TOMB-3, (18).	218
Table A3.3	Intramolecular Distances (Å) Involving the Nonhydrogen Atoms for TOMB-3, (18).	219
Table A3.4	Intramolecular Bond Angles Involving the Nonhydrogen Atoms for TOMB-3, (18).	219
Table A3.5	Torsional Angles for TOMB-3, (18).	220
Table A4.1	Summary of Crystal Data, Intensity Collection and Structure Refinement for $[Pd(CH_3CN)(TOMB-0)][BF_4]$, (21).	221
Table A4.2	Positional Parameters and β(eq) for $[Pd(CH_3CN)$-$(TOMB-0)][BF_4]$, (21).	222

Table A4.3	Intramolecular Distances (Å) Involving the Nonhydrogen Atoms for [Pd(CH_3CN)(TOMB-0)][BF_4], (21).	223
Table A4.4	Intramolecular Bond Angles Involving the Nonhydrogen Atoms for [Pd(CH_3CN)(TOMB-0)][BF_4], (21).	224
Table A5.1	Summary of Crystal Data, Intensity Collection and Structure Refinement for [Pd(CH_3CN)(TOMB-1)] [CF_3SO_3], (23).	225
Table A5.2	Positional Parameters and β(eq) for [Pd(CH_3CN)-(TOMB-1)][CF_3SO_3], (23).	226
Table A5.3	Intramolecular Distances (Å) Involving the Nonhydrogen Atoms for [Pd(CH_3CN)(TOMB-1)][CF_3SO_3], (23).	227
Table A5.4	Intramolecular Bond Angles Involving the Nonhydrogen Atoms for [Pd(CH_3CN)(TOMB-1)][CF_3SO_3], (23).	228
Table A6.1	Summary of Crystal Data, Intensity Collection and Structure Refinement for [Pd(TOMB-3)Cl], (24).	229
Table A6.2	Positional parameters and β(eq) for [Pd(TOMB-3)Cl], (24).	230
Table A6.3	Interatomic distances (Å) Involving the Nonhydrogen Atoms for [Pd(TOMB-3)Cl], (24).	231
Table A6.4	Intramolecular Bond Angles Involving the Nonhydrogen Atoms for [Pd(TOMB-3)Cl], (24).	232
Table A7.1	Summary of Crystal Data, Intensity Collection and Structure Refinement for [Pd(CH_3CN)(TOMB-3)][BF_4], (25).	233
Table A7.2	Positional parameters and β(eq) for [Pd(CH_3CN) (TOMB-3)][BF_4], (25).	234
Table A7.3	Intramolecular Distances (Å) Involving the Nonhydrogen Atoms for [Pd(CH_3CN)(TOMB-3)][BF_4], (25).	235
Table A7.4	Intramolecular Bond Angles Involving the Nonhydrogen Atoms for [Pd(CH_3CN)OMB-3)][BF_4], (25).	236
Table A8.1	Summary of Crystal Data, Intensity Collection and Structure Refinement for [Pd(CH_3CN)(TOMB-P4)][BF_4], (27).	237
Table A8.2	Positional Parameters and β(eq) for [Pd(CH_3CN)-(TOMB-P4)][BF_4], (27).	238
Table A8.3	Intramolecular Distances (Å) Involving the Nonhydrogen Atoms for [Pd(CH_3CN)(TOMB-P4)][BF_4], (27).	239
Table A8.4	Intramolecular Bond Angles Involving the Nonhydrogen Atoms for [Pd(CH_3CN)(TOMB-P4)][BF_4], (27).	240
Table A9.1	Summary of Crystal Data, Intensity Collection and Structure Refinement for [Pd(OAP)(TOMB-1)][BF_4], (31).	242
Table A9.2	Positional Parameters and β(eq) for [Pd(OAP)(TOMB-1)]$^+$ [BF_4], (31).	243
Table A9.3	Intramolecular Distances Involving the Nonhydrogen Atoms for [Pd(OAP)(TOMB-1)][BF_4], (31).	244
Table A9.4	Intramolecular Bond Angles Involving the Nonhydrogen Atoms for [Pd(OAP)(TOMB-1)][BF_4], (31).	245
Table A10.1	Summary of Crystal Data, Intensity Collection and Structure Refinement for [Pd(PYR)(TOMB-3)][BF_4], (32).	246

Table A10.2	Positional Parameters and β(eq) for [Pd(PYR)(TOMB-3)]$^{+}$ $[BF_4]$, (32).	247
Table A10.3	Intramolecular Distances (Å) Involving the Nonhydrogen Atoms for [Pd(PYR)(TOMB-3)][BF_4], (32).	248
Table A10.4	Intramolecular Bond Angles Involving the Nonhydrogen Atoms for [Pd(PYR)(TOMB-3)][BF_4], (32).	249
Table A11.1	Summary of Crystal Data, Intensity Collection and Structure Refinement for [Pd(PIC)(TOMB-3)][BF_4], (34).	250
Table A11.2	Positional Parameters and β(eq) for [Pd(PIC)(TOMB-3)] $[BF_4]$, (34).	251
Table A11.3	Intramolecular Distances (Å) Involving the Nonhydrogen Atoms for [Pd(PIC)(TOMB-3)][BF_4], (34).	252
Table A11.4	Intramolecular Bond Angles Involving the Nonhydrogen Atoms for [Pd(PIC)(TOMB-3)][BF_4], (34).	253
Table A12.1	Summary of Crystal Data, Intensity Collection and Structure Refinement for [Pd(CYT)(TOMB-3)][BF_4], (35).	254
Table A12.2	Positional parameters and β(eq) for [Pd(CYT)(TOMB-3)] $[BF_4]$, (35).	255
Table A12.3	Intramolecular Distances (Å) Involving the Nonhydrogen Atoms for [Pd(CYT)(TOMB-3)][BF_4], (35).	256
Table A12.4	Intramolecular Bond Angles Involving the Nonhydrogen Atoms for [Pd(CYT)(TOMB-3)][BF_4], (35).	257
Table A13.1	Summary of Crystal Data, Intensity Collection and Structure Refinement for [Pd(PAP)(TOMB-P4)][BF_4], (36).	258
Table A13.2	Positional Parameters and β(eq) for [Pd(PAP)(TOMB-P4)] $[BF_4]$, (36).	259
Table A13.3	Intramolecular Distances (Å) Involving the Nonhydrogen Atoms for [Pd(PAP)(TOMB-P4)][BF_4], (36).	260
Table A13.4	Intramolecular Bond Angles Involving the Nonhydrogen Atoms for [Pd(PAP)(TOMB-P4)][BF_4], (36).	261
Table A14.1	Summary of Crystal Data, Intensity Collection and Structure Refinement for [Pd(PAP)(TOMB-M4)][BF_4], (37).	263
Table A14.2	Positional parameters and β(eq) for [Pd(PAP)(TOMB-M4)] $[BF_4]$, (37).	264
Table A14.3	Intramolecular Distances (Å) Involving the Nonhydrogen Atoms for [Pd(PAP)(TOMB-M4)][BF_4], (37).	265
Table A14.4	Intramolecular Bond Angles Involving the Nonhydrogen Atoms for [Pd(PAP)(TOMB-M4)][BF_4], (37).	266
Table A15.1	Summary of Crystal Data, Intensity Collection and Structure Refinement for [Pd(NH_3)(TOMB-3)][BF_4], (38).	268
Table A15.2	Positional parameters and β(eq) for [Pd(NH_3)(TOMB-3)]$^{+}$ $[BF_4]$, (38).	269
Table A15.3	Intramolecular Distances (Å) Involving the Nonhydrogen Atoms for [Pd(NH_3)(TOMB-3)][BF_4], (38).	270
Table A15.4	Intramolecular Bond Angles Involving the Nonhydrogen Atoms for [Pd(NH_3)(TOMB-3)][BF_4], (38).	271

Table A16.1	Summary of Crystal Data, Intensity Collection and Structure Refinement for [Pd(H_2O)(TOMB-5)][BF_4], (42).	272
Table A16.2	Positional Parametersand β(eq) for [Pd(H_2O)(TOMB-5)][BF_4], (42).	273
Table A16.3	Intramolecular Distances Involving the Nonhydrogen Atoms for [Pd(H_2O)(TOMB-5)][BF_4], (42).	274
Table A16.4	Intramolecular Bond Angles Involving the Nonhydrogen Atoms for [Pd(H_2O)(TOMB-5)][BF_4], (42).	275
Table A17.1	Summary of Crystal Data, Intensity Collection and Structure Refinement for [Pd(NH_2NH_2)(TOMB-3)][BF_4], (43).	276
Table A17.2	Positional Parameters and β(eq) for [Pd(NH_2NH_2)(TOMB-3)][BF_4], (43).	277
Table A17.3	Intramolecular Distances (Å) Involving the Nonhydrogen Atoms for [Pd(NH_2NH_2)(TOMB-3)][BF_4], (43).	278
Table A17.4	Intramolecular Bond Angles Involving the Nonhydrogen Atoms for [Pd(NH_2NH_2)(TOMB-3)][BF_4], (43).	279
Table A18.1	Summary of Crystal Data, Intensity Collection and Structure Refinement for [Pd(NH_2NH_3)(TOMB-3)][CF_3SO_3]$_2$, (45).	280
Table A18.2	Positional Parameters and β(eq) for [Pd(NH_2NH_3) (TOMB-3)][CF_3SO_3]$_2$ (45).	281
Table A18.3	Intramolecular Distances (Å) Involving the Nonhydrogen Atoms [Pd(NH_2NH_3)(TOMB-3)][CF_3SO_3]$_2$ (45).	283
Table A18.4	Intramolecular Bond Anglesnvolving the Nonhydrogen Atoms for [Pd(NH_2NH_3)(TOMB-3)][CF_3SO_3]$_2$ (45).	284
Table A19.1	Summary of Crystal Data, Intensity Collection and Structure Refinement for [Pd(NH_2NH_3)(TOMB-5)][BF_4]$_2$, (46).	285
Table A19.2	Positional parameters and β(eq) for [Pd(NH_2NH_3)-(TOMB-5)][BF_4]$_2$, (46).	286
Table A19.3	Intramolecular Distances (Å) Involving the Nonhydrogen Atoms for [Pd(NH_2NH_3)(TOMB-5)] [BF_4]$_2$, (46).	287
Table A19.4	Intramolecular Bond Angles Involving the Nonhydrogen Atoms for [Pd(NH_2NH_3)(TOMB-5)] [BF_4]$_2$, (46).	288
Table A20.1	Summary of Crystal Data, Intensity Collection and Structure Refinement for TOMB-F2, (52).	289
Table A20.2	Positional parameters and β(eq) for TOMB-F2, (52).	290
Table A20.3	Intramolecular Distances Involving the Non-Hydrogen Atoms for TOMB-F2, (52).	291
Table A20.4	Intramolecular Bond Angles Involving the Non-Hydrogen Atoms for TOMB-F2, (52).	292

List of Abbreviations

Abbreviation	Meaning
Å	Angstrom (10^{-10} m)
ADE	adenine
ALL	allylamine
BDH	British Drug House
BPY	2,2'-bipyridine
br	broad
°C	degrees Celcius
COD	1,5-cyclooctadiene
cm	centimetres
CPK	Corey-Pauling-Koltun
CYT	cytosine
δ	chemical shift
d_6	hexa-deutero
d	doublet
D	deuterium
deg	degrees
DMF	N,N'-dimethylformamide
DMSO	dimethylsulfoxide
DNA	deoxyribonucleicacid
EPR	electron paramagnetic resonance
F_c	calculated structure factor
F_o	observed structure factor
g	grams
GUA	guanine
h	hours
Hz	hertz
IR	infrared
J	\J\, (coupling constant, Hz)
K	degrees Kelvin
λ	wavelength
μ	absorption coefficient
m	multiplet
MAP	*meta*-aminopyridine

Me	methyl
MHz	megahertz
min.	minutes
mL	millilitres
mmol	millimoles
μmol	micromoles
NMR	nuclear magnetic resonance
OAP	o-aminopyridine
ORTEP	Oak Ridge Thermal Ellpisoid Plot
PAP	*para*-aminopyridine
PCP	1,3-bis[(di-*t*-butylphosphino)methyl]-benzene
Ph	phenyl
PIC	2-amino-4-picoline
ppm	parts per million
pr-TOMB-1	6-oxa-2,10-dithia-[11]-*m*-cyclophane
PYR	pyridine
q	quartet
quin	quintet
ρ	density
R	agreement factor
R_w	weighted agreement factor
s	singlet
SGI	Silicon Graphics Indigo
t	triplet
T	temperature
t-Bu	*tertiary*-butyl
THY	thymine
TMEDA	N,N,N',N'-tetramethylethylenediamine
TOMB-0	2,14-dithia-[15]-*m*-cyclophane
TOMB-1	5-oxa-2,8-dithia-[9]-*m*-cyclophane
TOMB-3	5,8,11-trioxa-2,14-dithia-[15]-*m*-cyclophane
TOMB-5	5,8,11,14,17-pentacxa-2, 20-dithia-[21]-*m*-cyclophane

TOMB-F2	5,9-dioxa-2,12-dithia-6,8-ferrocenyl-[13]-*m*-cyclophane
TOMB-F4	2,18-dithia-5,8,12,15-tetraoxa-9,11-ferrocenyl-[19]-*m*-cyclophane
TOMB-M4	10,13,16,19-tetraoxa-2,27-dithia-3,19-*p*-phenyl-[28]-*m*-cyclophane
TOMB-P4	10,13,16,19-tetraoxa-2,27-dithia-3,19-*m*-phenyl-[28]-*m*-cyclophane
TT[9]MC	2,5,8-trithia[9]-*m*-cyclophane
TT[11]MC	2,6,10-trithia[11]-*m*-cyclophane
X-ray	X-ray diffraction
var	variables
V	unit cell volume
Z	number of molecules in the unit cell

Chapter 1

Introduction

Chapter 1

Introduction

1.1 Historical Background

In 1967 Charles Pedersen published an article in *The Journal of the American Chemical Society* detailing the synthesis of 33 cyclic polyether compounds which he coined "crown ethers"[1] (Figure 1.1). This article, though not the first to describe the synthesis of cyclic compounds[2], was enormously important to the field of macrocyclic chemistry. It was the first to recognize the potential that macrocycles had to bind alkali and alkaline earth metal cations using non-covalent interactions between the electron rich oxygen atoms and the electron poor metals ions. Over the next 20 years the area of macrocyclic chemistry proliferated and in 1987 the Nobel Prize in Chemistry was awarded to Charles Pedersen[3], Donald Cram[4] and Jean-Marie Lehn[5] for their work in pioneering, developing and investigating the now vast area of macrocyclic chemistry.

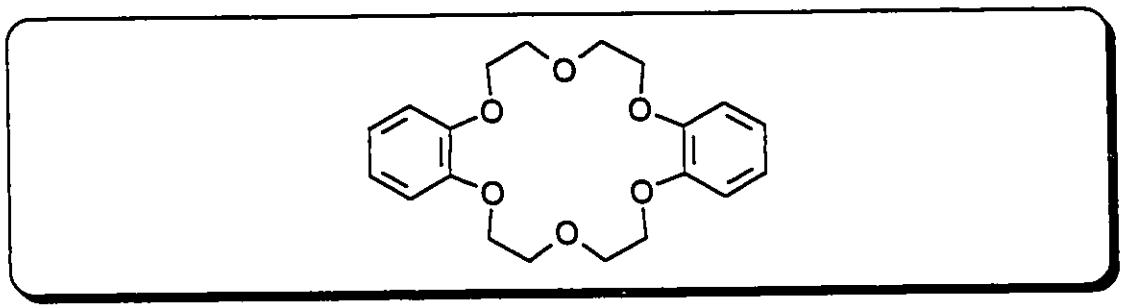

Figure 1.1 Dibenzo-18-Crown-6, first isolated and identified by Pedersen.

Pedersen's article described the synthetic procedure and utility of macrocycles ranging in size from 9 to 60 atoms and containing 3 to 20 oxygen

atoms using several different synthetic strategies. Although he was aware that there was 'an unusual mechanism' at work, now known as the template effect, Pedersen did not know why the formation of these large rings was allowed at the time he published his paper[6]. The template effect[7, 8, 9] can be easily understood by considering the interaction of a metal cation with a polyether chain containing a nucleophilic function on one end, and a leaving group on the other. The polyether chain wraps around the metal atom, and if the metal is the appropriate size (the right template), the nucleophile and electrophile on the same molecule are placed in close proximity and react to form the macrocycle (Figure 1.2).

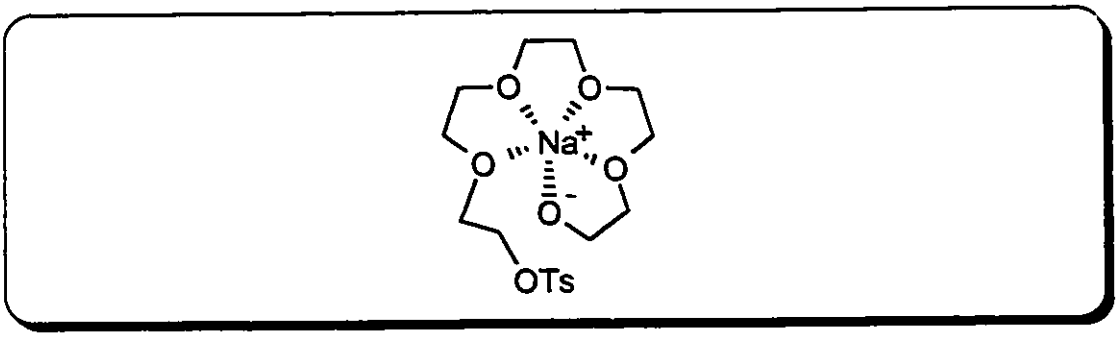

Figure 1.2 Na^+ acts as a template in the cyclization of 15-Crown-5.

With the advent of a facile route towards macrocycles of various sizes, peripheral groups and other donors were quickly added to the central core of macrocycles and their chemistry explored. At the forefront of those who caught on to this exciting new area of organic chemistry were Jean-Marie Lehn and Donald Cram.

Lehn's major contribution to the field of macrocyclic chemistry was to add a third strand of donor groups across Pedersen's crown ethers. In order to

distinguish his molecules from existing macrocycles Lehn coined the name "cryptands"[5, 10, 11]. While crown ethers complexed cations, the cryptands, because of their 3-dimensional shape, (Figure 1.3) were designed to fully encapsulate metal cations, in effect replacing the first solvation sphere.

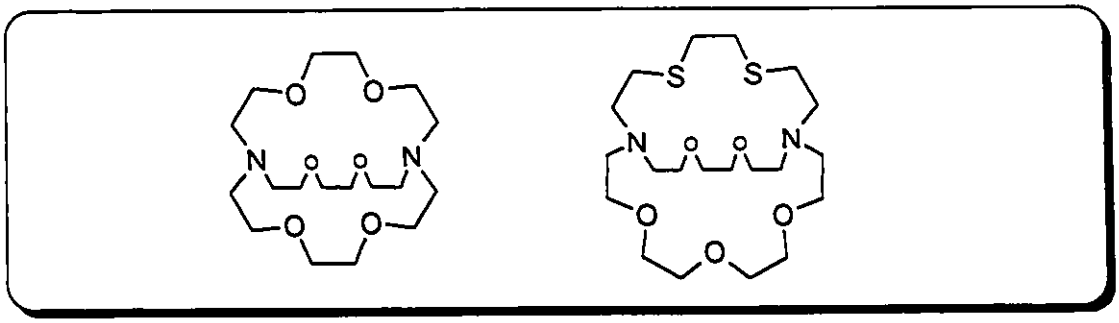

Figure 1.3 Lehn's [2.2.2]-cryptand and [3.2.2$_S$]-cryptand.

After reading Pedersen's paper on macrocyclic ethers, Cram realized work he previously considered with cyclic tetramers derived from furan and acetone had been too narrow in scope[6]. He soon found his own niche in the field, developing chiral macrocycles which could in principle permit the stereochemical differentiation of racemic mixtures of optically active ammonium salts[4, 12] (Figure 1.4a). He also developed a variety of rigidly reinforced concave molecules he termed "hemispherands" (Figure 1.4b) and spherands[13, 14, 15, 16].

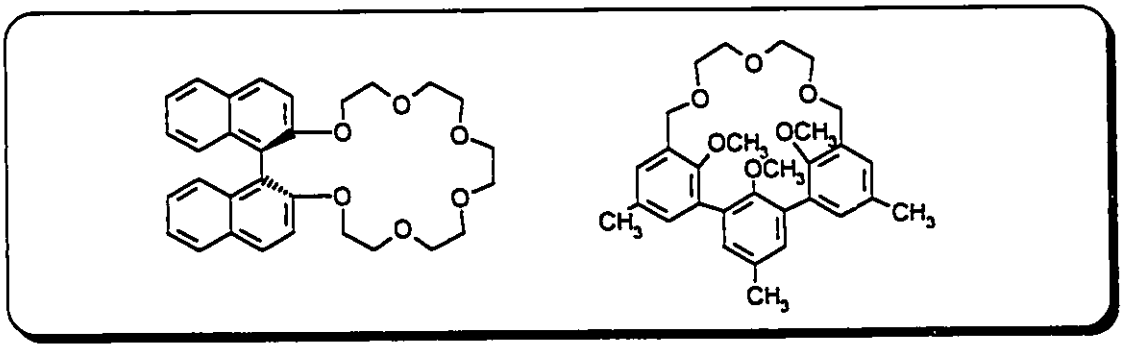

Figure 1.4 a) Cram's optically active binaphtho-20-crown-6. b) One of Cram's hemispherand molecules.

As research in the area continued the variety of macrocyclic structures increased. Workers such as Gutsche pioneered the area of "calixarenes"[17, 18] which are so named to describe the calix, or vase, shape resulting from the arrangement of arene rings. Donor groups attached to the bottom of the 'vase' complex metal cations. Gokel and co-workers developed "lariat ethers" in which pendant arms are attached to a crown ether such that a donor at the end of the arm can cap the planar coordination sphere of a complexed cation[19, 20]. These lariat ethers show increased binding and selectivity for metal cations over their crown ether predecessors.

It is perhaps wise at this point to also mention the class of macrocycles known as cyclophanes[21]. These molecules incorporate an aromatic ring(s) into the macrocycle and as such spherands and calixarenes may be included in this group. The term cyclophane is, however, intended to refer to macrocycles containing aromatic rings that are not already a class unto themselves[22, 23].

1.2 Crown Thioethers.

(i) Synthesis. At about the same time that Pedersen discovered the crown ethers, the group of Daryle Busch and others had been working on macrocyclic complexes containing nitrogen and sulfur donor atoms for a number of years[24]. The synthetic route to thioether macrocycles at that time involved the reaction of the sodium salt of a dithiol with an appropriate dihalide[25]. Initially the synthesis of 1,4,8,11- tetrathiacyclotetradecane (14-S-4) resulted in only a 7.5% yield. This was later increased to 55% by performing the reaction at higher

dilution[26, 27].

In 1981, Buter and Kellogg reported a facile synthetic route towards sulfur containing macrocycles in yields ranging from 73% to 90%[28]. The method involved using Cs_2CO_3 as a base to remove the acidic thiol protons and form reasonably soluble cesium thiolates. Rather than a template mechanism, the method utilizes a large charge separation between the cesium atom and the thiolate in DMF solution to increase the attraction of the nucleophilic thiolate for electrophilic carbon atoms, as determined by a ^{133}Cs NMR experiment[29]. At moderate dilution conditions (4 mmol of dithiol and 4 mmol of dihalide in 700 mL DMF), moderate temperatures (50-55 °C) and relatively slow addition times (12-15 h) the intramolecular cyclization is favoured over intermolecular oligomer formation, yielding relatively pure ligands in good yields.

(ii) Ligand Conformation. In a conformational analysis of macrocyclic ligands, a good measure of the strain inherent in the ligand is found in the torsional angles. Deviations of these torsional angles from the optimal values of ± 60° (*gauche*) and ±180° (*anti*) (Figure 1.5) indicate that the ligand is relieving

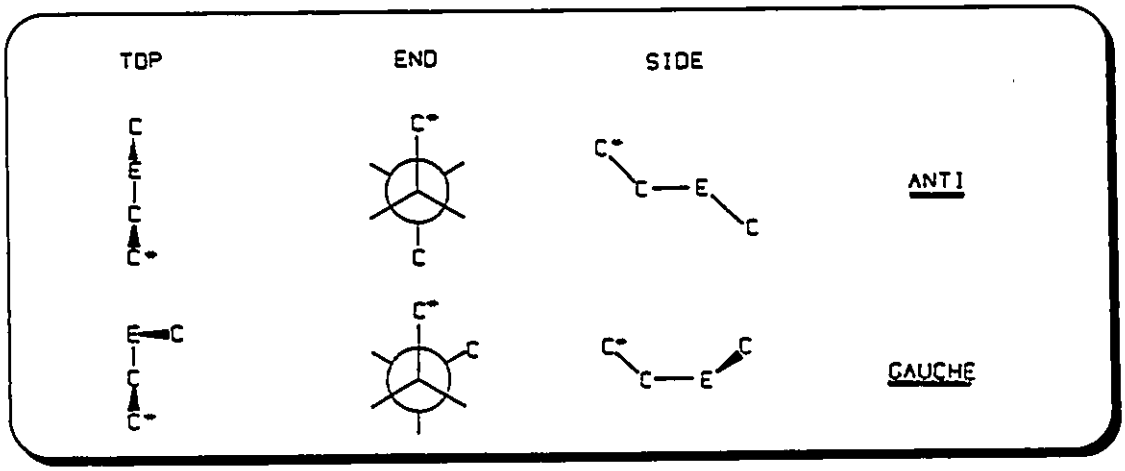

Figure 1.5 *Gauche* and *anti* placements at C-C-E-C bonds.

this strain. Dale first used this technique in a pioneering conformational analyses of crown ethers[30].

In an extension of Dale's research, Stephen Cooper and coworkers published an elegant paper[31] in which he applied the technique to crown thioethers. For a full description the reader is referred to that paper as only a brief synopsis will be given here. They observed in the crystal structures of several macrocyclic crown thioethers that the vast majority, if not all, of the torsional angles associated with the sulfur atoms adopt *gauche* placements (angles near 60°), whereas torsional angles associated with oxygen atoms typically adopt *anti* placements (angles near 180°) as much as possible.

These gauche placements result in the sulfur atoms being oriented outside of the macrocyclic cavity in an *exodentate*[32] conformation. This, then, requires that the ligand rearrange itself to turn the sulfur atoms into the macrocyclic cavity, with a concomitant energy requirement, in order to chelate to a single metal atom.

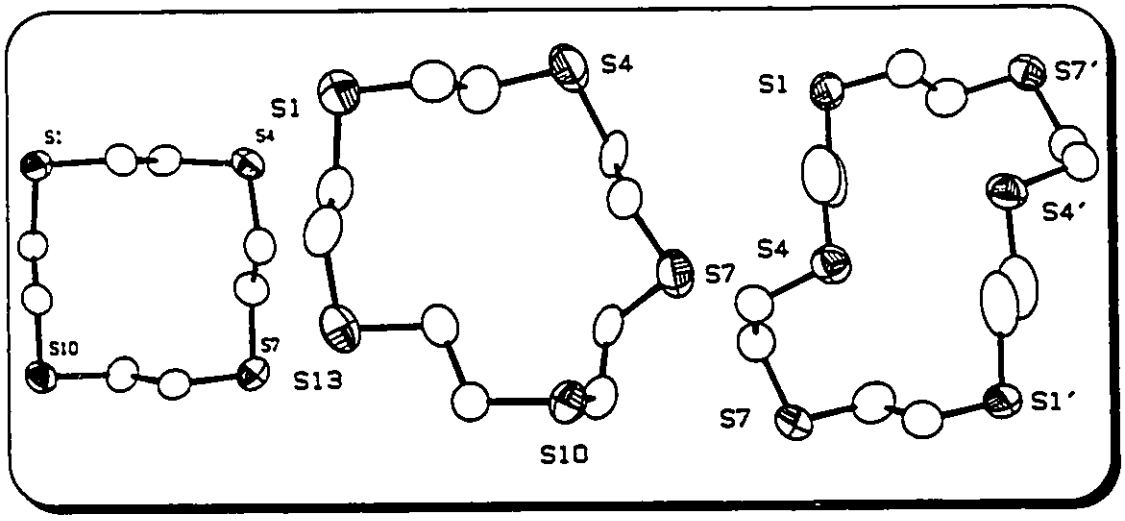

Figure 1.6 Crystal structures of 12-S-4, 15-S-5 and 18-S-6. Note that all C-S linkages in 12-S-4 and 18-S-6 and 8 of 10 in 15-S-5 are gauche.

(iii) Bonding of Thioethers. In 1981, Murray and Hartley reviewed the coordinative ability of thioether ligands[33]. They reported that relatively few thioether complexes had been isolated in comparison to phosphine and amine complexes due to their poor ability to act as electron donors. On going from phosphines (R_3P) to thioethers (R_2S) to organic chlorides (RCl) the number of lone pairs of electrons remaining after coordination increases from 0 to 1 to 2. Thus in phosphines there are no repulsive effects between metal based electrons and phosphine lone pair electrons. In thioethers repulsive effects increase, and in organic chlorides they increase once again.

Phosphine-metal bonding involves σ-donation by the phosphine and back donation from the metal atom to empty phosphine π-orbitals[34]. Thioether-metal bonding, however, can in principle involve σ- *and* π-donation to the metal atom[35]. The π-donation arises from the uncoordinated π-orbital on the sulfur atom which can fill an empty π– or *d*-orbital on the metal (Figure 1.7), giving rise to the aforementioned additional repulsion to metal based electrons. The sulfur atom

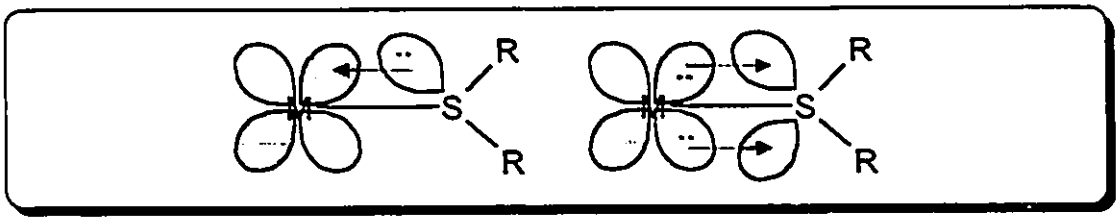

Figure 1.7 Metal-thioether bonding assuming sp^3 hybridization at sulfur. σ and π-donation to M, and π-back donation to S.

also has empty *d*-orbitals that may act as π-acceptors. Therefore, thioethers can potentially act simultaneously as σ- and π-donors, and as π-acceptors.

The questions then arise that if thioethers are poor ligands in comparison to phosphines, then why should they be studied and why do macrocyclic thioether complexes form at all?

In Cooper's review[36], it is stated that four considerations have fuelled recent interest in macrocyclic thioethers: 1) a possible analogy between the coordination chemistry of thioethers and phosphines; 2) the relevance of thioether coordination to blue copper proteins[37]; 3) synthetic improvements have made crown thioethers more readily available; 4) the increasing availability of X-ray diffraction facilities.

Crown thioether complexes form, as one might expect, because of the presence of more than one donor atom within the ligand; the chelate effect is a well known phenomenon in coordination chemistry[38]. Indeed, the stability constant for the Cu(II) complex of the reduced Curtis macrocycle is 10^4 times greater than the stability constant of the open chain analogue; about an order of magnitude more than expected based on the addition of a fourth chelate ring[39]. The term "macrocyclic effect" was coined to describe this additional stability. This effect has also observed in crown thioethers[40] (Figure 1.8).

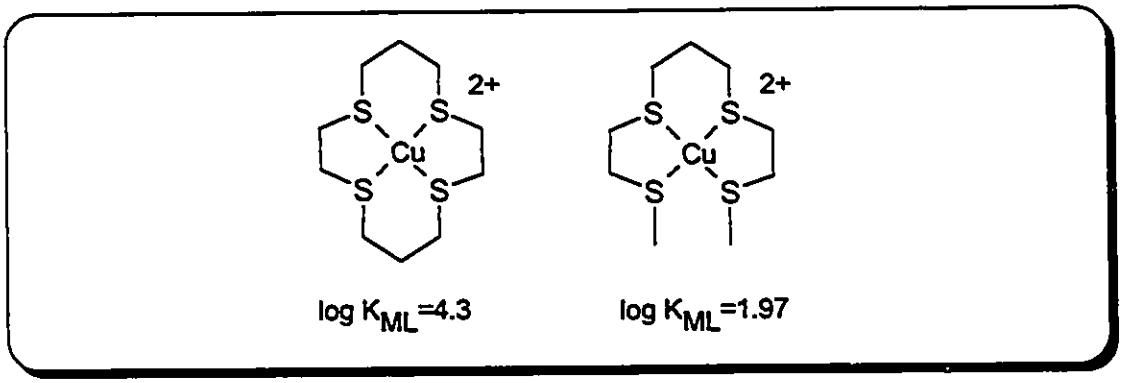

Figure 1.8 Copper(II) complex of 14-S-4, and its open chain analogue.

The general coordination chemistry of macrocyclic thioethers has been reviewed by Schröder[35] and by Cooper[36]. Since the focus of this dissertation is not on the coordination chemistry of thioethers but rather on simultaneous first- and second-sphere coordination and its application to molecular recognition, an extensive listing of these complexes will be avoided and the reader is referred to those reviews.

1.3 Second-Sphere Coordination

(i) Concept. The concept of second-sphere coordination was first eluded to by Werner as early as 1893. He found the concept necessary to explain solvents of crystallization, the dependence of optical rotation on the nature of the solvent and anion, and adduct formation between amines and saturated complexes[41]. It was only recently though that Stoddart and coworkers considered crown ethers and other macrocyclic receptors as models for solvent or anion interactions with the first-sphere ligands of metal complexes.

The intention of this section is not to provide the reader with a comprehensive review, which would be quite long. Rather, an introduction to the concept of second-sphere coordination is given along with a few illustrative examples to give the reader a basic understanding. For a comprehensive description of second-sphere coordination the reader is referred to an excellent review by Stoddart, Colquhoun and Williams[42].

At this point, a description of the terms "first-sphere coordination" and "second-sphere coordination" is in order. The concept of first-sphere

coordination is quite simple: ligands (ex. ammonia) directly bonded to a metal, exist in the *first sphere* of coordination of that metal. Next, if one considers the *non-covalent* interaction of a crown ether with the first-sphere ligands on the metal (ex. hydrogen-bonding, electrostatic attraction, charge transfer, Van Der Waal's interactions), the crown ether exists in the *second-sphere* of coordination of the metal atom. A schematic diagram of this concept is shown in Figure 1.9.

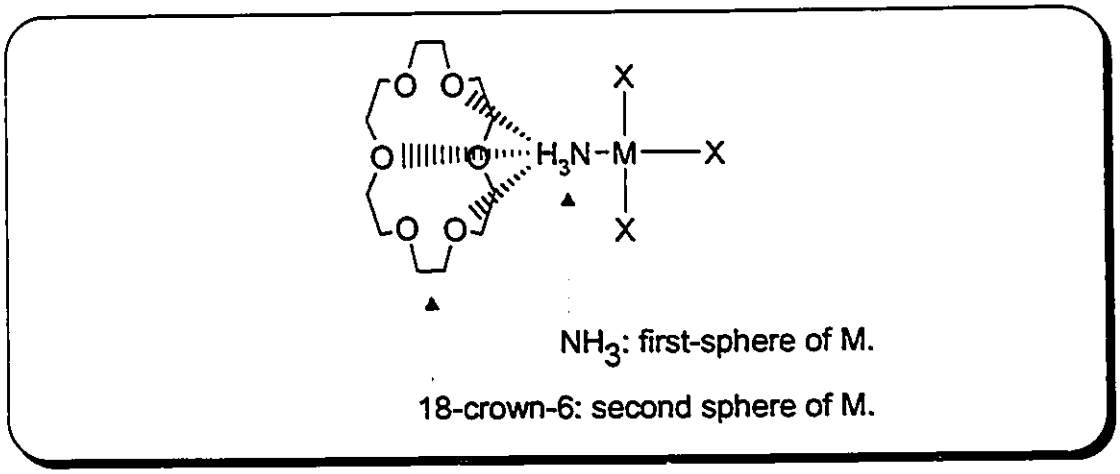

Figure 1.9 Schematic diagram of 18-crown-6 in the second sphere of M.

(ii) Second-Sphere Coordination. The first second-sphere complex structurally characterized, by Stoddart[43] *et al*, contains two molecules of *trans*-$[PtCl_2(PR_3)(NH_3)]$ hydrogen-bonded, *via* the ammonia ligand, to staggered oxygen atoms of a bifacial molecule of 18-crown-6; the crown ether exists in the second coordination sphere of two individual platinum atoms. The demonstrated ability of 18-crown-6 to act as a bireceptor led to formation of $\{$*trans*-$[PtCl_2(NH_3)_2]$ (18-crown-6)$\}_n$[43] which is polymeric by virtue of the *trans* orientation of the two ammonia ligands.

The antitumor drug Cisplatin, *cis*-$[PtCl_2(NH_3)_2]$, interacts with 18-crown-6 in much the same way that *trans*-$[PtCl_2(PR_3)(NH_3)]$ does, with one NH_3 ligand of each *cis*-$[PtCl_2(NH_3)_2]$ hydrogen-bonding with each face of the crown ether[44] (Figure 1.10). The second NH_3 ligand of each *cis*-$[PtCl_2(NH_3)_2]$ also hydrogen-bonds with the crown-ether, preventing polymerization and forming the complex $[\{cis\text{-}[PtCl_2(NH_3)_2] \cdot dma\}_2 \cdot (18\text{-crown-6})]$, with two molecules of dimethylacetamide included in the crystal lattice.

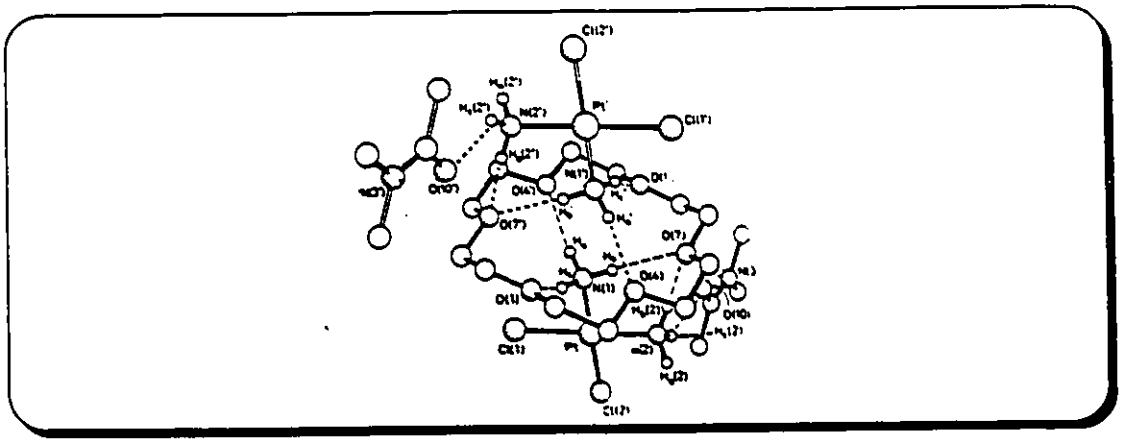

Figure 1.10 Crystal structure of $[\{cis\text{-}[PtCl_2(NH_3)_2] \cdot dma\}_2 \cdot (18\text{-crown-6})]$.

The receptor molecule in second-sphere coordination is not restricted to 18-crown-6; one such example is the interaction of dibenzo-30-crown-10 with $[Rh(COD)(NH_3)_2]^+$ (Figure 1.11)[45]. The X-ray crystal structure reveals that the large macrocycle adopts a V-shape conformation with a $[Rh(COD)(NH_3)_2]^+$ ion hydrogen-bonded *via* the Rh-amine ligands. The two amine ligands of the metal complex 'straddle' the polyether chain such that one amine ligand is hydrogen-bonded within the cavity and the other hydrogen-bonds with the oxygen atoms in the straddled chain.

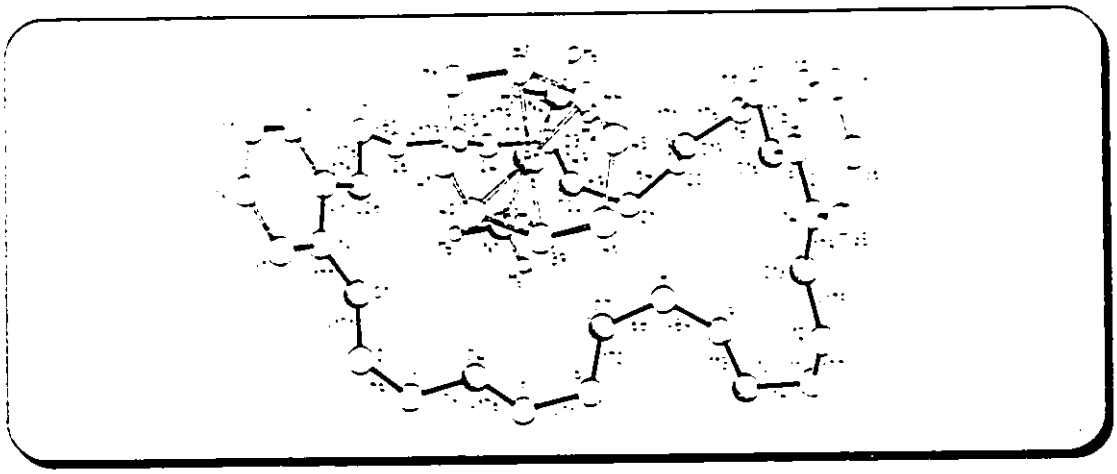

Figure 1.11 Crystal structure of [{Rh(COD)$(NH_3)_2$}$^+$ (dibenzo-30-crown-10)].

In complexes of dibenzo-3n-crown-n ethers with [Pt(2,2'-bipyridine)$(NH_3)_2$], it was observed that in addition to second-sphere hydrogen-bonding with the polyether chains, the 2,2' bipyridyl aromatic rings also π-stack with the phenyl rings of the receptor in the second-sphere, imparting additional stability on second-sphere complexes[46]. In order to qualitatively define the significance of the π-stacking interactions between the electron rich arene units of the receptor and the electron deficient BPY ligand, the benzo-units of dibenzo-30-crown-10 were replaced with naphtho-units and the second-sphere complex of [Pt(2,2'-bipyridine)$(NH_3)_2$] was isolated and structurally characterized (Figure 1.12)[47]. The structural data revealed that the platinum complex is significantly tilted in comparison to its position in the dibenzo receptor, in order to maximize charge transfer interactions between the arene units.

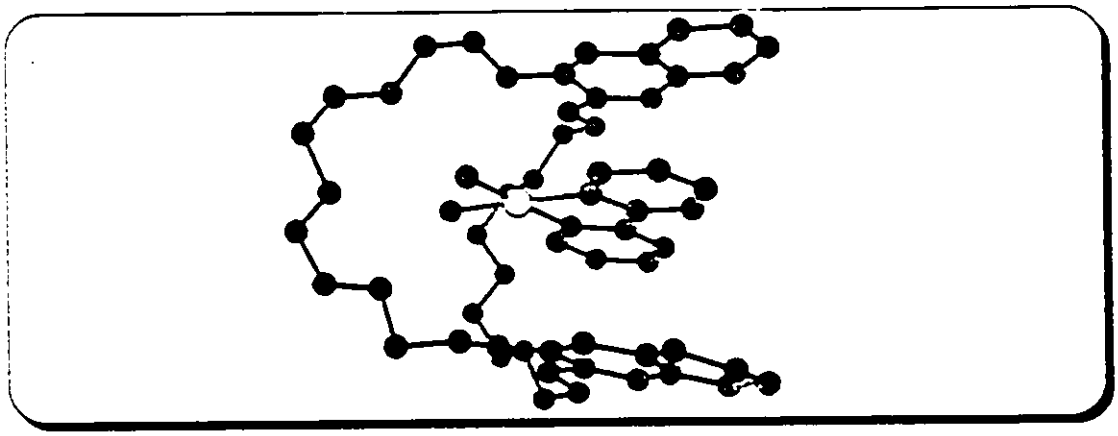

Figure 1.12 Crystal structure of [{Pt(2,2'-bipyridine)$(NH_3)_2$}$^{2+}$ - (dinaphtho-30-crown-10)].

With macropolycyclic receptors a more preorganized cavity for binding of $[Rh(COD)(NH_3)_2]$ is observed[48]. The macro-ring encircles the metal complex and stabilizes the structure by the formation of eight hydrogen-bonding interactions with distances in the range of 3.00-3.26 Å (Figure 1.13)[49].

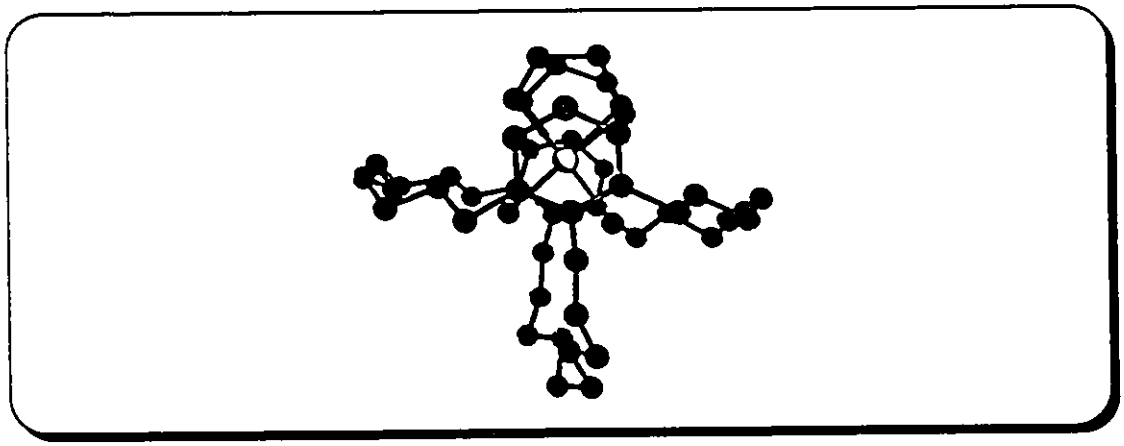

Figure 1.13 Crystal structure of macropolycyclic complex of $[Rh(COD)(NH_3)_2]$.

(iii) Simultaneous First- and Second-Sphere Coordination. It is possible for a ligand to interact with a metal complex such that it occupies sites in both the first and second coordination spheres of a metal. The first examples of

this were observed by Alcock *et al* in Rh (I) complexes of bis-phosphine ligands joined by polyether chains[50]. X-ray crystallcgraphyconfirmed that water and ethanol molecules coordinate to Rh (I) in the first-sphere, and hydrogen-bond to the polyether chain in the second-sphere of the metal (Figure 1.14).

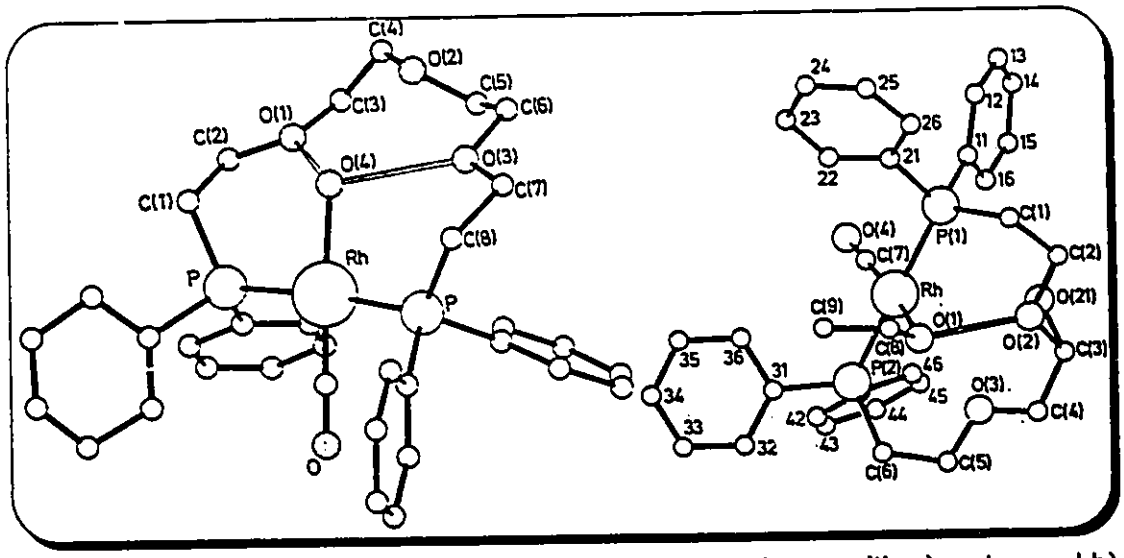

Figure 1.14 Crystal structures of Alcock's Rh (I) complexes with a) water and b) ethanol interacting in the first- and second-sphere of the metal atom.

The bis-phosphine ligand acts as a first-sphere ligand, coordinating directly to Rh (I). At the same time, it also acts as a second-sphere ligand, hydrogen-bonding with the first-sphere water/ethanol ligands. It is interesting to note that the opposite is also true. The water/ethanol ligand acts as a first-sphere ligand, coordinating directly to Rh (I). At the same time it also acts as a second-sphere ligand, hydrogen-bonding with the first-sphere bis-phosphine ligand. It follows then, that any non-covalent interaction between two distinct ligands in a metal complex can be termed simultaneous first- and second-sphere coordination. Since the isolation and characterization of these first examples, many more have

appeared in the literature. These are covered in the Introduction sections in Chapters 4 and 5 and will not be discussed here.

1.4 Molecular Recognition

Molecular recognition is the study of supramolecular complexes and assemblies, formed between two or more designed chemical species, and held together by intermolecular forces[21a]. It is controlled by the geometric and electronic complimentarity between the receptor (host) and the substrate (guest) (Figure 1.15). This involves a balance of the energetic and stereochemical features of non-covalent intermolecular forces within the resulting host-guest complex[5, 51].

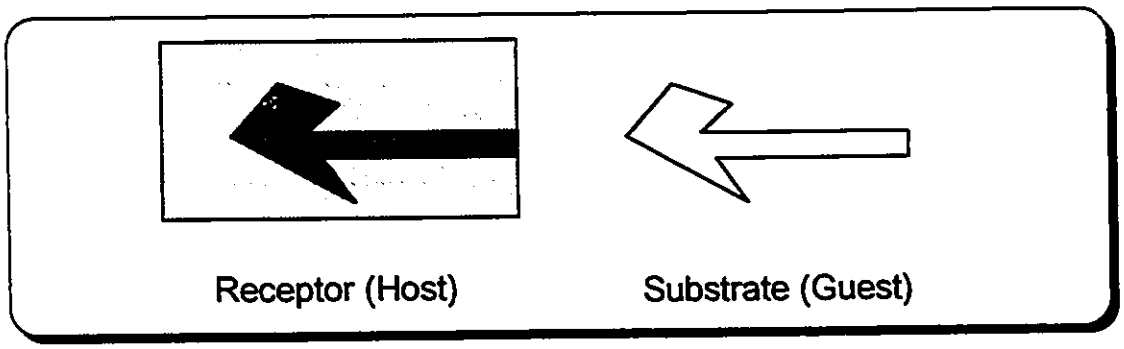

Figure 1.15 Schematic diagram of geometric complimentarity between a receptor and a substrate.

There has been considerable interest in the design of molecules capable exhibiting molecular recognition and binding of small molecules. Two general approaches have been taken in the design of these receptors. One has involved the use of solvophobic, π-π stacking and dispersion forces in water-soluble cyclophane frameworks[21] (Figure 1.16). This method has lead to important

quantitative results regarding hydrophobic and solvation effects, but these forces are essentially non-directional. The result is a receptor that uses only weakly oriented binding interactions, in contrast to systems in nature which show good substrate selectivity, chiral recognition and catalytic activity.

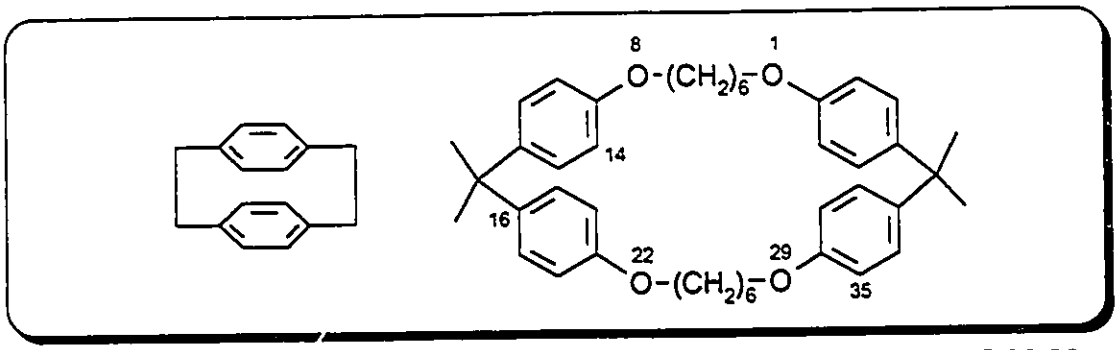

Figure 1.16 Schematic diagram of a) [2.2]paracyclophane and b) 15,15,36,36-tetramethyl-1,8,22,29-tetraoxa[8.1.8.1]paracyclophane.

With this in mind, the other approach to synthetic receptors is one in which the directional interactions of π-π stacking and multiple hydrogen-bonding groups are combined in a bracket or macrocyclic cavity with well defined geometry[52]. This combination makes these hosts a much more selective class of receptor.

The use of weak forces between neutral molecules, such as hydrogen-bonding and π-π stacking, has attracted recent attention and several research groups have demonstrated quite elegantly that selective binding of guests can occur by a combination of π-π interactions and directed hydrogen-bonds. Some selected examples of molecular recognition are given below.

The research group of Hamilton synthesized a macrocyclic receptor containing six endodentate hydrogen-bonding sites[53]. It was shown by NMR

titration to bind barbitol more strongly than two other barbiturates due to the maximal complimentarity between the substrate and receptor (Figure 1.17a). Whitlock and coworkers have synthesized cyclophane 'cage' receptors that were shown to bind *p*-nitrophenol utilizing π-hydrogen-bonds between substrate hydrogen atoms and an arene ring of the receptor[54] (Figure 1.17b).

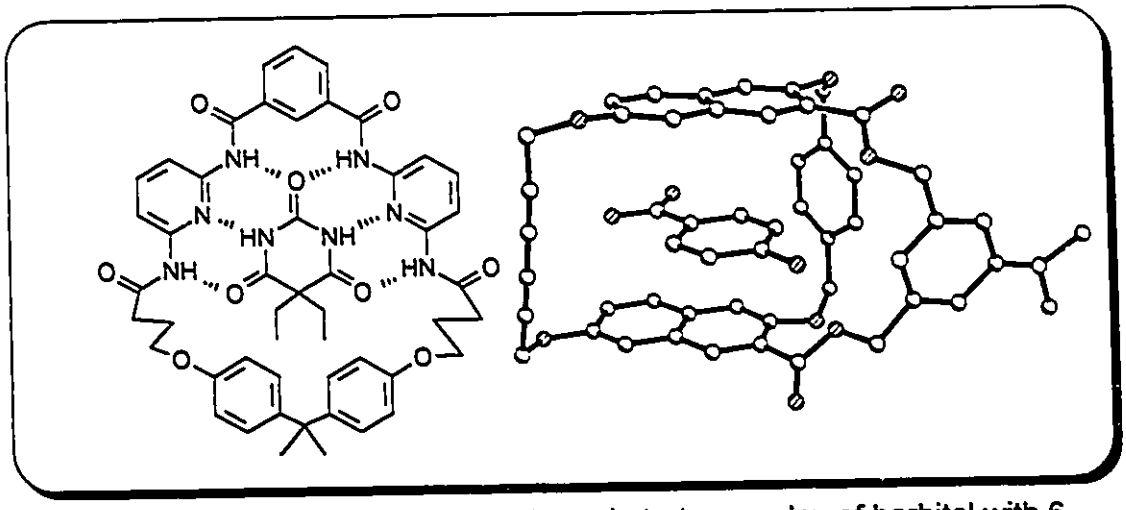

Figure 1.17 a) Hamilton *et al*'s receptor-substrate complex of barbitol with 6 hydrogen-bonds. b) Crystal structure of Whitlock's receptor-substrate complex with π-hydrogen-bonds.

One of ultimate goals of molecular recognition (to mimic biological processes) is almost realized in the elegant self replicating system by Rebek *et al*[55]. The molecule acts as a template, utilizing hydrogen-bonds and π–π stacking interactions to recognize precursors and catalyze the formation of itself; a primitive sign of a living system (Figure 1.18).

Synthetic receptors allow for a detailed study of the binding interactions that must occur in molecular recognition processes in biological systems. A large volume of research has been performed in this area (Hamilton[56], Nolte[57]

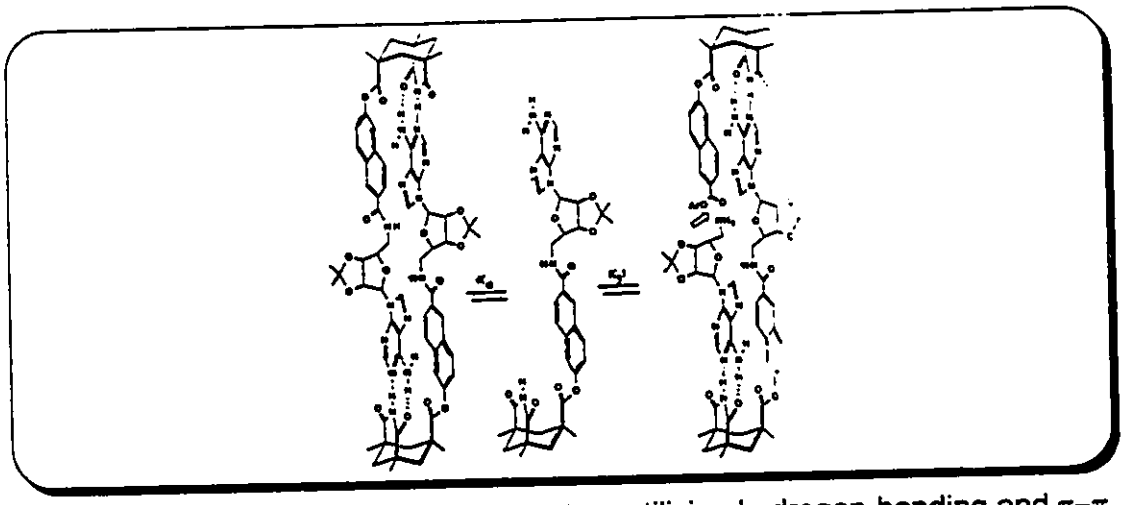

Figure 1.18 Rebek's self replicating system utilizing hydrogen-bonding and π–π stacking interactions for recognition.

Rebek[55], Whitlock[58] and Zimmerman[59]) and rather than describe all of it the reader is referred to the literature for a complete listing.

1.5 Scope of the Thesis

(i) Summary. This dissertation describes the incorporation of a stable organopalladium fragment into several macrocyclic structures, in which three of four coordination sites are permanently occupied by an S_2C "bracket". The remaining metal site is filled by a more labile donor, and is used for bonding of ancillary ligands (substrates).

Chapter 2 describes the synthesis and coordination chemistry of discrete macrocyclic complexes (TT[11]MC and *pr*-TOMB-1) in which one donor (S,O) is displaced by stronger ancillary ligands. Chapters 3, 4, 5 and 6 describe the synthesis and utility of several *metalated macrocyclic receptors* containing a palladium coordination site for first-sphere σ-donation by a substrate, and

polyether arrays for second-sphere hydrogen-bonding interactions with the substrates. The receptors were designed with the goal of achieving molecular recognition by cooperatively combining the coordination site with the polyether arrays to make selective receptors. Factors considered were preorganization of the receptor, the number of hydrogen-bonding sites available and methods of characterization.

(ii) Trivial Naming. As the acronym TOMB-X will be used throughout this dissertation to refer to cyclophanes containing both thioether and ether donors, (Figure 1.19) a brief description of its meaning is given here. The T refers to *thia*, O refers to *oxa*, M refers to *meta* and B refers to *benzenophane*. The proper naming of the series of macrocycles outlined in this work would place *'oxa'* before *'thia'* in alphabetical order. Also, molecules of this type are more correctly referred to as cyclophanes[21a] rather than *benzenophanes*, but as OTMC-X is not easily pronounced, the acronym TOMB-X was chosen. The number X follows the name in order to distinguish particular cyclophanes from one another and refers to the number of oxygen atoms contained within the macrocycle. As a rule, all the donor atoms in the aliphatic portion of the cyclophanes are joined by ethylene groups. As with every rule there are exceptions. The acronym *pr*-TOMB-1, for example, refers to the cyclophane in which the donors are joined by propylene groups, rather than ethylene groups.

It is also interesting that this trivial naming system has some support in the literature: *viz.* Lehn's "cryptands"[5]; Cram's "carcerands"[4].

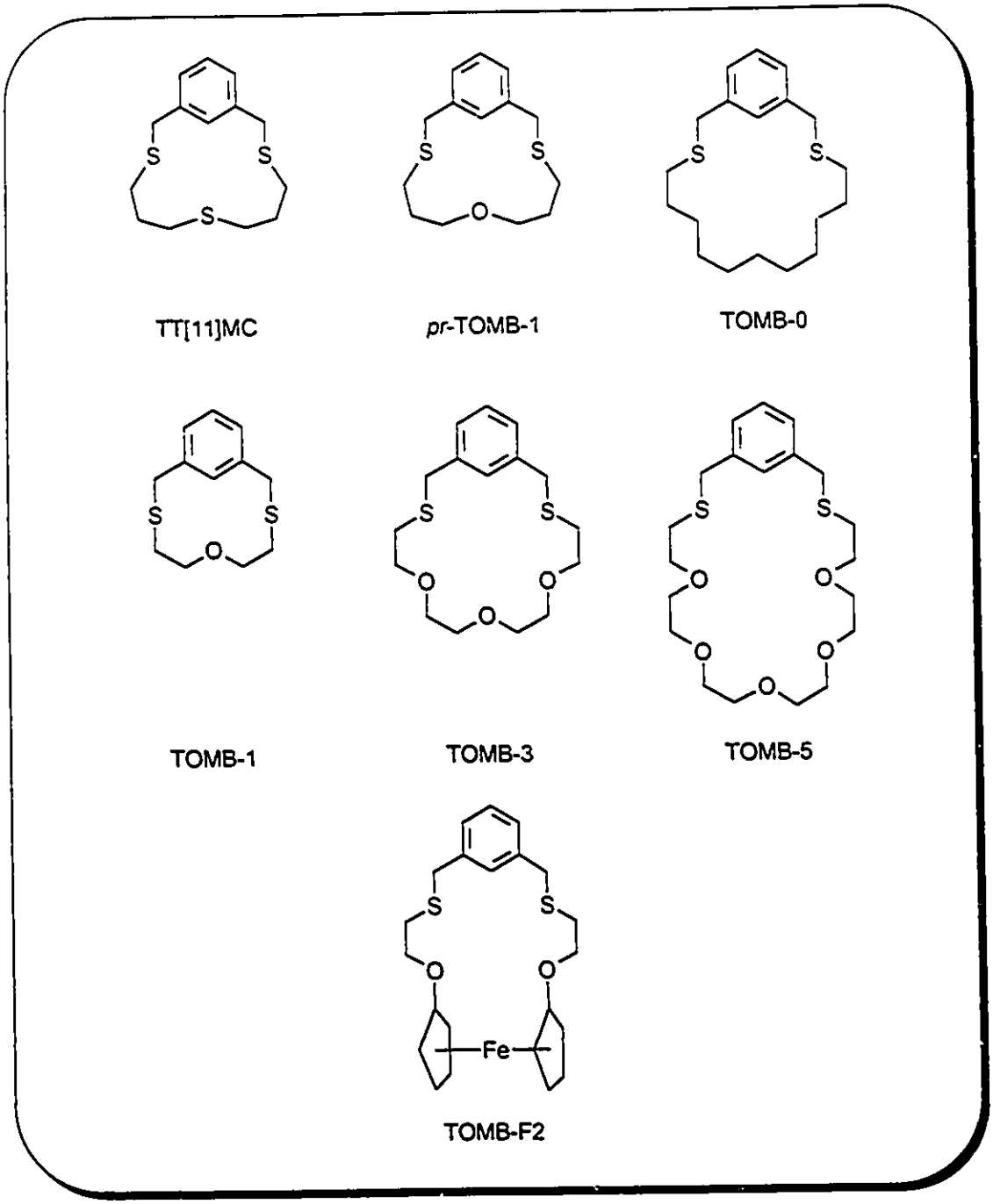

Figure 1.19 Macrocyclic TOMB ligands studied in this dissertation.

Chapter 2

Metalated Thioether Macrocycles

Chapter 2

2.1 Introduction

(i) Thought Process. In previous research done by Loeb *et al.*[60] the thiacyclophane molecule TT[9]MC was reacted with $Pd(PhCN)_2Cl_2$ to form the simple square planar complex $Pd(TT[9]MC)Cl_2$, in which two of the three S donor atoms displaced the benzonitrile ligands on the starting material.

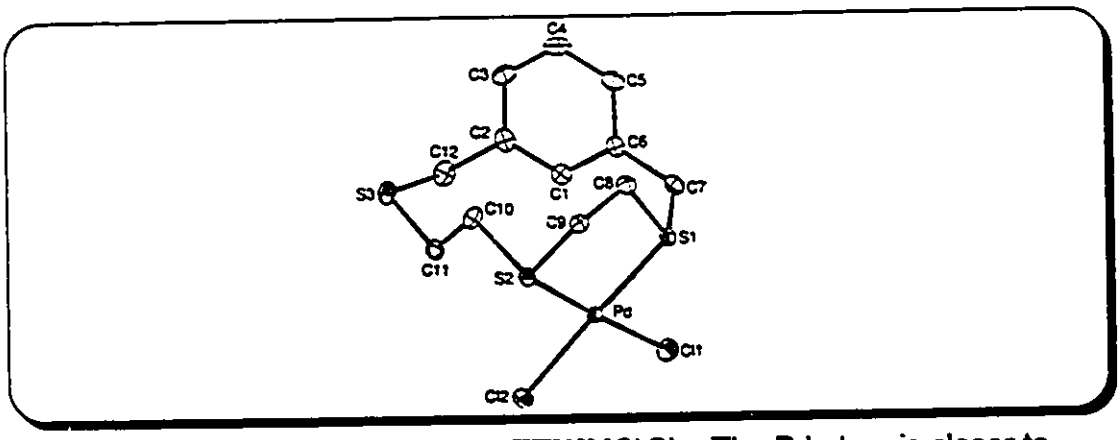

Figure 2.1 Crystal Structure of $Pd(TT[9]MC)Cl_2$. The Pd atom is closer to C1-H than to S3.

In the crystal structure of the complex (Figure 2.1)[60], it was observed that the Pd(II) centre was closer to the hydrogen atom on C1, than to the third S atom in the macrocycle. Furthermore, examination of molecular models indicated that removal of one of the chloride ligands, followed by intramolecular coordination of the third S donor to the Pd atom, would place the hydrogen atom on the 2-position of the aromatic ring in direct contact with the Pd(II) centre. However, attempts to *ortho*-metalate the aromatic ring in TT[9]MC by removal of one of the chloride ligands with Ag^+ failed. This result was attributed to the restricted size of the macrocyclic cavity. The strain the macrocycle would be required to endure in

supporting four fused 5-membered chelate rings probably prevents the formation of a square planar metalated complex; this is shown in Figure 2.2a.

In order to *ortho*-metalate the thiacyclophane, it is necessary to accommodate the size of the metal atom inside the macrocycle. This problem was solved by increasing the length of the linkages between the S atoms in

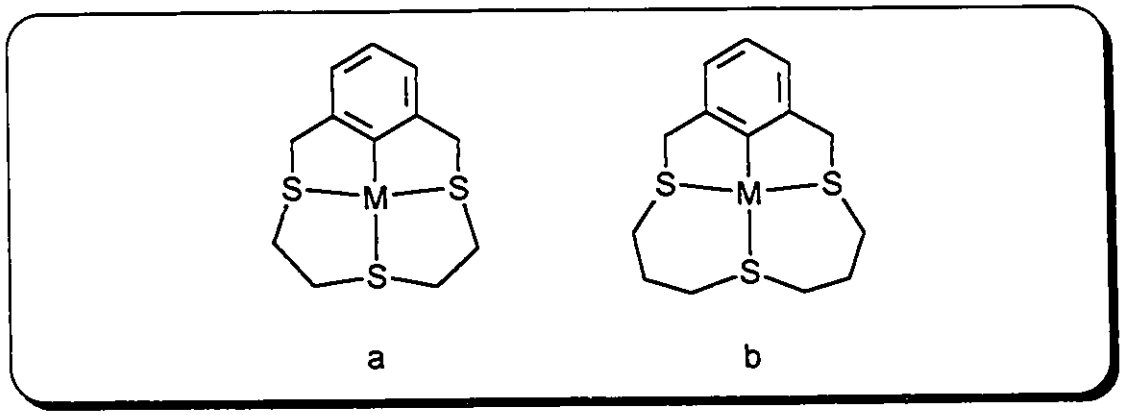

Figure 2.2 a) Four fused 5-membered chelate rings in metalated TT[9]MC prevent its formation. b) Propylene linkages form two 6-membered chelate rings, lowering strain on TT[11]MC.

TT[9]MC from ethylene to propylene chains to make TT[11]MC[61]. Two of the four chelate rings in an *ortho*-metalated complex of TT[11]MC would be 6-membered, reducing the strain placed on the macrocycle in accommodating the metal, as shown in Figure 2.2b.

This chapter, therefore, deals with the syntheses and complexation studies of the ligands 2,6,10-trithia[11]*m*-cyclophane (TT[11]MC) and 6-oxa-2,10-dithia-[11]*m*-cyclophane (*pr*-TOMB-1). The ligands contain a tridentate S-CH_2-C_6H_4-CH_2-S bracket (S_2C) (Figure 2.3), that is ideally suited to accommodating three of the four sites on a square planar metal atom. The fourth site on the metal atom is occupied by another donor joined to the two thioethers

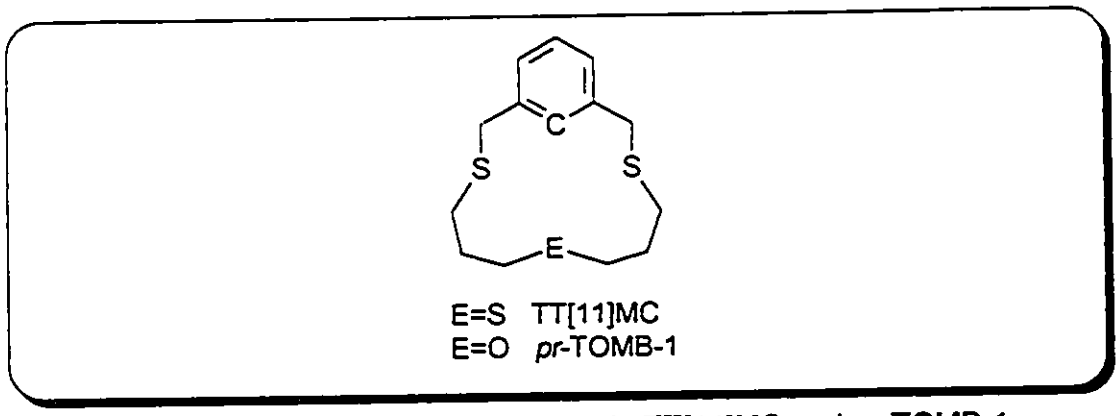

Figure 2.3 Placement of the donor atoms in TT[11]MC and *pr*-TOMB-1.

by propylene linkages. The macrocycles are easily metalated using palladium and platinum starting materials and the reaction chemistry of the metal containing complexes has been explored.

(ii) Literature Background. There have been several examples of *ortho*-metalation of ligands containing similar X-CH_2-C_6H_4-CH_2-X brackets with X=OR, NR_2, PR_2 and SR which are outlined below. Research by Friedrich Bickelhaupt *et al* incorporates the *m*-xylyl bracket described above, with all the donor atoms being oxygen. The reaction of 2-bromo-1,3-*m*-xylyl-15-crown-4 and 2-bromo-1,3-*m*-xylyl-18-crown-5 with magnesium starting materials afforded the Grignard reagents and diarylmagnesium complexes[62].

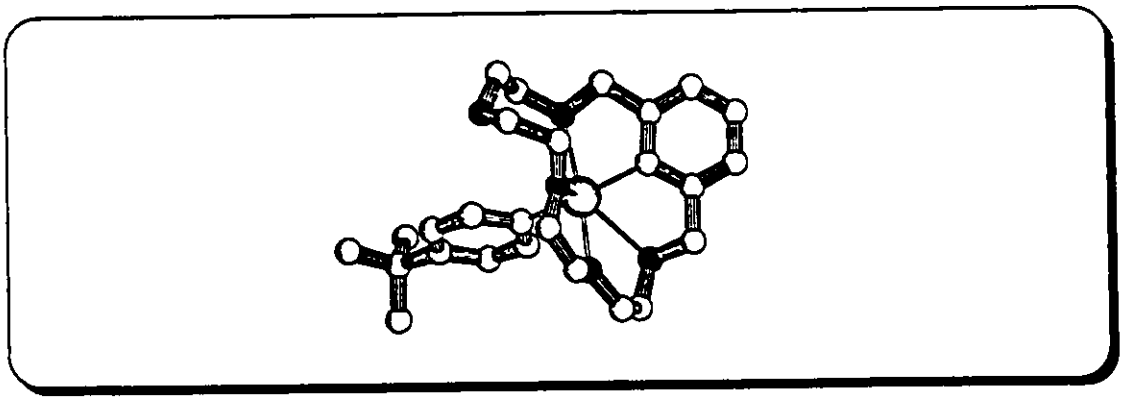

Figure 2.4. Crystal structure of 2-(phenylmagnesio)-1,3-xylylene-18-crown-5.

The authors illustrated that in addition to the proximity of the crown ether, the *m*-xylyl orientation of the donor atoms contributes significantly to the ease of halogen-metal exchange in these macrocycles. These ligands have also been used to stabilize mercury-carbon bonds which are formed by the reaction of the Grignard reagents described above with mercury starting materials[63].

A large amount of research has been done by Van Koten and co-workers on non-macrocyclic systems using the X-CH_2-C_6H_4-CH_2-X bracket with X=NR_2. Several complexes containing platinum(II) and nickel(II) exhibit interesting substitution chemistry at the fourth co-ordination site on the metal centre[64]. They have also isolated a metalated macrocyclic Pt(II) complex[65] (Figure 2.5).

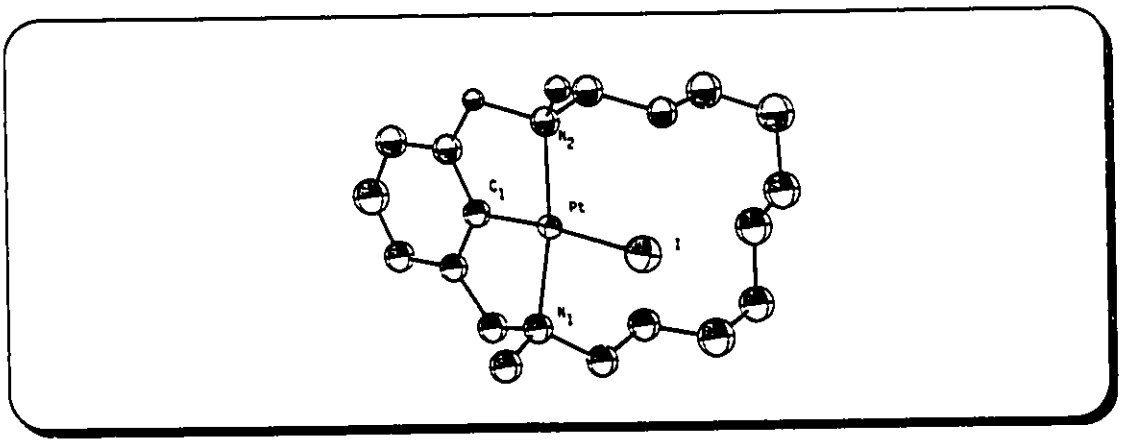

Figure 2.5. a) Crystal Structure of *trans*-[2,6-(dimethyl-2,13-diazatetradecanediyl)-phenyl-*N*-*N*']platinum(II) iodide.

In addition to the results on platinum and nickel complexes , Van Koten and coworkers have also synthesized a number of complexes with the same ligands and other metals such as Fe(III)[66], Sn(IV)[67], and Tl(III), Hg(II), and Pd(II)[68]. Van Koten has reviewed this and additional research from his and other laboratories[69].

Metalated complexes containing phosphines as the donor atoms have been synthesized by Shaw and co-workers[70] and others[71]. The ligand 1,3-bis[(di-*t*-butyl- phosphino)methyl]phenyl (PCP) reacts with several square planar starting materials to form the complexes [MX(PCP)] where M=Ni, Pd, Pt, Rh, Ir and X=Cl, CN, CCPh, CO, H^-. The complexes are all air stable compounds exhibiting the expected NMR spectra. Another similar complex was formed by the reaction of the bulky phosphalkene ligand 1,3-bis(2,4,6-tri-*t*-butylphenylphospha-2-alkene)phenyl with $Pd(PhCN)_2Cl_2$[72]. This ligand permits electrochemical reduction of the metal containing complex, with the electron residing on a ligand π-antibonding orbital as determined by EPR spectroscopy.

Thioether analogues having the X-CH_2-C_6H_4-CH_2-X bracket have also been synthesized by Pfeffer and co-workers. 1,3-bis(methylthiomethyl)benzene reacts with the complex $[\{Pd(C_6H_4CH_2NMe_2\text{-}2)Cl\}_2]$ in the presence of acetic acid to give the complex $[PdCl(C_6H_3(CH_2SMe)_2)\text{-}2,6)]$ in high yield[73]. The complex was found to react with an excess of *t*-butyl-NC to give a product in which one isocyanide ligand has inserted into the Pd-C bond and another has displaced one of the SMe donor groups[74]. Shaw and co-workers have also synthesized the thioether ligand 1,3-bis(*t*-butylthiomethyl)benzene and metalated it with $Na_2[PdCl_4]$ to give $[PdCl(C_6H_3(CH_2S\text{-}t\text{-}Bu)_2)\text{-}2,6)]$[75], as is shown in Figure 2.6

Until recently the appearance of *ortho*-metalated Pt(IV) complexes in the literature has been rare[76]. The complexes known to date include $[PtX_3(C_6H_3\{CH_2NMe_2\}_2\text{-}2,6)]$ (X=Cl, Br, I) and $[PtRX_2(C_6H_3\{CH_2NMe_2\}_2\text{-}2,6)]$ (X=Br,

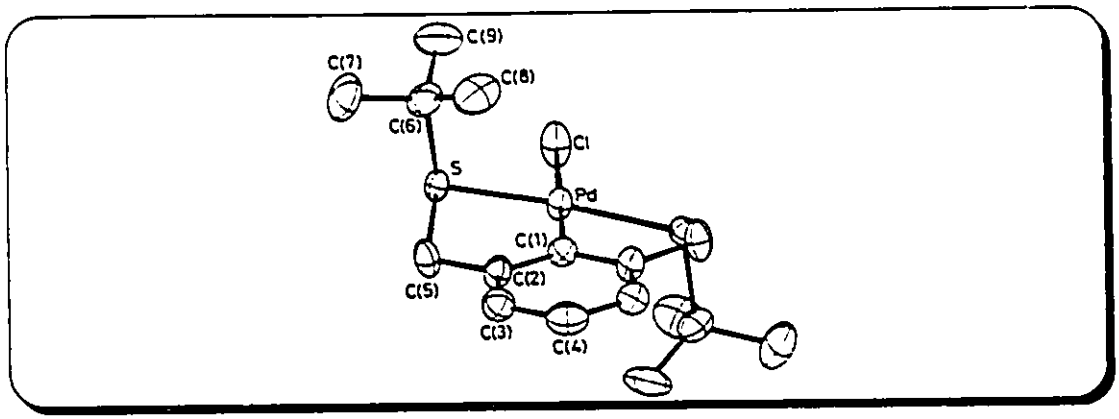

Figure 2.6. Crystal structure of [PdCl(SCS)].

I, R=*p*-tolyl), $[PtX_2(C_6H_4\{CH_2NMe_2\})_2]$ and $[PtX_2(C_{10}H_6\{CH_2NMe_2\})_2]$[77] (X=Br, I) and $[PtCl_3$((2-methylthio)azobenzene)$]$[78].

2.2 Experimental

General Comments. $Pt(COD)Cl_2$ was prepared by the literature method[79]. α,α'-Dibromo-*m*-xylene, *meta*-xylene-α,α'-dithiol, thiourea, cesium carbonate, *N,N'*-dimethylformamide, sodium sulfide nonahydrate, 1,3-propanediol, 3-bromopropanol, silver tetrafluoroborate, diphenylmethyl phosphine, $[Pd(CH_3CN)_4][BF_4]_2$, $[Pd(PhCN)_2Cl_2]$ and all deuterated solvents were purchased from Aldrich and used as received. I_2 and $CuCl_2$ were purchased from BDH and used as received. All reactions were performed under an atmosphere of N_2(g) using standard Schlenk techniques and all solvents were distilled and degassed prior to use. ^1H and $^{13}C\{^1H\}$ NMR spectra were recorded on a Bruker AC300 NMR spectrometer locked on the deuterated solvent at 300.1 and 75.5 MHz respectively. $^{31}P\{^1H\}$ NMR spectra were recorded on a Bruker AC200 NMR

spectrometer at 81.0 MHz with H_3PO_4 (85%) as the external reference. Infrared spectra were recorded on a Nicolet 5DX FTIR spectrometer and elemental analyses were performed by Canadian Microanalytical Services, New Westminister, British Columbia, Canada

(i) Preparation of 4-thiaheptane-1,7-diol, (1)[80]. Sodium sulfide nonahydrate (23.638 g, 0.098 mol) was dissolved in anhydrous ethanol (250 mL) and to this solution 3-bromopropanol (27.205 g, 0.196 mol) was added by syringe and the mixture stirred at reflux for 21.5 hours. The solution was cooled, filtered and the solvent was removed *in vacuo*. The remaining liquid was dissolved in CH_2Cl_2, filtered and the solvent was removed *in vacuo*. The resulting clear oil was vacuum distilled (bp. 134-138 °C, 1 mmHg). Yield 9.009g (61%). ^{1}H NMR ($CDCl_3$): δ (ppm) 3.64 (s, 2H, OH), 3.61 (t, 4H, OCH_2), 2.54 (t, 4H, SCH_2), 1.74 (m, 4H, CH_2). $^{13}C\{^1H\}$ NMR ($CDCl_3$): δ (ppm) 60.9 (CH_2OH), 31.9 (SCH_2), 28.4 (CH_2).

(ii) Preparation of 4-thiaheptane-1,7-dithiol, (2)[81]. 4-thiaheptane-1,7-diol (28.507 g, 190 mmol) and thiourea (32.215 g, 0.423mol) were dissolved in concentrated hydrochloric acid (95 mL, 1.143 mol) and stirred at reflux for 36 h during which time the solution turned from red to orange. Upon cooling, sodium hydroxide (45.911 g, 1.143 mol) dissolved in water (200 mL), was added through a slow addition funnel and the solution was refluxed for a further 2 h. The reaction mixture was reacidified to pH 2 and then extracted with CH_2Cl_2 (3 x 200 mL) (*Caution, Extremely irritating odour!*). The extracts were combined, dried over $MgSO_4$, filtered and the solvent was removed *in vacuo* leaving a brown

liquid. Vacuum distillation (bp. 108° C, 5 x 10^{-2} mmHg) gave a clear oil. Yield: 17.149 g, (49%). ^{1}H NMR ($CDCl_3$): δ (ppm) 2.59-2.50 (m, 8H, SCH_2), 1.79 (m, 4H, CH_2), 1.32 (t, 2H, SH). $^{13}C\{^1H\}$ NMR ($CDCl_3$): δ (ppm) 33.1 (CH_2SCH_2), 30.1 ($HSCH_2$), 23.2 (CH_2).

(iii) Preparation of 2,6,10-Trithia[11]-*m*-cyclophane, TT[11]MC, (3), Method A. To a stirred suspension of cesium carbonate (9.191 g, 28.2 mmol) in DMF (400 mL) was added a solution of α,α'-dibromo-*m*-xylene (3.717 g, 14.1 mmol) and 4-thiaheptane-1,7-dithiol (2.573 g, 14.1 mmol) in DMF (200 mL). The addition was performed over 27 h with the solution temperature at 50-55 °C. After addition, the mixture was stirred at room temperature for 24 hours. The DMF was removed *in vacuo* and the resulting solid was dissolved in CH_2Cl_2 (150 mL) and filtered. The CH_2Cl_2 solution was washed with 0.1 M NaOH (2 x 50 mL) and the organic layer was dried over $MgSO_4$. After filtration and removal of the solvent the crude product was recrystallized from acetone/absolute ethanol. Yield: 3.282 g, (82%); m.p. 57-58 °C. ^{1}H NMR ($CDCl_3$): δ (ppm) 7.43 (s, 1H, aromatic), 7.17-7.25 (m, 3H, aromatic), 3.70 (s, 4H, benzylic), 2.48 (t, 4H, ^{2}J=7.1 Hz, S-CH_2), 2.38 (t, 4H, ^{2}J=7.1 Hz, S-CH_2), 1.58 (m, 4H, CH_2). $^{13}C\{^1H\}$ NMR ($CDCl_3$): δ (ppm) 139.5, 129.4, 128.8, 127.7 (aromatic), 36.9 (benzylic), 31.2 (CH_2), 30.2 (CH_2S), 29.9 (CH_2S). Anal. Calcd. for $C_{14}H_{20}S_3$: C, 59.09; H, 7.10; S, 33.81. Found: C, 58.88; H, 7.00; S, 33.54.

(iv) Preparation of 2,6,10-Trithia[11]-*m*-cyclophane, TT[11]MC, (3), Method B. To a stirred suspension of cesium carbonate (7.691 g, 23.6 mmol) in

DMF (300 mL) was added a solution of *m*-xylene-α,α'-dithiol (2.003 g, 11.8 mmol) and 4-thiaheptane-1,7-ditosylate (5.402 g, 11.8 mmol) in DMF (200 mL). The slow addition was performed over 17 hours with the solution temperature at 60 °C. After addition, the mixture was stirred at room temperature for 12 hours and the product was isolated as in method A. Yield 2.693 g, (80%).

(v) Preparation of [Pt(TT[11]MC)][BF_4], (4). $PtCl_2$(COD) (0.399 g, 1.07 mmol), TT[11]MC (0.303 g, 1.07 mmol), and $AgBF_4$ (0.216 g, 1.11 mmol) were combined in acetonitrile (100 mL) and the solution was refluxed for 48 h. The resulting mixture was filtered to remove AgCl and the solvent was removed *in vacuo* to give an off white solid which was recrystallized from acetonitrile/diethyl ether. Yield: 0.521 g (87%). ^{1}H NMR (CD_3CN): δ (ppm) 7.12 (m, 3H, aromatic), 3.91 (d, 2H, ^2J=15.9 Hz, $^3J_{Pt\text{-}H}$=70.4 Hz, benzylic), 4.41 (d, 2H, ^2J=15.9 Hz, benzylic), 3.67 (m, 2H, $^3J_{Pt\text{-}H}$=81.1 Hz, SCH_2), 3.33-3.12 (m, 4H, SCH_2), 2.89 (m, 2H, SCH_2), 2.60 (m, 2H, CH_2), 2.00 (m, 2H, CH_2). $^{13}C\{^1H\}$ NMR (CD_3CN): δ (ppm) 157.9 ($^1J_{Pt\text{-}C}$=854.6 Hz, Pt-C1), 147.4 ($^2J_{Pt\text{-}C}$=111.1 Hz, aromatic) 126.6, 122.1 ($^3J_{Pt\text{-}C}$~30 Hz, aromatic), 52.5 ($^3J_{Pt\text{-}C}$~30 Hz, benzylic), 38.6 ($^3J_{Pt\text{-}C}$=23.5 Hz, SCH_2), 35.8 ($^3J_{Pt\text{-}C}$, SCH_2), 28.2 ($^3J_{Pt\text{-}C}$=29.9 Hz, CH_2). Anal. Calcd. for $C_{14}H_{19}BF_4S_3Pt$: C, 29.74; H, 3.39; S, 17.02. Found: C, 29.55; H, 3.26; S, 17.29.

(vi) Preparation of [Pt(PPh_2Me)(TT[11]MC)][BF_4], (5). [Pt(TT[11]MC)][BF_4] (0.098 g, 0.177 mmol) was dissolved in acetonitrile (15 mL) and PPh_2Me (0.035 g, 0.177 mmol) was added with stirring at room temperature. After 24 h, the solvent was removed *in vacuo* leaving an off-white solid which was recrystallized from acetonitrile/diethyl ether. Yield: 0.110 g, (81%). ^{1}H NMR

(CD_3CN): δ (ppm) 7.67 (m, 4H, aromatic PPh_2Me), 7.53 (m, 6H, aromatic PPh_2Me), 7.17 (m, 3H, aromatic TT[11]MC), 4.92 (d, 2H, ^2J=17.0 Hz, benzylic), 4.43 (d, 2H, ^2J=17.0 Hz, $^3J_{Pt-H}$=37.0 Hz, benzylic), 3.14 (m, 2H, SCH_2), 2.54 (m, 6H, aliphatic TT[11]MC), 2.32 (m, 4H, aliphatic TT[11]MC), 1.77 (br s, 3H, CH_3 PPh_2Me). $^{13}C\{^1H\}$ NMR (CD_3CN): δ (ppm) 169.1 ($^2J_{P-C}$=103.3 Hz, Pt-C1), 150.1 ($^2J_{Pt-C}$=105.6 Hz, aromatic TT[11]MC), 127.0, 122.2 (TT[11]MC), 133.4 (d, $^1J_{P-C}$=48.3 Hz, aromatic PPh_2Me), 133.4 ($^2J_{P-C}$=10.6 Hz, aromatic PPh_2Me), 132.4 (aromatic PPh_2Me), 130.0 ($^3J_{P-C}$=7.5 Hz, aromatic PPh_2Me), 52.6 (benzylic), 40.3 (SCH_2), 29.4 (SCH_2), 28.6 ($^3J_{Pt-C}$=38.1 Hz, CH_2), 13.7 ($^1J_{P-C}$=30.2 Hz, CH_3 PPH_2Me). $^{31}P\{^1H\}$ NMR (CD_3CN): δ (ppm) -0.3 ($^1J_{Pt-P}$=1950.4 Hz). Anal. Calcd. for $C_{27}H_{32}BF_4PS_3Pt$: C, 42.35; H, 4.22; S, 12.66. Found: C, 42.11; H, 4.03; S, 12.69.

(vii) Reactions of [Pt(TT[11]MC)][BF_4] with CO, H_2 and C_2H_4. [Pt(TT[11]MC)][BF_4] was dissolved in acetonitrile (25 mL); the solution was placed under 1 atm. of CO(g), H_2(g), or C_2H_4(g) and stirred at room temperature for 24 h. The atmosphere was then replaced by N_2(g) and the solvent was removed leaving a colourless solid which was recrystallized from acetonitrile/diethyl ether and identified as [Pt(TT[11]MC)][BF_4] by NMR spectroscopy.

(viii) Reactions of [Pt(TT[11]MC)][BF_4] with CH_3I, PPh_3, and DMAD. [Pt(TT[11]MC)][BF_4] (0.116 g, 0.205 mmol) was dissolved in acetonitrile (25 mL) and 1 equiv. of the reagent (0.205 mmol) was added with stirring. After 24 h, the solvent was removed leaving a colourless solid which was recrystallized from

acetonitrile/diethyl ether and identified as [Pt(TT[11]MC)][BF_4] by NMR spectroscopy.

(ix) Preparation of [PtI_2(TT[11]MC)][BF_4], (6). [Pt(TT[11]MC)][BF_4] (0.080 g, 0.142 mmol) was dissolved in acetonitrile (20 mL) and I_2 (0.037 g, 0.146 mmol) was added with stirring. The red solution stirred for 12 h and the solvent was then removed *in vacuo* leaving a dark red solid which was recrystallized from acetonitrile/diethyl ether. Yield: 0.083 g (71%). ^{1}H NMR (CD_3CN): δ (ppm) 7.27 (m, 2H, aromatic), 7.11 (m, 1H, aromatic), 4.93 (m, 4H, benzylic), 3.45 (m, 2H, SCH_2), 3.37 (m, 4H, SCH_2), 3.10 (m, 2H, SCH_2), 2.89 (ddd, 2H, $^3J_{Pt-H}$=60.0 Hz, CH_2), 2.41 (m, 2H, CH_2). $^{13}C\{^1H\}$ NMR (CD_3CN): δ (ppm) 149.6 ($^1J_{Pt-C}$=634 Hz, Pt-C1), 144.8 ($^2J_{Pt-C}$=51.8 Hz, aromatic), 132.7, 128.4 ($^3J_{Pt-C}$ ~30 Hz, aromatic), 48.3 ($^2J_{Pt-C}$ ~20 Hz, benzylic), 34.3 (SCH_2), 32.7 (SCH_2), 22.0 ($^3J_{Pt-C}$=19.5 Hz, CH_2). Anal. Calcd. for $C_{14}H_{19}BF_4S_3I_2Pt$: C, 20.52; H, 2.34; S, 11.74. Found: C, 20.77; H, 2.43; S, 11.85.

(x) Preparation of [$PtCl_2$(TT[11]MC)][BF_4], (7). [Pt(TT[11]MC)][BF_4] (0.100 g, 0.177 mmol) was dissolved in acetonitrile (20 mL) and $CuCl_2.2H_2O$ (0.061 g, 0.358 mmol) was added with stirring. The colourless solution immediately turned orange and a yellow solid precipitated. The solid was isolated by filtration, washed with diethyl ether and dried *in vacuo*. Yield: 0.064 g (57%). ^{1}H NMR (DMSO-d_6): δ (ppm) 7.22 (s br, 3H, aromatic), 4.95 (d br, 4H, benzylic), 3.35 (m br, 8H, SCH_2), 2.85 (m br, 4H, CH_2). $^{13}C\{^1H\}$ NMR (DMSO-d_6): δ (ppm) 143.8 ($^1J_{Pt-C}$=625 Hz, Pt-C1), 142.9 (J_{Pt-C}=43.7 Hz), 127.4, 125.3 (aromatic), 44.8 (benzylic), 33.3 (SCH_2), 32.2 (SCH_2), 21.1 (CH_2). Anal. Calcd. for

$C_{14}H_{19}BF_4S_3Cl_2Pt$: C, 26.42; H, 3.02; S, 15.12. Found: C, 26.22; H, 3.14; S, 15.21.

(xi) Preparation of [Pd(TT[11]MC)][BF_4], (8). $Pd(PhCN)_2Cl_2$ (0.404 g, 1.05 mmol), TT[11]MC (0.297 g, 1.04 mmol), and $AgBF_4$ (0.234 g, 1.20 mmol) were combined in acetonitrile (70 mL), and the mixture was refluxed for 48 hours. The resulting mixture was filtered to remove AgCl and the solvent was removed to give an orange solid which was recrystallized from acetonitrile/diethyl ether. Yield: 0.348 g (75%). ^1H NMR (CD_3CN): δ (ppm) 7.06 (br s, 3H, aromatic), 4.71 (d, 2H, ^2J=16.0 Hz, benzylic), 4.31 (d, 2H, ^2J=16.0 Hz, benzylic), 3.44 (ddd, 2H, ^2J=1.8, 7.6, 11.9 Hz, SCH_2), 3.21 (td, 2H, ^2J=1.9, 11.1 Hz, SCH_2), 3.10 (t, 2H, ^2J=5.0 Hz, SCH_2), 2.86 (t, 2H, ^2J=11.4 Hz, SCH_2), 2.58 (m, 2H, ^2J=7.3 Hz, CH_2), 2.00 (t, 2H, ^2J=10.6 Hz, CH_2). $^{13}C\{^1H\}$ NMR (CD_3CN): δ (ppm) 165.8 (Pd-C1), 149.8, 126.6, 123.0 (aromatic), 50.0 (benzylic), 38.3 (CH_2S), 35.1 (CH_2S), 27.7 (CH_2). Anal. Calcd. for $C_{14}H_{19}BF_4PdS_3$: C, 35.27; H, 4.03; S, 20.18. Found: C, 35.11; H, 3.92; S, 20.29.

(xii) Preparation of [Pd(PPh_2Me)(TT[11]MC)][BF_4], (9). [Pd(TT[11]MC)][BF_4] (0.103 g, 0.216 mmol) dissolved in acetonitrile (15 mL) and PPh_2Me (0.043 g, 0.215 mmol) was added with stirring. After 10 minutes the solvent was removed leaving an orange/yellow solid which was recrystallized from acetonitrile/diethyl ether. Yield: 0.125 g (86%). ^1H NMR (CD_3CN): δ (ppm) 7.70 (m, 4H, aromatic PPh_2Me), 7.54 (m, 6H, aromatic PPh_2Me), 7.06 (br s, 3H, aromatic TT[11]MC), 4.75 (d, 2H, ^2J=16.7 Hz, benzylic), 4.25 (d, 2H, ^2J=16.7 Hz, benzylic), 3.11 (m, 2H, aliphatic), 2.70 (m, 6H, aliphatic), 2.14 (br s, 4H, aliphatic),

1.87 (d, 3H, $^2J_{PH}$=3.6 Hz, CH_3 PPh_2Me). $^{13}C\{^1H\}$ NMR (CD_3CN): δ (ppm) 169.8 (Pd-C1), 151.5, 126.7, 123.5 (aromatic TT[11]MC), 136.0 ($^1J_{P-C}$=23.4 Hz, aromatic PPh_2Me), 133.0, 131.1, 129.9 (aromatic PPh_2Me), 49.7 (benzylic), 38.2 (CH_2S), 32.2 (CH_2S), 28.5 (CH_2), 12.9 (d, $^2J_{P-C}$=9.8 Hz, CH_3 PPh_2Me). $^{31}P\{^1H\}$ NMR (CD_3CN): δ (ppm) -11.2. Anal Calcd for $C_{27}H_{32}BF_4PS_3Pd$: C, 50.16; H, 5.00; S, 14.89. Found C, 49.89; H, 4.83; S, 14.99.

(xiii) Preparation of [$PdCl_2$(TT[11]MC)], (10). $PdCl_2(PhCN)_2$ (0.092 g, 0.24 mmol) and TT[11]MC (0.066 g, 0.23 mmol) were combined in acetonitrile (10 mL) and stirred at room temperature for 12 h. The resulting yellow precipitate was filtered and washed with acetonitrile (5 mL) and diethyl ether (10 mL). Yield: 0.084 g (78%). ^1H NMR (DMSO-d_6): δ (ppm) 8.29 (s, 1H, aromatic), 7.41 (br m, 2H, aromatic), 7.30 (br s, 1H, aromatic), 4.73 (br d, 1H, benzylic), 4.30 (br m, 1H, benzylic), 3.92 (br d, 1H, benzylic), 3.72 (br m, 1H, benzylic), 2.94 (br m, 2H), 2.57 (m, 5H), 2.16 (br m, 2H), 1.88 (m, 2H), 1.30 (m, 1H). Anal. calcd. for $C_{14}H_{20}S_3Cl_2Pd$: C, 36.40; H, 4.37; S, 20.83. Found: C, 36.12; H, 4.22; S, 20.67.

(xiv) Attempted oxidation of [Pd(TT[11]MC)][BF_4]. To a solution of $CuCl_2$ (0.072 g, 0.422 mmol) in acetonitrile (25 mL) was added [Pd(TT[11]MC)][BF_4] (0.104 g, 0.218 mmol). The initially green solution turned orange/red with a red precipitate present in the solution. After gentle heating for 20 h an orange precipitate was filtered and washed with acetonitrile, dried *in vacuo*, and identified by NMR spectroscopy as [$PdCl_2$(TT[11]MC)]. Yield: 0.080 g, (82%).

(xv) Metalation of [$PdCl_2$(TT[11]MC)]. To a suspension of [$PdCl_2$(TT[11]MC)] (0.076 g, 0.165 mmol) in acetonitrile (10 mL) was added $AgBF_4$ (0.038 g, 0.195 mmol). The mixture was refluxed for 24 h, filtered and the solvent was removed *in vacuo* leaving an orange solid which was identified by NMR spectroscopy (in CD_3CN) as [Pd(TT[11]MC)][BF_4]. Yield: 0.052 g (66%).

(xvi) Preparation of 4-oxaheptane-1,7-diol, (11). Sodium metal (3.068 g, 133 mmol) was dissolved in 1,3-propanediol (49.568 g, 651 mmol) at 60° C to give a yellow solution. 3-bromopropanol (18.290 g, 132 mmol) was syringed into the solution and the reaction maintained at 80° C for 12 h. The excess 1,3-propanediol was removed *in vacuo* leaving a light brown oil which was distilled on a Kugelrohr apparatus to give a clear liquid. Yield: 12.601 g (71%). ^{1}H NMR (DMSO-d_6): δ (ppm) 4.36 (^{2}J=7.6 Hz, 2H, OH), 3.41 (m, 8H, OCH_2), 1.61 (m, 4H, CH_2). ^{13}C{^{1}H} NMR (DMSO-d_6): δ (ppm) 67.2 (OCH_2, ether), 57.8 ($HOCH_2$, alcohol), 32.7 (CH_2).

(xvii) Preparation of 4-oxaheptane-1,7-dithiol, (12). This preparation follows that used for the synthesis of compound 2[81]. 4-oxaheptane-1,7-diol: (4.687 g, 34.9 mmol); thiourea: (5.866 g, 76.8 mmol); concentrated hydrochloric acid: (17.5 mL, 210 mmol). The crude product was distilled *in vacuo* (bp 70° C at $5x10^{-2}$ torr) to give a clear oil. (*Caution! Extremely irritating odour.*) Yield: 2.35 g (40%). ^{1}H NMR ($CDCl_3$): δ (ppm) 3.48 (t, 4H, OCH_2), 2.60 (m, 4H, SCH_2), 1.82 (m, 4H, CH_2), 1.33 (t, 2H, SH). ^{13}C{^{1}H} NMR ($CDCl_3$): δ (ppm) 68.6 (OCH_2), 33.7 ($HSCH_2$), 21.4 (CH_2).

(xviii) Preparation of 6-oxa-2,10-dithia[11]-*m*-cyclophane, (*pr*-TOMB-1), (13). To a stirred suspension of cesium carbonate (6.060 g, 18.6 mmol) in DMF (400 mL) was added a solution of α,α'-dibromo-*m*-xylene (2.392 g, 9.06 mmol) and 4-oxaheptane-1,7-dithiol (1.476 g, 9.04 mmol) in DMF (150 mL). The addition was performed over 40 h with the temperature at 50-55 °C. After addition, the mixture was stirred at room temperature for 15 hours and the product was isolated in the same manner as TT[11]MC (procedure (iii)). The crude product was recrystallized from hot *iso*propanol. Yield: 1.407 g (58%). ^{1}H NMR ($CDCl_3$): δ (ppm) 7.32-7.22 (m, 4H, aromatic), 3.64 (s, 4H, benzylic), 3.38 (t, 4H, OCH_2), 2.37 (t, 4H, SCH_2), 1.79 (m, 4H, CH_2). $^{13}C\{^{1}H\}$ NMR ($CDCl_3$): δ (ppm) 138.2, 130.6, 129.2, 127.8 (aromatic), 68.8 (OCH_2), 34.8 (benzylic), 29.6 (SCH_2), 25.9 (CH_2).

(xix) Preparation of [Pd(*pr*-TOMB-1)][BF_4]$_2$ (14). *pr*-TOMB-1 (0.150 g, 0.559 mmol) and $[Pd(CH_3CN)_4][BF_4]_2$ (0.252 g, 0.567 mmol) were dissolved in acetonitrile (40 mL). The orange solution was refluxed for 15 min. during which time it turned yellow. The solvent was removed *in vacuo* and the pasty solid was washed with chloroform (10 mL) and then recrystallized from chloroform. Yield: 0.185 g (72%). ^{1}H NMR (CD_3CN): δ (ppm) 7.01-6.94 (m, 3H, aromatic), 4.45 (d, 2H, ^{2}J=16.9 Hz, benzylic), 4.08 (d, 2H, ^{2}J=16.9 Hz, benzylic), 4.72 (m, 2H, OCH_2), 3.55 (m, 2H, OCH_2), 3.29 (m, 2H, SCH_2), 3.13 (m, 2H, SCH_2), 2.09 (m, 4H, CH_2). $^{13}C\{^{1}H\}$ NMR (CD_3CN): δ (ppm) 151.7, 125.2, 122.3 (aromatic, Pd-C1 not observed), 70.0 (OCH_2), 43.6 (benzylic), 37.2 (SCH_2), 26.0 (CH_2).

(xx) Preparation of [Pd(PPh_2Me)(*pr*-TOMB-1)][BF_4], (15).

[Pd(*pr*-TOMB-1)][BF_4] (0.026 g, 56.4 μmol) was dissolved in acetonitrile (5 mL) and PPh_2Me (0.012 g, 61.8 μmol) was added by syringe after which the solution was brighter yellow. The solution stirred for 24 h and the solvent was removed *in vacuo*. The remaining solid recrystallized from acetonitrile/diethyl ether. Yield: 0.020 g (55%). ^{1}H NMR (CD_3CN): δ (ppm) 7.67 (m, 4H, aromatic PPh_2Me), 7.52 (m, 6H, aromatic PPh_2Me), 7.09 (m, 3H, aromatic *pr*-TOMB-1), 4.73 (d, 2H, ^2J=17.1 Hz, benzylic), 4.26 (d, 2H, ^2J=17.1 Hz, benzylic), 3.53 (m, 2H, OCH_2), 3.33 (m, 2H, OCH_2), 3.09 (m, 2H, SCH_2), 2.58 (m, 2H, SCH_2), 2.14 (d, 3H, ^2J=7.4 Hz, CH_3 PPh_2Me), 1.88 (m, 2H, CH_2), 1.72 (m, 2H, CH_2). $^{13}C\{^1H\}$ NMR (CD_3CN): δ (ppm) 171.7 (Pd-C1), 152.2, 126.5, 123.0 (aromatic *pr*-TOMB-1), 133.4, 131.9, 130.0 (aromatic PPh_2Me), 71.0 (OCH_2), 49.4 (d, ^2J=12.9 Hz, benzylic), 38.1 (SCH_2), 26.5 (CH_2), 13.1 (d, $^1J_{P\text{-}C}$=21.8 Hz, CH_3 PPh_2Me). $^{31}P\{^1H\}$ NMR (CD_3CN): δ (ppm) -4.0.

2.3 X-Ray Diffraction Data Collection, Solution, and Refinement.

(i) General Procedures. Diffraction experiments were performed on a four-circle Rigaku AFC6S diffractometer with graphite-monochromatized MoKα radiation. The unit cell constants and orientation matrices for data collection were obtained from 20 centred reflections ($15° < 2\theta < 35°$). Machine parameters, crystal data, and data collection parameters are summarized in Appendix A. The intensities of three standard reflections were recorded every 150 reflections and

showed no statistically significant changes over the duration of the data collections. The intensity data were collected using the $\omega-2\theta$ scan technique, in four shells ($2\theta < 30$, 40, 45, and 50°). Absorption coefficients were calculated and absorption as well as decay corrections applied to the data. The data were processed using the TEXSAN software[82] package running on a VAX 3520 or a SGI Challenge computer. Refinements were carried out by using full-matrix least-squares techniques on F by minimizing the function $\Sigma w(F_o - F_c)^2$, where $w = 1/\sigma^2(F_o)$ and F_o and F_c are the observed and calculated structure factors. Atomic scattering factors[83] and anomalous dispersion terms[84] were taken from the usual sources. In the final cycles of refinement, all non-H atoms were assigned anisotropic thermal parameters with exceptions noted for the carbon atoms in some structures in the individual Structure Determination sections. Fixed hydrogen-atom contributions were included with C-H distances of 0.95 A and thermal parameters 1.2 times the isotropic thermal parameter of the bonded C atoms. These H atoms were not refined, but were updated and included in the structure factor calculations as refinement continued. All atomic positional parameters, bonding parameters and thermal parameters are listed in Appendix A.

(ii) Structure Determinations of TT[11]MC (3), [Pt(TT[11]MC)][BF_4] (4), [Pt(PPh_2Me)(TT[11]MC)][BF_4] (5), [PtI_2(TT[11]MC)][BF_4] (6). The X-ray structural analyses for compounds 3, 4, 5 and 6 were performed by Professor Stephen J. Loeb and full details of the solutions are given in the literature[64, 76].

(iii) Structure Determination of 6-oxa-2,10-dithia[11]-*m*-cyclophane, *pr*-TOMB-1, (13). Colourless crystals of *pr*-TOMB-1 were grown by slow evaporation of a $CDCl_3$ solution of the compound. A statistical analysis of the intensity distributions and a determination of observed extinctions were consistent with the *ortho*rhombic space group Pnma, and this was confirmed by a successful solution refinement. A total of 1461 reflections were collected, and 712 unique reflections with $F_o^2>3\sigma(F_o^2)$ were used in the refinement. The positions of the sulfur and oxygen atoms were determined by direct methods from the *E*-map with the highest figure of merit. The remaining carbon atoms were located from a difference Fourier map calculation. In the final cycles of refinement, all atoms were assigned anisotropic thermal parameters. This resulted in $R = \Sigma||F_o|-|F_c||/\Sigma|F_o|| = 0.0385$ and $R_w = (\Sigma_w(|F_o|-|F_c|)^2/\Sigma_w F_o^2)^{1/2} = 0.0233$ at final convergence. The Δ/σ value for any parameter in the final cycle was less than 0.0002. A final difference Fourier map calculation showed no peaks of chemical significance; the largest was 0.201 electron /Å^3 and was associated with the S1 atom. Crystal data, intensity collection and structure refinement details, as well as all atomic positional parameters, bond distances and angles are summarized in Appendix Table A1.

(iv) Structure Determination of [Pd(*pr*-TOMB-1)][BF_4], (14). Colourless crystals of [Pd(*pr*-TOMB-1)][BF_4] were grown by recrystallization from a $CDCl_3$ solution of the compound. A statistical analysis of the intensity distributions was consistent with space group $P\bar{1}$, and this was confirmed by a successful solution refinement. A total of 3721

reflections were collected, and 2116 unique reflections with $F_o^2>3\sigma(F_o^2)$ were used in the refinement. The positions of the palladium and sulfur atoms were determined by direct methods from the *E*-map with the highest figure of merit. The remaining carbon and oxygen atoms were located from a difference Fourier map calculation. In the final cycles of refinement, all atoms were assigned anisotropic thermal parameters. This resulted in R = 0.0462 and R_w = 0.0367 at final convergence. The Δ/σ value for any parameter in the final cycle was less than 0.003. A final difference map Fourier map calculation showed no peaks of chemical significance; the largest was 0.850 electron /Å^3 and was associated with the BF_4 anion. Crystal data, intensity collection and structure refinement details, as well as all atomic positional parameters, bond distances and angles are summarized in Appendix Table A2.

2.4 Results and Discussion

(i) Synthesis and Characterization of TT[11]MC, (3). TT[11]MC can be readily prepared by using the Cs^+ ion mediated cyclization method of Buter and Kellogg[28]. The synthesis involves the formation of two carbon-sulfur bonds and can be performed as a one-pot reaction from commercially available or easily prepared starting materials in one of two methods. A) Reaction of 4-thiaheptane-1,7-dithiol[81] with an equimolar amount of α,α'-dibromo-*m*-xylene or B) reaction of *m*-xylene-α,α'-dithiol with 4-thiaheptane-1,7-ditosylate[80b], in the presence of cesium carbonate, both give TT[11]MC in high yields (Scheme 2.1).

The ligand is air stable, colourless, and easily crystallized from a variety of organic solvents (CH_3COCH_3, CH_2Cl_2, $CHCl_3$, C_6H_6, CH_3CN).

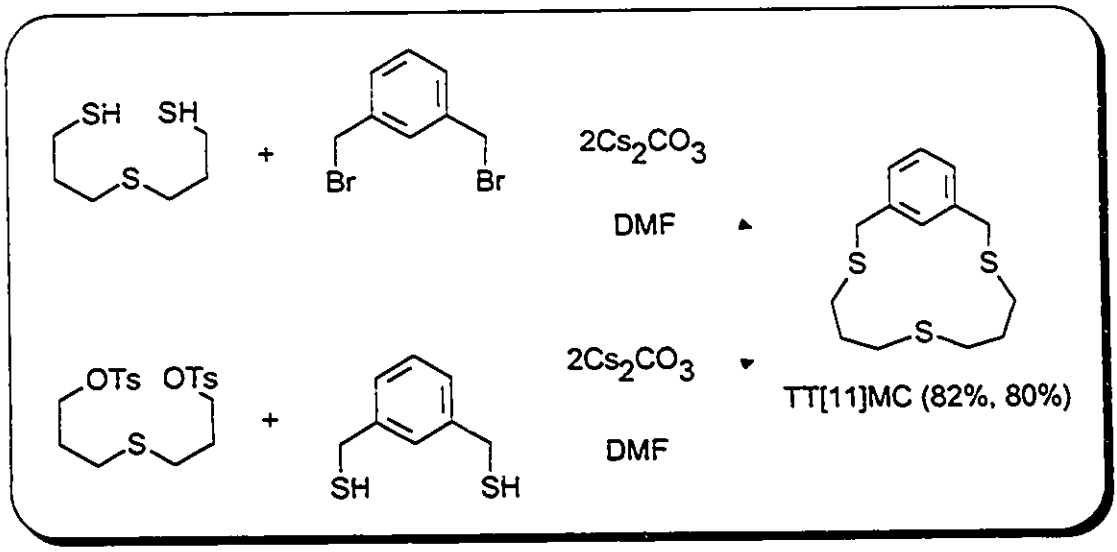

Scheme 2.1 These two routes can both be used to synthesize TT[11]MC.

The macrocycle was characterized first by NMR spectroscopy. In the ^1H NMR spectrum the expected *meta* substitution pattern is observed in the aromatic region of the spectrum, with the H-atom at the 2-position of the aromatic ring appearing slightly downfield (7.42 ppm) of the other aromatic hydrogens (7.25-7.15 ppm). A single resonance for the benzylic CH_2 groups appears at 3.70 ppm and triplets for the methylene units adjacent to S1 and S3, and to S2 appear at 2.48 ppm and 2.38 ppm respectively. The central CH_2 groups in the propylene chains appear as a pseudo quintet at 1.58 ppm. Single resonances for pairs of methylene groups indicate that the ligand is symmetrical in solution.

The $^{13}C\{^1H\}$ spectrum is equally diagnostic with a resonance at 139.5 ppm for the quaternary carbons and resonances at 129.4, 128.8 and 127.7 ppm for the remainder of the aromatic nuclei. Resonances for symmetrical aliphatic carbon

atoms appear at 36.9 ppm for the benzylic CH_2 group, at 31.2 ppm for the central CH_2, and at 30.3 and 29.9 ppm for the CH_2 groups adjacent to sulfur atoms.

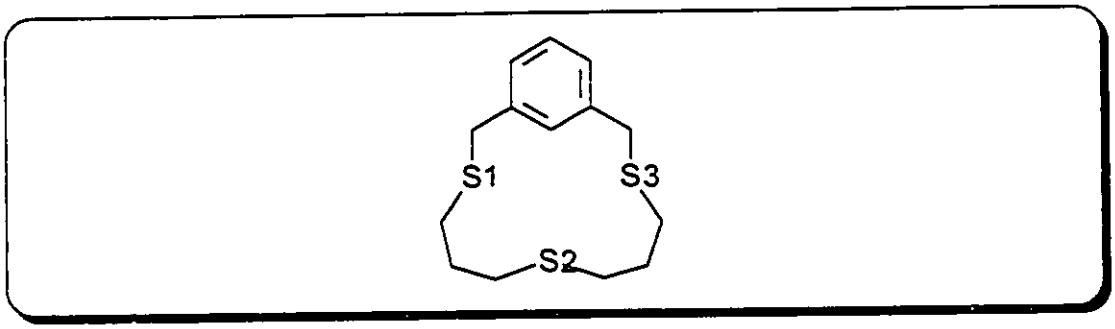

Figure 2.7 TT[11]MC with heteroatom numbering scheme consistent with crystal structure and NMR discussion.

In addition to the evidence described above, crystals of TT[11]MC were grown by slow evaporation of an acetone solution of the compound and the crystal structure was determined.

(ii) Crystal Structure of TT[11]MC (3). The unit cell is monoclinic and contains four molecules of TT[11]MC. A perspective view of the molecule with the atom numbering scheme is shown in Figure 2.8. Complete listings of crystallographic parameters including atomic positions, bonding parameters and details of data collection are listed in the literature[61]. Selected parameters are given in the figure caption.

Sulfur-carbon distances range from 1.792(6) to 1.806(5) Å and $C(sp^2)$-$C(sp^2)$ distances range 1.373(6) to 1.384(6) Å. The two $C(sp^2)$-$C(sp^3)$ bonds are 1.514(6) and 1.507(7) Å and the $C(sp^3)$-$C(sp^3)$ bonds average 1.47(9) Å with a relatively large range from 1.31(1) to 1.54(1) Å, resulting from a slight disorder in the C11-C12 linkage. These distances compare well with those found

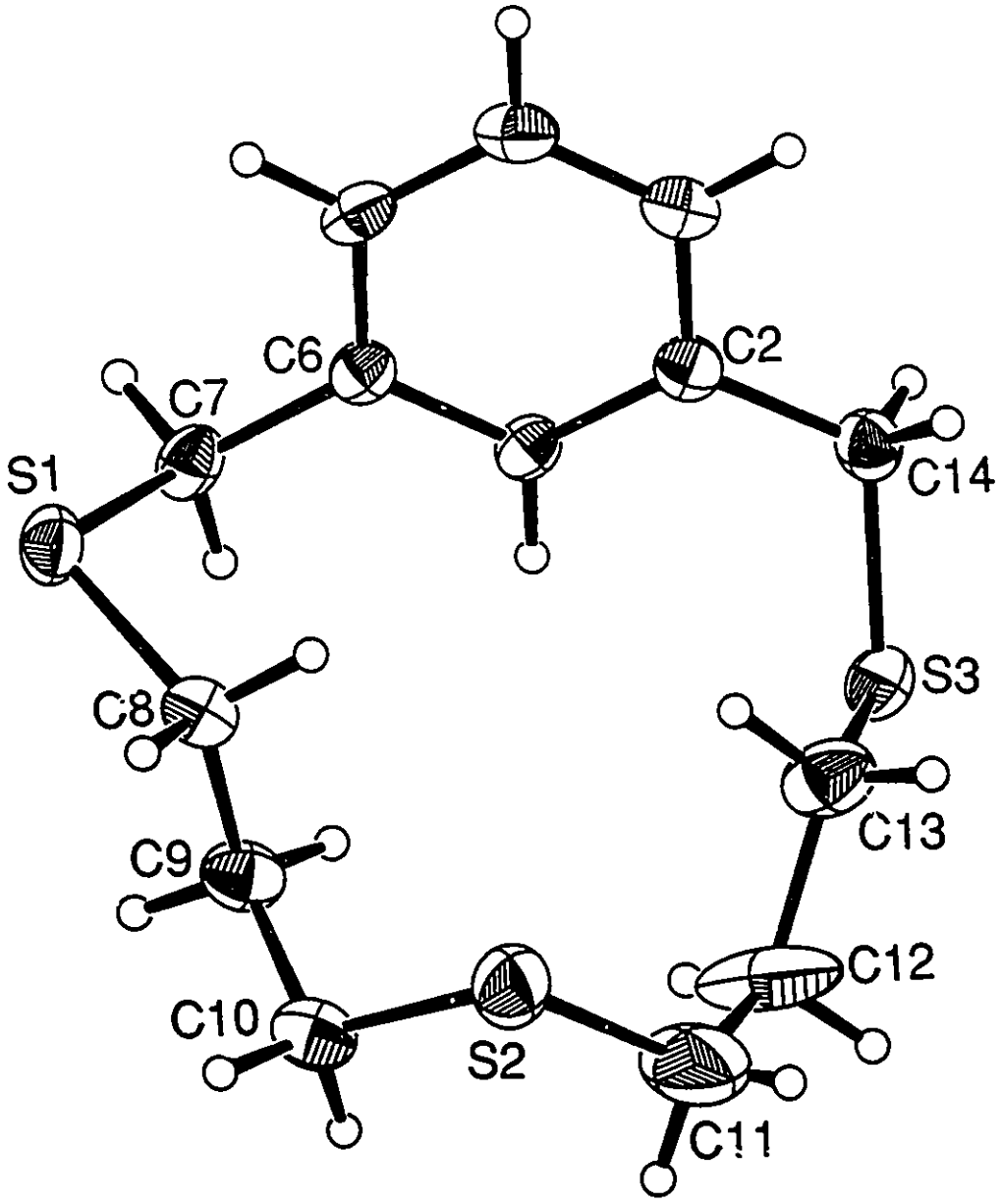

Figure 2.8 Perspective ORTEP drawing of TT[11]MC (3) showing the atom numbering scheme with 30% thermal ellipsoids. Selected bond distances (Å) are: S1-C7 =1.806(5), S1-C8 = 1.805(6), S2-C10 = 1.817(6), S2-C11 = 1.750(8), S3-C13 = 1.792(6), S3-C14 = 1.795(5). C6-C7 = 1.514(6), C2-C14 = 1.507(7) Å. $C(sp^2)$-$C(sp^2)$ distances range from 1.373(6) to 1.384(6) Å. $C(sp^3)$-$C(sp^3)$ bonds average 1.47(9) Å.

for other thiacyclophanes and macrocyclic thioethers[31, 85].

In examining the structure of TT[11]MC, two main features are observed. The two C(benzylic)-S bonds are positioned on the same side of the aromatic ring which has the effect of orienting the aliphatic chain approximately perpendicular to the aromatic ring. This is consistent with the structures of the smaller thiacyclophanes TT[9]OC and TT[9]MC[60] and in contrast to the structure of TT[11]OC[61] and to TOMB-3 (vide infra) which both have the C(benzylic)-S bonds oriented on opposite sides of the aromatic moiety, forcing the aliphatic chain to loop around from one side of the aromatic ring to the other.

It is well known that thioether macrocycles prefer to adopt exodentate conformations as uncoordinated ligands[31, 86] and examination of Figure 2.8 verifies that the sulfur donor atoms point out of the macrocycle. Closer examination of the torsional angles about the sulfur atoms reveals that 4 of 6 adopt *gauche* placements (Table 2.1) and one is intermediate between *gauche* and *anti*; only C12-C13-S3-C14 has an *anti* conformation and it deviates significantly from the 180° torsional angle in an ideal *anti* placement.

Table 2.1 Torsional Angles about Sulfur Atoms in TT[11]MC.

Linkage	Angle (°)
C6-C7-S1-C8	-62.0(4)
C7-S1-C8-C9	-65.7(4)
C9-C10-S2-C11	-56.3(6)
C10-S2-C11-C12	-97.4(5)
C12-C13-S3-C14	161.5(5)
C13-S3-C14-C2	-66.5(4)

(iii) Formation of [Pt(TT[11]MC)][BF_4], (4). The reaction of equimolar amounts of TT[11]MC, Pt(COD)Cl_2 and $AgBF_4$ in refluxing acetonitrile yields [Pt(TT[11]MC)][BF_4] (Figure 2.9) as an off white solid which is easily recrystallized from acetonitrile/diethyl ether to give the complex as a colouriess crystalline solid.

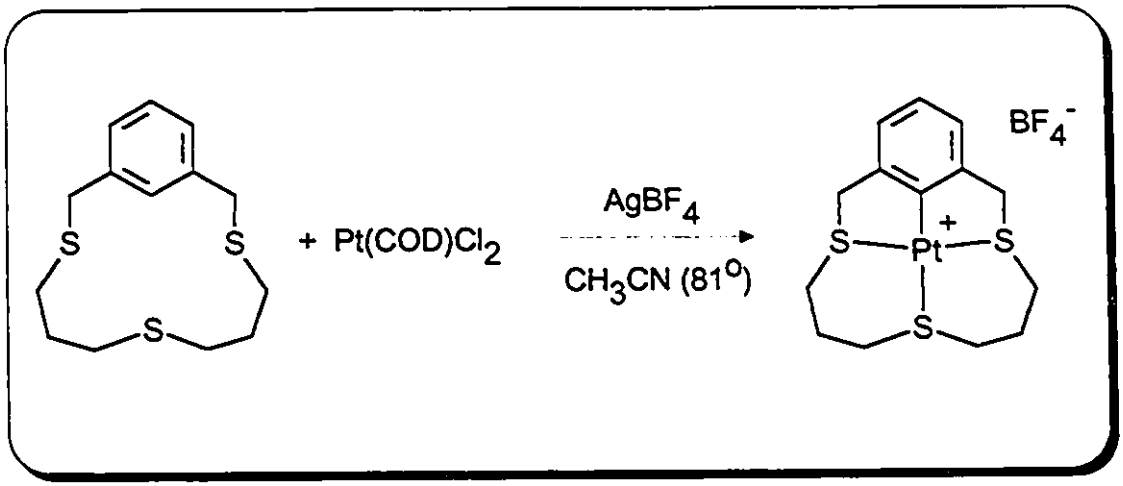

Figure 2.9 Metalation Reaction for formation of [Pt(TT[11]MC)][BF_4].

^1H and $^{13}C\{^1H\}$ NMR spectroscopy both indicate that a symmetrical *ortho*-metalated product was formed. The absence of a ligand proton resonance at 7.43 ppm[61, 76] and the downfield shift and splitting of the benzylic resonance into a pair of doublets, with a large three-bond ^{195}Pt coupling of 70.4 Hz to the downfield signal centred at 4.90 ppm, offer strong evidence for the metalation product. In addition, large one- and two-bond couplings of 855 and 111.1 Hz to $^{13}C\{^1H\}$ resonances at 157.9 and 147.4 ppm for the carbon atoms at the 2- and 1-positions of the aromatic ring (shifted downfield from 128.8 and 139.5 ppm respectively) are strong evidence for the formation of the Pt-C bond. The resonances for the carbon atoms adjacent to the sulfur atoms are also shifted

downfield upon coordination from about 30 ppm to 38.6 and 35.8 ppm, offering more evidence for the inclusion of the Pt(II) centre inside the macrocyclic cavity.

(iv) Crystal Structure of [Pt(TT[11]MC)][BF_4], (4). The unit cell is monoclinic and contains four molecules of [Pt(TT[11]MC)][BF_4]. A perspective view of the molecule with the atom numbering scheme is shown in Figure 2.10. Complete listings of crystallographic parameters including atomic positions, bonding parameters and details of data collection are tabulated in the literature[76]. Selected bonding parameters are given in the figure caption.

The platinum atom is in a square planar environment with three sulfur atoms and one carbon atom providing the coordination sphere for the metal. The Pt-S2 bond distance of 2.365(6) Å is significantly longer that the Pt-S1 and Pt-S3 distances of 2.255(6) and 2.266(4) Å respectively, due to the strong *trans* influence of the aromatic group and the relaxed nature of the 6-membered chelate rings. The Pt-C1 distance is 1.99(3) Å. The ligand bite angles at the Pt centre are S1-Pt-C1 = 83.0(9)° and S3-Pt-C1 = 86.4(9)° for the rigid metalated fragment containing the strained 5-membered chelate rings and S1-Pt-S2 = 98.2 (2)° and S3-Pt-S2 = 94.3 (2)° for the more flexible 6-membered chelate rings. The effect of constraining the Pt(II) centre inside the macrocycle is evident from a number of bonding parameters. First the mutually *trans* Pt-S distances are significantly shorter than those recently found for a series of Pt(II) complexes with open chain thioether ligands, $[PtX(RS(CH_2)_3S(CH_2)_3SR)]^+$ (X=halide, R=Et, Ph, *i*-Pr)[80b]. The Pt-S bond distances in these complexes range from 2.290 (4) to 2.308 (5) Å when no chelate strain was present. There is also a

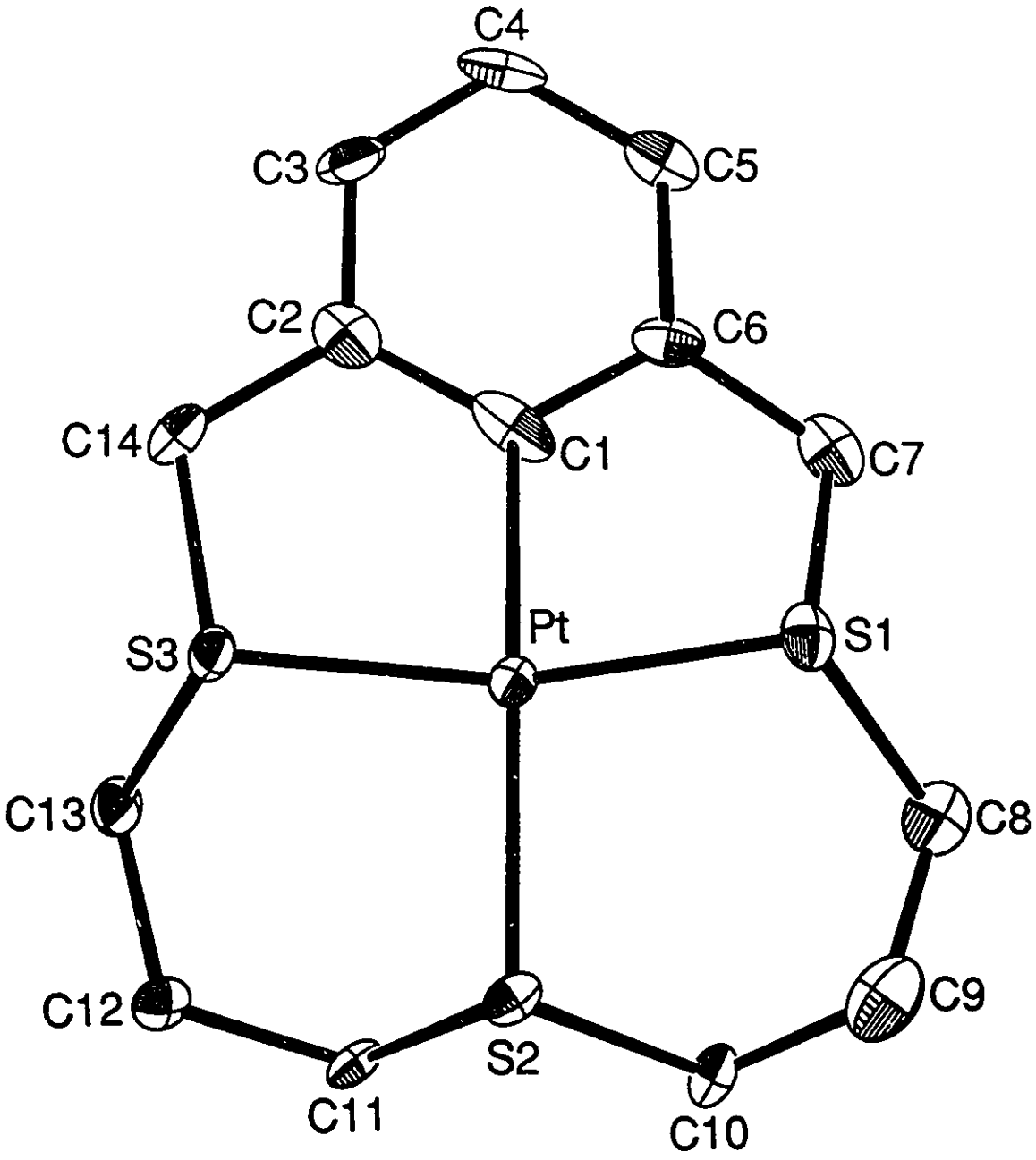

Figure 2.10 Perspective ORTEP drawing of the $[Pt(TT[11]MC)]^+$ (4) cation showing the atom numbering scheme with 30% thermal ellipsoids. Selected distances (Å) and angles are Pt-C1 = 1.99 (3), Pt-S1 = 2.255 (6), Pt-S2 = 2.365 (6), Pt-S3 = 2.266 (4). S1-Pt-C1 = 83.0(9)°, S3-Pt-C1 = 86.4(9)°, S1-Pt-S2 = 98.2 (2)°, S3-Pt-S2 = 94.3(2)°, C1-Pt-S2 = 170.4 (6), S1-Pt-S3 = 163.6 (2)°

tetrahedral distortion at Pt evidenced by the C1-Pt-S2 and S1-Pt-S3 angles of 170.4 (6) and 163.6 (2)°. This distortion presumably arises from the angular constraints of the rigid S_2C bracket in the ligand.

(v) Substitution Chemistry of [Pt(TT[11]MC)][BF_4]; Preparation of [Pt(PPh_2Me)(TT[11]MC)][BF_4], (5). A number of substitution reactions were attempted with simple two-electron donor groups and [Pt(TT[11]MC)][BF_4]. With CO, C_2H_4, and RCCR (R = Ph, COOMe) no reaction could be detected by NMR spectroscopy, while with PPh_3 and PPh_2Me competition for the Pt-S2 site was evident in solution. The -$S(CH_2)_3S(CH_2)_3S$- chain is flexible enough to accommodate substitution of the central sulfur atom by strong donor groups. However, PPh_2Me was the only donor group strong enough to compete successfully with S2 for the coordination site and give an isolable product.

The ^1H and $^{13}C\{^1H\}$ NMR spectra of the adduct confirm the presence of the PPh_2Me. A comparison of the $^{13}C\{^1H\}$ NMR chemical shifts for the aliphatic chain of [Pt(TT[11]MC)][BF_4] and [Pt(PPh_2Me)(TT[11]MC)][BF_4] following the atom numbering scheme in Figure 2.10 for [Pt(TT[11]MC)][BF_4] is given in Table 2.2. Upon addition of the phosphine, the resonance for C10 and C11 moves upfield from 35.8 to 29.4 ppm, near where it appears in the spectrum of the uncoordinated ligand. This evidence, coupled with the fact that the $^{31}P\{^1H\}$ NMR spectrum contains a single resonance (δ -0.3 ppm) with $^1J_{Pt\text{-}P}$= 1950.4 Hz, indicates that the central S2 atom has been displaced by PPh_2Me. In addition to the NMR evidence given above, X-ray quality crystals of the phosphine adduct were grown by vapour diffusion of diethyl ether into an acetonitrile solution of

Table 2.2 $^{13}C\{^1H\}$ NMR Chemical Shifts for TT[11]MC, $[Pt(TT[11]MC)]^+$ and $[Pt(PPh_2Me)(TT[11]MC)]^+$.

Carbon Atom#	TT[11]MC	$[Pt(TT[11]MC)]^+$	$[Pt(PPh_2Me)(TT[11]MC)]^+$
C7, C14	36.9	52.5	52.6
C8, C13	30.2	38.6	40.3
C9, C12	31.2	28.2	28.6
C10, C11	**29.9**	**35.8**	**29.4**

$[Pt(PPh_2Me)(TT[11]MC)][BF_4]$ and the crystal structure was determined.

(vi) Crystal Structure of $[Pt(PPh_2Me)(TT[11]MC)][BF_4]$, (5). The unit cell is monoclinic and contains four molecules of $[Pt(PPh_2Me)(TT[11]MC)][BF_4]$. A perspective view of the molecule with the atom numbering scheme is shown in Figure 2.11. Complete listings of crystallographic parameters including atomic positions, bonding parameters and details of data collection are tabulated in the literature[76]. Selected bonding parameters are listed in the figure caption.

The X-ray structure of the complex shows that the Pt atom is in a square planar environment and that the aliphatic chain is flexible enough to allow the central sulfur atom to be displaced from the platinum by the phosphine. Bond distances to the platinum are Pt-S1 = 2.290(4), Pt-S3 = 2.292 (4), Pt-P1 = 2.344 (5) and Pt-C1 = 1.99 (2).. The angles at the Pt centre are S1-Pt-C1 = 84.4 (5)° and S3-Pt-C1 = 84.7 (5)° for the 5-membered chelate rings in the metalated portion of the cyclophane and S1-Pt-P1 = 96.6 (2)° and S3-Pt-P1 = 94.2 (2)° for the non-chelating PPh_2Me ligand. Since the Pt atom is no longer constrained inside the macrocycle there is less tetrahedral distortion, as shown by the C1-Pt-P1 and S1-Pt-S3 angles of 172.7 (5)° and 169.1 (3)°. This relaxation of the

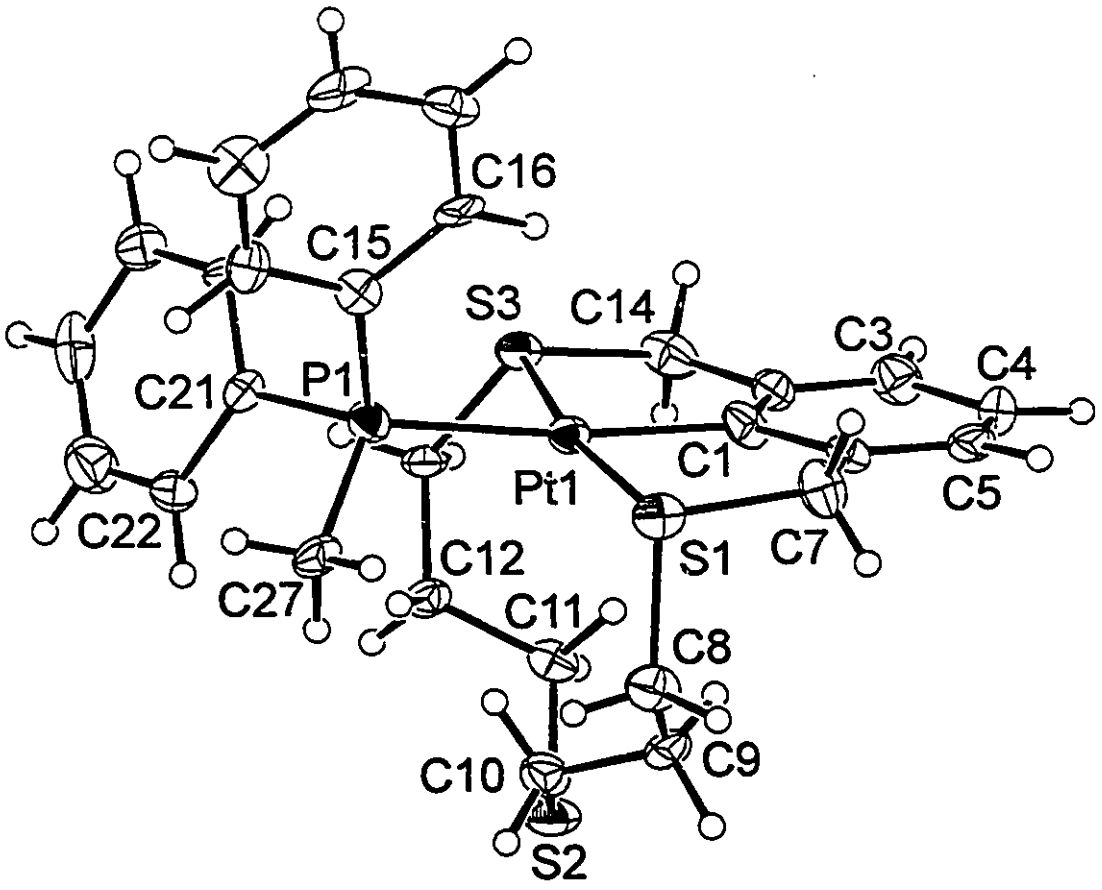

Figure 2.11 Perspective ORTEP drawing of the $[Pt(PPh_2Me)(TT[11]MC)]^+$ (5) cation showing the atom numbering scheme with 30% thermal ellipsoids. Selected distances (Å) and angles are: Pt-S1 = 2.290 (4), Pt-S3 = 2.292 (4), Pt-P1 = 2.344 (5), Pt-C1 = 1.99 (2). S1-Pt-C1 = 84.4 (5)°, S3-Pt-C1 = 84.7 (5)°, S1-Pt-P1 = 96.6 (2)°, S3-Pt-P1 = 94.2 (2)°, C1-Pt-P1 = 172.7 (5) °, S1-Pt-S3 = 169.1 (3)°

macrocycle results in significantly longer Pt-S distances and slightly larger S-Pt-C angles as compared to those in [Pt(TT[11]MC)][BF_4].

(vii) Oxidation Reactions of [Pt(TT[11]MC)][BF_4]; Preparation of [PtI_2(TT[11]MC)][BF_4] (6), and [$PtCl_2$(TT[11]MC)][BF_4], (7). The demonstrated flexibility of the aliphatic chain in TT[11]MC suggested that [Pt(TT[11]MC)][BF_4] might also accommodate the structural changes required for oxidative addition to Pt(IV) complexes. The reactions of [Pt(TT[11]MC)][BF_4] with 1 equivalent of either $CuCl_2$ or I_2[77] yielded the oxidative-addition products [PtX_2(TT[11]MC)][BF_4], where X = I (6), Cl (7), however no reaction was detected with MeI. NMR spectroscopy, particularly $^{13}C\{^1H\}$, confirms that oxidation from Pt(II) to Pt(IV) has occurred. The resonances for the metalated carbon atoms in both oxidation products [$PtCl_2$(TT[11]MC)][BF_4] and [PtI_2(TT[11]MC)][BF_4] undergo upfield shifts from δ = 157.9 ppm to 143.8 and 149.6 ppm for X = Cl and I respectively, and a reduction in the Pt-C coupling constants from 855 Hz to 625 Hz and 634 Hz respectively. This is a well established trend and can be attributed to less electron density on the Pt(IV) centre as compared to Pt(II)[87]. The actual geometry about the metal atom was established from the X-ray crystal structure of [PtI_2(TT[11]MC)][BF_4].

(viii) Crystal Structure of [PtI_2(TT[11]MC)][BF_4], (6). The unit cell is monoclinic and contains four molecules of [PtI_2(TT[11]MC)][BF_4]. A perspective view of the molecule with the atom numbering scheme is shown in Figure 2.12. Complete listings of crystallographic parameters including atomic positions, bonding parameters and details of data collection are tabulated in the literature[76].

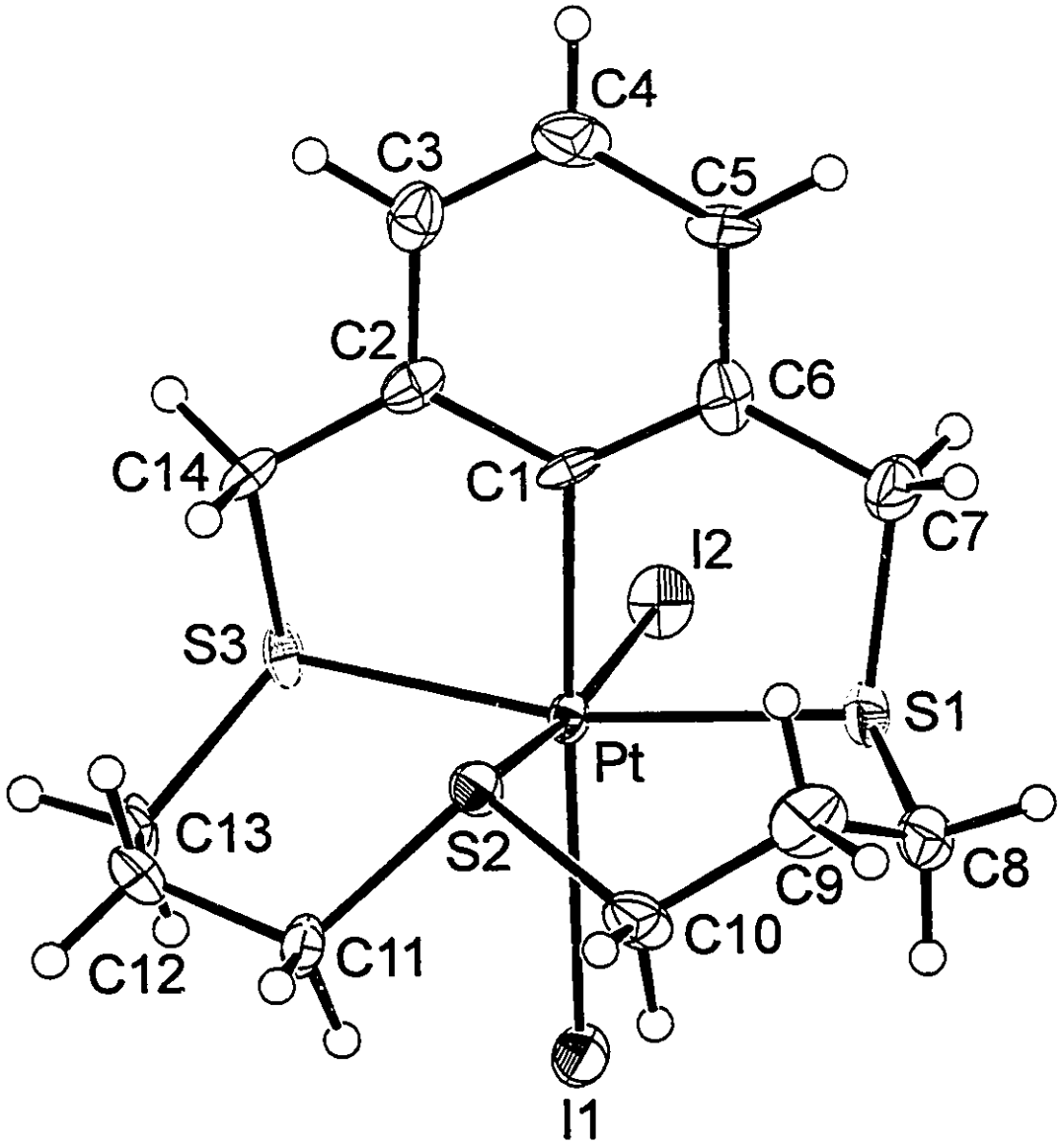

Figure 2.12 Perspective ORTEP drawing of the $[PtI_2(TT[11]MC)]^+$ (6) cation showing the atom numbering scheme with 30% thermal ellipsoids. Selected distances (Å) and angles are: Pt-C1 = 2.04 (2), Pt-S1 = 2.325 (5), Pt-S2 = 2.346 (5), Pt-S3 = 2.331 (5), Pt-I1 = 2.739 (2), Pt-I2 = 2.681 (2). S1-Pt-C1 = 86.1 (5)°, S3-Pt-C1 = 83.6 (6)°, S2-Pt-C1 = 84.6(5)° , I1-Pt-I2 = 91.31(5)°, I1-Pt-C1 = 177.6(5)°, I2-Pt-S2 = 173.7(1)°, S1-Pt-S3 = 166.2(2)°

Selected bonding parameters are given in the figure caption.

Octahedral Pt(IV) with a $PtCS_3I_2$ coordination sphere is formed in which the iodine atoms are *cis* to one another and the ligand is folded such that the aliphatic chain is perpendicular to the aromatic ring and S2 is coordinated to the Pt(IV) centre *cis* to the metalated carbon atom. Pt-C1 = 2.04(2), Pt-S1 = 2.325(5), Pt-S2 = 2.346(5), Pt-S3 = 2.331(5), Pt-I1 = 2.739(2), Pt-I2 = 2.681(2). Pt-L distances for the complex show that the Pt-S2 distance *trans* to I2 is slightly longer than the other two Pt-S distances. The Pt-I1 distance is longer than the Pt-I2 distance reflecting the *trans* influence of the aromatic group, similar to that observed for Pt-S2 in [Pt(TT[11]MC)][BF_4]. The significantly longer Pt-C1 distance of 2.04(2) Å compared to 1.99(3) Å in [Pt(TT[11]MC)][BF_4] can be attributed to the higher oxidation state on the metal, the change in coordination geometry, and the presence of extra donors in this six coordinate complex. The chelate angles associated with the folded macrocycle are S1-Pt-C1 = 86.1 (5)°, S3-Pt-C1 = 83.6 (6)° and S2-Pt-C1 = 84.6(5)°. The I1-Pt-I2 angle is 91.31(5)°. The slightly distorted octahedral geometry is exemplified by the *trans* angles I1-Pt-C1 = 177.6(5)°, I2-Pt-S2 = 173.7(1)° and S1-Pt-S3 = 166.2(2)°.

In order to further explore the chemistry of TT[11]MC and to observe the effect that including a different metal atom inside the macrocyclic cavity would have on the reaction chemistry of TT[11]MC complexes, metalation experiments were also carried out using Pd(II).

(ix) Formation of [Pd(TT[11]MC)][BF_4] (8). The reaction of TT[11]MC with one equivalent of $Pd(PhCN)_2Cl_2$ in acetonitrile yields the simple adduct

$Pd(TT[11]MC)Cl_2$ in which two of the three sulfur atoms in TT[11]MC displace the labile benzonitrile ligands in a manner analogous to reaction of $Pd(PhCN)_2Cl_2$ with TT[9]MC[60]. The complex is a bright yellow powder with limited solubility in polar organic solvents such as DMF and DMSO. The ^1H and $^{13}C\{^1H\}$ NMR spectra (d_6-DMSO) are similar to that observed for $Pd(TT[9]MC)Cl_2$ in which coordination in a bidentate fashion results in non-equivalent halves of the macrocycle; separate resonances for all hydrogen and carbon atoms are observed.

Addition of one equivalent of $AgBF_4$ to a suspension of $Pd(TT[11]MC)Cl_2$ in acetonitrile followed by refluxing for 48 h yielded an orange compound which was identified by ^1H and $^{13}C\{^1H\}$ NMR spectroscopy as the palladation product $[Pd(TT[11]MC)][BF_4]$. Reaction of one equivalent each of TT[11]MC, $AgBF_4$ and $Pd(NCPh)_2Cl_2$ in refluxing acetonitrile also yielded the same compound.

The proton resonance for the hydrogen atom on the 2-position of the aromatic ring appearing at 7.43 ppm in the spectrum of the free ligand is absent in the spectrum of the metalated product, and the aromatic region integrates to only 3 hydrogens. The benzylic resonance at 3.70 ppm in the spectrum of the free ligand is split into 2 doublets at 4.71 and 4.31 ppm. This is evidence that inversion of the sulfur atoms has been slowed down in solution by coordination to the palladium. The individual hydrogens on the benzylic carbons are rendered inequivalent on the NMR time scale and as a result couple to each other (Figure 2.13).

Further evidence for the metalation product is found in the $^{13}C\{^1H\}$ NMR spectrum. The resonance for the carbon atom at the 2-position of the aromatic

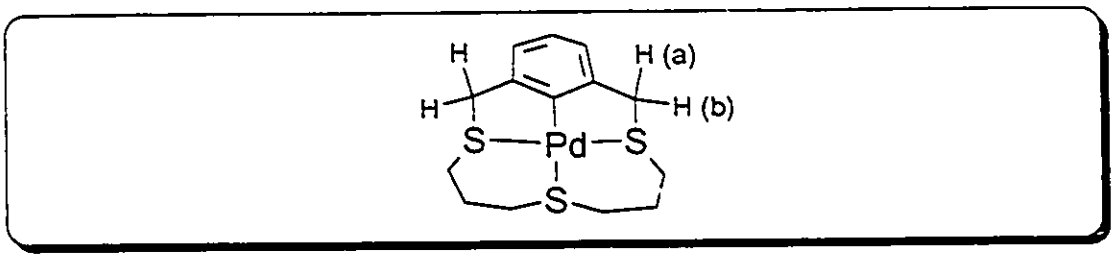

Figure 2.13 Sulfur coordination renders adjacent benzylic H-atoms inequivalent resulting in AB splitting pattern.

ring has a large downfield shift of 165.8 ppm. The resonances for the carbon atoms adjacent to the sulfur atoms are also shifted downfield from their position in the spectrum of the free ligand due to coordination by the adjacent sulfur atoms. The $^{13}C\{^1H\}$ NMR spectrum is consistent with a symmetrical complex in solution by the presence of only 8 peaks: 4 for the aromatic ring and 4 for the 8 aliphatic carbon atoms, in a pattern similar to that for [Pt(TT[11]MC)][BF_4].

The isolation and subsequent metalation of Pd(TT[11]MC)Cl_2 gives information about a possible mechanism of formation of the metalated complex. The macrocycle displaces the solvent ligands from Pd(Sol)$_2Cl_2$ and the $AgBF_4$ most probably reacts in a concerted process with the $PdCl_2$ solvate to remove one of the chloride ligands. The palladium cation then reacts with TT[11]MC to form a third Pd-S bond. This process places the remaining Pd-Cl bond in direct contact with the C-H bond at the 2-position of the aromatic ring (Scheme 2.2). The metalation most likely proceeds via electrophilic aromatic substitution pathway[88], with mass balance requiring the loss of HCl.

In addition to the information outlined above, a crystal structure of the complex was solved and confirmed that the *ortho*-metalated product was indeed

formed[61] (Figure 2.14).

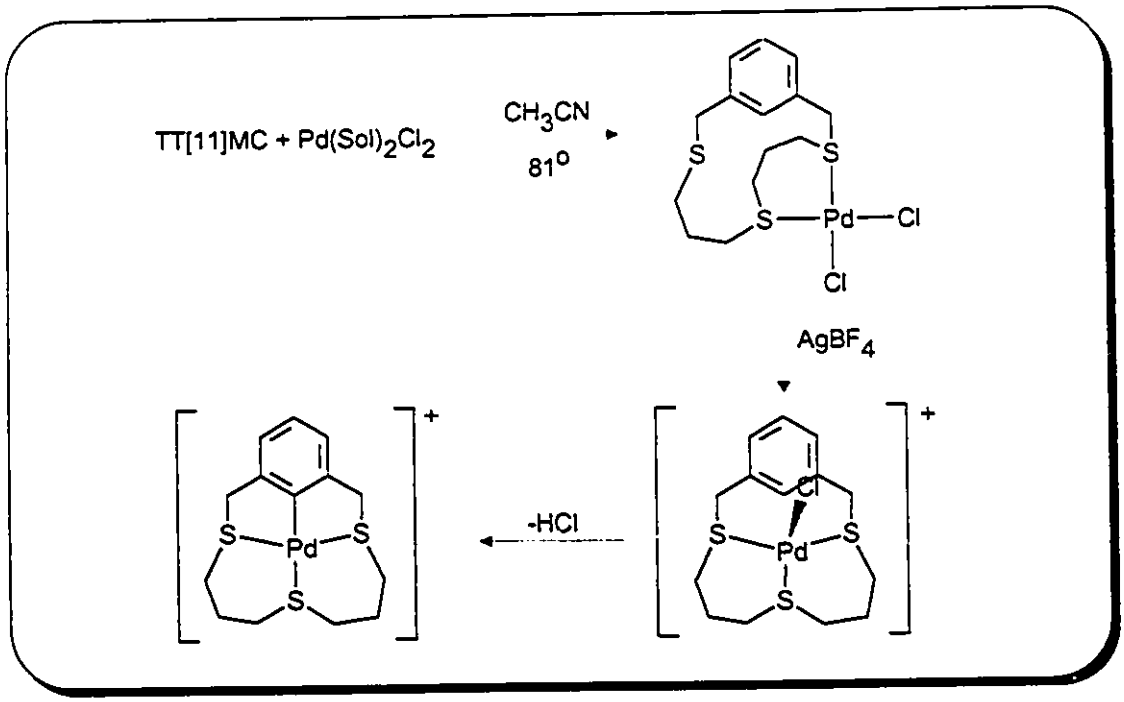

Scheme 2.2 Process of formation of [Pd(TT[11]MC)][BF_4].

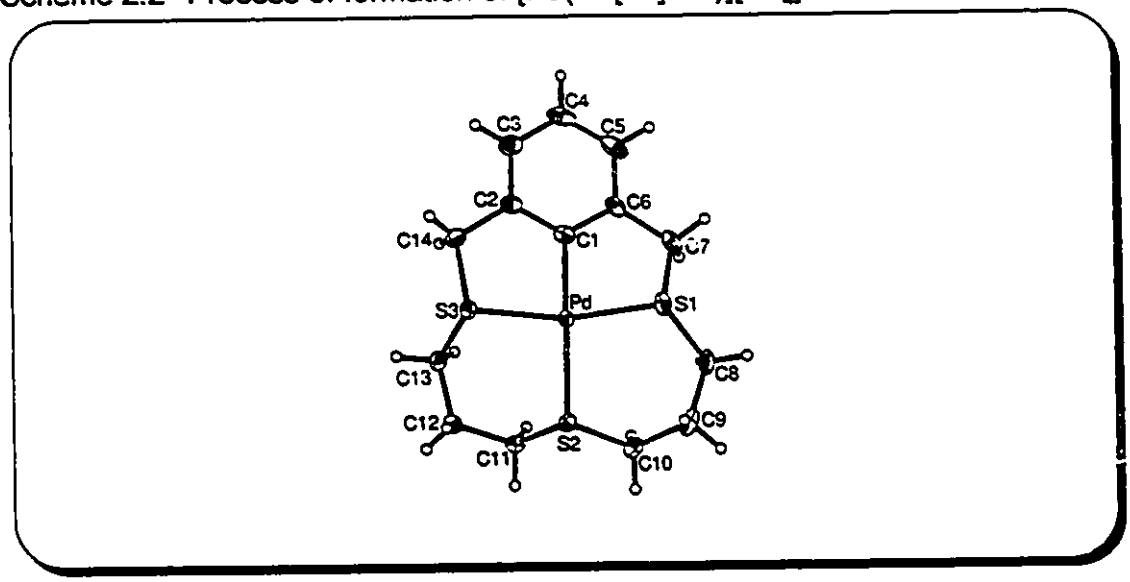

Figure 2.14 Crystal Structure of the $[Pd(TT[11]MC)]^+$ cation.

(x) Comparison of [Pt(TT[11]MC)][BF_4] (4) and [Pd(TT[11]MC)][BF_4] (8). When the ^1H NMR spectra for the palladium and platinum complexes of

TT[11]MC are compared to one another, despite the lack of NMR active isotopic satellites in the spectrum of the palladium complex and some minor chemical shift differences, the two spectra are almost superimposable in a variety of solvents. This is a strong indication that the two complexes are rigid and isostructural in solution.

In comparing the lattice parameters of the crystal structures of [Pd(TT[11]MC)][BF_4] and [Pt(TT[11]MC)][BF_4], it can be seen that there are definite similarities (Table 2.3) demonstrating that the two compounds are isostructural in the solid state as well as in solution.

Table 2.3 Comparison of some X-ray structural parameters for [Pt(TT[11]MC][BF_4] and [Pd(TT[11]MC][BF_4][61, 76].

Compound	[Pd(TT[11]MC)][BF_4]	[Pt(TT[11]MC)][BF_4]
Space Group	$P2_1/c$	$P2_1/c$
a, Å	8.383 (2)	8.373 (1)
b, Å	21.889 (5)	21.784 (7)
c, Å	9.437 (3)	9.517 (4)
β, deg	95.89 (2)	95.09 (2)
V, Å^3	1722.5 (14)	1729.1 (16)

(xi) Reaction Chemistry of [Pd(TT[11]MC)][BF_4], (4). A number of reactions were attempted with [Pd(TT[11]MC)][BF_4] and 2 electron donor groups such as CO, C_2H_4, DMAD, diphenyl acetylene and PPh_2Me. However, only the strongest donor PPh_2Me reacted to give the isolable adduct [Pd(PPh_2Me)-(TT[11]MC)][BF_4]. The ^1H, $^{13}C\{^1H\}$, and $^{31}P\{^1H\}$ NMR spectra all confirm the presence of PPh_2Me and TT[11]MC in this adduct.

Based on a comparison of ^{1}H and $^{13}C\{^{1}H\}$ NMR spectra of the palladated complex and the phosphine adduct (Figure 2.15) it was concluded that the phosphine containing complex is a 5-coordinate Pd(II) adduct with pseudo trigonal bipyramidal geometry. If the sulfur atom had been completely displaced by the phosphine, the resonance for the carbon atoms adjacent to the central sulfur atom would be shifted upfield from 35.1 ppm to about 30 ppm, where

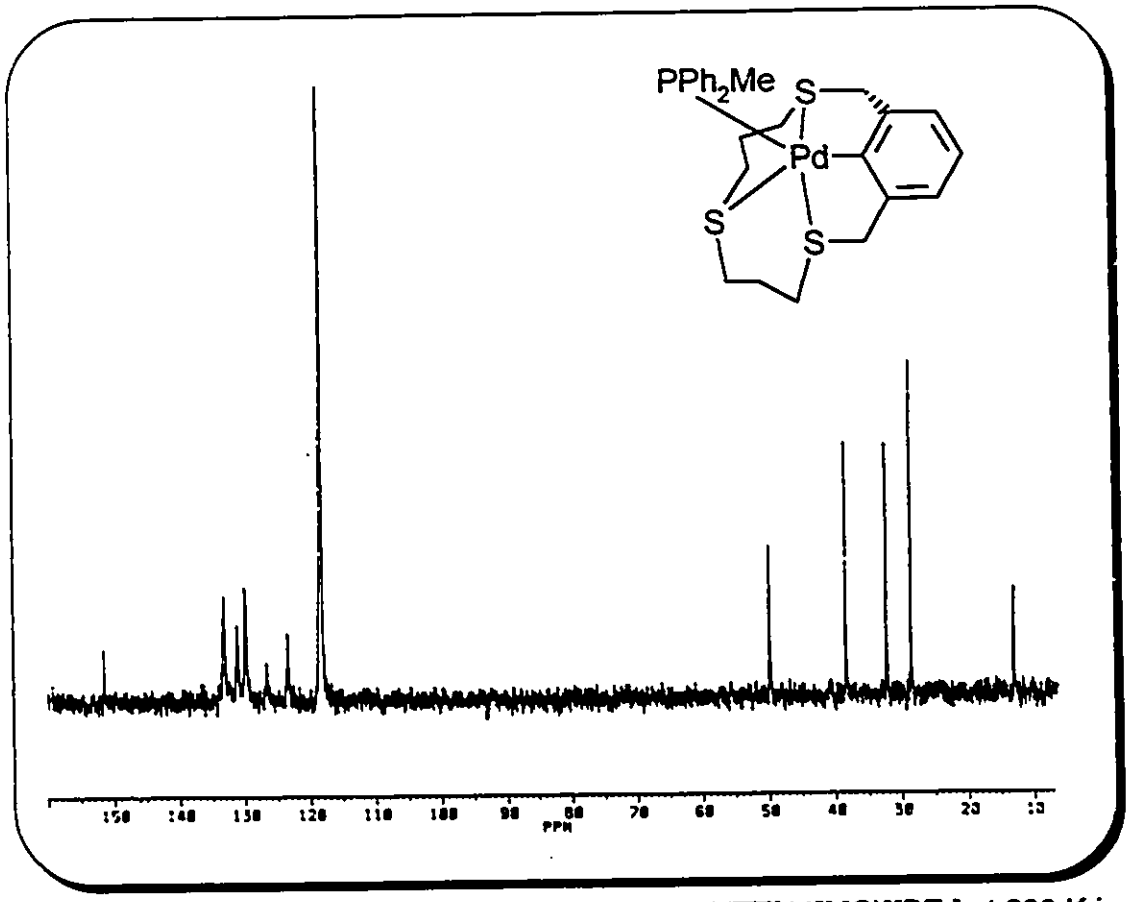

Figure 2.15 $^{13}C\{^{1}H\}$ NMR spectrum of [Pt(PPh_2Me)(TT[11]MC)][BF_4] at 298 K in CD_3CN with inset diagram of the cation.

it appears in the spectra of TT[11]MC and [Pt(PPh_2Me)(TT[11]MC)][BF_4]. Instead the chemical shift observed is 32.2 ppm, consistent with the sulfur atom remaining coordinated to the Pd(II) centre in the presence of PPh_2Me.

Another interesting feature of the $^{13}C\{^1H\}$ NMR spectrum is the chemical shift of the metalated carbon atom. The resonance appears at 169.8 ppm, 4.0 ppm downfield from that [Pd(TT[11]MC)][BF_4], indicating that the carbon atom is deshielded in comparison to [Pd(TT[11]MC)][BF_4]. This can be attributed to π-back bonding from the metal to the phosphine[89] reducing the electron density on the carbon atom. The $^{31}P\{^1H\}$ NMR spectrum exhibits a single resonance at -11.0 ppm, shifted downfield from -27.0 ppm in the spectrum of the free phosphine.

An attempt was also made to oxidize the Pd(II) centre in [Pd(TT[11]MC)][BF_4] to Pd(IV) using $CuCl_2$ as the oxidizing agent. The isolated product was shown, however, to be Pd(TT[11]MC)Cl_2 by NMR spectroscopy. The addition of Cl^- could be easily reversed by addition of one equivalent of $AgBF_4$ to an acetonitrile suspension of the product, regenerating the metalated complex.

Because we were interested in investigating substrates that would not be as strong a donor group as PPh_2Me, the next step in the development of these metalated complexes was to increase the lability of the central donor group in order to increase the reactivity of the complex. The approach taken was to replace the central sulfur atom with a weaker donor, such as an oxygen atom.

(xii) Preparation of 6-oxa-2,10-dithia[11]-*m*-cyclophane, (*pr*-TOMB-1) (13). The method used to make the oxygen containing analogue of TT[11]MC was to employ the Buter and Kellogg ring closure method[28] and react $HS(CH_2)_3O(CH_2)_3SH$ with α,α'-dibromo-*m*-xylene. The 4-oxa-1,7-heptanedithiol

was synthesized (Scheme 2.3) by first reacting 3-bromopropanol with the monosodium salt of 1,3-propanediol to make dipropylene glycol. The dialcohol was then converted to the dithiol by reaction with thiourea in refluxing HCl[81].

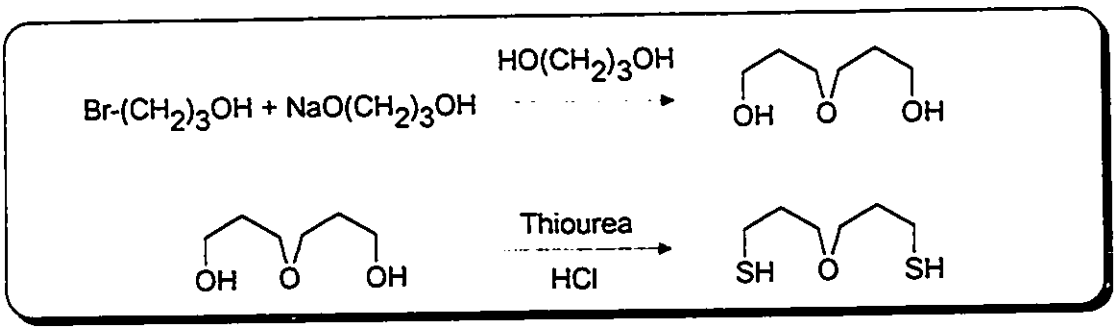

Scheme 2.3 Preparation of 4-oxa-1,7-heptanedithiol.

Reaction of 4-oxa-1,7-heptanedithiol and α,α'-dibromo-*m*-xylene in the presence of two equivalents of Cs_2CO_3 in DMF at 55° C gave the ligand *pr*-TOMB-1 in good yield. The ^1H NMR spectrum of the ligand contains the expected *meta* substitution pattern ranging from 7.29-7.22 ppm for the aromatic hydrogens atoms. The benzylic hydrogens appear as a singlet at 3.64 ppm, the CH_2 group adjacent to the oxygen atom appears as a triplet at 3.38 ppm, the CH_2 group adjacent to the sulfur atoms appears as a triplet at 2.37 ppm and the central CH_2 group in the propylene chain is a multiplet at 1.79 ppm. The $^{13}C\{^1H\}$ NMR spectrum is equally diagnostic with the expected *meta* substitution pattern observed in the aromatic region, a peak at 68.8 ppm for the OCH_2 group and peaks at 34.8 (benzylic), 29.6 (SCH_2) and 25.9 (CH_2) for the remainder of the methylene groups in the macrocycle.

In addition to the NMR evidence outlined above, X-ray quality crystals of the ligand were grown by slow evaporation of a chloroform solution of the ligand and the crystal structure of *pr*-TOMB-1 was determined.

(xiii) Crystal Structure of 6-oxa-2,10-dithia[11]-*m*-cyclophane, (*pr*-TOMB-1), (13). The unit cell is *ortho*rhombic and contains four molecules of *pr*-TOMB-1. A perspective view of the molecule with the atom numbering scheme is shown in Figure 2.16. Complete listings of crystallographic parameters including atomic positions, bonding parameters and details of data collection are collected in Appendix Table A1. Selected bonding parameters are given in the figure caption.

Each asymmetric unit contains one half of the molecule with the other half being related to it by a mirror plane through C1, C4 and O1. As is the case for TT[11]MC, the C(benzylic)-S bonds are perpendicular to the aromatic ring. The remainder of the aliphatic portion of the macrocycle bends back up towards the aromatic ring with the oxygen atom pointed into the macrocyclic cavity. C5-S1 = 1.822(3), S1-C6 = 1.803(3), O1-C8 = 1.409(3). C5-S1-C6 = 101.0(1)°, C8-O1-C8 = 113.9(3)°. All the bond distances are similar to those observed previously for thiacyclophanes and for crown ethers[61, 90]. The torsional angles C2-C5-S1-C6 = 66.9 (3)° and C5-S1-C6-C7 = 73.9 (3)° are both consistent with an exodentate orientation of the sulfur atom. The torsional angle C7-C8-O1-C8^{*80c} = -173.1 (2)° is alternately consistent with an endodentate conformation of oxygen. As observed previously[90], *pr*-TOMB-1 shows a tendancy for sulfur atoms to be exodentate and oxygen atoms to be simultaneously endodentate.

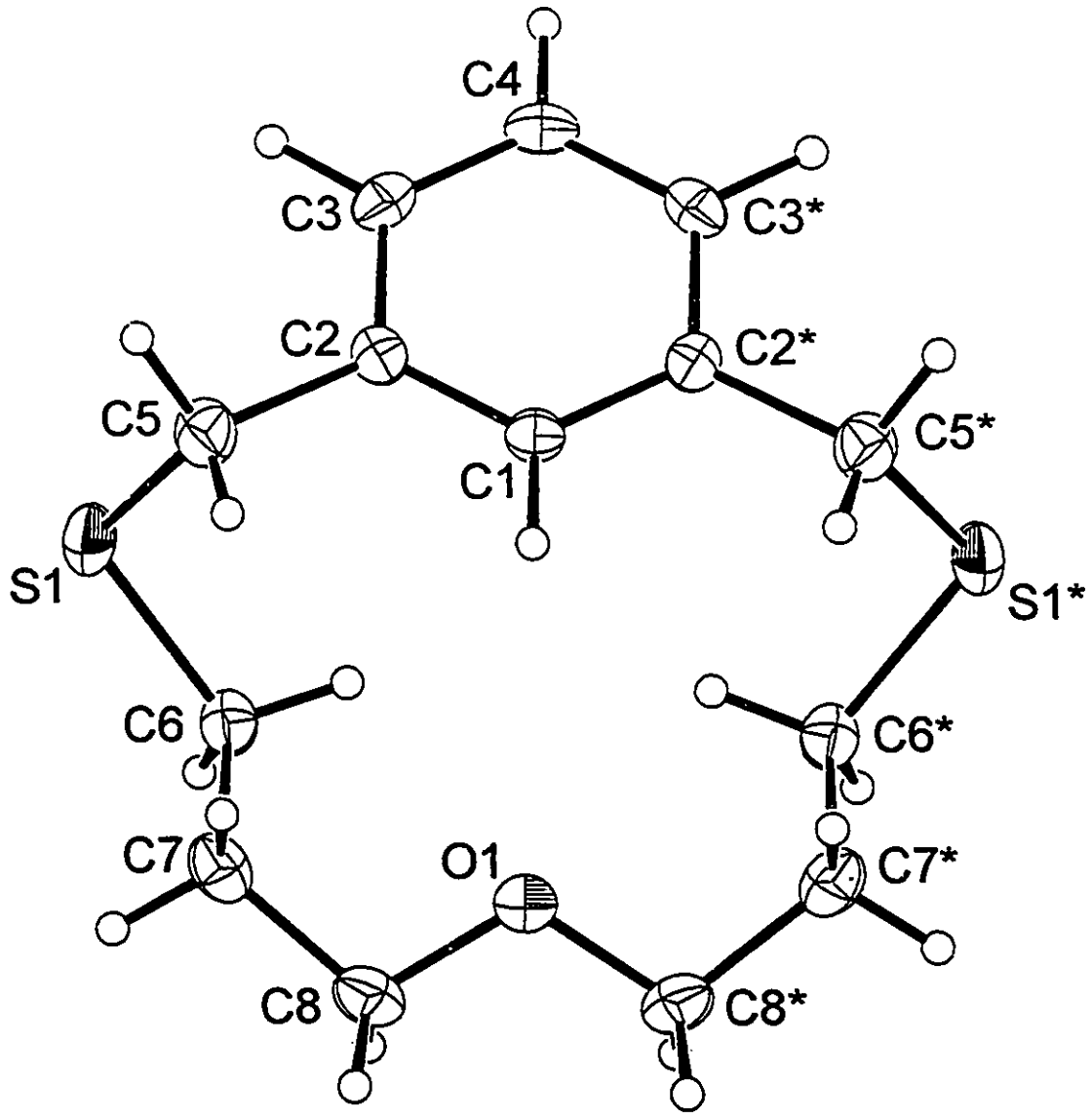

Figure 2.16. Perspective ORTEP drawing of *pr*-TOMB-1 (13) showing the atom numbering scheme with 30% thermal ellipsoids. Selected bond distances (Å) and angles are: C5-S1 = 1.822 (3), S1-C6 = 1.803 (3), O1-C8 = 1.409(3). C5-S1-C6 = 101.0 (1)°, C8-O1-C8 = 113.9 (3)°. C2-C5-S1-C6 = 66.9 (3)°, C5-S1-C6-C7 = 73.9 (3)°, C7-C8-O1-C8* = -173.1 (2)°.

(xiv) Preparation of [Pd(*pr*-TOMB-1)][BF_4], (14). The palladium centre was incorporated into the macrocycle by direct metalation of the aromatic ring employing [Pd(CH_3CN)$_4$][BF_4]$_2$ in acetonitrile solution[88]. Removal of the solvent followed by recrystallization from chloroform or acetonitrile affords the clean product in 72% yield. The complex was characterized by ^{1}H and ^{13}C{^{1}H} NMR spectroscopy. The ^{1}H NMR spectrum contains a multiplet at δ 7.01-6.94 ppm which integrates to 3 H atoms, indicating the loss of the hydrogen atom at the 2-position of the aromatic ring. The benzylic hydrogen atoms have been shifted downfield from δ 3.64 ppm and split into two pairs of doublets at 4.45 and 4.08 ppm, consistent with sulfur coordination to the Pd(II) centre. The remainder of the methylene hydrogen resonances have all been shifted downfield and split into complex multiplets by oxygen coordination to the palladium atom. The ^{13}C{^{1}H} NMR spectrum exhibits resonances at δ 151.7 ppm for the metalated carbon atom, at 70.0 ppm for the oxygen bonded carbon atoms and at 37.2 ppm for the carbon atoms adjacent to the sulfur atoms. Other carbon resonances appear as expected, and both spectra indicated symmetry in the molecule. In addition to the evidence outlined above, crystals of the complex were grown from chloroform and the crystal structure was determined.

(xv) Crystal Structure of [Pd(*pr*-TOMB-1)][BF_4], (14). The unit cell is triclinic and contains two molecules of [Pd(*pr*-TOMB-1)][BF_4] and two molecules of chloroform solvate. A perspective view of the molecule with the atom numbering scheme is shown in Figure 2.17. Complete listings of crystallographic parameters including atomic positions, bonding parameters and details of data

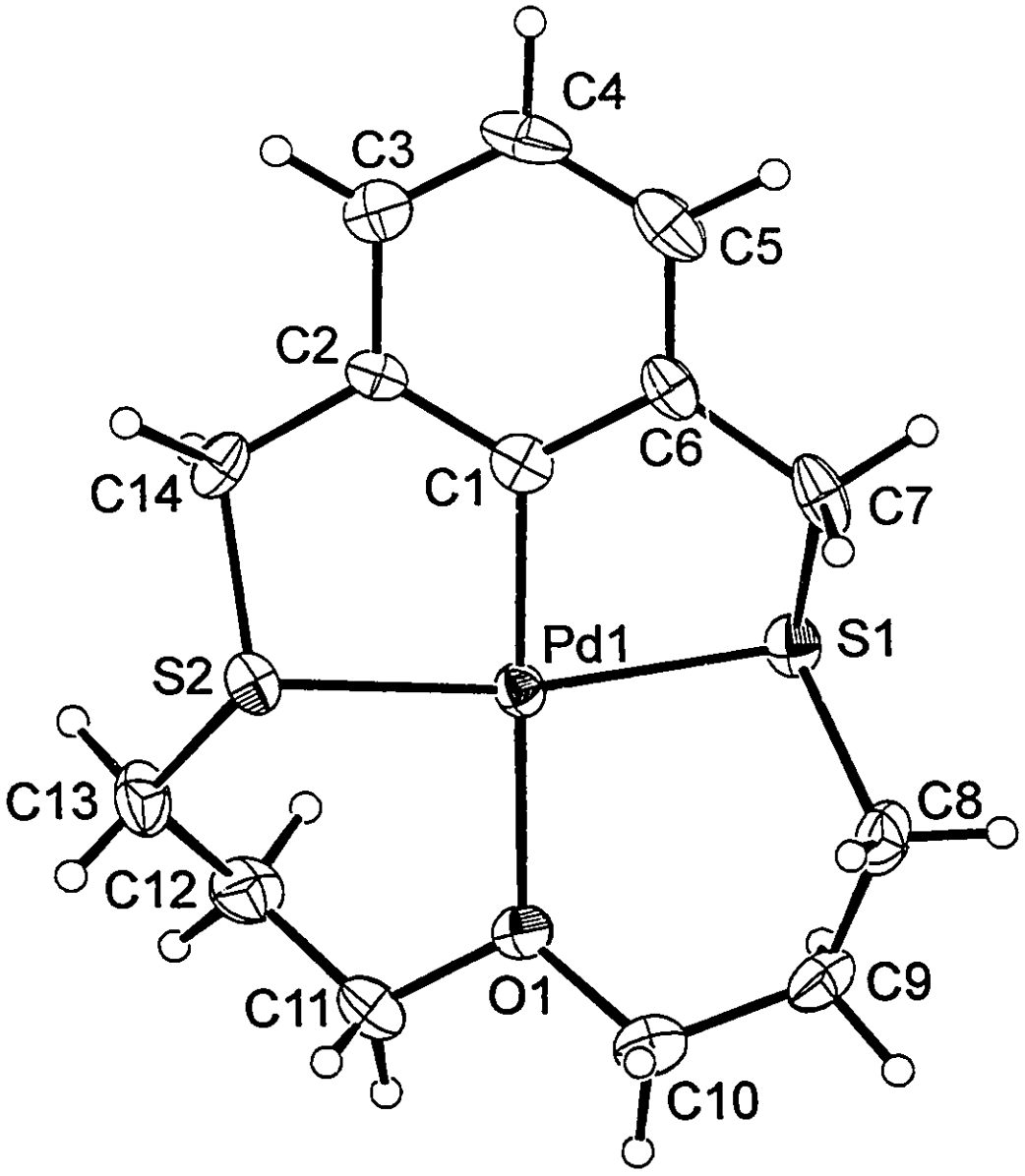

Figure 2.17. Perspective ORTEP drawing of the [Pd(*pr*-TOMB-1)]$^{+}$ (14) cation showing the atom numbering scheme with 30% thermal ellipsoids. Selected bond distances (Å) and angles are: Pd-S1 = 2.286 (2), Pd-S2 = 2.284 (3), Pd-C1 = 1.951 (8), Pd-O1 = 2.119 (5). S1-Pd-C1 = 84.1 (3)°, S2-Pd-C1 = 83.5 (3)°, S1-Pd-O1 = 94.3 (2)°, S2-Pd-O1 = 98.2 (2)°, C1-Pd-O1 = 176.7 (3)°, S1-Pd-S2 = 167.20 (8)°

collection are collected in Appendix Table A2. Selected bonding parameters are given in the figure caption.

The palladium atom is in a square planar environment defined by the two sulfur atoms, the ether oxygen atom and the metalated carbon atom. Pd-S1 = 2.286(2), Pd-S2 = 2.284(3), Pd-C1 = 1.951(8), Pd-O1 = 2.119(5). The Pd-S distances compare well with the mutually trans Pd-S distances in [Pd(TT[11]MC)][BF_4]. The Pd-O distance is significantly shorter than the Pd-S2 distance in [Pd(TT[11]MC)][BF_4]. This shorter bond distance can be explained by the smaller size of oxygen. The O1-C10 and O1-C11 bond distances average 1.44 (1) Å while the S2-C10 and S2-C11 bond distances in [Pd(TT[11]MC)][BF_4] average 1.825 (7) Å. The smaller bond distances 'tighten up' the macrocycle, pulling the oxygen atom closer to the metal centre. The S1-Pd-C1 and S2-Pd-C1 bond angles for the two strained 5-membered chelate rings are 84.1 (3)° and 83.5 (3)° respectively while the 6-membered chelate rings contain bond angles around the palladium of 94.3 (2)° and 98.2 (2)° for S1-Pd-O1 and S2-Pd-O1. There is a slight tetrahedral distortion at Pd as evidenced by the C1-Pd-O1 and S1-Pd-S2 angles of 176.7 (3)° and 167.20 (8)° . The presence of a bond between an ether oxygen and a palladium(II) centre is unusual but can be explained by the chelate/macrocyclic effect placing the donor in close proximity to the metal.

(xvi) Preparation of [Pd(PPh_2Me)(*pr*-TOMB-1)][BF_4], (15). Addition of PPh_2Me to an acetonitrile solution of [Pd(*pr*-TOMB-1)][BF_4] affords the phosphine adduct in moderate yield. The ^1H and $^{13}C\{^1H\}$ NMR spectra both indicate that the phosphine is coordinated to the palladium atom. Multiplets appear centred at δ

7.7 and 7.5 ppm for the aromatic hydrogens on the phosphine and at 7.1 ppm for the aromatic ring of the cyclophane. Doublets at 4.73 and 4.25 ppm for the benzylic hydrogens have been shifted downfield by 0.28 and 0.13 ppm respectively due to the presence of phosphine. The remainder of the chemical shifts arising from the aliphatic chain of the macrocycle are shifted upfield from their position in the spectrum of [Pd(*pr*-TOMB-1)][BF_4], indicating higher electron density on the aliphatic chain. The methyl group on the phosphine appears as a doublet at 2.14 ppm with a $^2J_{P\text{-}H}$=7.4 Hz. The $^{13}C\{^1H\}$ NMR spectrum contains a resonance at δ 171.70 ppm for the metalated carbon atom as well as resonances for the remainder of the aromatic carbon atoms in a pattern similar to that observed for [Pd(PPh_2Me)(TT[11]MC)][BF_4]. The resonance for the carbon atoms adjacent to the oxygen atom appears at 70.99 ppm, the benzylic carbons appear as a doublet at 49.40 ppm with $^3J_{P\text{-}C}$ = 13 Hz, and the remainder of the carbon atoms in the macrocycle appear at 38.14 and 26.46 ppm. The methyl carbon atom on the phosphine appears as a doublet at 13.1 ppm with $^1J_{P\text{-}C}$= 22.1 Hz.

The $^{31}P\{^1H\}$ NMR spectrum contains a single resonance at δ -4.0 ppm. The placement of this peak indicates that the phosphine has completely displaced the oxygen as one would expect. As shown in Table 2.4, coordination to the palladium atom in [Pd(PPh_2Me)(TT[11]MC)][BF_4] results in a chemical shift of -11.2 ppm for the phosphorus atom in the presence of the thioether donor atom. In the absence of the strong thioether donor atom, as in [Pd(PPh_2Me)(*pr*-TOMB-1)][BF_4], the $^{31}P\{^1H\}$ NMR resonance shifts further

Table 2.4 $^{31}P\{^{1}H\}$ NMR Chemical Shifts of PPh_2Me.

Phosphine environment	δ (ppm)
Uncoordinated	-27.0
[Pd(PPh_2Me)(TT[11]MC)][BF_4]	-11.2
[Pd(PPh_2Me)(*pr*-TOMB-1)][BF_4]	-4.0

downfield from -27.0 ppm for the uncoordinated phosphine to -4.0 ppm, indicating that the phosphorus atom is coordinated to a greater extent that it is in the presence of the thioether donor and that the oxygen atom has been completely displaced by the stronger phosphine donor group. In addition, the chemical shift of the metalated carbon atom, which is 171.7 ppm, indicates that the phosphine has completely displaced the ether donor atom. This chemical shift is almost 2 ppm downfield of the same resonance in [Pd(PPh_2Me)(TT[11]MC)][BF_4], indicating that the carbon atom is further deshielded by more efficient π-back bonding to the phosphine from the palladium atom. For this to occur the σ-donation from the phosphine must be more efficient than it was in the TT[11]MC complex.

2.5 Conclusion

The formation of [Pt(TT[11]MC)][BF_4] was found to proceed in good yield by the one pot reaction of one equivalent each of TT[11]MC, Pt(COD)Cl_2 and $AgBF_4$. Substitution reactions with several 2-electron donors were attempted but only the strong donors PPh_3 and PPh_2Me are able to displace the central sulfur atom and only PPh_2Me gives an isolable square planar adduct. Oxidative

addition reactions with the oxidants $CuCl_2$ and I_2 gave the *cis* dihalo-Pt(IV) complexes.

Ortho-metalation of TT[11]MC with $Pd(PhCN)_2Cl_2$ in the presence of $AgBF_4$ was found to proceed in good yield to form the complex $[Pd(TT[11]MC][BF_4]$, presumably via an electrophilic substitution mechanism. Substitution reactions with several 2-electron donors were attempted but only the strong donor PPh_2Me was able to displace the central sulfur atom to form the 5-coordinate trigonal bipyramidal adduct $[Pd(TT[11]MC)(PPh_2Me)][BF_4]$. Attempts to oxidize the palladium centre with $CuCl_2$ failed, yielding $Pd(TT[11]MC)Cl_2$.

Replacement of the central sulfur donor atom in TT[11]MC with a weaker oxygen donor to make *pr*-TOMB-1 followed by metalation gave the palladation product $[Pd(pr\text{-}TOMB\text{-}1)][BF_4]$. PPh_2Me was shown to fully displace the weaker oxygen donor in comparison to $[Pd(TT[11]MC)][BF_4]$ to form the square planar complex $[Pd(pr\text{-}TOMB\text{-}1)(PPh_2Me)][BF_4]$.

Chapter 3

Preparation of Receptors

Chapter 3

3.1 Introduction

(i) Thought Process. In the previous chapter, two approaches were taken to increase the affinity of the metalated complexes for ancillary ligands, or substrates as they will commonly be referred to. The first was to change the metal atom from platinum to palladium, which resulted in less strongly coordinated PPh_2Me in $[Pd(PPh_2Me)(TT[11]MC)][BF_4]$ in comparison to that in $[Pt(PPh_2Me)(TT[11]MC)][BF_4]$. The second was to replace the central thioether donor in TT[11]MC with a weaker donor oxygen atom, which resulted in more strongly coordinated PPh_2Me in $[Pd(pr\text{-}TOMB\text{-}1)(PPh_2Me)][BF_4]$ in comparison to $[Pd(TT[11]MC)(PPh_2Me)][BF_4]$. To further increase the ability of the 'receptors' outlined in this work to bind substrates, a third approach was taken.

The metalation and formation of four fused 5-membered chelate rings was shown to be precluded in TT[9]MC[60]. Although the central sulfur atom in this ligand is as good a donor as the two thioethers in the S_2C bracket, the ligand prefers to coordinate in a bidentate *cis* fashion rather than ortho-metalate and endure the strain imposed by four 5-membered chelate rings. In addition, oxygen has already been shown to be a weaker donor for palladium than sulfur (vide supra), as one would expect. We, therefore, reasoned that placing oxygen atoms within the aliphatic chain and arranging them in such a way that they would be forced to form 5-membered S-Pd-O chelate rings would create very labile Pd-O bonds. The interaction of the oxygen atom(s) with the palladium would not,

however, interfere with the *trans* coordination of the bracket sulfur atoms necessary for the metalation reaction, as the central sulfur atom did in TT[9]MC.

Towards this end the macrocyclic mixed thioether/ether ligands 5-Oxa-2,8-dithia[9]-*m*-cyclophane (TOMB-1), 5,8,11-Trioxa-2,14-dithia[15]-*m*-cyclophane (TOMB-3) and 5,8,11,14,17-pentaoxa-2,20-dithia[21]-*m*-cyclophane (TOMB-5), along with the oxygen deficient model ligand 2,14-Dithia[15]-*m*-cyclophane (TOMB-0), were synthesized and subsequently metalated yielding the four receptors shown in Figure 3.1.

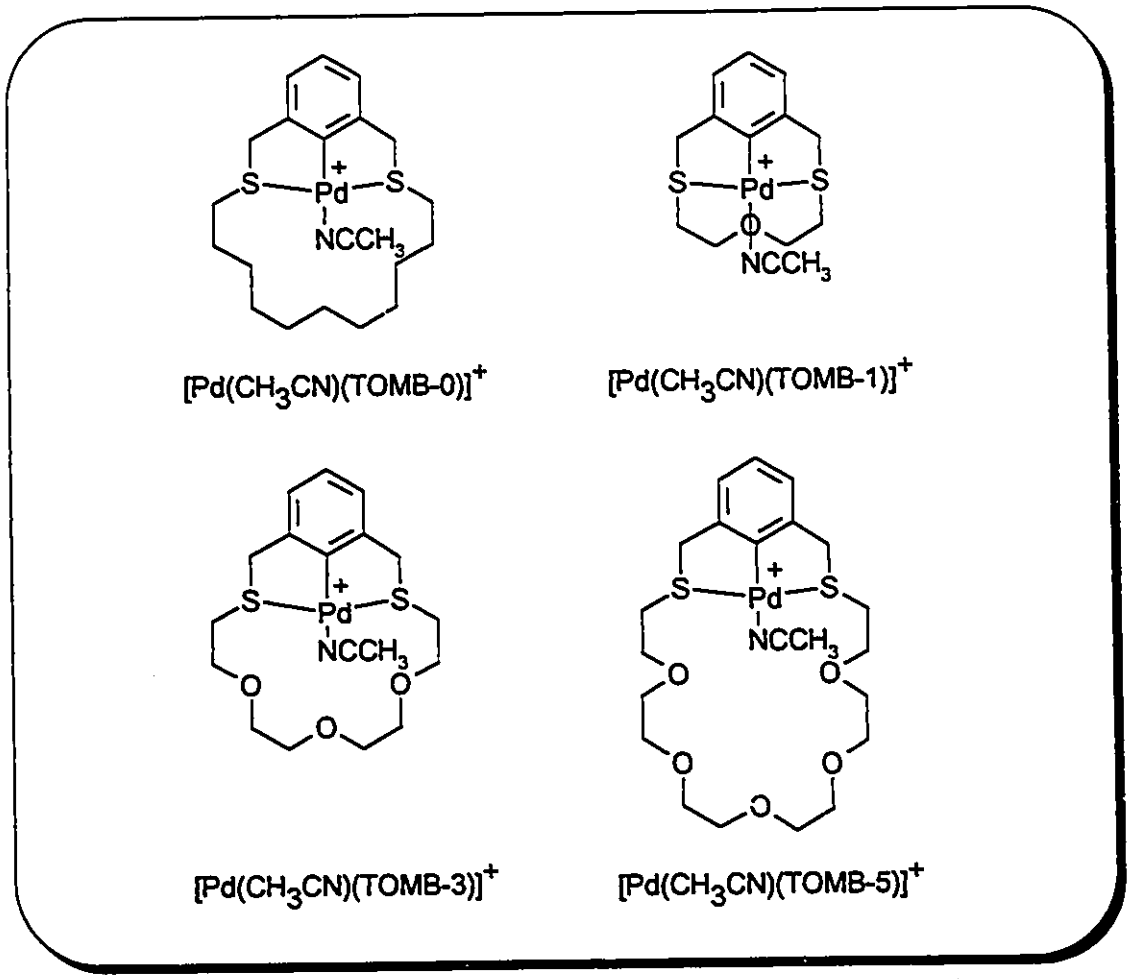

Figure 3.1 Schematic diagrams of the four $[Pd(CH_3CN)(TOMB\text{-}0)]^+$, $[Pd(CH_3CN)(TOMB\text{-}1)]^+$, $[Pd(CH_3CN)(TOMB\text{-}3)]^+$ and $[Pd(CH_3CN)(TOMB\text{-}5)]^+$ cationic receptors.

The metalated ligands, or 'receptors', were designed to incorporate a Lewis acidic metal centre readily available for dative bonds, and ether oxygens available as simultaneous hydrogen-bond acceptors.

(ii) Background Literature. There have been several examples of systems incorporating metal centres for ligand to metal coordination, and ancillary frameworks for weaker secondary interactions. Among these is tetrakis-(μ-acetoxylato)dirhodium (II)[91] shown in Figure 3.2. The rhodium centres can accept coordination bonds and the acetoxy oxygens are available as hydrogen-bond acceptors.

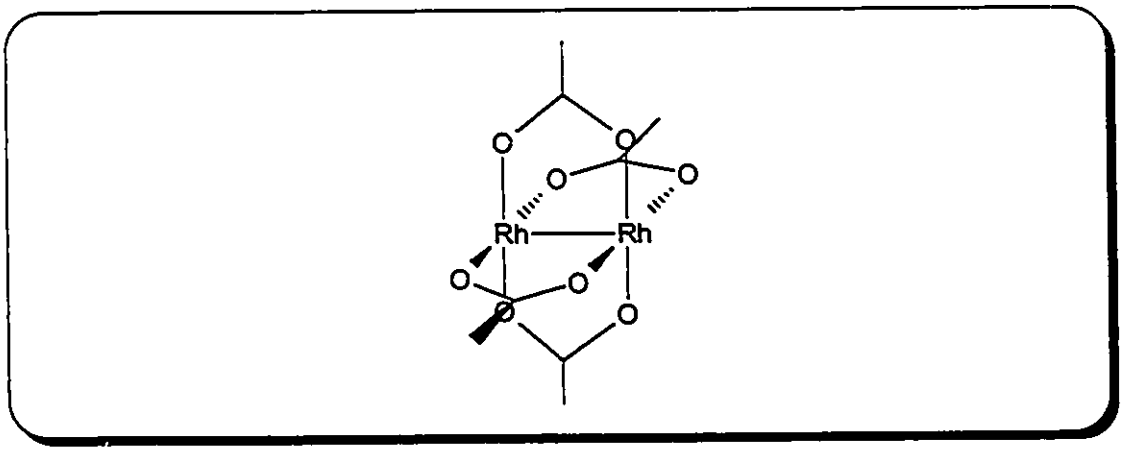

Figure 3.2 Structure of tetrakis-(μ-acetoxylato)dirhodium (II).

There have also been examples of receptor molecules with various secondary groups attached to porphyrins[92]. These include research done by Ogoshi and co-workers, as shown below in Figure 3.3.

Elegant work from the Kimura laboratory[93] utilizes N-H hydrogens and a pendant-arm acridine group (Figure 3.4) available for secondary interactions with complimentary substrates, along with a readily available metal coordination site.

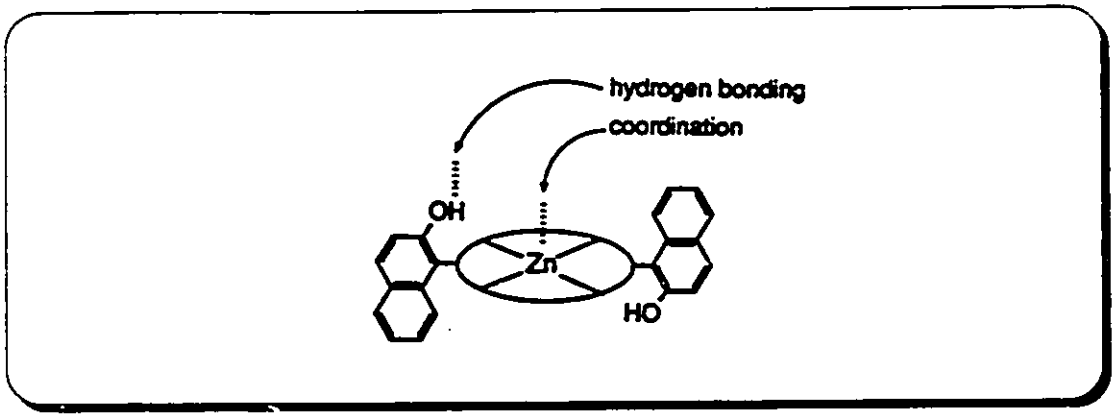

Figure 3.3 Ogoshi's porphyrin receptor containing coordination site and hydrogen bond donors.

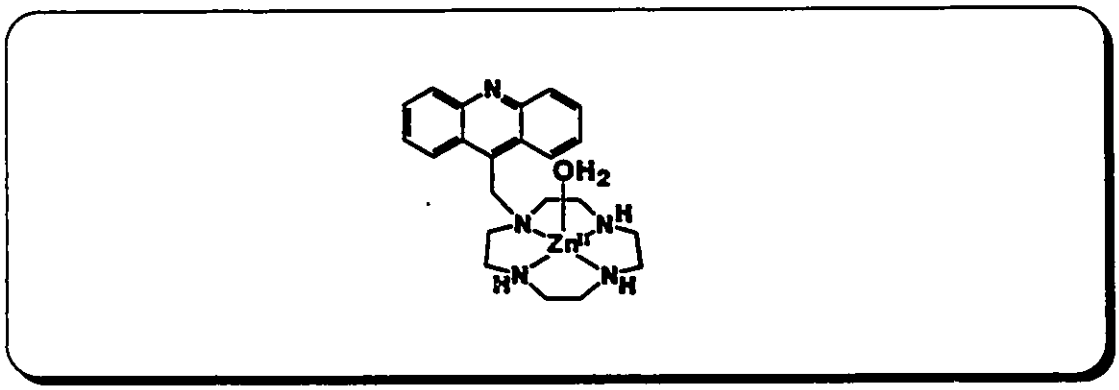

Figure 3.4 Kimura's Zn(II)-cyclen receptor with pendant arm acridine group and N-H hydrogens for secondary interactions with substrates.

Manfred Reetz and coworkers have synthesized a number of receptor molecules containing a Lewis acidic boron atom as an anion receptor and a polyether macrocyclic chain for simultaneous complexation of either cationic metal ions or ammonium ions[94].

Interesting results relevant to this dissertation has been produced by the Reinhoudt lab[95]. Their systems incorporate large polyether chains for hydrogen-bonding and a *N,N'*-ethylenebis(salicylideneaminato) moiety for the complexation of metal centres such as Ni(II) and UO_2 as shown in Figure 3.5.

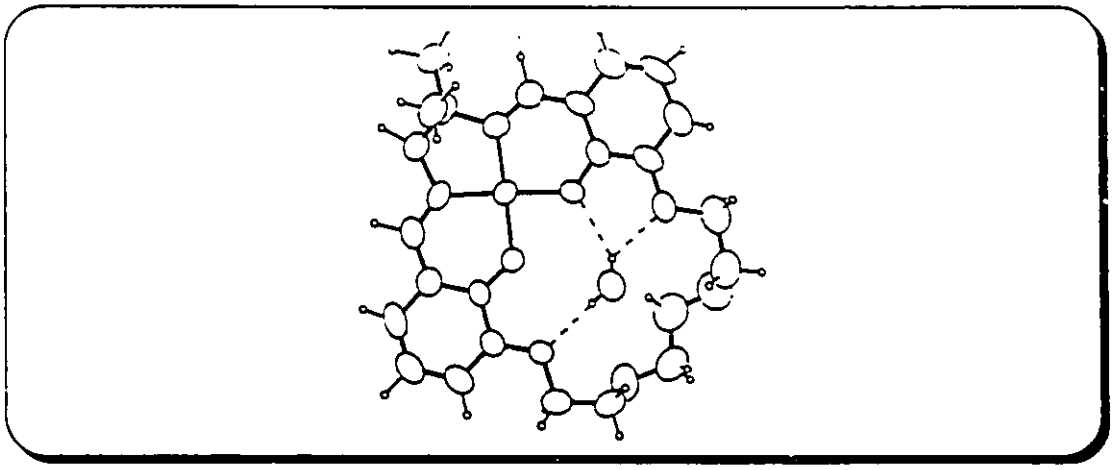

Figure 3.5 Reinhoudt's receptor molecule with a Ni(II) centre as the Lewis acid and polyether chains as hydrogen-bond acceptors.

Lehn and others have synthesized receptor molecules containing an X_2N bracket[96]. The bracket is linked to an azacrown ether creating a 'lateral macrobicyclic cryptand' with a soft chelating unit (the bracket) and a polyether unit for interaction with hydrogen-bond donors or hard metal centres (Figure 3.6).

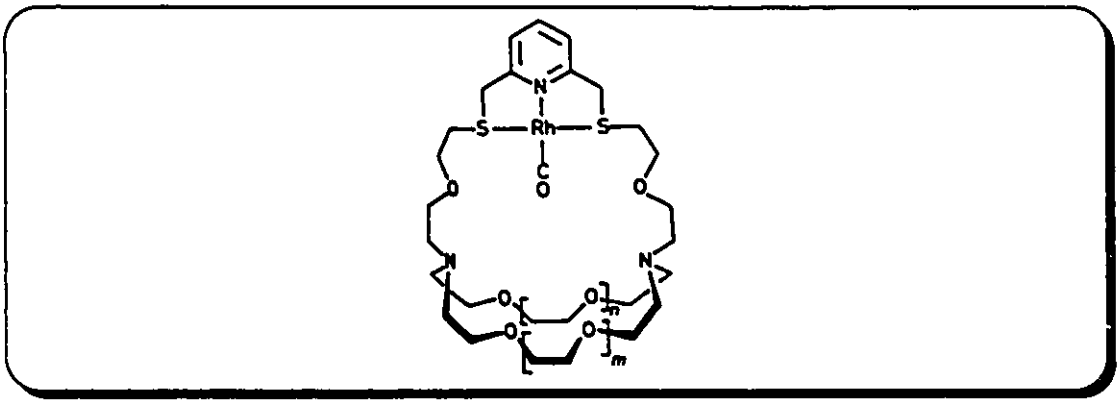

Figure 3.6 Lehn's cryptand containing soft and hard donor sets.

Several years ago Fritz Vogtle and co-workers synthesized a large series of ligands[97] of the general form shown in Figure 3.6a. Included in this series are the two ligands TOMB-1 and TOMB-3, shown in Figure 3.7b,c.

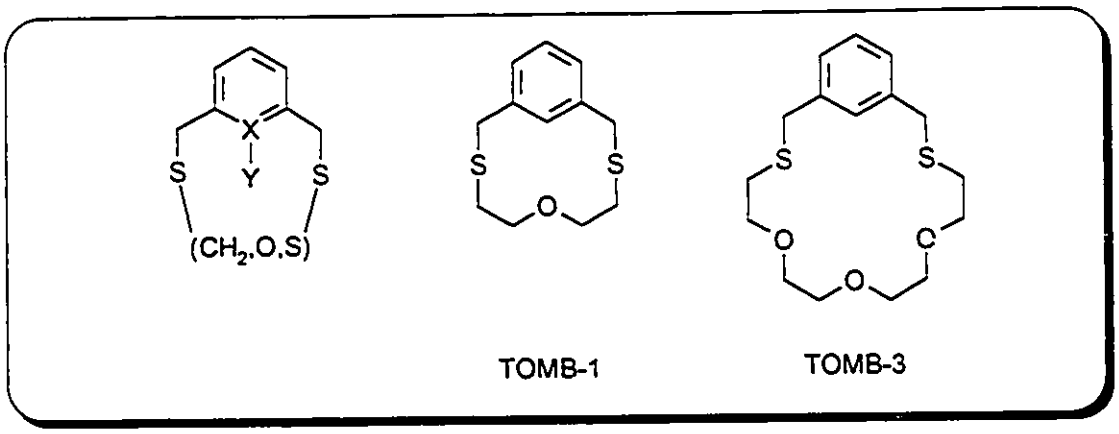

Figure 3.7 a) General form of ligands synthesized in the Vogtle lab. b) TOMB-1 and c) TOMB-3.

Systems closely related to the ones discussed in this dissertation[98] have been synthesized by Loeb's lab[99] and others[100]. The receptor molecules contain a metal centre available for dative bonding, a polyether chain for hydrogen-bonding and aromatic rings for π- stacking of substrates (Figure 3.8).

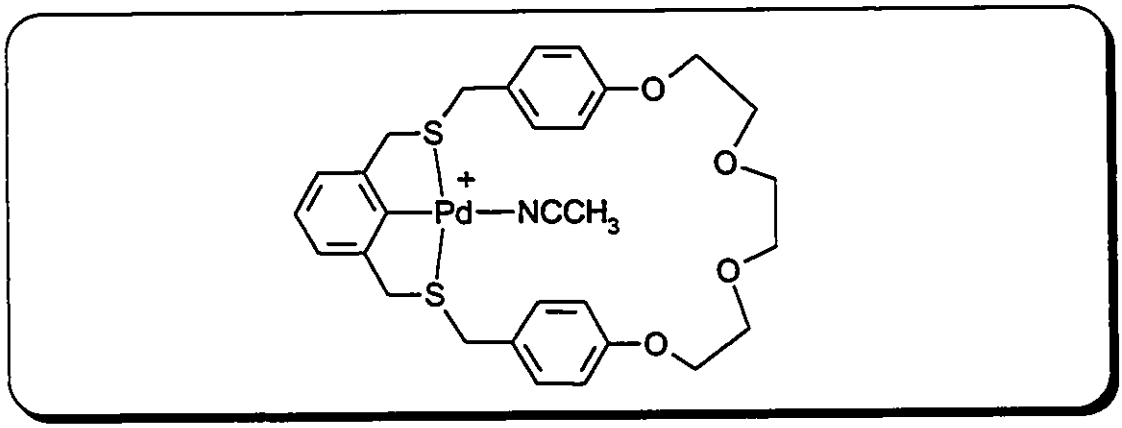

Figure 3.8 Receptor molecule synthesized by Loeb *et al*, containing a metal centre, hydrogen-bond acceptors and π-stacking units.

Part of the work described in this chapter has been previously described by us[101].

3.2 Experimental

General Comments. All starting materials, deuterated solvents and anhydrous N,N'-dimethylformamide (DMF) were purchased from Aldrich Chemicals and used without further purification. Acetonitrile was distilled from CaH_2 under N_2(g). All reactions were performed under an atmosphere of N_2(g) using standard Schlenk techniques and all solvents and liquid starting materials were degassed prior to use. ^1H and $^{13}C\{^1H\}$ NMR spectra were recorded on a Brüker AC300 spectrometer locked to the deuterated solvent at 300.1 and 75.5 MHz respectively, and infrared spectra were recorded on a Nicolet 5DX FTIR spectrometer. Elemental analyses were performed by Canadian Microanalytical Service, Delta, British Columbia.

(i) Preparation of 2,14-Dithia[15]-*m*-cyclophane, (TOMB-0), (16). To a suspension of Cs_2CO_3 (7.274 g, 22.3 mmol) in DMF (500 mL) at 60 °C, was added a solution of 1,11-dibromo-undecane (3.500 g, 11.1 mmol) and *m*-xylene-α,α'-dithiol (1.900 g, 11.2 mmol) in DMF (120 mL) over 24 h. Upon completion of the slow-addition, the suspension was cooled for 2 h and the DMF removed *in vacuo* leaving a brown oil and cesium salts. The oil was dissolved in CH_2Cl_2 (200 mL), filtered and washed with 0.1 M NaOH (2 x 50 mL) and distilled water (50 mL). The solution was dried over anhydrous $MgSO_4$ for 3 h, filtered, and the CH_2Cl_2 reduced to 25 mL. This solution was then added to boiling anhydrous ethanol (250 mL) which was cooled to -10 °C, filtered, and the resulting solid dried *in vacuo*. Crude yield: 2.679 g (75 %). Further purification was accomplished by concentrating a petroleum ether solution of TOMB-0 and

stirring it over silica gel (10g, 70-230 mesh, 60 Å) for 0.5 h, filtering and then evaporating the solution to dryness. Yield: 2.179 g (61 %); m.p. 27 °C. ^{1}H NMR ($CDCl_3$): δ (ppm) 7.25-7.19 (m, 4H, aromatic), 3.68 (s, 4H, benzylic), 2.39 (t, 4H, SCH_2), 1.45 (q, 4H , β-CH_2), 1.32 (q, 4H, γ-CH_2), 1.25 (s br, 10H, CH_2). $^{13}C\{^{1}H\}$ NMR ($CDCl_3$): δ (ppm) 138.77, 129.23, 128.78, 127.38 (aromatic), 36.16 (benzylic), 30.98 (SCH_2), 28.50, 27.52, 27.12, 26.84 (CH_2). Anal. Calcd. for $C_{19}H_{30}S_2$: C, 70.37; H, 9.39. Found: C, 71.68; H, 9.39.

(ii) Preparation of 5-Oxa-2,8-dithia[9]-*m*-cyclophane, (TOMB-1), (17). To a suspension of Cs_2CO_3 (4.756 g, 14.59 mmol) in DMF (350 mL) at 56 °C was added a solution of 3-oxapentane-1,5-dithiol (0.965 g, 6.98 mmol) and α,α'-dibromo-*m*-xylene (1.839 g, 6.97 mmol) in DMF (140 mL) over 36 h. The solution stirred for an additional 8 h at 56 °C after which the DMF was removed *in vacuo* leaving a brown oil and cesium salts. The residue was dissolved in CH_2Cl_2 (200 mL), filtered, and washed with 0.1 M NaOH (2 x 50 mL) and distilled water (50 mL). The solution was stirred over anhydrous $MgSO_4$/charcoal for 12 h, filtered twice, the solvent evaporated, and the white solid dried *in vacuo*. Yield: 1.114 g (66 %); m.p. 46 °C. ^{1}H NMR ($CDCl_3$): δ (ppm) 7.61 (s, 1H, aromatic), 7.31-7.17 (m, 3H, aromatic), 3.76 (s, 4H, benzylic), 2.98 (t, 4H, CH_2O), 2.55 (t, 4H, SCH_2). $^{13}C\{^{1}H\}$ NMR ($CDCl_3$): δ (ppm) 138.61, 130.26, 129.20, 127.87 (aromatic), 67.63 (CH_2O), 37.04 (benzylic), 29.82 (SCH_2). Anal. Calcd. for $C_{12}H_{16}OS_2$: C, 59.95; H, 6.72. Found: C, 59.84; H, 6.72.

(iii) Preparation of 5,8,11-Trioxa-2,14-dithia[15]-*m*-cyclophane, (TOMB-3), (18). To a suspension of Cs_2CO_3 (3.790 g, 11.6 mmol) in DMF (250 mL), at 62 °C, was added a solution of *m*-xylene-α,α'-dithiol (0.960 g, 5.64 mmol) and tetraethylene glycol di-*p*-tosylate (2.833 g, 5.64 mmol) in DMF (125 mL) over 48 h. After the slow addition was complete, the DMF was removed *in vacuo* leaving a brown oil and cesium salts. The residue was dissolved in CH_2Cl_2 (200 mL), filtered, washed with 0.1 M NaOH (2 x 50 mL) and distilled water (50 mL) and then dried over anhydrous $MgSO_4$/charcoal for 3 h. The solution was then filtered and the CH_2Cl_2 evaporated to dryness *in vacuo*. Column chromatography using 50/50 petroleum ether/diethyl ether as eluent (R_f = 0.30) and 40 g of (70-230 mesh 60 Å) silica gel gave a white solid upon evaporation of the solvent. Yield: 1.110 g (60 %); m.p. 53 °C. ^1H NMR ($CDCl_3$): δ (ppm) 7.33 (s, 1H, aromatic), 7.29-7.21 (m, 3H, aromatic), 3.81 (s, 4H, benzylic), 3.67-3.58 (m, 12H, CH_2O), 2.51 (t, 4H, SCH_2). $^{13}C\{^1H\}$ NMR ($CDCl_3$): δ (ppm) 138.41, 130.82, 129.23, 127.51 (aromatic), 72.13, 70.92, 70.37 (CH_2O), 36.22 (benzylic), 29.59 (SCH_2). Anal. Calcd. for $C_{16}H_{24}O_3S_2$: C, 58.49; H, 7.38. Found: C, 58.46; H, 7.34.

(iv) Preparation of 1,17-dichloro-3,6,9,12,15-pentaoxaheptadecane, (19). To a solution of $SOCl_2$ (8.7 g, 73 mmol) in 100 mL of CH_2Cl_2 was added a solution of hexaethylene glycol (10.015 g, 35.5 mmol) and pyridine (5.9 g, 74 mmol) in CH_2Cl_2 (100 mL) over a 4h period. The solvent was reduced to 75 mL and the solution was washed with water (25 mL), 0.1 M HCl (25 mL) and water (25 mL) and then dried over $MgSO_4$ overnight. The solution was filtered and the

solvent was removed leaving a yellow oil which was vacuum distilled. Yield: 9.143 g (81%). ^{1}H NMR ($CDCl_3$): δ (ppm) 3.73 (t, 4H, OCH_2), 3.64 (s br, 16 H, OCH_2), 3.60 (t, 4H, CH_2Cl). $^{13}C\{^1H\}$ NMR ($CDCl_3$): δ (ppm) 71.45 (OCH_2), 70.77, 70.71 (OCH_2), 42.81 (CH_2Cl).

(v) Preparation of 5,8,11,14,17-pentaoxa-2,20-dithia[21]-*m*-cyclophane, (TOMB-5), (20). To a suspension of Cs_2CO_3 (7.718 g, 23.7 mmol) in DMF (500 mL), at 56 °C, was added a solution of *m*-xylene-α,α'-dithiol (1.977 g, 11.6 mmol) and 1,17-dichloro-3,6,9,12,15-pentaoxaheptadecane (3.705 g, 11.6 mmol) in DMF (115 mL) over 36 h. After the slow addition was complete, the DMF was removed *in vacuo* leaving a brown oil and cesium salts. The residue was dissolved in CH_2Cl_2 (200 mL), filtered, washed with 0.1 M NaOH (2 x 50 mL) and distilled water (50 mL) and then dried over anhydrous $MgSO_4$ overnight. The solution was then filtered and the CH_2Cl_2 evaporated to dryness *in vacuo*. Column chromatography using diethyl ether as eluent (R_f = 0.30) and 60 g of silica gel (70-230 mesh 60 Å) gave a clear oil upon evaporation of the solvent. Yield: 1.448 g, (30%). ^{1}H NMR ($CDCl_3$): δ (ppm) 7.26-7.15 ppm (m, 4H, aromatic), 3.74 (s, 4H, benzylic), 3.63-3.51 (m, 20H, OCH_2), 2.56 (t, ^{3}J=6.7 Hz, 4H, SCH_2). $^{13}C\{^1H\}$ NMR ($CDCl_3$): δ (ppm) 138.81, 129.65, 128.91, 127.67 (aromatic), 71.10, 70.80, 70.45, 70.35 (OCH_2), 36.54 (benzylic), 30.50 (SCH_2).

Preparation of Receptor Complexes. In a typical metalation reaction, one equivalent each of $[Pd(CH_3CN)_4][BF_4]_2$ and TOMB-X (X=0,1,3,5) were added to a Schlenk flask (100 mL) and dissolved in *ca.* 40 mL of dry CH_3CN with stirring.

Within 5-10 minutes, the solution changed colour from orange to pale yellow. The solution was then refluxed for 2-12 h. Upon cooling, the solution was concentrated to 3-5 mL and the complex crystallized by vapour diffusion of diethyl ether into the CH_3CN solution of the complex.

(vi) Preparation of [Pd(TOMB-0)(CH_3CN)][BF_4], (21). $[Pd(CH_3CN)_4][BF_4]_2$ (0.162 g, 0.366 mmol), TOMB-0 (0.117 g, 0.363 mmol). Yield of pale yellow crystals: 0.180g (89 %). ^1H NMR ($CDCl_3$): δ (ppm) 7.04-6.93 (m, 3H, aromatic), 4.35 (d, 2H, benzylic, J = 16.0 Hz), 4.06 (d, 2H, benzylic), 3.05 (m, 4H, SCH_2), 2.38 (s br, 3H, CH_3CN), 1.96 (m, 4H, β-CH_2), 1.62-1.18 (m, 14H, CH_2). Anal. Calcd. for $C_{21}H_{32}BF_4NPdS_2$: C, 45.37; H, 5.81. Found: C, 45.01; H, 5.75.

(vii) Preparation of [Pd(TOMB-1)(CH_3CN)][BF_4], (22). $[Pd(CH_3CN)_4][BF_4]_2$ (0.185 g, 0.416 mmol), TOMB-1 (0.103 g, 0.429 mmol). Yield of deep orange crystals: 0.117 g (60 %). ^1H NMR ($CDCl_3$): δ (ppm) 7.01-6.92 (m, 3H, aromatic), 4.49 (d, 2H, benzylic, J = 17.0 Hz), 4.11 (d, 2H, benzylic), 3.95 (dt, 2H, CH_2O), 3.54-3.40 (m, 4H, SCH_2CH_2O), 2.89 (td, 2H, SCH_2). $^{13}C\{^1H\}$ NMR (CD_3CN): δ (ppm) 157.04 (Pd-C, aromatic), 154.60, 125.72, 122.88 (aromatic), 67.39 (CH_2O), 45.06 (benzylic), 24.96 (SCH_2).

(viii) Preparation of [Pd(TOMB-1)(CH_3CN)][CF_3SO_3], (23). $PdCl_2$ (0.091 g, 0.513 mmol) and [Ag][CF_3SO_3] (0.127 g, 1.05 mmol) were dissolved in dry CH_3CN (30 mL) and protected from light. The solution was refluxed for 1 h and then filtered from the AgCl precipitate onto TOMB-1 (0.127 g, 0.528 mmol). The resulting solution was then refluxed for 2 h. A floculent white precipitate was filtered from a yellow solution and the solvent reduced to 5 mL. The product was

crystallized by vapour diffusion of diethyl ether into a CH_3CN solution of the complex. Yield of deep orange crystals: 0.168 g (61 %). ^1H NMR and $^{13}C\{^1H\}$ NMR (CD_3CN, 295 K) were identical to that found for $[Pd(L^1)(CH_3CN)][BF_4]$. Anal. Calcd. for $C_{15}H_{18}F_3NO_4PdS_3$: C, 33.62; H, 3.39. Found: C, 33.84; H, 3.49.

(ix) Preparation of [Pd(TOMB-3)Cl], (24). $[PdCl_2(PhCN)_2]$ (0.227 g, 0.592 mmol), $[Ag][CF_3SO_3]$ (0.171 g, 0.667 mmol) and TOMB-3 (0.194 g, 0.591 mmol) were dissolved in CH_3CN (50 mL). The yellow solution was refluxed for 48 h, cooled, filtered from a yellow precipitate, and the solvent was removed in vacuo. The orange residue was dissolved in acetonitrile (10 mL) and diffusion of diethyl ether into this solution gave [Pd(TOMB-3)Cl] as a yellow crystalline solid. Yield: 0.179 g (64%). ^1H NMR (CD_3CN): δ (ppm) 6.98 (m, 3H, aromatic), 4.41 (s, 4H, benzylic), 4.06 (s, br, 4H, OCH_2CH_2S), 3.58 (s, 4H, OCH_2CH_2O), 3.51 (s, 4H, OCH_2CH_2O), 3.20 (s, br, 4H, SCH_2CH_2O). $^{13}C\{^1H\}$ NMR (CD_3CN): δ(ppm) 155.89, (aromatic, Pd-C), 151.68, 126.33, 123.49 (aromatic), 72.22, 71.20, 71.11 (CH_2O), 45.05 (benzylic), 38.07 (-SCH_2).

(x) Preparation of [Pd(TOMB-3)(CH_3CN)][BF_4], (25). $[Pd(CH_3CN)_4][BF_4]_2$ (0.272 g, 0.612 mmol), TOMB-3 (0.201 g, 0.612 mmol). Yield of yellow crystals: 0.295 g (86 %). ^1H NMR ($CDCl_3$): δ (ppm) 7.00-6.91 (m, 3H, aromatic), 4.37 (s, 4H, benzylic), 4.09 (s br, 4H, CH_2O), 3.73 (s, 4H, CH_2O), 3.61 (s, 4H, CH_2O), 3.39 (s br, 4H, SCH_2), 2.20 (s, 3H, CH_3CN). Anal. Calcd. for $C_{18}H_{26}BF_4NO_3PdS_2$: C, 38.48; H, 4.67. Found: C, 38.25; H, 4.66

(xi) Preparation of [Pd(TOMB-5)(CH_3CN)][BF_4], (26). $[Pd(NCCH_3)_4][BF_4]_2$ (0.116 g, 2.61×10^{-4} mol), TOMB-5 (0.108 g, 2.59×10^{-4} mol).

Yield of yellow paste: 0.129 g, (82%). ^{1}H NMR ($CDCl_3$): δ (ppm) 6.91 (m, 3H, aromatic), 4.44 (m vbr, 4H, benzylic), 3.93 (s br, 4H, OCH_2), 3.71-3.58 (m br, 16 H, OCH_2), 3.30 (s br, 4H, SCH_2), 2.31 (s, 3H, CH_3CN).

(xii) Preparation of [Pd(CH_3CN)(TOMB-P4)][BF_4], (27). [Pd(CH_3CN)(TOMB-P4)][BF_4] (27) was synthesized by Shannon L. Murphy in partial fulfilment of her fourth year research project and details of the synthesis and crystallization of these compounds can be found in her written report[99].

3.3 X-Ray Diffraction Data Collection, Solution, and Refinement.

(i) General Procedures. The general procedure for data collection and solution refinement is identical to that outlined in section 2.3 (i) and the reader is referred to it for the sake of brevity.

(ii) Structure Determination of 5,8,11-trioxa-2,14-dithia[15]-*m*-cyclophane, TOMB-3, (18). Colourless crystals of TOMB-3 were grown by slow evaporation of a $CDCl_3$ solution of the compound. A statistical analysis of the intensity distributions and a determination of observed extinctions were consistent with the monoclinic space group $P2_1/c$, and this was confirmed by a successful solution refinement. A total of 3214 reflections were collected, and 853 unique reflections with $F_o^2 > 3\sigma(F_o^2)$ were used in the refinement. The positions of the sulfur and oxygen atoms were determined by direct methods from the *E*-map with the highest figure of merit. The remaining carbon atoms were located from a difference Fourier map calculation. In the final cycles of refinement, all atoms were assigned anisotropic thermal parameters. This

resulted in $R = 0.0628$ and $R_w = 0.0441$ at final convergence. The Δ/σ value for any parameter in the final cycle was less than 0.0002. A final difference Fourier map calculation showed no peaks of chemical significance; the largest was 0.292 electron /Å^3 and was associated with the O3 atom. Crystal data, intensity collection and structure refinement as well as all atomic positional parameters, bond distances and angles are summarized in Appendix Table A3.

(iii) Structure Determination of [Pd(CH_3CN)(TOMB-0)][BF_4], (21). Pale yellow crystals of [Pd(CH_3CN)(TOMB-0)][BF_4] were grown by vapour diffusion of diethyl ether into an acetonitrile solution of the compound. A statistical analysis of the intensity distributions and a determination of observed extinctions were consistent with the monoclinic space group C2/c, and this was confirmed by a successful solution refinement. A total of 4703 reflections were collected, and 2959 unique reflections with $F_o^2 > 3\sigma(F_o^2)$ were used in the refinement. The positions of the palladium and sulfur atoms were determined by direct methods from the *E*-map with the highest figure of merit. The remaining carbon atoms were located from a difference Fourier map calculation. In the final cycles of refinement, all atoms were assigned anisotropic thermal parameters. This resulted in $R = 0.0562$ and $R_w = 0.0528$ at final convergence. The Δ/σ value for any parameter in the final cycle was less than 0.04. A final difference Fourier map calculation showed no peaks of chemical significance; the largest was 0.711 electron /Å^3 and was associated with the F1 atom. Crystal data, intensity collection and structure refinement details, as well as all atomic positional parameters, bond distances and angles are summarized in Appendix Table A4.

(iv) Structure Determination of [Pd(CH_3CN)(TOMB-1)][CF_3SO_3], (23). Deep orange crystals of [Pd(CH_3CN)(TOMB-1)][CF_3SO_3] were grown by vapour diffusion of diethyl ether into an acetonitrile solution of the compound. A statistical analysis of the intensity distributions and a determination of observed extinctions were consistent with the monoclinic space group $P2_1/c$, and this was confirmed by a successful solution refinement. A total of 3558 reflections were collected, and 1333 unique reflections with $F_o^2 > 3\sigma(F_o^2)$ were used in the refinement. The positions of the palladium and sulfur atoms were determined by direct methods from the *E*-map with the highest figure of merit. The remaining atoms were located from a difference Fourier map calculation. In the final cycles of refinement, all the heteroatoms and C1 were assigned anisotropic thermal parameters. This resulted in $R = 0.0469$ and $R_w = 0.0407$ at final convergence. The Δ/σ value for any parameter in the final cycle was less than 0.0002. A final difference Fourier map calculation showed no peaks of chemical significance; the largest was 0.566 electron /Å^3 and was associated with the Pd1 atom. Crystal data, intensity collection and structure refinement details, as well as all atomic positional parameters, bond distances and angles are summarized in Appendix Table A5.

(v) Structure Determination of [Pd(TOMB-3)Cl], (24). Yellow crystals of [PdCl(TOMB-3)] were grown by vapour diffusion of diethyl ether into an acetonitrile solution of the compound. A statistical analysis of the intensity distributions and a determination of observed extinctions were consistent with the triclinic space group $P\bar{1}$, and this was confirmed by a successful solution

refinement. A total of 3261 reflections were collected, and 2647 unique reflections with $F_o^2>3\sigma(F_o^2)$ were used in the refinement. The positions of the palladium and sulfur and chlorine atoms were determined by direct methods from the *E*-map with the highest figure of merit. The remaining atoms were located from a difference Fourier map calculation. In the final cycles of refinement, all atoms were assigned anisotropic thermal parameters. This resulted in R = 0.0515 and R_w = 0.0410 at final convergence. The Δ/σ value for any parameter in the final cycle was less than 0.001. A final difference Fourier map calculation showed no peaks of chemical significance; the largest was 1.489 electron /Å^3 and was associated with the Pd1 atom. Crystal data, intensity collection and structure refinement as well as all atomic positional parameters, bond distances and angles are summarized in Appendix Table A6.

(vi) Structure Determination of [Pd(CH$_3$CN)(TOMB-3)][BF$_4$], (25).

Yellow crystals of [Pd(CH$_3$CN)(TOMB-3)][BF$_4$] were grown by vapour diffusion of diethyl ether into an acetonitrile solution of the compound. A statistical analysis of the intensity distributions and a determination of observed extinctions were consistent with the triclinic space group $P\bar{1}$, and this was confirmed by a successful solution refinement. A total of 3957 reflections were collected, and 2226 unique reflections with $F_o^2>3\sigma(F_o^2)$ were used in the refinement. The positions of the palladium and sulfur atoms were determined by direct methods from the *E*-map with the highest figure of merit. The remaining atoms were located from a difference Fourier map calculation. In the final cycles of refinement, all atoms were assigned anisotropic thermal parameters. This

resulted in $R = 0.0459$ and $R_w = 0.0367$ at final convergence. The Δ/σ value for any parameter in the final cycle was less than 0.0005. A final difference Fourier map calculation showed no peaks of chemical significance; the largest was 0.612 electron /Å^3 and was associated with the BF_4 anion. Crystal data, intensity collection and structure refinement details, as well as all atomic positional parameters, bond distances and angles are summarized in Appendix Table A7.

(vii) Structure Determination of [Pd(CH_3CN)(TOMB-P4)][BF_4], (27). Yellow crystals of [Pd(CH_3CN)(TOMB-P4)][BF_4] were grown an acetonitrile/ chloroform solution of the complex. A statistical analysis of the intensity distributions and a determination of observed extinctions were consistent with the monoclinic space group $P\bar{1}$, and this was confirmed by a successful solution refinement. A total of 5480 reflections were collected, and 3818 unique reflections with $F_o^2 > 3\sigma(F_o^2)$ were used in the refinement. The positions of the palladium and sulfur atoms were determined by direct methods from the *E*-map with the highest figure of merit. The remaining atoms were located from a difference Fourier map calculation. In the final cycles of refinement, all atoms were assigned anisotropic thermal parameters. This resulted in $R = 0.0418$ and $R_w = 0.0423$ at final convergence. The Δ/σ value for any parameter in the final cycle was less than 0.01. A final difference Fourier map calculation showed no peaks of chemical significance. Crystal Data, Intensity Collection and Structure Refinement as well as all atomic positional parameters, bond distances and angles are summarized in Appendix Table A8.

3.4 Results and Discussion

(i) Synthesis of the ligands TOMB-0,1,3,5. The thiacyclophanes employed in this study were prepared from the reaction of *meta*-xylene-α,α'-dithiol with the appropriate dihalide or ditosylate, or from the reaction of α,α'-dibromo-*meta*-xylene with the appropriate dithiol employing Buter and Kellogg's Cs^+-ion mediated method in DMF solution[28] as outlined in Scheme 3.1 for TOMB-1 and TOMB-3. This synthetic route produced these compounds as colourless, crystalline materials (or as an oil for TOMB-5) in yields of 60-66 %.

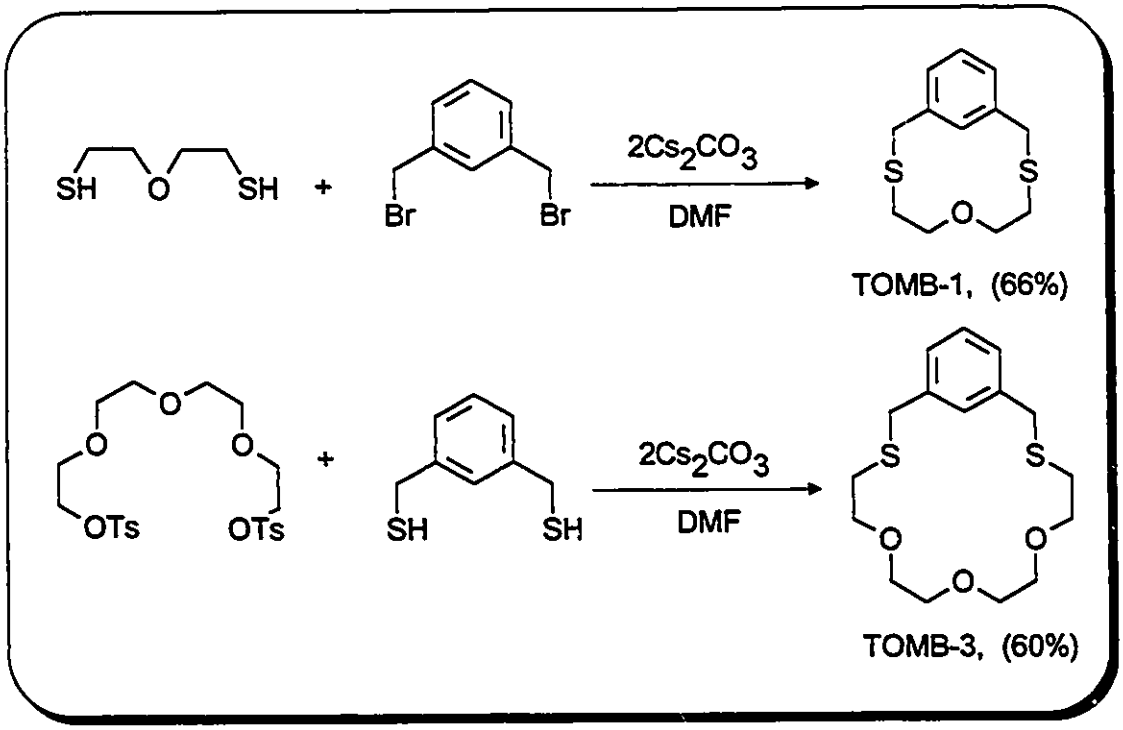

Scheme 3.1 Preparation of TOMB ligands by two methods.

The ^1H NMR spectra of TOMB-1, TOMB-3 (Figure 3.9), and TOMB-5 contain four well separated sets of resonances attributable to aromatic, benzylic OCH_2 and SCH_2 hydrogen atoms, with the proton at the 2-position of the aromatic

ring assigned to a singlet slightly downfield of the other three aromatic protons. For TOMB-0 the ^{1}H NMR spectrum has the same SCH_2 and benzylic resonances; aliphatic CH_2 resonances further upfield replace the -OCH_2 resonances, and the aromatic protons appear as a multiplet similar to those observed for TOMB-X, X=1,3,5. The $^{13}C\{^1H\}$ NMR spectra for these ligands show well resolved peaks for all carbon atoms which are assigned in Table 3.1.

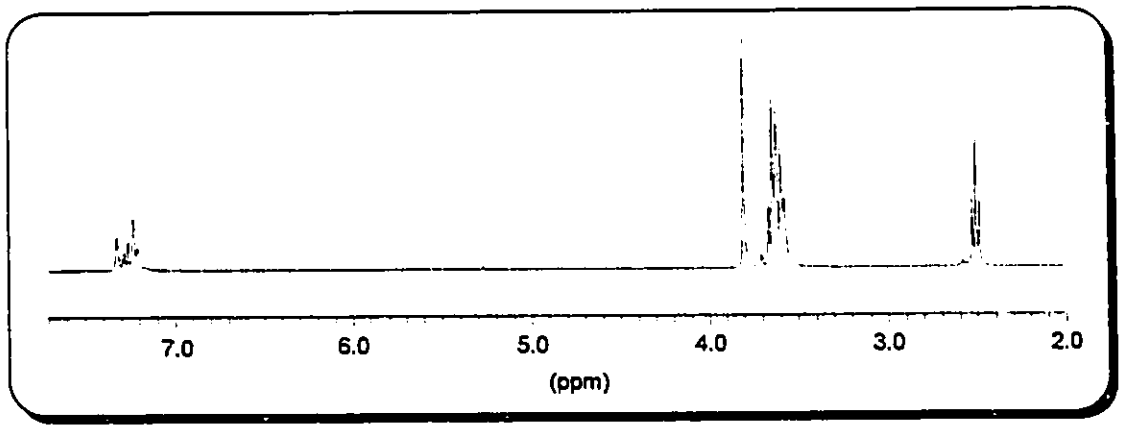

Figure 3.9 ^{1}H NMR spectrum of 5,8,11-Trioxa-2,14-dithia[15]-*m*-cyclophane, (TOMB-3).

Table 3.1 $^{13}C\{^1H\}$ NMR assignments ($CDCl_3$) for TOMB-X (X=0,1,3,5).

Ligand	Aromatic	O-CH_2[a]	Benzyllic	S-CH_2
TOMB-0	138.8, 129.2, 128.8, 127.4	28.5, 27.5, 27.1, 26.8	36.2	31.0
TOMB-1	138.6, 130.3, 129.2, 127.9	67.6	37.0	29.8
TOMB-3	138.4, 130.8, 129.2, 127.5	72.1, 70.9, 70.4	36.2	29.6
TOMB-5	138.8, 129.6, 128.9, 127.7	71.1, 70.8, 70.4, 70.3	36.5	30.5

a) O-CH_2 resonances are replaced by CH_2 resonances for TOMB-0

In addition to the spectroscopic information observed for TOMB-3, X-ray quality crystals were grown by slow evaporation of a dichloromethane solution of

the ligand and the crystal structure was determined.

(ii) Crystal Structure of TOMB-3, (18). The unit cell is monoclinic and contains four molecules of TOMB-3. A perspective view of the molecule with the atom numbering scheme is shown in Figure 3.10. Complete listings of crystallographic parameters including atomic positions, bonding parameters and details of data collection are listed in Appendix Table A3. Selected bonding parameters are given in the figure caption. Sulfur-carbon distances range from 1.799(9) to 1.825(9) Å and $C(sp^2)$-$C(sp^2)$ distances range 1.34(1) to 1.40(1) Å. The two $C(sp^2)$-$C(sp^3)$ bonds are 1.50(1) Å and the $C(sp^3)$-$C(sp^3)$ bonds average 1.46(1) Å. These distances compare well with those found for other thiacyclophanes and macrocyclic ethers[30, 31, 85a, 86].

In examining the structure of TOMB-3, the main feature that should be noted is the orientation of the aliphatic chain to the aromatic ring. As observed for TT[11]MC[61], the two C(benzylic)-S bonds are approximately perpendicular to the plane of the aromatic ring with C7-S1-C8 = 102.5(4)° and C15-S2-C16 = 102.5(4)°. The difference between TT[11]MC and TOMB-3, in this respect, is that the two C(benzylic)-S bonds are oriented on opposite sides of the aromatic ring whereas in TT[11]MC they are arranged on the same side of the aromatic ring. This has the effect of looping the aliphatic chain from one side of the aromatic ring to the other. The torsional angles for TOMB-3 are listed in Table 3.1. The two sulfur atoms are exodentate with torsional angles ranging from -55.9(8)° to -80.5(9)°, consistent with the range found for other thiacyclophanes[31]. The torsional angles about the oxygen atoms are consistent with the endodentate

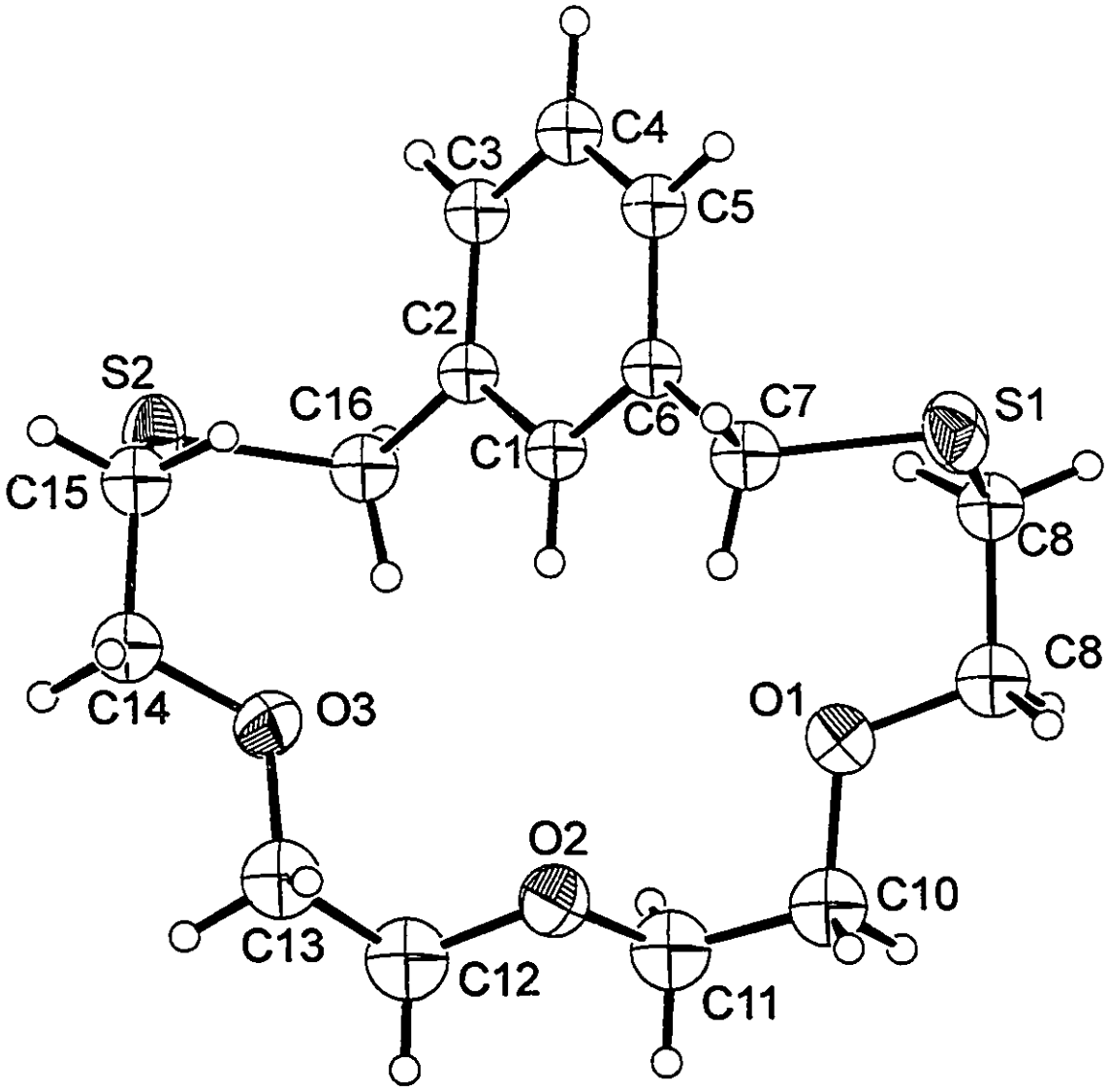

Figure 3.10 Perspective ORTEP drawing of TOMB-3 (18) showing the atom numbering scheme with 30% thermal ellipsoids. Selected bond distances (Å) are: S1-C7 = 1.815(9), S1-C8 = 1.791(8), S2-C15 = 1.799(9), S2-C16 = 1.825(9), average C-O = 1.40(1), average $C(sp^2)$-$C(sp^2)$ = 1.38(1), average $C(sp^3)$-$C(sp^3)$ = 1.46(1).

Table 3.2 Selected Torsional Angles for TOMB-3, (18).

linkage	angle (°)
C14-C15-S2-C16	-80.5(9)
C2-C16-S2-C15	-55.9(8)
C6-C7-S1-C8	-59.0(8)
C7-S1-C8-C9	-77.7(8)
C8-C9-O1-C10	-175.3(7)
C9-O1-C10-C11	-164.9(8)
C10-C11-O2-C12	-174.2(9)
C11-O2-C12-C13	-167.4(9)
C12-C13-O3-C14	161.7(8)
C13-O3-C14-C15	171.8(8)

conformation observed for ether functional groups in other mixed ether/thioether ligands[90, 30], with angles ranging from 161.7(8)° to 175.2(7)°. The endodentate and exodentate nature of the oxygen and sulfur atoms can easily be seen in Figure 3.10.

(iii) Metalation of the Ligands TOMB-0 (16), TOMB-1 (17), TOMB-3 (18), and TOMB-5 (20). The palladium centre was incorporated into the macrocycles by direct metalation of the aromatic ring employing $[Pd(CH_3CN)_4][BF_4]_2$ in acetonitrile solution. The metalation most likely proceeds via an electrophilic aromatic substitution pathway[88], with the law of conservation of mass requiring the loss of HBF_4. As was expected, the formation of 5-membered chelate rings containing oxygen is not favoured in these complexes and as a result an acetonitrile solvent molecule, rather than an ether oxygen, resides on the fourth coordination site of the palladium atom (Figure 3.11). The

resulting complexes [Pd(TOMB-X)(CH_3CN)][BF_4] (X = 0,1,3), obtained in high yields, are yellow air-stable crystalline solids although

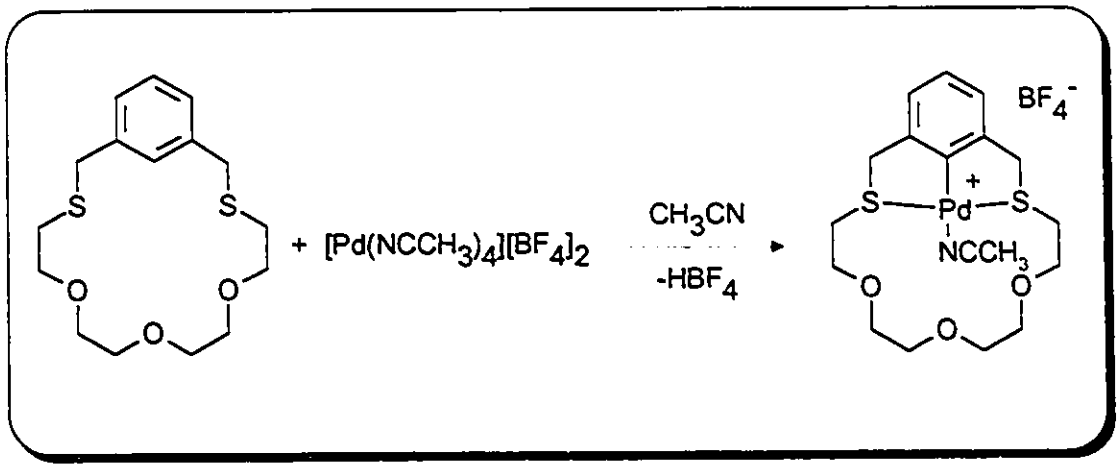

Figure 3.11 Typical Preparation of a [Pd(TOMB-X)(CH_3CN)][BF_4] complex.

[Pd(TOMB-0)(CH_3CN)][BF_4] shows a slight sensitivity to moisture.

[Pd(TOMB-0)(CH_3CN)][BF_4], [Pd(TOMB-3)(CH_3CN)][BF_4] and [Pd(CH_3CN)(TOMB-5)][BF_4] are quite soluble in most polar organic solvents, however, [Pd(TOMB-1)(CH_3CN)][BF_4] was considerably less soluble in the same solvents and was converted to the [CF_3SO_3]$^-$ salt for most manipulations including X-ray diffraction and substrate competition experiments in $CDCl_3$ (Chapter 4). The isolation of [Pd(TOMB-5)(CH_3CN)][BF_4] is not quite as straightforward as the isolation of the other [Pd(TOMB-X)(CH_3CN)][BF_4] (x=0,1,3) complexes. This complex exhibits high sensitivity to atmospheric moisture and is isolated as a paste rather than a crystalline solid.

The ligand TOMB-3 was also reacted with $Pd(PhCN)_2Cl_2$ in the presence of one equivalent of $AgBF_4$ to give the neutral ortho-metalated compound

[Pd(TOMB-3)Cl] in moderate yield. It is interesting to note that the absence of a third thioether donor atom in the macrocycle leaves a chloride anion coordinated to the palladium centre, as was determined by X-ray crystallography (vide infra).

(iv) NMR Spectroscopy of $[Pd(TOMB\text{-}X)(CH_3CN)]^+$ Cations (X=0,1,3,5). Four features in the ^1H NMR spectra of the reaction products (Figure 3.12a-d) indicate that metalation of the ligands has occurred: (i) the absence of a downfield resonance in the aromatic region of the ^1H NMR spectra; (ii) the splitting of the benzylic protons into a pair of doublets for $[Pd(CH_3CN)(TOMB\text{-}0)][BF_4]$ and $[Pd(CH_3CN)(TOMB\text{-}1)][BF_4]$; (iii) the downfield shift of the $-SCH_2$ resonances; (iv) the downfield shift of coordinated acetonitrile. These observations are consistent with other metalated thiacyclophanes[61, 76].

Because $[Pd(TOMB\text{-}3)(CH_3CN)][BF_4]$ and $[Pd(TOMB\text{-}5)(CH_3CN)][BF_4]$ do not exhibit the same sharpening of peaks in the ^1H NMR spectra that $[Pd(TOMB\text{-}0)(CH_3CN)][BF_4]$ and $[Pd(TOMB\text{-}1)(CH_3CN)][CF_3SO_3]$ do, it was thought that a process whereby the aliphatic chain 'flips' from one side of the aromatic ring to the other was occurring. This process requires the ancillary CH_3CN ligand to be displaced from the palladium centre by one of the ether oxygen atoms (Figure 3.13) and would be accompanied by inversion of the sulfur atoms, possibly explaining the broad benzylic resonances. In order to test this hypothesis a low temperature NMR experiment was performed on $[Pd(TOMB\text{-}3)(CH_3CN)][BF_4]$ (Figure 3.14).

Upon cooling the chloroform solution of the receptor down to 213 K, the broad CH_2 resonances become sharp. In addition, the peak at 2.2 ppm at 298 K,

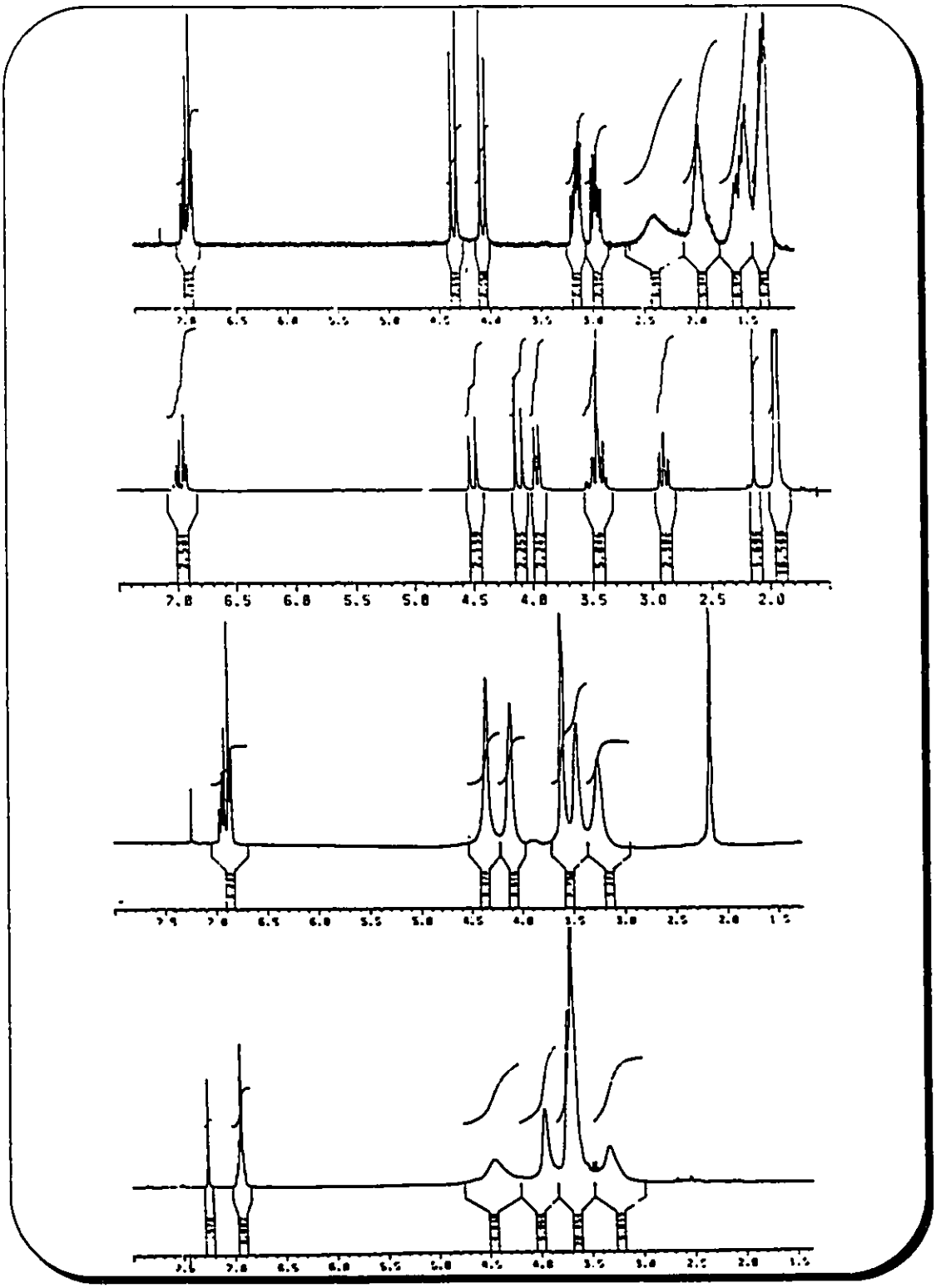

Figure 3.12 ^{1}H NMR Spectra (ppm) of a) [Pd(TOMB-0)(CH_3CN)]$^+$ (21) ($CDCl_3$), b) [Pd(TOMB-1)(CH_3CN)]$^+$ (23) (CD_3CN), c) [Pd(TOMB-3)$^+$ (CH_3CN)]$^+$ (25) ($CDCl_3$), d) [Pd(TOMB-5)(CH_3CN)]$^+$ (26) ($CDCl_3$)

assigned as the CH_3CN peak, separates into 2 peaks. One peak appears at 2.43 ppm for coordinated CH_3CN, accounting for 40% of the total. The other appears

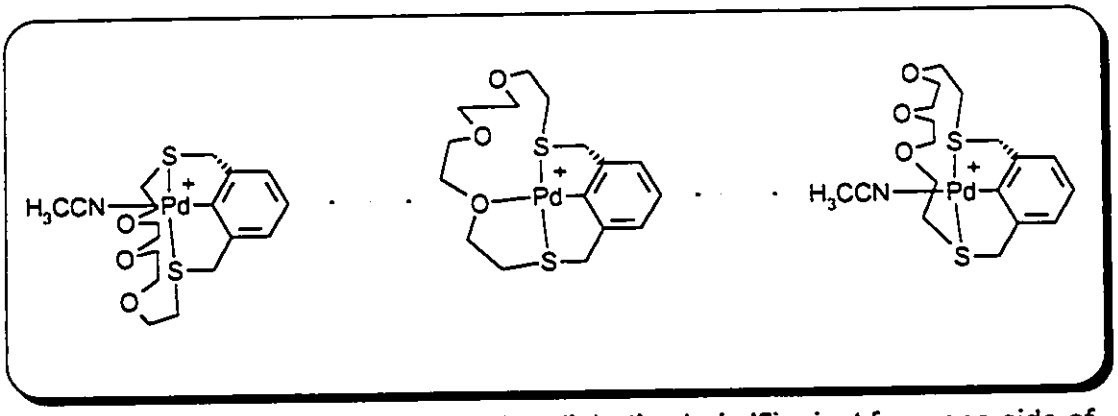

Figure 3.13 Schematic diagram of the aliphatic chain 'flipping' from one side of the aromatic ring to the other in the $[Pd(TOMB\text{-}3)(CH_3CN)]^+$ (25) cation.

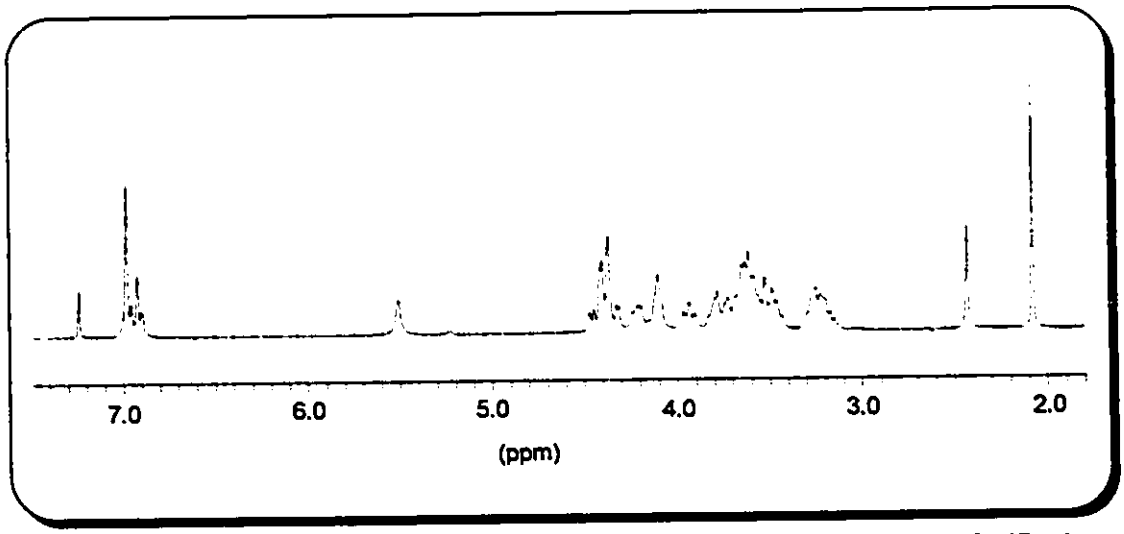

Figure 3.14 Low temperature (213 K) ^1H NMR spectrum of the $[Pd(TOMB\text{-}3)(CH_3CN)]^+$ cation in $CDCl_3$. At low temperature free and coordinating acetonitrile appear at 2.05 and 2.43 ppm respectively.

at 2.05 ppm for uncoordinated CH_3CN and accounts for the remaining 60% of the acetonitrile.

This result indicates that the aliphatic chain undergoes the 'flipping' process shown in Figure 3.13. The presence of oxygen donors in the aliphatic chain, coupled with the flexibility of the chain, allow for dissociation and recomplexation of the acetonitrile ligand. The asymmetric nature of the CH_2 (benzylic) resonances indicate that one of the ether oxygen atoms replaces the ancillary CH_3CN ligand to form a 5-membered chelate ring, leaving the complex asymmetric. Recomplexation of the acetonitrile to palladium can result in the aliphatic chain being oriented on either side of the square plane of the palladium atom; the polyether chain 'flips'.

The NMR spectra of [Pd(TOMB-3)Cl] recorded in CD_3CN as well as in $CDCl_3$ are similar to the spectra of [Pd(TOMB-3)(CH_3CN)][BF_4] recorded in the same solvents. This indicates that in solution the chloride ligand is at least partially dissociated from the cation and the vacant coordination site is filled by acetonitrile or one of the ether oxygen atoms.

In addition to the NMR evidence discussed above, yellow or orange X-ray quality crystals of [Pd(TOMB-0)(CH_3CN)][BF_4], [Pd(TOMB-1)(CH_3CN)][CF_3SO_3], [Pd(TOMB-3)Cl] and [Pd(TOMB-3)(CH_3CN)][BF_4] were grown by vapour diffusion of diethyl ether into CH_3CN solutions of the receptors.

(v) Crystal Structure of [Pd(TOMB-0)(CH_3CN)][BF_4], (21). The unit cell is monoclinic and contains eight molecules of [Pd(TOMB-0)(CH_3CN)][BF_4] and four CH_3CN molecules of crystallization. A perspective view of the cation with the atom numbering scheme is shown in Figure 3.15. Complete listings of crystallographic parameters including atomic positions, bonding parameters and

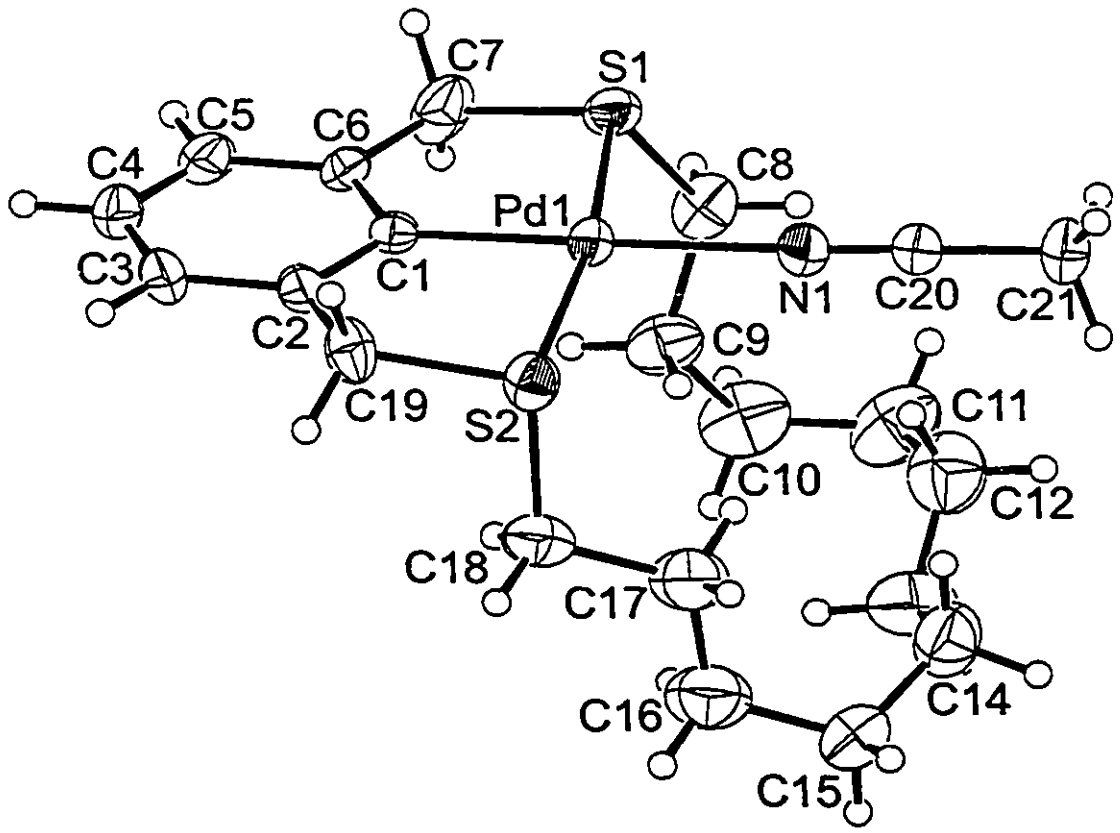

Figure 3.15 Perspective ORTEP drawing of $[Pd(CH_3CN)(TOMB\text{-}0)]^+$ cation (21) showing the atom numbering scheme with 30% thermal ellipsoids. Selected bond distances (Å) and angles are: Pd1-S1 = 2.299(2), Pd1-S2 = 2.327 (2), Pd1-C1 = 1.987(7), Pd1-N1 = 2.125(6). S1-Pd1-C1 = 85.1(2)°, S2-Pd1-C1 = 85.3(2)°, S1-Pd1-N1 = 92.6(2)°, S2-Pd1-N1 = 97.0(2)°, C1-Pd1-N1 = 177.6(3)°, S1-Pd1-S2 = 169.86(8)°.

details of data collection are listed in Appendix Table A4. Selected bonding parameters are given in the figure caption.

The palladium atom is in a square planar environment with the S_2C bracket occupying three sites and an ancillary CH_3CN ligand occupying the fourth site. The Pd-S distances are significantly longer than those found for [M(TT[11]MC)][BF_4], (M=Pd, Pt)[61, 76] or for [Pd(*pr*-TOMB-3)][BF_4], averaging 2.313(2) Å. The long aliphatic chain is more flexible than that in TT[11]MC or *pr*-TOMB-1 and the metal atom is strictly speaking not contained in a macrocyclic environment. As a result the Pd-S bonds are allowed to lengthen and are more comparable with Pt-S distances in open chain analogues[80b]. The Pd1-C1 distance is 1.987(7) Å and the Pd1-N1 distance is 2.125(6) Å[102]. The angles at the palladium atom are S1-Pd1-C1 = 85.1(2)° and S2-Pd1-C1 = 85.3(2)° for the 5-membered chelate rings, and are larger at the non chelating acetonitrile group with S1-Pd1-N1 = 92.6(2)° and S2-Pd1-N1 = 97.0(2)°. There is a slight distortion at the palladium atom with S1-Pd1-S2 = 169.86(8)° while the C1-Pd1-N1 bond is almost linear at 177.6(3)°.

(vi) Crystal Structure of [Pd(TOMB-1)(CH_3CN)][CF_3SO_3], (23). The unit cell is monoclinic and contains four cations and anions each of [Pd(CH_3CN)(TOMB-1)][CF_3SO_3]. A perspective view of the molecule with the atom numbering scheme is shown in Figure 3.16. Complete listings of crystallographic parameters including atomic positions, bonding parameters and details of data collection are listed in Appendix Table A5. Selected bonding parameters are given in the figure caption.

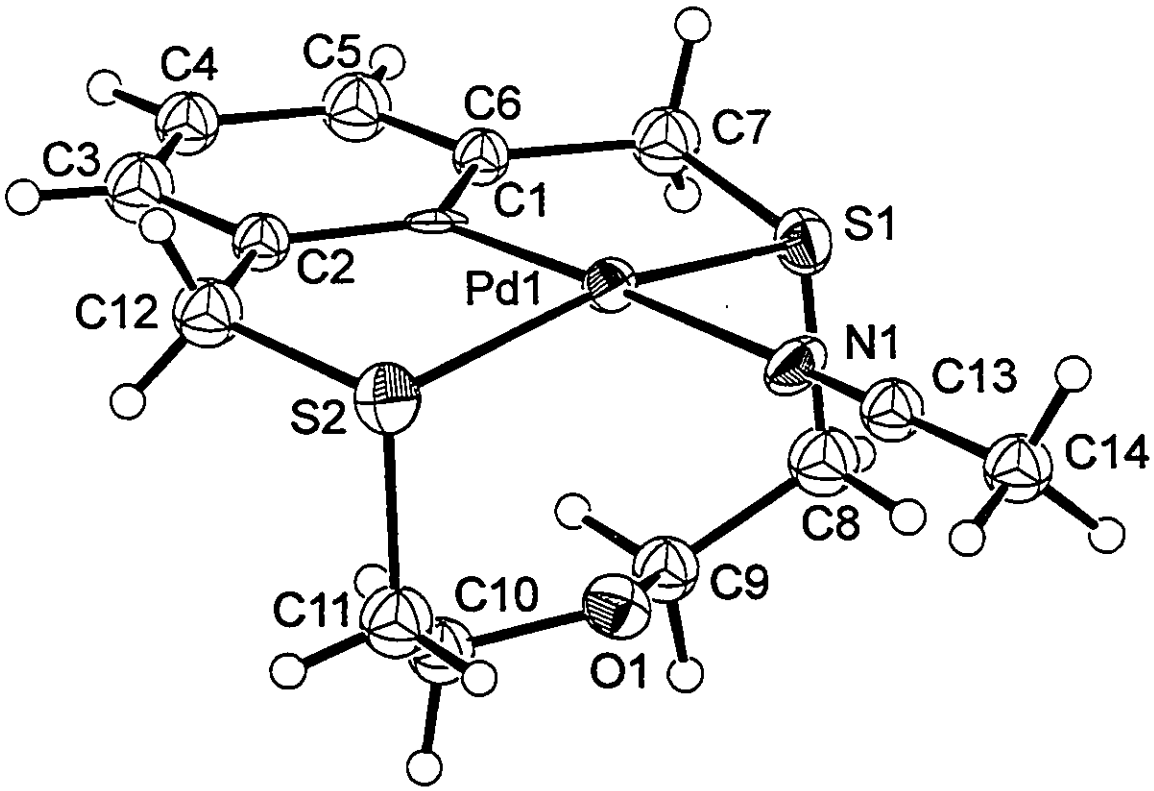

Figure 3.16 Perspective ORTEP drawing of $[Pd(CH_3CN)(TOMB\text{-}1)]^+$ cation (23) showing the atom numbering scheme with 30% thermal ellipsoids. Selected bond distances (Å) and angles are: Pd1-S1 = 2.315(4), Pd1-S2 = 2.316(4), Pd1-C1 = 1.98(1), Pd1-N1= 2.13(1), Pd...O1 = 2.714(8). S1-Pd1-C1 = 85.4(4)°, S2-Pd1-C1 = 85.4(4)°, S1-Pd1-N1 = 95.3(3)°, S2-Pd1-N1 = 93.3(3)°, S1-Pd1-S2 = 160.6(1)°, C1-Pd1-N1 = 177.6(5)°.

The palladium atom is in a square planar environment with the S_2C bracket occupying three sites, and an ancillary CH_3CN ligand occupying the fourth site on the metal atom. The Pd-S distances are again longer than those found for [M(TT[11]MC)][BF_4], (M=Pd, Pt) or for [Pd(*pr*-TOMB-3)][BF_4], averaging 2.316(4) Å. The Pd1-C1 distance is 1.98(1) Å and the Pd1-N1 distance is 2.13(1) Å, similar to those observed for the [Pd(CH_3CN)(TOMB-0)]$^+$ cation. The angles at the palladium atom are S1-Pd1-C1 = 85.4(4)° and S2-Pd1-C1 = 85.4(4)° for the 5-membered chelate rings, and are larger at the non chelating acetonitrile group with S1-Pd1-N1 = 95.3(3)° and S2-Pd1-N1 = 93.3(3)°. There is a significant distortion at the palladium atom with S1-Pd1-S2 = 160.6(1)°, due to the short five-atom chain joining the two sulfurs. The C1-Pd1-N1 bond is almost linear at 177.6(5)°.

(vii) Crystal Structure of [Pd(TOMB-3)Cl], (24). The unit cell is triclinic and contains two molecules of [Pd(TOMB-3)Cl]. A perspective view of the molecule with the atom numbering scheme is shown in Figure 3.17. Complete listings of crystallographic parameters including atomic positions, bonding parameters and details of data collection are listed in Appendix Table A6. Selected bonding parameters are given in the figure caption.

The palladium atom is in a square planar environment with the S_2C bracket occupying three sites, and a Cl^- ligand occupying the fourth site on the metal atom. The Pd-S distances are similar to those found for [M(TT[11]MC)][BF_4], (M=Pd, Pt) and for [Pd(*pr*-TOMB-3)][BF_4], averaging 2.284(2) Å. The Pd1-C1 distance is 1.982(7) Å and the Pd1-Cl1 distance 2.405(2) Å. The angles at the

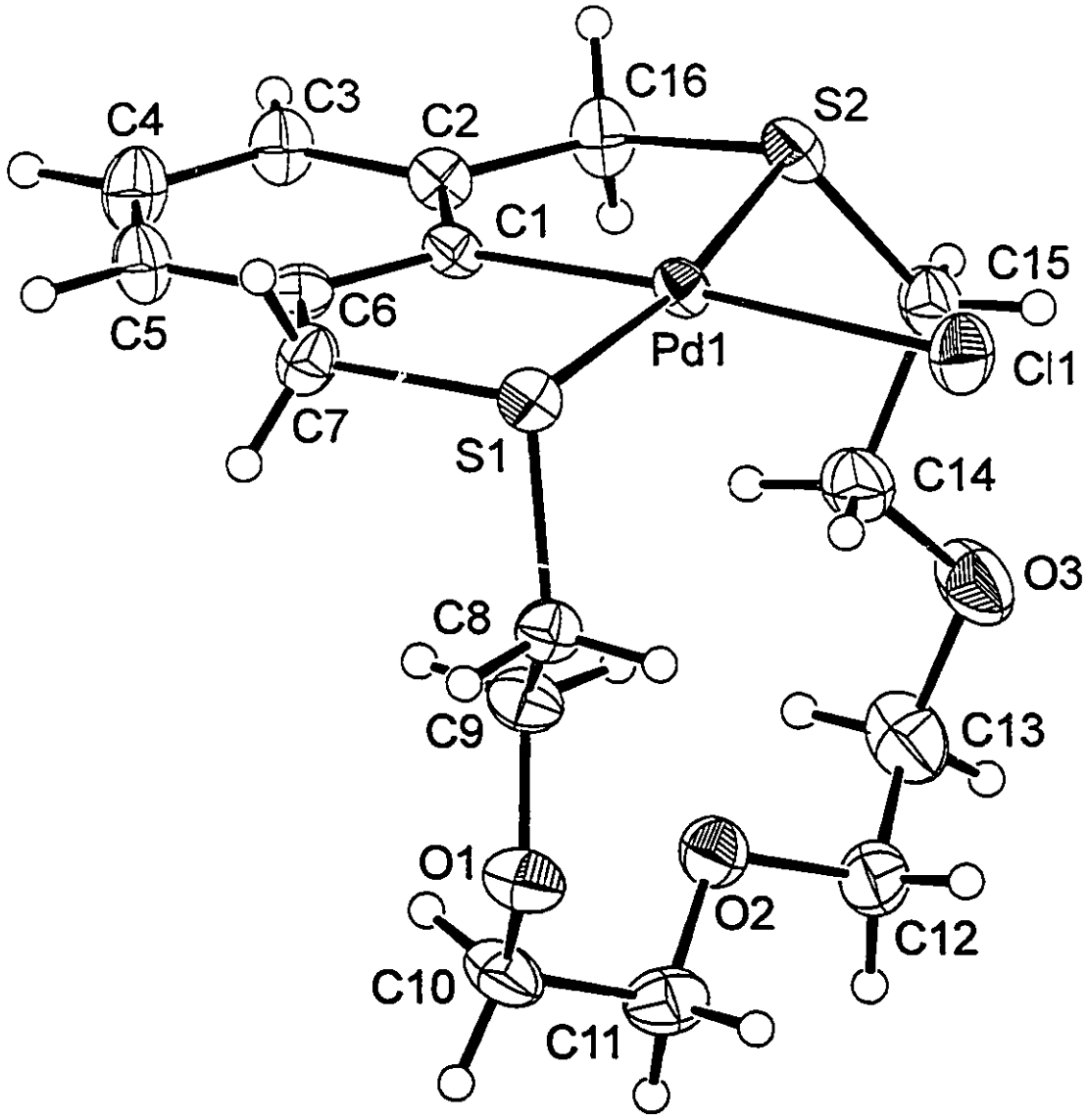

Figure 3.17 Perspective ORTEP drawing of [Pd(TOMB-3)Cl] (24) showing the atom numbering scheme with 30% thermal ellipsoids. Selected bond distances (Å) and angles are: Pd1-S1 = 2.284(2), Pd1-S2 = 2.285(2), Pd1-C1 = 1.982(7), Pd1-Cl1 = 2.405(2). S1-Pd1-C1 = 85.4(2)°, S2-Pd1-C1 = 86.0(2)°, S1-Pd1-Cl1 = 94.96(7)°, S2-Pd1-Cl1 = 93.91(8)°, S1-Pd1-S2 = 170.54(8)°, C1-Pd1-Cl1 = 175.7(2)°.

palladium atom are S1-Pd1-C1 = 85.4(2)° and S2-Pd1-C1 = 86.0(2)° for the 5-membered chelate rings, and are larger at the chloride ligand with S1-Pd1-Cl1 = 94.96(7)° and S2-Pd1-Cl1 = 93.91(8)°. There is a slight distortion at the palladium atom with S1-Pd1-S2 = 170.54(8)° and the C1-Pd1-Cl1 bond is almost linear at 175.7(2)°. The polyether chain is almost perpendicular to the square plane of the palladium atom, with the C-S-C angles averaging 103.2(2)°.

(viii) Crystal Structure of [Pd(TOMB-3)(CH_3CN)][BF_4], (25). The unit cell is triclinic and contains two cations and anions of [Pd(TOMB-3)(CH_3CN)]-[BF_4]. A perspective view of the molecule with the atom numbering scheme is shown in Figure 3.18. Complete listings of crystallographic parameters including atomic positions, bonding parameters and details of data collection are listed in Appendix Table A7. Selected bonding parameters are given in the figure caption.

The palladium atom is in a square planar environment with the S_2C bracket occupying three sites and an ancillary CH_3CN ligand occupying the fourth site on the metal atom. The Pd-S distances are similar to those found for the other [Pd(TOMB-X)(CH_3CN)]$^+$ receptors, averaging 2.303(3) Å. The Pd1-C1 distance is 1.984(6) Å and the Pd1-N1 distance 2.120(6) Å, similar to those observed for the other [Pd(TOMB-X)(CH_3CN)]$^+$ cations. The angles at the palladium atom are S1-Pd1-C1 = 85.7(2)° and S2-Pd1-C1 = 85.8(2)° for the 5-membered chelate rings, and are larger at the non chelating acetonitrile group with S1-Pd1-N1 = 94.2(2)° and S2-Pd1-N1 = 94.4(2)°. There is a slight distortion at the palladium atom with S1-Pd1-S2 = 171.27(7)° and the C1-Pd1-N1 bond is almost linear at 177.2(3)°.

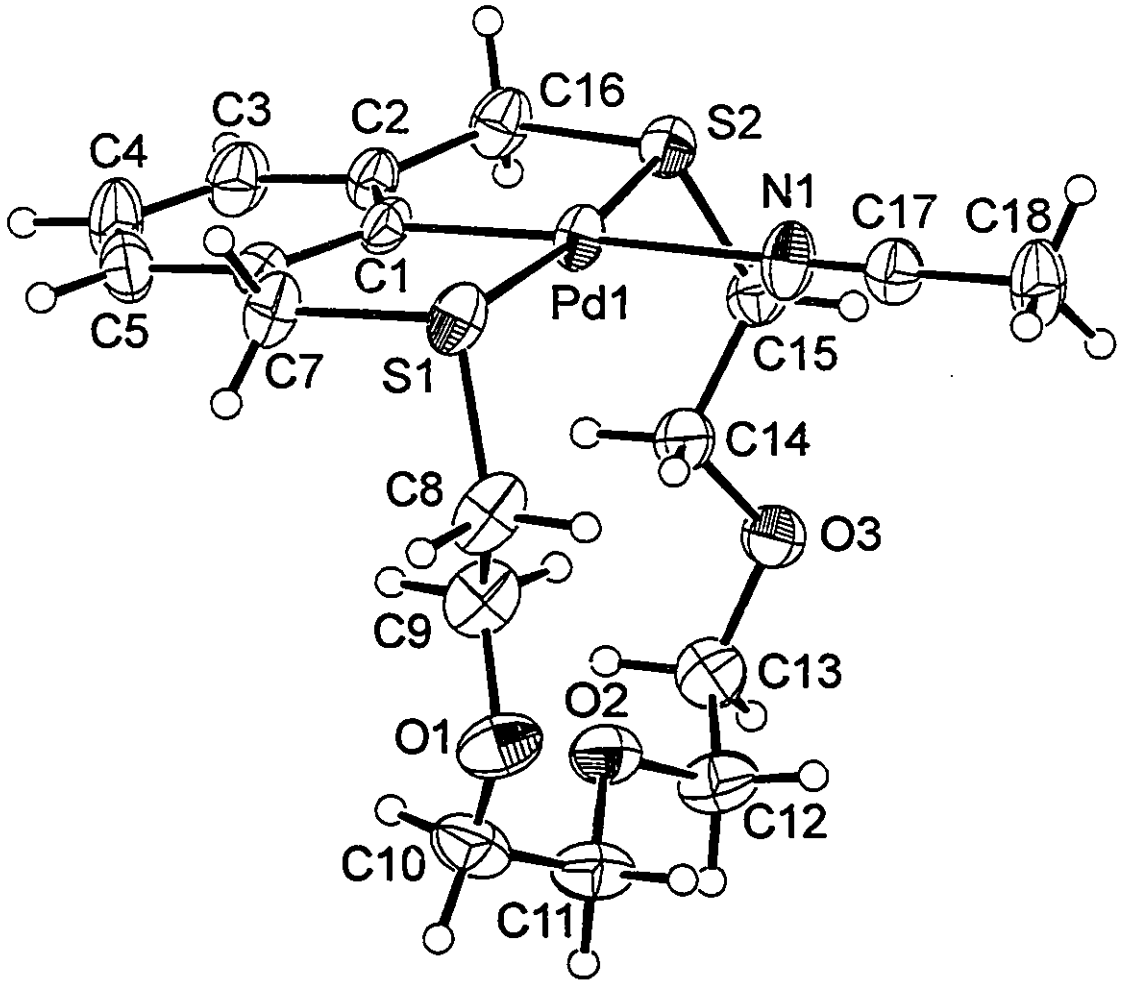

Figure 3.18 Perspective ORTEP drawing of $[Pd(CH_3CN)(TOMB\text{-}3)]^+$ cation (25) showing the atom numbering scheme with 30% thermal ellipsoids. Selected bond distances (Å) and angles are: Pd1-S1 = 2.307(3), Pd1-S2 = 2.299(3), Pd1-C1 = 1.984(6), Pd-N1 = 2.120(6). S1-Pd1-C1 = 85.7(2)°, S2-Pd1-C1 = 85.8(2)°, S1-Pd1-N1 = 94.2(2)°, S2-Pd1-N1 = 94.4(2)°, S1-Pd1-S2 = 171.27(7)°, C1-Pd1-N1 = 177.2(3)°.

In addition to the work done on the receptors outlined above, receptors containing aromatic spacing units in addition to polyether chains were synthesized in order to utilize π-stacking interactions with aromatic substrates. These receptors and their host-guest complexes were synthesized and crystallized by Shannon Murphy as part of her fourth year project and crystal structures of three compounds are detailed in this work. One is described in section 3.4 and two others in section 4.4.

(ix) Crystal Structure of [Pd(CH_3CN)(TOMB-P4)][BF_4], (27). The unit cell is monoclinic and contains two cations and anions of [Pd(PAP)(TOMB-P4)]$^+$ [BF_4]. A perspective view of the cation with the atom numbering scheme is shown in Figure 3.19. Complete listings of crystallographic parameters including atomic positions, bonding parameters and details of data collection are listed in Appendix Table A8. Selected bonding parameters are given in the figure caption.

The palladium atom is in a square planar environment with the S_2C bracket occupying three sites and the acetonitrile ligand occupying the fourth site on the metal atom. The Pd-S distances are Pd1-S1 = 2.313(2) Å and Pd1-S2 = 2.307(2) Å. Pd1-N1 = 2.137(5) Å and Pd1-C1 = 1.995(5) Å. The angles at the palladium atom are S1-Pd1-C1 = 84.8(2)° and S2-Pd1-C1 = 83.6(2)° at the 5-membered chelate rings and S1-Pd1-N1 = 92.3(1)° and S2-Pd1-N1 = 99.1(1)° at the non-chelating ligand. The palladium atom is significantly distorted from an ideal square planar geometry with S1-Pd1-S2 = 167.70(5)°. The N1-Pd1-C1 angle is almost linear at 175.7(2)°. There is a π–π interaction between the acetonitrile ligand and the aromatic rings in the receptor. Contacts ranging from 3.34 Å to

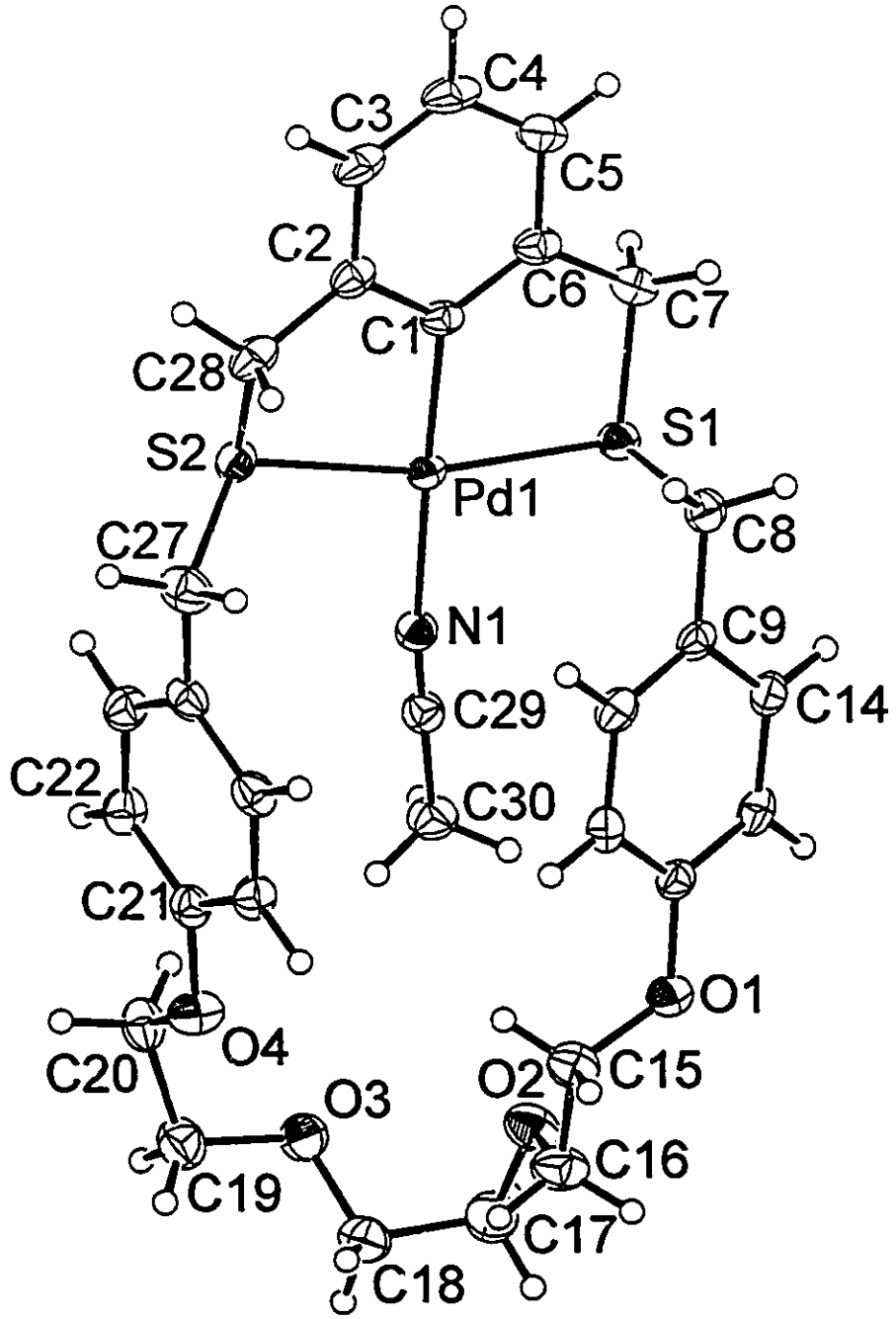

Figure 3.19 Perspective ORTEP drawing of $[Pd(CH_3CN)(TOMB\text{-}P4)]^+$ cation (35) showing the atom numbering scheme with 30% thermal ellipsoids. Selected bond distances (Å) and angles are: Pd1-S1 = 2.313(2), Pd1-S2 = 2.307(2), Pd1-N1 = 2.137(5), Pd1-C1 = 1.995(5). S1-Pd1-C1 = 84.8(2)°, S2-Pd1-C1 = 83.6(2)°, S1-Pd1-N1 = 92.3(1)°, S2-Pd1-N1 = 99.1(1)°, S1-Pd1-S2 = 167.70(5)°, N1-Pd1-C1 = 175.7(2)°.

3.69 Å are observed for N1 and C29 of the acetonitrile ligand to the C9-C11 atoms and to the C22-C24 atoms in one of the aromatic spacing units of the receptor. The two aromatic spacer units are almost perpendicular to each other, with an angle between the mean plane of the two aromatic rings of 96.31°.

(x) Comparative Structural Analysis for the [Pd(TOMB-0)]$^+$ (21), [Pd(TOMB-1)]$^+$ (23), [Pd(TOMB-3)]$^+$ (25) cations. The major structural difference between these complexes is the composition and spatial orientation of the chain joining the two sulfur atoms. For [Pd(CH_3CN)(TOMB-0)]$^+$, the purely hydrocarbon chain bends back towards the square planar palladium as the chain is traced away from the sulfur atoms. This is presumably a result of minimizing repulsive contacts and optimizing packing forces in the solid state. For [Pd(CH_3CN)(TOMB-1)]$^+$ the short length of the ether chain joining the sulfurs results in a potential hydrogen-bonding site directly below the metal coordination plane in which is oriented parallel to the Pd-N1 bond. Therefore, both the coordination site on the palladium and the ether oxygen are directed towards any incoming substrate. The longer polyether chain for [Pd(CH_3CN)(TOMB-3)]$^+$, which contains three ether oxygen atoms, is also oriented perpendicular to the coordination plane and contains three potential hydrogen-bonding sites. Similar to [Pd(CH_3CN)(TOMB-1)]$^+$, this results in a solid state orientation appropriate to allowing simultaneous hydrogen-bonding with a substrate to accompany metal coordination.

3.5 Conclusion

In this chapter the general synthetic procedure for the macrocyclic mixed ether/thioether ligands TOMB-1, TOMB-3 and TOMB-5 and that for the model thioether ligand TOMB-0 was discussed. The ligands are easily synthesized using the method of Buter and Kellogg to give products in approximately 60% yield. The crystal structure of TOMB-3 was determined.

The ligands are easily ortho-metalated using $[Pd(CH_3CN)_4][BF_4]_2$ as the palladium (II) source and give the receptor molecules in high yields (60-89%). The receptors $[Pd(CH_3CN)(TOMB\text{-}3)][BF_4]$ and $[Pd(CH_3CN)(TOMB\text{-}5)][BF_4]$ do not exhibit sharp ^1H NMR resonances in $CDCl_3$ as is observed for the receptors $[Pd(CH_3CN)(TOMB\text{-}0)][BF_4]$ and $[Pd(CH_3CN)(TOMB\text{-}1)][CF_3SO_3]$. A low temperature NMR experiment on $[Pd(CH_3CN)(TOMB\text{-}3)][BF_4]$ demonstrated that the receptor undergoes a dynamic dissociation process whereby the ancillary CH_3CN ligand is displaced by one of the ether oxygen atoms.

Three of the four receptor molecules can be isolated as crystalline solids and the crystal structures of $[Pd(CH_3CN)(TOMB\text{-}0)][BF_4]$, $[Pd(CH_3CN)(TOMB\text{-}1)][CF_3SO_3]$ and $[Pd(CH_3CN)(TOMB\text{-}3)][BF_4]$ were determined. The structures of the $[Pd(CH_3CN)(TOMB\text{-}1)]^+$ and $[Pd(CH_3CN)(TOMB\text{-}3)]^+$ cations in the solid state are such that they are ideally suited to substrate-receptor complex formation by simultaneously utilizing both coordination bonds to the palladium (II) centre and hydrogen-bonds to the polyether chains.

Chapter 4

Towards Molecular Recognition

Chapter 4

4.1 Introduction

(i) Thought Process. This chapter deals with the application of the receptor molecules synthesized in Chapter 3 for use in Simultaneous First- and Second-Sphere Coordination. The goal of the research outlined in this chapter was to determine whether the presence of second-sphere hydrogen-bonding interactions accompanying the normal coordination of a ligand/substrate would allow for selectivity or molecular recognition by the receptor molecule. Towards this end, substrates were chosen such that they contained hydrogen-bond donors in addition to groups capable of forming dative bonds. In order to test for this selectivity, it was also necessary to study the interaction of the receptors with substrates that contained no hydrogen-bonding groups and compare the two types of interactions. The first substrates chosen were o-aminopyridine (OAP), which contains a hydrogen-bond donor group in addition to the strong N donor, and pyridine (PYR) which contains only the aromatic nitrogen donor (Figure 4.1).

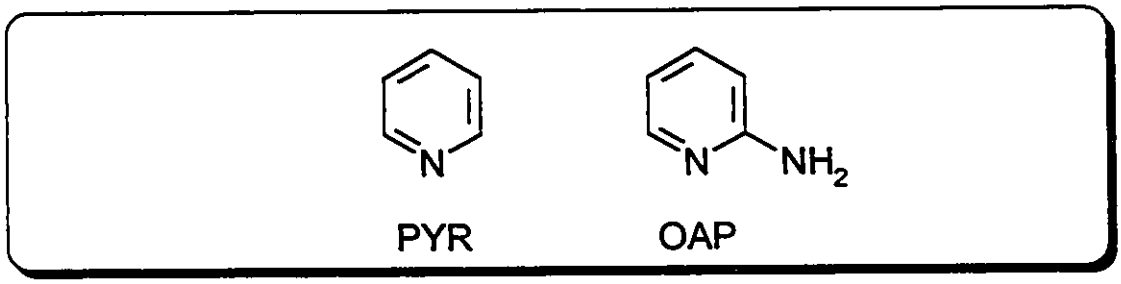

Figure 4.1 Structures of pyridine and o-aminopyridine.

These substrates were chosen because (i) they are commercially available at low cost, (ii) they are soluble in a variety of solvents, (iii) the orientation of the

amino group to the aromatic nitrogen in OAP directs both the first- and second-sphere interactions towards the receptor and (iv) the orientation of the amino group to the aromatic nitrogen in OAP is similar to that in the second set of substrates studied: adenine, guanine, cytosine and thymine (Figure 4.2). As such they are a model for interactions between the nucleobases and the receptors.

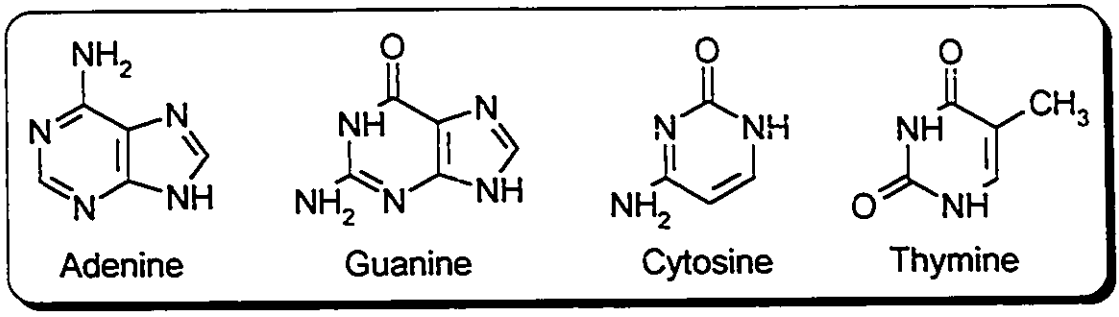

Figure 4.2 Structure of the four biological nucleobases in DNA.

(ii) Background Literature. Molecular recognition is currently a popular topic in the literature. It has been observed in systems supported by frameworks such as calix[4]arenes[103], large ring macrocycles[104], supramolecular bicyclic systems[105], cyclodextrins[106], macrotricyclic hosts[58b] and non-macrocyclic systems as well[52, 107]. It has also been used to affect chemical transformations[108]. A more detailed review of the subject can be found in Chapter 1.

The interaction of metal atoms with adenine, guanine or cytosine, or their sugar/phosphate derivatives, has been observed in the absence of second-sphere coordination[109].

In the previous chapter receptors synthesized by Reinhoudt's lab were mentioned. They utilized these receptors in binding urea, and other neutral organic guests, in which the guest molecule coordinates to a lithium atom in one

case[110] and to an immobilized UO_2 centre in two other cases[95a, e, 111] (Figure 4.3) in the first-sphere, and to a polyether chain in the second sphere of the metal.

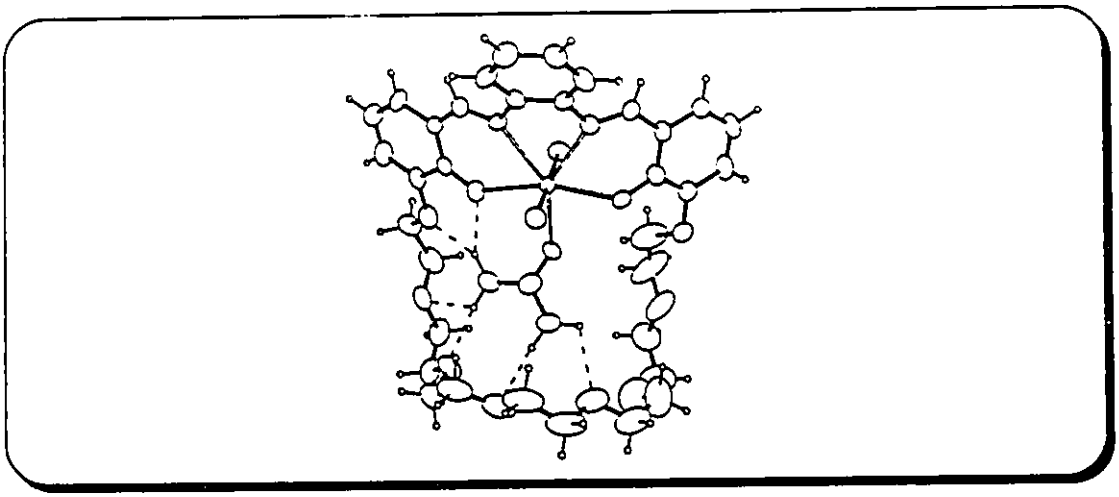

Figure 4.3 Crystal structure of uranyl containing receptor-urea complex.

Hisanobu Ogoshi and coworkers have developed a series of receptor molecules containing 2-hydroxynaphthyl groups attached to metalated porphyrins. These receptors have been shown to complex amino acid guests[92, 112] via simultaneous first- and second-sphere coordination, as shown in Figure 4.4.

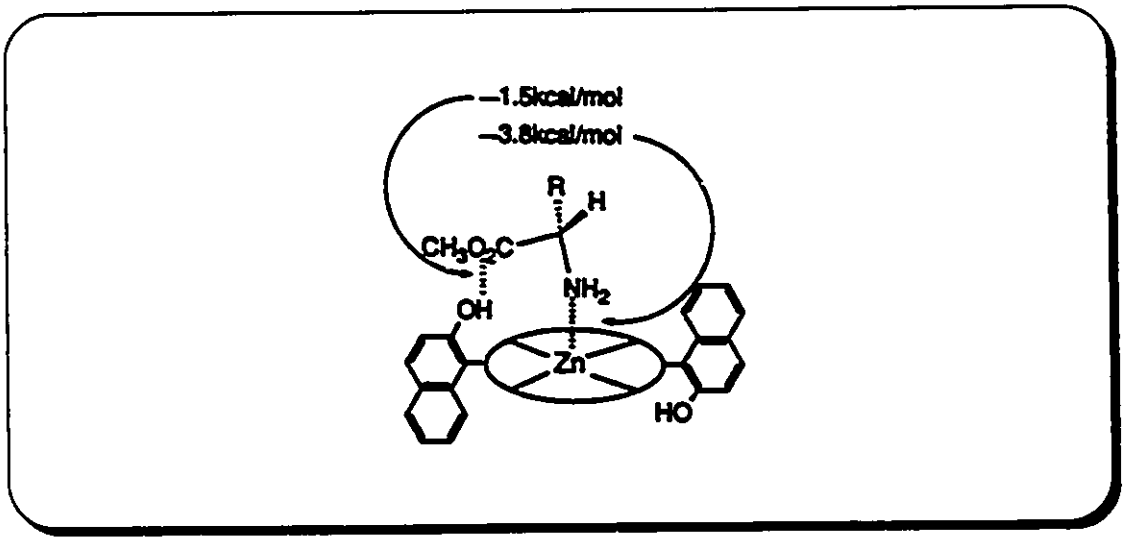

Figure 4.4 Simultaneous first- and second sphere coordination of the methyl ester of leucine by bis(2-hydroxynaphthyl)porphyrins.

The molecular recognition of biomolecules such as DNA nucleobases has attracted a lot of interest recently. Eiichi Kimura *et al* have done elegant work in this area with his Zn(II) cyclen complex[93] in which multi-point binding of deoxythymidine and uridine allows for selectivity of these two biomolecules using first-sphere coordination and second-sphere hydrogen-bonding and π-stacking interactions (Figure 4.5).

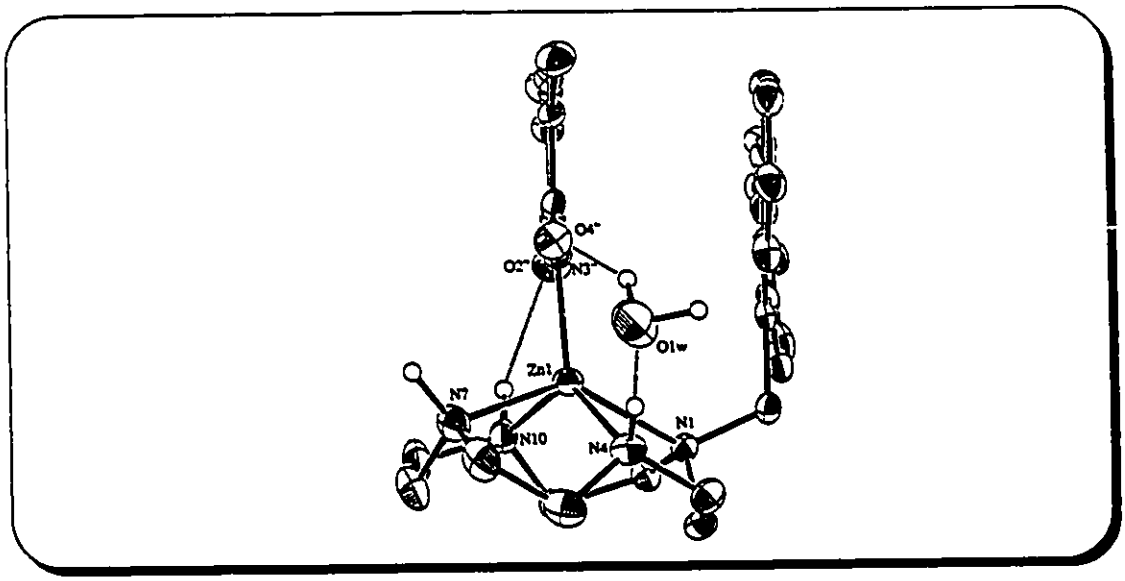

Figure 4.5 Zn(II) cyclen receptor binding 1-methylthymidine *via* first-sphere coordination and second-sphere hydrogen-bonding and π-stacking.

The tetrakis-(μ-carboxylato)dirhodium(II) dimer mentioned in Chapter 3 has been implicated in carcinostatic activity, and as a result great interest has been stimulated in this area[91a]. Aoki and coworkers, and others have studied the interactions with biomolecules[113] and other model substrates[91b, 114] in which the substrate binds to the receptor in the first sphere at rhodium, and in the second sphere at the carboxylato, or at the acetamido (Figure 4.6) framework. Other similar work has been done by Marzilli with a Co(III)-$(acac)_2$ receptor[115].

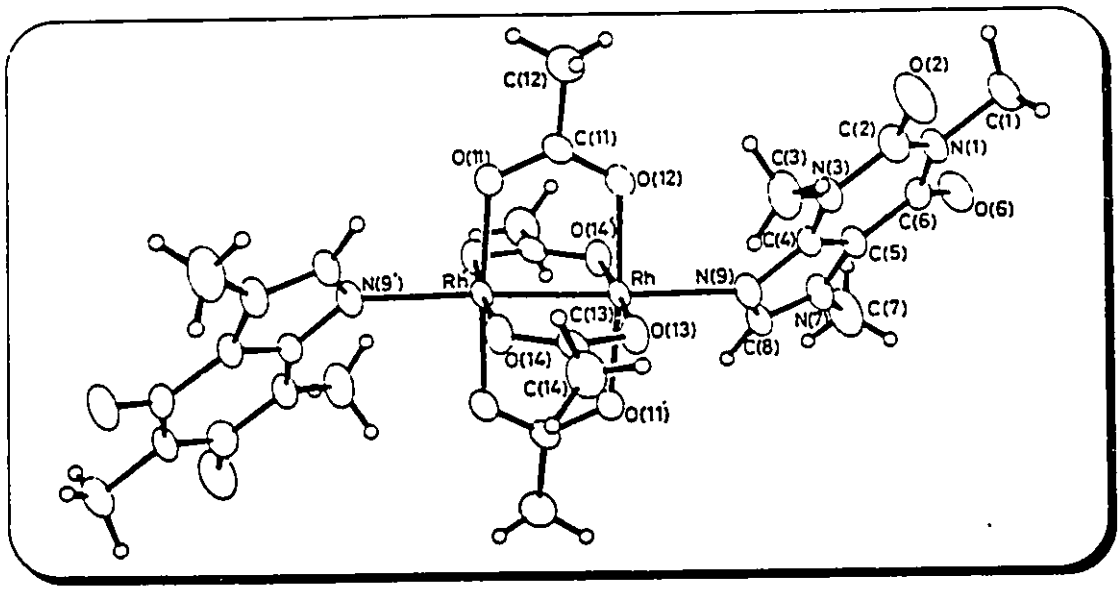

Figure 4.6 Crystal structure of tetrakis-(μ-acetato)dirhodium(II) dimer complexing caffeine in first and second sphere[113b].

Recently Loeb's research group has been able to trap the biological nucleobase guanine in a receptor containing palladium for first-sphere coordination, and ether oxygens for hydrogen-bonding and aromatic rings for π-stacking in the second sphere of the palladium[98].

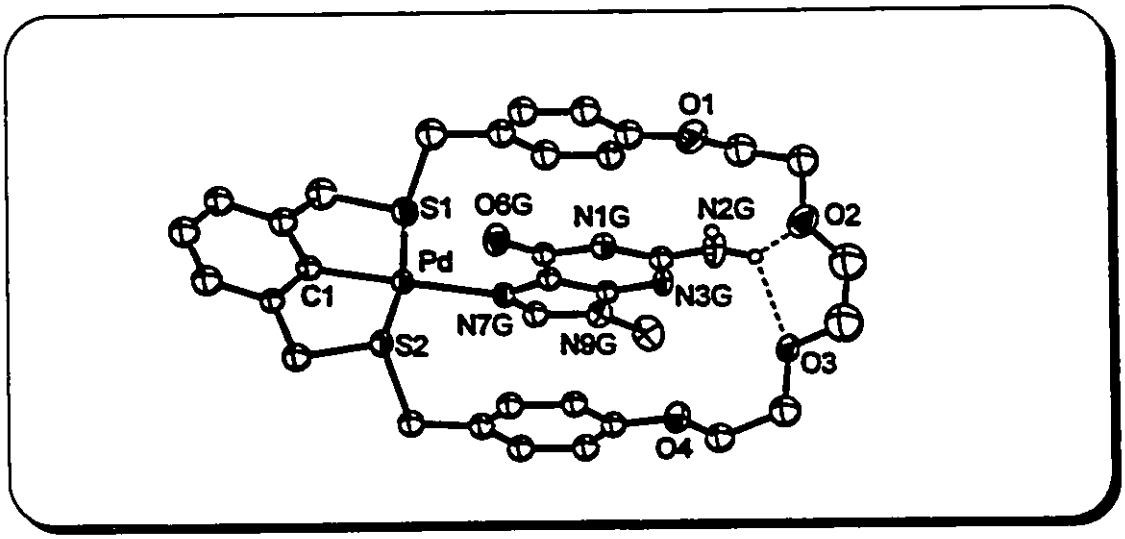

Figure 4.7 Crystal Structure of guanine coordinating to palladium in the first sphere and hydrogen bonding and π-stacking in the second sphere of the palladium.

4.2 Experimental

General Comments. All starting materials, pyridine (PYR), 2-amino-4-picoline (PIC), *o*-aminopyridine (OAP), cytosine (CYT), adenine (ADE) and guanine (GUA) and thymine (THY), deuterated solvents and anhydrous N,N-dimethylformamide (DMF) were purchased from Aldrich Chemicals and used without further purification, except acetonitrile which was distilled from CaH_2 under N_2(g). All reactions were performed under an atmosphere of N_2(g) using standard Schlenk or dry-box techniques and all solvents and liquid starting materials were degassed prior to use. ^1H and $^{13}C\{^1H\}$ NMR spectra were recorded on a Brüker AC300 spectrometer locked to the deuterated solvent at 300.1 and 75.5 MHz respectively, and infrared spectra were recorded on a Nicolet 5DX FTIR spectrometer. Elemental analyses were performed by Canadian Microanalytical Service, Delta, British Columbia.

(i) Preparation of Receptor-Substrate Complexes. In a typical reaction, 5 mL of an acetonitrile solution of $[Pd(CH_3CN)(TOMB\text{-}0)][BF_4]$, $[Pd(CH_3CN)(TOMB\text{-}1)][CF_3SO_3]$, $[Pd(CH_3CN)(TOMB\text{-}1)][BF_4]$ or $[Pd(CH_3CN)(TOMB\text{-}3)][BF_4]$ was combined with the appropriate amount of substrate solution (pyridine, *o*-aminopyridine, 2-amino-4-picoline in CH_3CN) and shaken for 5 min. The solvent was removed *in vacuo* and the pasty solid triturated with 5 mL of diethyl ether for 1 h to remove excess substrate and solvent. The solid was then dried *in vacuo* for 1 h providing essentially quantitative yields of receptor-substrate complex.

(ii) Preparation of [Pd(PYR)(TOMB-0)][BF_4], (28).

[$Pd(CH_3CN)$(TOMB-0)][BF_4] (5.0 mL, 7.4 x 10^{-3} M, 37 μmol), pyridine (0.25 mL, 0.16 M, 40 μmol). Yield of white solid: 0.021 g (95 %). ^{1}H NMR ($CDCl_3$): δ (ppm) 8.56 (d, 2H, pyr), 8.02 (t, 1H, pyr), 7.70 (t, 2H, pyr), 7.09-6.91 (m, 3H, aromatic), 4.52 (d, 2H, benzylic, J = 16.4 Hz), 4.17 (d, 2H, benzylic), 2.95-2.79 (m, 4H, SCH_2), 1.95 (m, 4H, β-CH_2), 1.49-1.34 (m, 14H, CH_2). Anal. Calcd. for $C_{24}H_{34}BF_4NPdS_2$: C, 48.53; H, 5.78. Found: C, 48.60; H, 5.71.

(iii) Preparation of [Pd(OAP)(TOMB-0)][BF_4], (29).

[$Pd(CH_3CN)$(TOMB-0)][BF_4] (5.0 mL, 7.4 x 10^{-3} M, 37 μmol). *o*-aminopyridine (0.23 mL, 0.16 M, 37 μmol). Yield of white powder: 0.022g (100%). ^{1}H NMR ($CDCl_3$): δ (ppm) 7.67 (d, 1H, oap), 7.51 (t, 1H, oap), 7.06-6.96 (m, 3H+1H, aromatic + oap), 6.66 (t, 1H, oap), 5.92 (s, 2H, NH_2), 4.53 (d, 2H, benzylic, J = 16.2 Hz), 4.17 (d, 2H, benzylic), 2.80 (dm, 4H, SCH_2), 2.01-1.84 (m, 4H, β-CH_2), 1.50 (s br, 6H, CH_2), 1.35 (s br, 8H, CH_2). Anal. Calcd. for $C_{34}H_{35}BF_4N_2PdS_2$: C, 47.33; H, 5.81. Found: C, 47.05; H, 5.77.

(iv) Preparation of [Pd(PYR)(TOMB-1)][CF_3SO_3], (30).

[$Pd(CH_3CN)$(TOMB-1)][CF_3SO_3] (5.0 mL, 7.5 x 10^{-3} M, 37 μmol), pyridine (0.25 mL, 0.16 M, 40 μmol). Yield of an orange-yellow powder: 0.019 g (89 %). ^{1}H NMR ($CDCl_3$): δ (ppm) 8.66 (d, 2H, pyr), 7.99 (t, 1H, pyr), 7.58 (t, 2H, pyr), 7.02-6.95 (m, 3H, aromatic), 4.62 (d, 2H, benzylic, J = 17.5 Hz), 4.54 (d, 2H, benzylic), 4.10 (dt, 2H, SCH_2), 3.43 (dt, 4H, SCH_2), 3.01 (dt, 2H, SCH_2). Anal. Calcd. for $C_{18}H_{20}F_3NO_4PdS_3$: C, 37.66; H, 3.52. Found: C, 37.34; H, 3.57.

[Pd(TOMB-1)(PYR)][BF_4] was prepared in exactly the same manner from [Pd(TOMB-1)(CH_3CN)][BF_4] and was identical to the triflate salt by spectroscopic analysis.

(v) Preparation of [Pd(OAP)(TOMB-1)][CF_3SO_3], (31).

[Pd(CH_3CN)(TOMB-1)][CF_3SO_3] (5.0 mL, 7.5 x 10^{-3} M, 37 μmol), *o*-aminopyridine (0.24 mL, 0.16 M, 37 μmol). Yield of an orange powder: 0.023 g (100%). ^1H NMR ($CDCl_3$): δ (ppm) 8.16 (dd, 1H, oap), 7.56 (dt, 1H, oap), 6.98 (m, 3H, aromatic), 6.73 (t, 1H, oap), 6.68 (d, 1H, oap), 6.03 (s, 2H, NH_2), 4.61 (d, 2H, benzylic, J = 17.5 Hz), 4.20 (d, 2H, benzylic), 4.05 (dt, 2H, SCH_2), 3.44 (dt, 4H, SCH_2), 2.99 (dt, 2H, SCH_2). Anal. Calcd. for $C_{18}H_{21}F_3N_2O_4PdS_3$: C, 36.70; H, 3.60. Found: C, 36.76; H, 3.65. [Pd(TOMB-1)(oap)][BF_4] was prepared in the same manner from [Pd(TOMB-1)(CH_3CN)][BF_4] and was identical to the triflate salt by NMR spectroscopic analysis.

(vi) Preparation of [Pd(PYR)(TOMB-3][BF_4], (32).

[Pd(CH_3CN)(TOMB-3)][BF_4] (5.0 mL, 7.1 x 10^{-3} M, 36 μmol), pyridine (0.25 mL, 0.16 M, 40 μmol). Yield of a pale yellow powder: 0.021g (100 %). ^1H NMR ($CDCl_3$): δ (ppm) 8.77 (d, 2H, pyr), 7.93 (t, 1H, pyr), 7.60 (t, 2H, pyr), 6.99 (s br, 3H, aromatic), 4.55-4.43 (q br, 4H, benzylic), 4.00 (s br, 4H, SCH_2CH_2O), 3.60 (s br, 4H, CH_2O), 3.60 (s br, 4H, CH_2O), 3.05 (dm, 4H, SCH_2). Anal. Calcd. for $C_{21}H_{28}BF_4NO_3PdS_2$: C, 42.05; H, 4.71. Found: C, 42.15; H, 4.66.

(vii) Preparation of [Pd(OAP)(TOMB-3)][BF_4], (33).

[Pd(CH_3CN)(TOMB-3)][BF_4] (5.0 mL, 7.1 x 10^{-3} M, 36 μmol), *o*-aminopyridine

(0.23 mL, 0.16 M, 36 μmol). Yield of a white powder: 0.022g (100 %). ^{1}H NMR ($CDCl_3$): δ (ppm) 7.88 (d, 1H, oap), 7.45 (t, 1H, oap), 7.01-6.99 (m, 3H, aromatic), 6.94 (d, 1H, oap), 6.56 (t, 1H, oap), 6.40 (s br, 2H, NH_2), 4.67 (d, 2H, benzylic, J = 15.3 Hz), 4.41 (d, 2H, benzylic), 3.88-3.37 (m, 12H, CH_2O), 3.20-3.02 (m, 4H, SCH_2). Anal. Calcd. for $C_{21}H_{29}BF_4N_2O_3PdS_2$: C, 41.02; H, 4.76. Found: C, 40.76; H, 4.77.

(viii) Preparation of [Pd(PIC)(TOMB-3)][BF$_4$], (34). 0.5 mL of a 2.25 x 10^{-2} M solution of [Pd(CH_3CN)(TOMB-3)][BF_4] in $CDCl_3$ and 14.9 μL of a 0.753 M solution of 2-amino-4-picoline in $CDCl_3$ were mixed and the NMR recorded. The product was crystallized by vapour diffusion of diethyl ether into this $CDCl_3$ solution of the complex. Yield of yellow crystals: 0.005 g (71%). ^{1}H NMR ($CDCl_3$): δ (ppm) 7.75 (d, 1H, pic), 6.98 (m, 3H, aromatic), 6.70 (s, 1H, pic), 6.40 (d, 1H, pic), 6.20 (s br, 2H, NH_2), 4.65 (d, 2H, benzylic, J = 15.4 Hz), 4.47 (d, 2H, benzylic), 3.87-3.37 (m, 12H, CH_2O), 3.15-3.01 (m, 4H, SCH_2), 2.22 (s, 3H, CH_3). Anal. Calcd. for $C_{22}H_{31}BF_4N_2O_3PdS_2$: C, 42.01; H, 4.98. Found: C, 41.94; H, 4.95.

(ix) Preparation of [Pd(CYT)(TOMB-3)][BF$_4$], (35). 0.75 mL of a 9.6 x 10^{-3} M $CDCl_3$ solution of [Pd(TOMB-3)(CH_3CN)][BF_4] was added to *ca.* 10-fold excess of cytosine and sonicated for 15 min. The excess solid was filtered off and washed with CH_3CN (2 mL). Diethyl ether (5 mL) was added to the CH_3CN solution and it was cooled to -10 °C to yield colourless crystals. ^{1}H NMR ($CDCl_3$): δ (ppm) 9.20 (s, br, 1H, NH, cyt), 7.39 (d, 1H, aromatic, cyt), 7.29 (s, br, 1H, NH_2), 7.00-6.95 (m, 3H, aromatic), 6.49 (s br, 1H, NH_2), 5.81 (d, 1H, aromatic,

cyt), 4.57 (d, 2H, benzylic, J = 15.9 Hz), 4.45 (d, 2H, benzylic), 4.21-3.85 (m, 4H, CH_2O), 3.58-3.33 (m, 8H, CH_2O), 3.20-2.99 (m, 4H, SCH_2). Anal. Calcd. for $C_{20}H_{28}BF_4N_3O_4PdS_2$: C, 38.02; H, 4.48. Found: C, 37.99; H, 4.44.

(x) Nucleobase Extractions. In a typical extraction experiment, 0.8 mL of a 0.01 M solution of $[Pd(CH_3CN)(TOMB\text{-}0)][BF_4]$, $[Pd(CH_3CN)(TOMB\text{-}1)]^+$ $[CF_3SO_3]$ or $[Pd(CH_3CN)(TOMB\text{-}3)][BF_4]$ in CD_3CN or CD_3COCD_3 was sonicated for 15 min in the presence of a 10-fold excess of solid nucleobase, the mixture was filtered, and the ^1H NMR spectrum was recorded.

(xi) Competition Reactions. A 1:1 mixture of PYR and OAP was mixed with 1 equivalent of $[Pd(CH_3CN)(TOMB\text{-}0)][BF_4]$, $[Pd(CH_3CN)(TOMB\text{-}1)]^+$ $[CF_3SO_3]$ or $[Pd(CH_3CN)(TOMB\text{-}3)][BF_4]$ in $CDCl_3$ solution, and the ^1H NMR was recorded at 213, 233, 253, 273 and 293K. The ratio OAP/PYR for complexed substrate was determined by integrating the lowest field resonances of coordinated and uncoordinated pyridine.

(xii) Syntheses not performed by the author.

$[Pd(PAP)(TOMB\text{-}P4)][BF_4]$ (36) and $[Pd(PAP)(TOMB\text{-}M4)][BF_4]$ (37) were synthesized by Shannon L. Murphy in partial fulfilment of her fourth year research project and details of the synthesis and crystallization of these compounds can be found in her written report. The free ligands contain aromatic spacing units between the polyether chain and the S_2C bracket, and the "P" or "M" in the name of the complexes above, refers to *para* or *meta* substitution on these aromatic spacer units.

4.3 X-Ray Diffraction Data Collection, Solution, and Refinement.

(i) General Procedures. The general procedure for data collection and solution refinement is identical to that outlined in section 2.3 (i) and the reader is referred to it for the sake of brevity.

(ii) Structure Determination of [Pd(OAP)(TOMB-1)][BF_4], (31). Deep yellow crystals of [Pd(OAP)(TOMB-1)][BF_4] were grown by vapour diffusion of diethyl ether into an acetonitrile solution of the complex. A statistical analysis of the intensity distributions and a determination of observed extinctions were consistent with the monoclinic space group $P2_1/c$, and this was confirmed by a successful solution refinement. A total of 3915 reflections were collected, and 2326 unique reflections with $F_o^2 > 3\sigma(F_o^2)$ were used in the refinement. The positions of the palladium and sulfur atoms were determined by direct methods from the *E*-map with the highest figure of merit. The remaining atoms were located from a difference Fourier map calculation. In the final cycles of refinement, all atoms were assigned anisotropic thermal parameters. This resulted in $R = 0.0695$ and $R_w = 0.0614$ at final convergence. The Δ/σ value for any parameter in the final cycle was less than 0.001. A final difference Fourier map calculation showed no peaks of chemical significance. Crystal data, intensity collection and structure refinement as well as all atomic positional parameters, bond distances and angles are summarized in Appendix Table A9.

(iii) Structure Determination of [Pd(PYR)(TOMB-3)][BF_4], (32). Yellow crystals of [Pd(PYR)(TOMB-3)][BF_4] were grown by slow evaporation of a $CDCl_3$ solution of the complex. A statistical analysis of the intensity distributions and a

determination of observed extinctions were consistent with the monoclinic space group $P\bar{1}$, and this was confirmed by a successful solution refinement. A total of 3304 reflections were collected and 2079 unique reflections with $F_o^2>3\sigma(F_o^2)$ were used in the refinement. The positions of the palladium and sulfur atoms were determined by direct methods from the *E*-map with the highest figure of merit. The remaining atoms were located from a difference Fourier map calculation. In the final cycles of refinement, all heteroatoms were assigned anisotropic thermal parameters. This resulted in $R = 0.0514$ and $R_w = 0.0462$ at final convergence. The Δ/σ value for any parameter in the final cycle was less than 0.001. A final difference Fourier map calculation showed no peaks of chemical significance. Crystal Data, Intensity Collection and Structure Refinement as well as all atomic positional parameters, bond distances and angles are summarized in Appendix Table A10.

(iv) Structure Determination of [Pd(PIC)(TOMB-3)][BF_4], (34). Yellow crystals of [Pd(PIC)(TOMB-3)][BF_4] were grown by vapour diffusion of diethyl ether into an acetonitrile solution of the complex. A statistical analysis of the intensity distributions and a determination of observed extinctions were consistent with the monoclinic space group $P\bar{1}$, and this was confirmed by a successful solution refinement. A total of 4929 reflections were collected, and 3084 unique reflections with $F_o^2>3\sigma(F_o^2)$ were used in the refinement. The positions of the palladium and sulfur atoms were determined by direct methods from the *E*-map with the highest figure of merit. The remaining atoms were located from a difference Fourier map calculation. In the final cycles of refinement, all atoms

were assigned anisotropic thermal parameters. This resulted in R = 0.0438 and R_w = 0.0472 at final convergence. The Δ/σ value for any parameter in the final cycle was less than 0.001. A final difference Fourier map calculation showed no peaks of chemical significance. Crystal Data, Intensity Collection and Structure Refinement as well as all atomic positional parameters, bond distances and angles are summarized in Appendix Table A11.

(v) Structure Determination of [Pd(CYT)(TOMB-3)][BF_4], (35).

Colourless crystals of [Pd(CYT)(TOMB-3)][BF_4] were grown by cooling a diethyl ether/acetonitrile solution of the complex to -10 °C. A statistical analysis of the intensity distributions and a determination of observed extinctions were consistent with the monoclinic space group $P2_1/n$, and this was confirmed by a successful solution refinement. A total of 5258 reflections were collected, and 2335 unique reflections with $F_o^2 > 3\sigma(F_o^2)$ were used in the refinement. The positions of the palladium and sulfur atoms were determined by direct methods from the *E*-map with the highest figure of merit. The remaining atoms were located from a difference Fourier map calculation. In the final cycles of refinement, all heteroatoms were assigned anisotropic thermal parameters. This resulted in R = 0.0461 and R_w = 0.0354 at final convergence. The Δ/σ value for any parameter in the final cycle was less than 0.001. A final difference Fourier map calculation showed no peaks of chemical significance. Crystal Data, Intensity Collection and Structure Refinement as well as all atomic positional parameters, bond distances and angles are summarized in Appendix Table A12.

(vi) Structure Determination of [Pd(PAP)(TOMB-P4)][BF_4], (36).

Yellow crystals of [Pd(PAP)(TOMB-P4)][BF_4] were grown from an acetonitrile/dichloromethane solution of the complex. A statistical analysis of the intensity distributions and a determination of observed extinctions were consistent with the monoclinic space group $P\bar{1}$, and this was confirmed by a successful solution refinement. A total of 5902 reflections were collected, and 3241 unique reflections with $F_o^2 > 3\sigma(F_o^2)$ were used in the refinement. The positions of the palladium and sulfur atoms were determined by direct methods from the *E*-map with the highest figure of merit. The remaining atoms were located from a difference Fourier map calculation. In the final cycles of refinement, all atoms were assigned anisotropic thermal parameters. This resulted in $R = 0.0400$ and $R_w = 0.0348$ at final convergence. The Δ/σ value for any parameter in the final cycle was less than 0.0002. A final difference Fourier map calculation showed no peaks of chemical significance. Crystal Data, Intensity Collection and Structure Refinement as well as all atomic positional parameters, bond distances and angles are summarized in Appendix Table A13.

(vii) Structure Determination of [Pd(PAP)(TOMB-M4)][BF_4], (37).

Yellow crystals of [Pd(PAP)(TOMB-M4)][BF_4] were grown by vapour diffusion of diethyl ether into an acetonitrile solution of the complex. A statistical analysis of the intensity distributions and a determination of observed extinctions were consistent with the monoclinic space group $P2_1/c$, and this was confirmed by a successful solution refinement. A total of 5047 reflections were collected, and 1404 unique reflections with $F_o^2 > 3\sigma(F_o^2)$ were used in the refinement. The

positions of the palladium and sulfur atoms were determined by direct methods from the *E*-map with the highest figure of merit. The remaining atoms were located from a difference Fourier map calculation. In the final cycles of refinement, all heteroatoms were assigned anisotropic thermal parameters. This resulted in $R = 0.0547$ and $R_w = 0.0482$ at final convergence. The Δ/σ value for any parameter in the final cycle was less than 0.0006. A final difference Fourier map calculation showed no peaks of chemical significance. Crystal Data, Intensity Collection and Structure Refinement as well as all atomic positional parameters, bond distances and angles are summarized in Appendix Table A14.

4.4 Results and Discussion

(i) Formation and NMR Spectroscopy of Receptor-Substrate Complexes. $[Pd(CH_3CN)(TOMB\text{-}0)]^+$, $[Pd(CH_3CN)(TOMB\text{-}1)]^+$ and $[Pd(CH_3CN)(TOMB\text{-}3)]^+$ were reacted with pyridine or *o*-aminopyridine in a 1:1 ratio to produce the aromatic amine adducts in essentially quantitative yield.

The ^1H NMR spectra of the pyridine adducts contain downfield shifted resonances for the substrates consistent with coordination. Only a slight sharpening of the receptor CH_2 peaks in the spectrum of $[Pd(PYR)(TOMB\text{-}3)]^+$ is observed, consistent with competition between pyridine and the ether oxygen atoms. The receptor CH_2 resonances for $[Pd(CH_3CN)(TOMB\text{-}0)]^+$ and $[Pd(CH_3CN)(TOMB\text{-}1)]^+$ however, remain sharp and essentially unchanged upon addition of pyridine; the aliphatic chain in $[Pd(CH_3CN)(TOMB\text{-}0)]^+$ does not compete with the substrate for the palladium coordination site and the ether in

$[Pd(CH_3CN)(TOMB\text{-}1)]^+$ is locked in a rigid conformation.

Coordination of *o*-aminopyridine to Pd in all three receptors was evidenced by significant changes in the chemical shifts of the aromatic protons of the substrates (Figure 4.8). In the adduct $[Pd(OAP)(TOMB\text{-}0)]^+$, in which there can

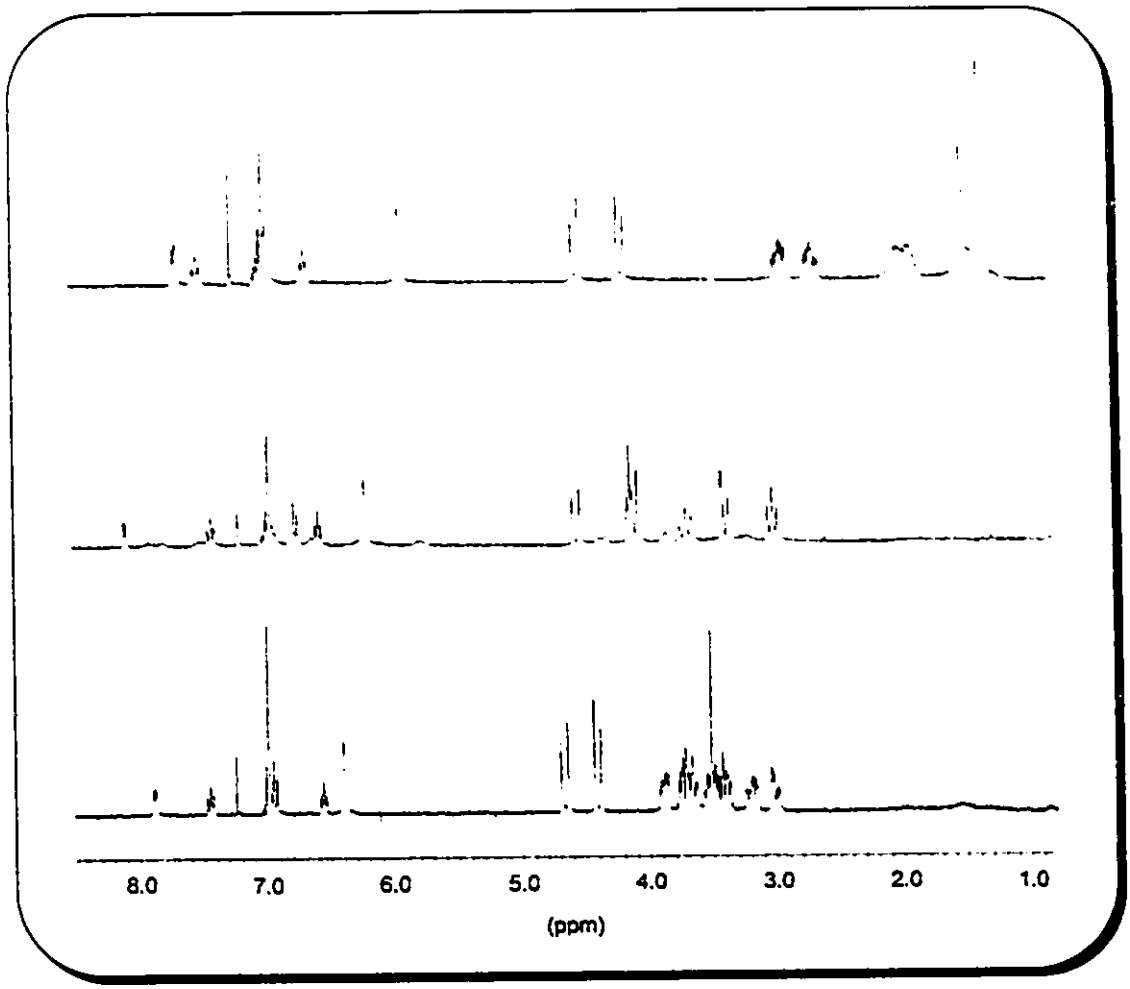

Figure 4.8 Comparison of the ^1H NMR spectra of the $[Pd(OAP)(TOMB\text{-}0)]^+$ (top), $[Pd(OAP)(TOMB\text{-}1)]^+$ (middle) and $[Pd(OAP)(TOMB\text{-}3)]^+$ (bottom) cations. Hydrogen bonding shifts the NH_2 resonances further downfield in the spectra of $[Pd(OAP)(TOMB\text{-}1)]^+$ and $[Pd(OAP)(TOMB\text{-}3)]^+$.

be no hydrogen-bonding, the NH_2 peak shifts downfield from 4.54 ppm to 5.92 ppm due solely to coordination by the aromatic nitrogen. For the adducts

[Pd(OAP)(TOMB-1)]$^+$ and [Pd(OAP)(TOMB-3)]$^+$ where substrate/receptor hydrogen-bonding can occur, further deshielding of the NH_2 protons was observed in the ^1H NMR spectra. This is indicative of hydrogen-bonding and is quite comparable to similar shifts observed for purely organic hydrogen-bonding receptors[52]. Additionally, the resonances for the aliphatic portion of [Pd(OAP)(TOMB-3)]$^+$ are sharp, with the benzylic splitting indicating that polyether chain does not compete with the substrate on the NMR time scale but rather hydrogen-bonds with the NH_2 group.

It is also interesting to note that in several NMR experiments with [Pd(CH_3CN)(TOMB-3)]$^+$ and 2-aminopicolines the splitting pattern observed for the aliphatic portion of the macrocycle at 4.0-2.9 ppm is identical to that observed

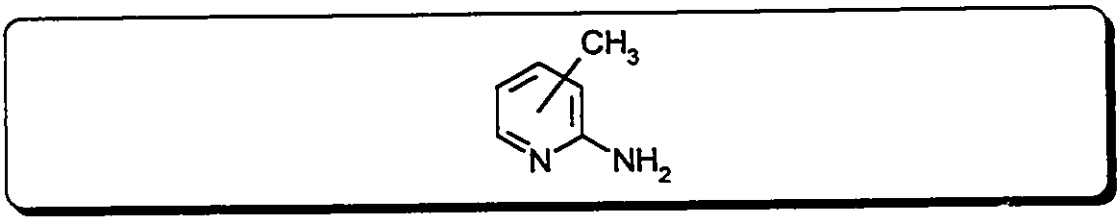

for the OAP adduct. This indicates that the aliphatic portion of the receptor is in the same conformation in solution regardless of the placement or presence of the methyl group on the substrate.

In addition to the NMR evidence observed for the substrate-receptor complexes, X-Ray quality crystals were isolated for [Pd(OAP)(TOMB-1)][BF_4], [Pd(PYR)(TOMB-3)][BF_4] and [Pd(PIC)(TOMB-3)][BF_4] and the crystal structures were determined.

(ii) Crystal Structure of [Pd(OAP)(TOMB-1)][BF_4], (30). The unit cell is monoclinic and contains 4 cations and anions each of [Pd(OAP)(TOMB-1)][BF_4].

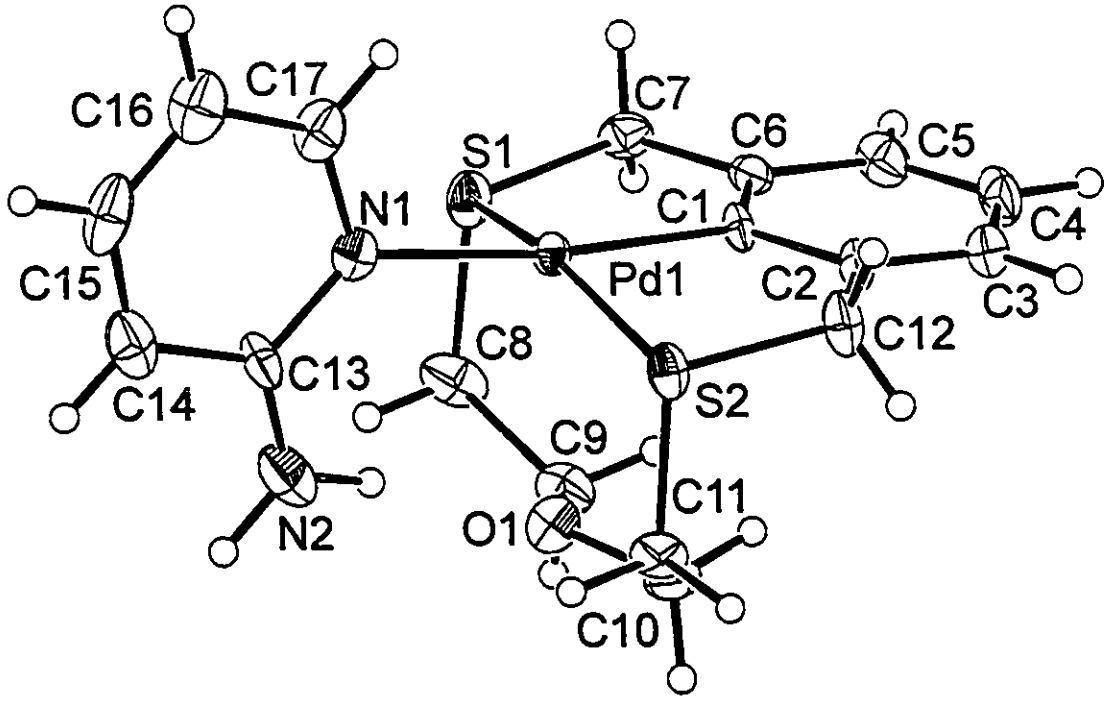

Figure 4.9 Perspective ORTEP drawing of the [Pd(OAP)(TOMB-1)]$^{+}$ cation (30) showing the atom numbering scheme with 30% thermal ellipsoids. Selected bond distances (Å) and angles are: Pd1-S1 = 2.298(4), Pd1-S2 = 2.312(4), Pd1-N1 = 2.14(1), Pd1-C1 = 1.99(1), Pd1-O1 = 2.75(1), N2-O1 = 2.95(2). S1-Pd1-C1 = 85.5(4)°, S2-Pd1-C1 = 85.3(4)°, S1-Pd1-N1 = 96.1(3)°, S2-Pd1-N1 = 95.4(3)°, S1-Pd1-S2 = 160.8(1)°, C1-Pd1-N1 = 172.0(4)°.

A perspective view of the cation with the atom numbering scheme is shown in Figure 4.9. Complete listings of crystallographic parameters including atomic positions, bonding parameters and details of data collection are listed in Appendix Table A9. Selected bonding parameters are given in the figure caption.

The palladium atom is in a square planar environment with the S_2C bracket occupying three sites and the *o*-aminopyridine aromatic nitrogen atom occupying the fourth site on the metal atom. The Pd-S distances are Pd1-S1 = 2.298(4) Å and Pd1-S2 = 2.312(4) Å. Pd1-N1 = 2.14(1) Å and Pd1-C1 = 1.99(1) Å. The angles at the palladium atom are S1-Pd1-C1 = 85.5(4)° and S2-Pd1-C1 = 85.3(4)° at the 5-membered chelate rings and S1-Pd1-N1 = 96.1(3)° and S2-Pd1-N1 = 95.4(3)° at the non-chelating substrate. The S1-Pd1-S2 angle is 160.8(1)° which is the same as that observed in the free receptor within experimental error, again small due to the short chain tying the two sulfur atoms together. C1-Pd1-N1 = 172.0(4)° deviates slightly from linearity, presumably due to the substrate being oriented in order to maximize hydrogen-bonding between the substrate and the receptor. The Pd-O1 distance is essentially unchanged from that of the free receptor at 2.75(1) Å and the O1 atom forms a hydrogen-bond with the N2 atom of the substrate with N2...O1 = 2.95(2) Å[42-49].

(iii) Crystal Structure of [Pd(PYR)(TOMB-3)][BF_4], (31). The unit cell is triclinic and contains two cations and anions of [Pd(PYR)(TOMB-3)][BF_4] and two $CDCl_3$ molecules of crystallization. A perspective view of the cation with the atom numbering scheme is shown in Figure 4.10. Complete listings of crystallographic parameters including atomic positions, bonding parameters and details of data

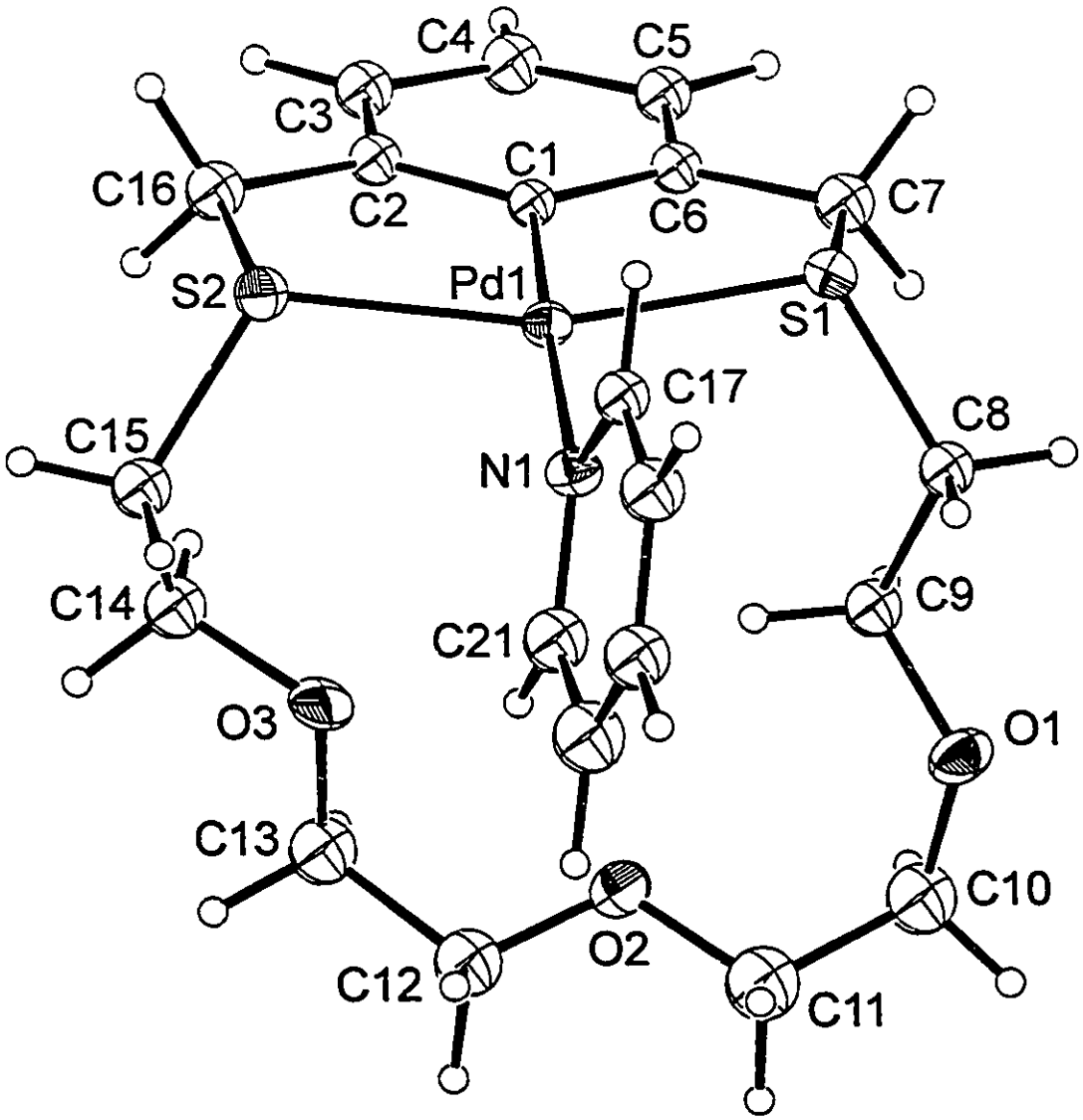

Figure 4.10 Perspective ORTEP drawing of the [Pd(PYR)(TOMB-3)]$^{+}$ cation (31) showing the atom numbering scheme with 30% thermal ellipsoids. Selected bond distances (Å) and angles are: Pd1-S1 = 2.294(3), Pd1-S2 = 2.285(3), Pd1-N1 = 2.144(8), Pd1-C1 = 1.98(1) S1-Pd1-C1 = 84.7(3)°, S2-Pd1-C1 = 85.6(3)°, S1-Pd1-N1 = 93.7(3)°, S2-Pd1-N1 = 96.8(3)°, S1-Pd1-S2 = 163.7(1)°, C1-Pd1-N1 = 175.4(4)°.

collection are listed in Appendix Table A10. Selected bonding parameters are given in the figure caption.

The palladium atom is in a square planar environment with the S_2C bracket occupying three sites and aromatic nitrogen atom occupying the fourth site on the metal atom. The Pd-S distances are Pd1-S1 = 2.294(3) Å and Pd1-S2 = 2.285(3) Å. Pd1-N1 = 2.144(8) Å and Pd1-C1 = 1.98(1) Å. The angles at the palladium atom are S1-Pd1-C1 = 84.7(3)° and S2-Pd1-C1 = 85.6(3)° at the 5-membered chelate rings and S1-Pd1-N1 = 93.7(3)° and S2-Pd1-N1 = 96.8(3)° at the non-chelating substrate. S1-Pd1-S2 = 163.7(1)°, which is significantly smaller than the same angle of 171.27(7)° in the free $[Pd(CH_3CN)(TOMB\text{-}3)]^+$ receptor. The angle is reduced due to a reorientation of the aliphatic chain, possibly a result of crystal packing forces and steric interaction with the substrate. The C1-Pd1-N1 angle is almost linear at 175.4(4)°.

(iv) Crystal Structure of [Pd(PIC)(TOMB-3)][BF_4], (33). The unit cell is triclinic and contains two cations and anions of [Pd(PIC)(TOMB-3)][BF_4]. A perspective view of the cation with the atom numbering scheme is shown in Figure 4.11. Complete listings of crystallographic parameters including atomic positions, bonding parameters and details of data collection are listed in Appendix Table A11. Selected bonding parameters are given in the figure caption.

The palladium atom is in a square planar environment with the S_2C bracket occupying three sites and the aromatic nitrogen occupying the fourth site on the metal atom. The Pd-S distances are Pd1-S1 = 2.299(2) Å and Pd1-S2 = 2.304(2) Å. Pd1-N1 = 2.139(5) Å and Pd1-C1 = 1.983(6) Å. The angles at the palladium

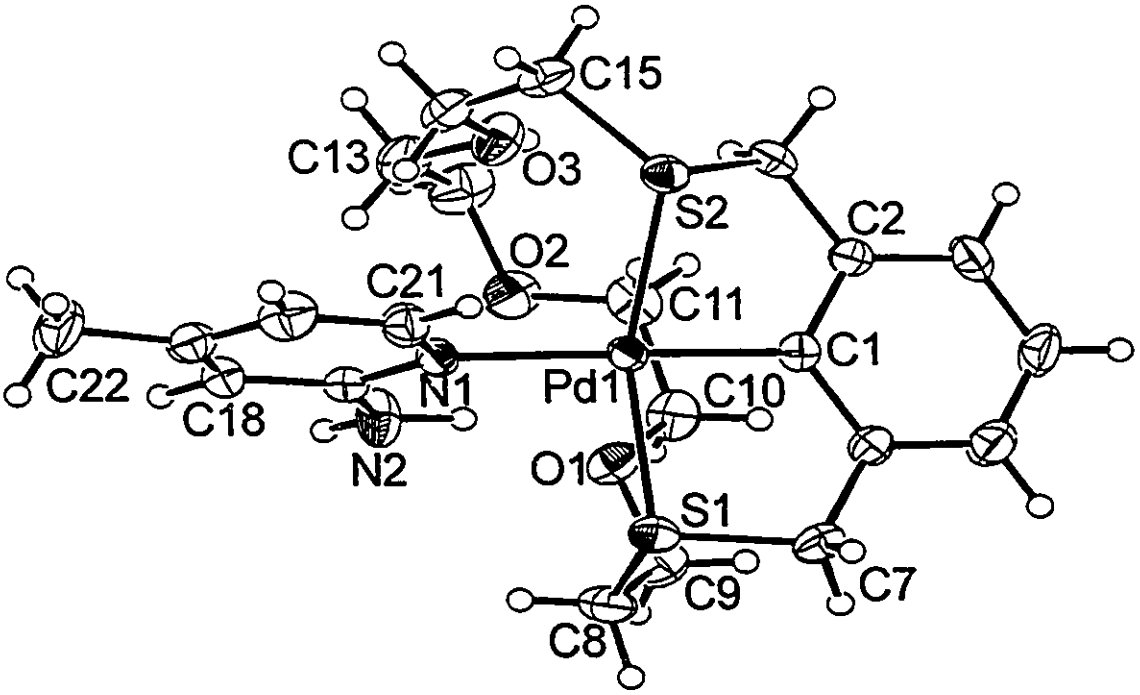

Figure 4.11 Perspective ORTEP drawing of [Pd(PIC)(TOMB-3)]$^+$ cation (33) showing the atom numbering scheme with 30% thermal ellipsoids. Selected bond distances (Å) and angles are: Pd1-S1 = 2.299(2), Pd1-S2 = 2.304(2), Pd1-N1 = 2.139(5), Pd1-C1 = 1.983(6), N2...O1 = 2.980(8). S1-Pd1-C1 = 85.1(2)°, S2-Pd1-C1 = 81.1(2)°, S1-Pd1-N1 = 94.7(2)°, S2-Pd1-N1 = 99.7(2)°, S1-Pd1-S2 = 159.93(7)°, N1-Pd1-C1 = 177.2(2)°.

atom are S1-Pd1-C1 = 85.1(2)° and S2-Pd1-C1 = 81.1(2)° at the 5-membered chelate rings and S1-Pd1-N1 = 94.7(2)° and S2-Pd1-N1 = 99.7(2)° at the non-chelating substrate. The significantly smaller S2-Pd1-C1 angle in comparison to [Pd(CH_3CN)(TOMB-3)][BF_4], accompanied by the significantly larger S2-Pd1-N1 angle are a result of the aliphatic chain reorienting itself in order to form a hydrogen-bond between O1 and N2, with a hydrogen bonding distance of N2...O1 = 2.980(1) Å. The S1-Pd1-S2 angle of 159.93(7)° is smaller still than the same angle in the pyridine adduct. This is again due to the aliphatic chain reorienting itself to form the hydrogen-bond, as can be seen in Figure 4.11. The N1-Pd1-C1 angle is almost linear at 177.2(2)°.

(v) Comparative Structural Analysis of the Receptor-Substrate Complexes [Pd(OAP)(TOMB-1)][BF_4] (30), [Pd(PYR)(TOMB-3)][BF_4].$CHCl_3$, (31), and [Pd(PIC)(TOMB-3)][BF_4] (33). In [Pd(OAP)(TOMB-1)]$^+$, [Pd(PYR)(TOMB-3)]$^+$ and [Pd(PIC)(TOMB-3)]$^+$, the plane of the pyridyl ring is approximately perpendicular to the square plane of the palladium centre. For [Pd(OAP)(TOMB-1)]$^+$, the NH_2 group is oriented on the same side of the square plane as the aliphatic chain, and the ether oxygen atom which is positioned below the Pd atom hydrogen-bonds to the amino group with a N2...O1 distance of 2.95(2) Å. For [Pd(PYR)(TOMB-3)]$^+$, the polyether chain maintains the open configuration observed in the free receptor complex [Pd(CH_3CN)(TOMB-3)]$^+$. For [Pd(PIC)(TOMB-3)][BF_4] the amino group is positioned on the same side of the square plane as the ether oxygen atoms and there is a hydrogen-bond between N2 and O1 at a distance of 2.980(8) Å. In order to form the hydrogen bond

between N2 and O1, the S2 atom moves away from the substrate and the polyether chain reorients itself to bring the O1 atom closer to the N2 atom. This results in a decrease of the S1-Pd1-S1 bond angle from 171.27(7)° down to 159.93(7)°.

(vi) Crystal Structure of [Pd(PAP)(TOMB-P4)][BF_4], (35). The unit cell is triclinic and contains two cations and anions each of [Pd(PAP)(TOMB-P4)]$^+$ [BF_4]. A perspective view of the cation with the atom numbering scheme is shown in Figure 4.12. Complete listings of crystallographic parameters including atomic positions, bonding parameters and details of data collection are listed in Appendix Table A13. Selected bonding parameters are given in the figure caption.

The palladium atom is in a square planar environment with the S_2C bracket occupying three sites and the aromatic nitrogen atom occupying the fourth site on the metal atom. The Pd-S distances are Pd1-S1 = 2.311(2) Å and Pd1-S2 = 2.301(2) Å. Pd1-N1 = 2.147(5) Å and Pd1-C1 = 1.992(6) Å. The angles at the palladium atom are S1-Pd1-C1 = 84.7(2)° and S2-Pd1-C1 = 83.6(2)° at the 5-membered chelate rings and S1-Pd1-N1 = 91.1(1)° and S2-Pd1-N1 = 101.1(1)° at the non-chelating substrate. The S1-Pd1-S2 angle is significantly distorted from linearity at 159.98(6)°. The N1-Pd1-C1 angle is almost linear at 175.1(2)°. The small S1-Pd1-S2 angle and the large S2-Pd1-N1 angle are due to the macrocyclic chain of the receptor and the substrate arranging themselves in order to maximize π-stacking and hydrogen bonding interactions. The aromatic rings of the receptor π-stack with the PAP substrate in an offset manner with the

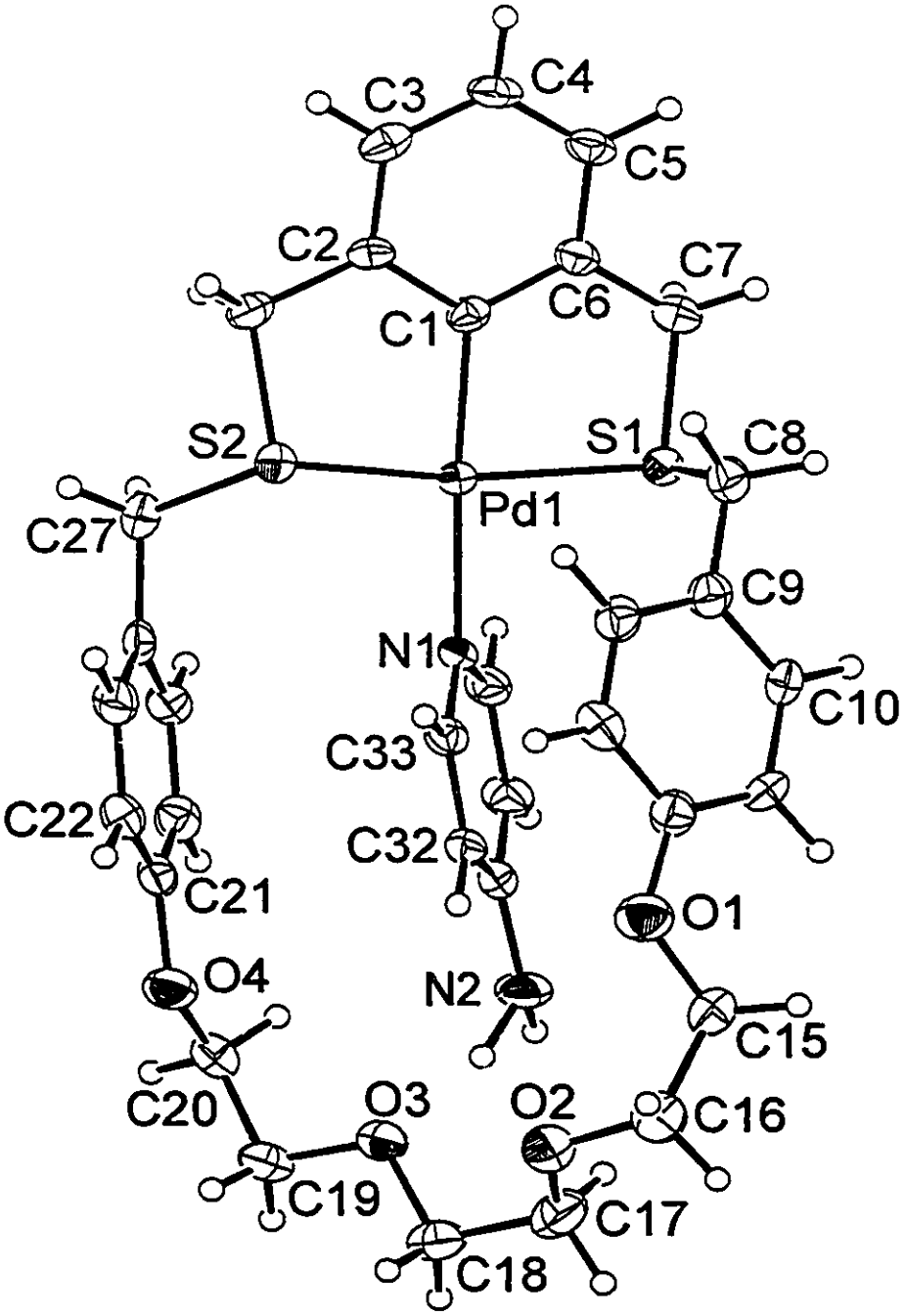

Figure 4.12 Perspective ORTEP drawing of $[Pd(PAP)(TOMB\text{-}P4)]^+$ cation (35) showing the atom numbering scheme with 30% thermal ellipsoids. Selected bond distances (Å) and angles are: Pd1-S1 = 2.311(2), Pd1-S2 = 2.301(2), Pd1-N1 = 2.147(5), Pd1-C1 = 1.992(6), N2-O3 = 3.12(1). S1-Pd1-C1 = 84.7(2)°, S2-Pd1-C1 = 83.6(2)°, S1-Pd1-N1 = 91.1(1)°, S2-Pd1-N1 = 101.1(1)°, S1-Pd1-S2 = 159.98(6)°, N1-Pd1-C1 = 175.1(2)°.

top of the ring defined by C25-C26 and the bottom of the ring defined by C32-C33-N1 separated by about 3.3 Å. These two rings are almost perfectly coplanar at an angle of 1.98° to each other. The closest contact between the substrate and the other aromatic ring in the receptor is between C32-C33 and C12-C13-C14 averaging about 3.4 Å; these aromatic rings aren't coplanar, at 37.27° to each other. The N2...O3 hydorgen-bonding distance is 3.12(1) Å.

(vii) Crystal Structure of [Pd(PAP)(TOMB-M4)][BF_4], (36). The unit cell is monoclinic and contains two cations and anions of [Pd(PAP)(TOMB-M4)][BF_4]. A perspective view of the cation with the atom numbering scheme is shown in Figure 4.13. Complete listings of crystallographic parameters including atomic positions, bonding parameters and details of data collection are listed in Appendix Table A14. Selected bonding parameters are given in the figure caption.

The palladium atom is in a square planar environment with the S_2C bracket occupying three sites and the aromatic nitrogen atom occupying the fourth site on the metal atom. The Pd-S distances are Pd1-S1 = 2.310(6) Å and Pd1-S2 = 2.306(6) Å. Pd1-N1 = 2.11(1) Å and Pd1-C1 = 2.00(2) Å. The angles at the palladium atom are S1-Pd1-C1 = 82.5(5)° and S2-Pd1-C1 = 81.5(5)° at the 5-membered chelate rings and S1-Pd1-N1 = 98.4(4)° and S2-Pd1-N1 = 97.6(4)° at the non-chelating substrate. The S1-Pd1-S2 angle of 163.8(2)° is significantly distorted from 180°, presumably due to rearrangement of the macrocyclic chain to maximize π-stacking and hydrogen-bonding interactions with the substrate. The N1-Pd1-C1 angle of 178.3(6)° is essentially linear. The PAP substrate π-stacks with the aromatic ring C21-C26 of the receptor with the average distance

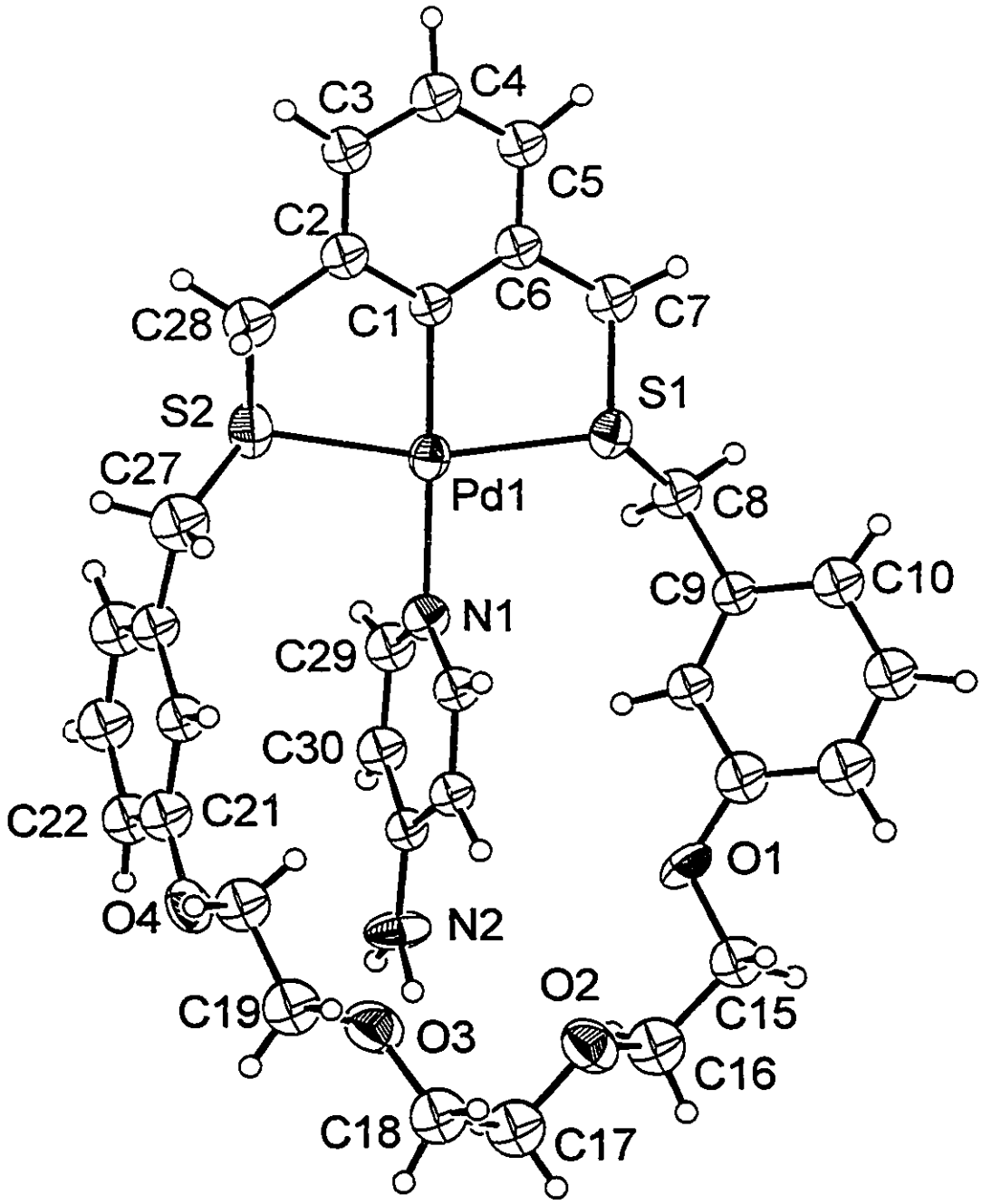

Figure 4.13 Perspective ORTEP drawing of [Pd(PAP)(TOMB-M4)]$^{+}$ cation (36) showing the atom numbering scheme with 30% thermal ellipsoids. Selected bond distances (Å) and angles are: Pd1-S1 = 2.310(6), Pd1-S2 = 2.306(6), Pd1-N1 = 2.11(1), Pd1-C1 = 2.00(2), N2-O2 = 3.51(1), N2-O3 = 3.12(1). S1-Pd1-C1 = 82.5(5)°, S2-Pd1-C1 = 81.5(5)°, S1-Pd1-N1 = 98.4(4)°, S2-Pd1-N1 = 97.6(4))°, S1-Pd1-S2 = 163.8(2)°, N1-Pd1-C1 = 178.3(6)°.

between carbon atoms being about 3.55 Å and the angle between the two rings being 2.33°, making them essentially coplanar. The angle between the second aromatic ring C9-C14 in the receptor and the substrate is 47.68° and there is a close contact between C14 and the C32 and C33 carbon atoms of the substrate at 3.52 and 3.30 Å respectively. One N-H proton hydrogen-bonds in a bifurcating fashion, with N2...O2 = 3.52(1) Å and N2...O3 = 3.12(1) Å.

(viii) Selectivity Experiment on $[Pd(CH_3CN)(TOMB\text{-}X)]^+$ (X=0,1,3) for o-aminopyridine (OAP) and pyridine (PYR). In order to test whether the presence of second sphere hydrogen-bonding would lead to selectivity by the receptor molecules for OAP over PYR, competition experiments were performed in which receptor, OAP, and PYR were mixed in $CDCl_3$ in a 1:1:1 ratio, and the ^1H NMR spectrum was recorded, as is shown in Figure 4.14. Selectivity was determined by integrating the lowest field resonance for uncoordinated and

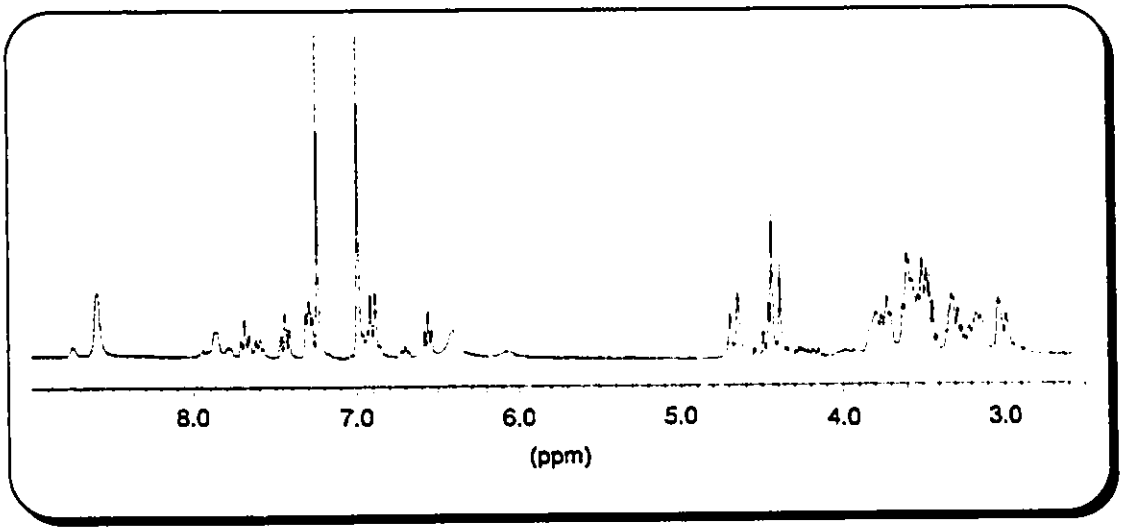

Figure 4.14 ^1H NMR spectrum a 1:1:1 mixture of $[Pd(CH_3CN)(TOMB\text{-}3)][BF_4]$, OAP and PYR in $CDCl_3$ at 253 K. The ratio of coordinated OAP:PYR is 6.33:1.

coordinated pyridine, at 8.59 and 8.73 ppm respectively in Figure 4.14. The results of this experiment are summarized in Table 4.1. As the temperature is lowered there is no substantial change in the OAP:PYR ratios for either the $[Pd(TOMB\text{-}0)]^+$ or $[Pd(TOMB\text{-}1)]^+$ receptors. However, as the temperature is

Table 4.1 Results of variable temperature NMR selectivity experiment listing OAP:PYR ratios and percentage of OAP bound by the receptor[a].

T (K)	$[Pd(TOMB\text{-}0)]^+$ OAP:PYR ratios		$[Pd(TOMB\text{-}1)]^+$ OAP:PYR ratios		$[Pd(TOMB\text{-}3)]^+$ OAP:PYR ratios	
293	(1.94:1)	(66%)	3.79:1	79%	4.42:1	81%
273	2.11:1	68%	3.28:1	77%	(5.33:1)	(84%)
253	2.23:1	69%	3.46:1	78%	6.33:1	86%
233	2.66:1	73%	3.59:1	78%	6.96:1	87%
213	2.56:1	72%	3.92:1	80%	12.34:1	92%

a) Numbers in parentheses are extrapolated from observed data points

lowered for the $[Pd(TOMB\text{-}3)]^+$ OAP/PYR solution, the ratio of coordinated OAP:PYR shows an increase. This is possibly because the decrease in the rate the aliphatic chain 'flips' results in more non-chelating ether oxygen atoms, providing more hydrogen-bonding sites for the substrate to interact with.

Ortho-aminopyridine is expected to be a stronger σ-donor than the unsubstituted pyridine, and this is demonstrated by the OAP:PYR ratio of 2.23:1 employing $[Pd(CH_3CN)(TOMB\text{-}0)]^+$ at 253 K in which no hydrogen-bonds can form. The increase in this ratio to 3.46 and 6.33 when $[Pd(CH_3CN)(TOMB\text{-}1)]^+$ and $[Pd(CH_3CN)(TOMB\text{-}3)]^+$ are used demonstrates that the observed second-sphere interactions have a significant effect on the interaction between receptor and substrate. Since only one intramolecular hydrogen-bond is formed

with both $[Pd(CH_3CN)(TOMB\text{-}1)]^+$ and $[Pd(CH_3CN)(TOMB\text{-}3)]^+$, it is difficult to explain why the OAP:PYR ratio is larger for $[Pd(CH_3CN)(TOMB\text{-}3)]^+$. It is possible that additional *inter*molecular hydrogen-bonding between an unused ether oxygen and the remaining amino hydrogen atom accounts for the increased ratio. Similar trends, where a receptor's ability to select OAP over PYR increases as the number of ether oxygen atoms increases, are observed at temperatures ranging from 213 K to 293 K (Figure 4.15).

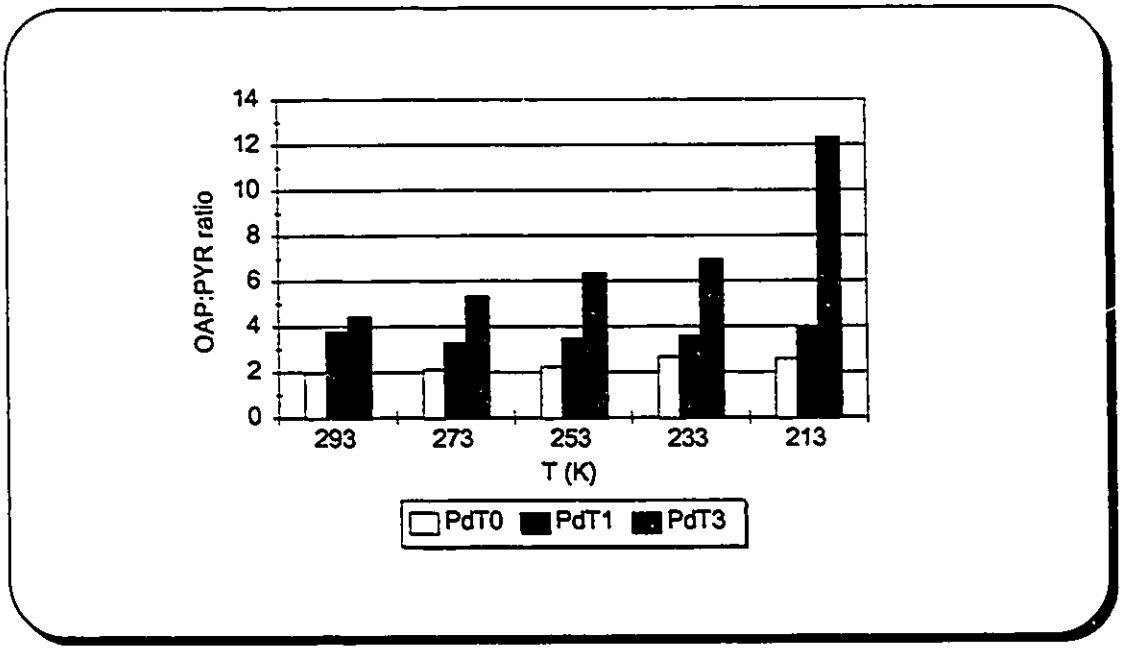

Figure 4.15 OAP:PYR ratio for each receptor at various temperatures. More ether oxygen atoms in a receptor results in a higher OAP:PYR ratio.

(ix) Molecular Recognition of Biological Nucleobases. Extraction experiments with adenine, cytosine, guanine and thymine were performed in CD_3COCD_3 and CD_3CN solutions[98]. The results are summarized in graphical form in Figure 4.16 and provide a qualitative picture of the relative affinities of the receptors for the four nucleobases.

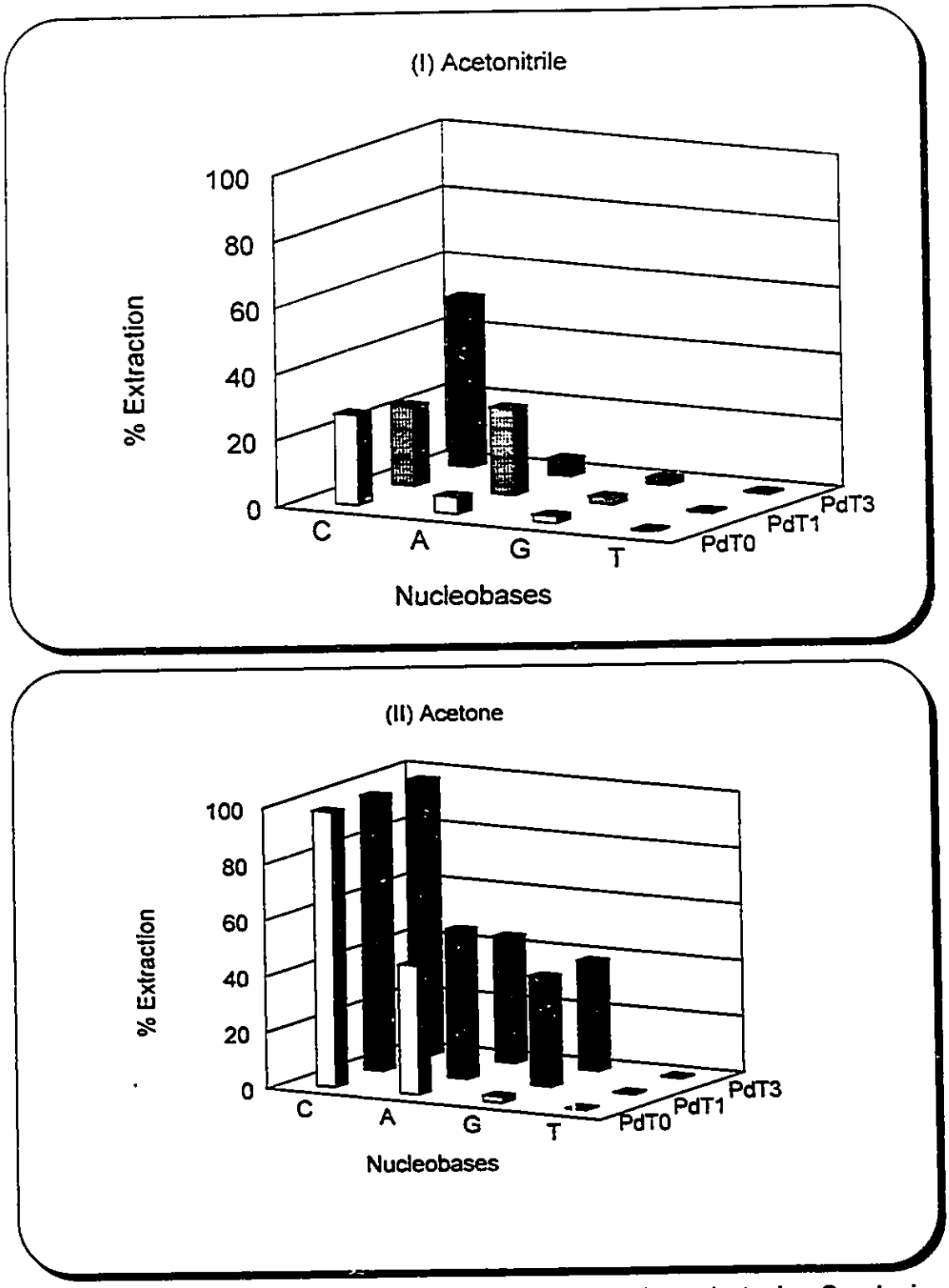

Figure 4.16 Plots of percent extraction of solid nucleobase (cytosine C, adenine A, guanine G, thymine T) into a solution of PdTX ($[Pd(CH_3CN)(TOMB\text{-}X)][BF_4]$, X=0,1,3) in CD_3CN and CD_3COCD_3.

Cytosine has potential metal coordination and hydrogen bonding sites at N3 and N4, two of the three sites employed in Watson-Crick base pairing. Figure 4.16 shows that in CD_3CN solution $[Pd(CH_3CN)(TOMB\text{-}3)]^+$ exhibits molecular recognition for cytosine, with a 56% extraction value compared to less than 5% for the other nucleobases. The ^1H NMR spectrum (CD_3CN) of an isolated sample of $[Pd(CYT)(TOMB\text{-}3)][BF_4]$ (Figure 4.17) shows the typical benzylic splitting, and free and hydrogen-bonded NH_2 signals at 6.71 and 7.28 ppm for bound cytosine, as compared to a single resonance at 6.69 ppm for $[Pd(CYT)(TOMB\text{-}0)]^+$ in which no hydrogen-bonding can occur[42-49].

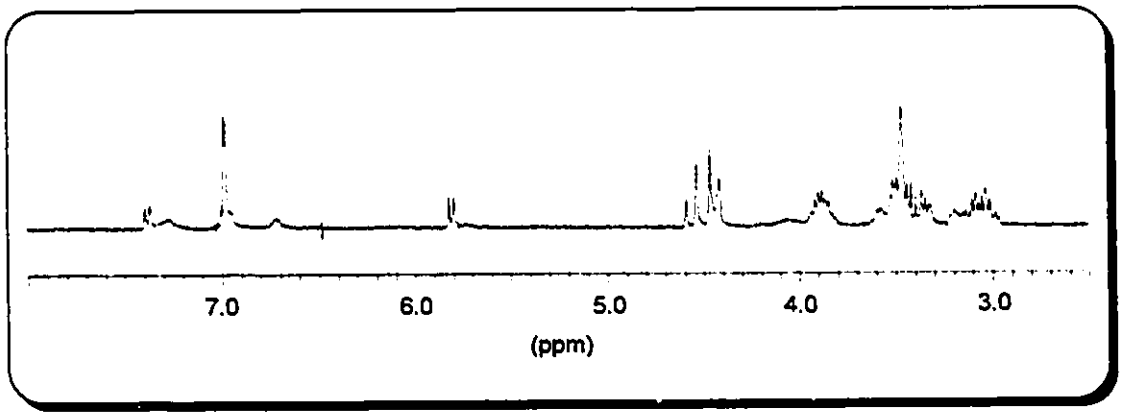

Figure 4.17 ^1H NMR spectrum of $[Pd(CYT)(TOMB\text{-}3)]^+$ (CD_3CN). Free and hydrogen-bonded N-H protons are observed at 6.71 and 7.28 ppm.

Guanine has potential metal coordination and hydrogen-bonding sites at either N7 and N2 or N3 and N2, however only one isomer was observed by NMR. Extraction experiments show guanine to be the least extracted of adenine, cytosine and guanine, while thymine was not extracted in any appreciable amount as it lacks the aromatic nitrogen-donor for σ-donation to Pd.

Adenine has potential metal coordination and hydrogen-bonding sites at either N1 and N6 employed in Watson-Crick base pairing, N7 and N6 employed in Hoogsteen base pairing[113a, 115, 116], or N3 and N6, Type III (Figure 4.18). In extraction experiments performed in acetonitrile, only $[Pd(CH_3CN)(TOMB\text{-}1)]^+$ was able to extract adenine in an appreciable amount at 26%, compared to <5% for the other 2 receptors.

In performing extraction experiments, two isomers for a bound adenine substrate were observed with the receptors. ^1H NMR spectra in CD_3COCD_3 employing 1:1 solutions of the receptors and 9-ethyladenine showed isomer ratios of 1:1, 1.96:1 and 1.64:1 respectively. These ratios are a result of competition between Watson-Crick and Hoogsteen type binding modes while Type III binding is not observed. Watson-Crick type binding allows for optimization of the hydrogen-bonding interaction but the higher basicity of N7 favours the Hoogsteen type binding mode. In the case of $[Pd(CH_3CN)(TOMB\text{-}0)]^+$, in which

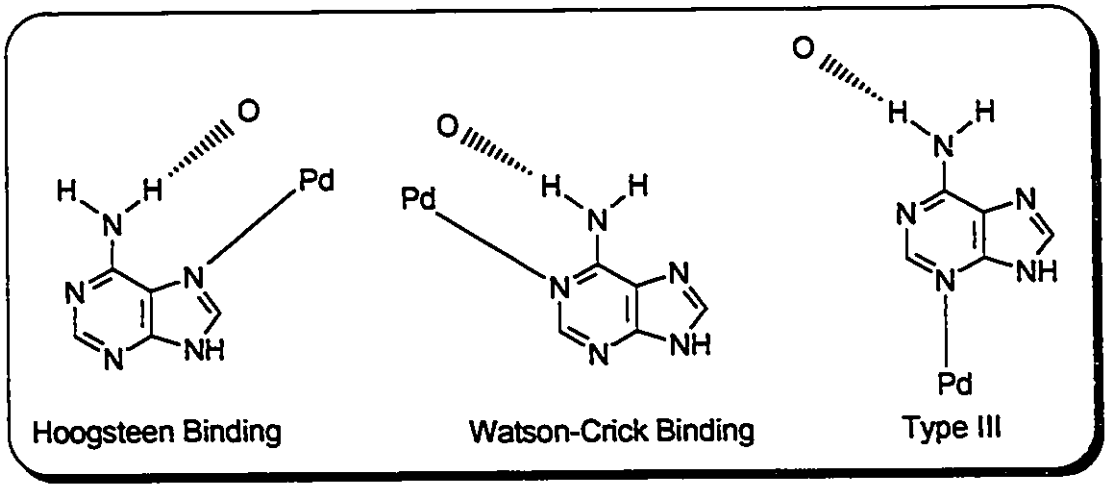

Figure 4.18 Three types of binding modes possible for adenine.

no hydrogen-bonding occurs the ratio is 1:1, but when the possibility of hydrogen-

bonding is introduced for $[Pd(CH_3CN)(TOMB\text{-}1)]^+$ and $[Pd(CH_3CN)(TOMB\text{-}3)]^+$ the Watson-Crick type interaction is favoured. This is more pronounced for $[Pd(CH_3CN)(TOMB\text{-}1)]^+$ and CPK models show that although both receptors can undergo hydrogen-bonding, the short polyether chain for $[Pd(CH_3CN)(TOMB\text{-}1)]^+$ is locked in a rigid, preorganized conformation with a smaller spacing between the Pd and O binding sites which favours Watson-Crick type binding.

In addition to the NMR evidence observed in the extraction experiments, X-Ray quality crystals of the $[Pd(CYT)(TOMB\text{-}3)][BF_4]$ were grown from an acetonitrile/diethyl ether solution and the crystal structure was solved.

(x) Crystal Structure of $[Pd(CYT)(TOMB\text{-}3)][BF_4]$, (34). The unit cell is monoclinic and contains 4 cations and anions of $[Pd(CYT)(TOMB\text{-}3)][BF_4]$ and four acetonitrile solvent molecules. A perspective view of the cation with the atom numbering scheme is shown in Figure 4.19. Complete listings of crystallographic parameters including atomic positions, bonding parameters and details of data collection are listed in Appendix Table A12. Selected bonding parameters are given in the figure caption.

The palladium atom is in a square planar environment with the S_2C bracket occupying three sites and the cytosine substrate occupying the fourth site on the metal atom. The Pd-S distances are Pd1-S1 = 2.309(3) Å and Pd1-S2 = 2.299(3) Å. Pd1-N1 = 2.164(4) Å and Pd1-C1 = 1.992(7) Å. The angles at the palladium atom are S1-Pd1-C1 = 85.4(2)° and S2-Pd1-C1 = 81.8(2)° at the 5-membered chelate rings and S1-Pd1-N1 = 92.0(2)° and S2-Pd1-N1 = 101.2(2)° at the non-chelating substrate. As was observed for $[Pd(PIC)(TOMB\text{-}3)]^+$, the angle

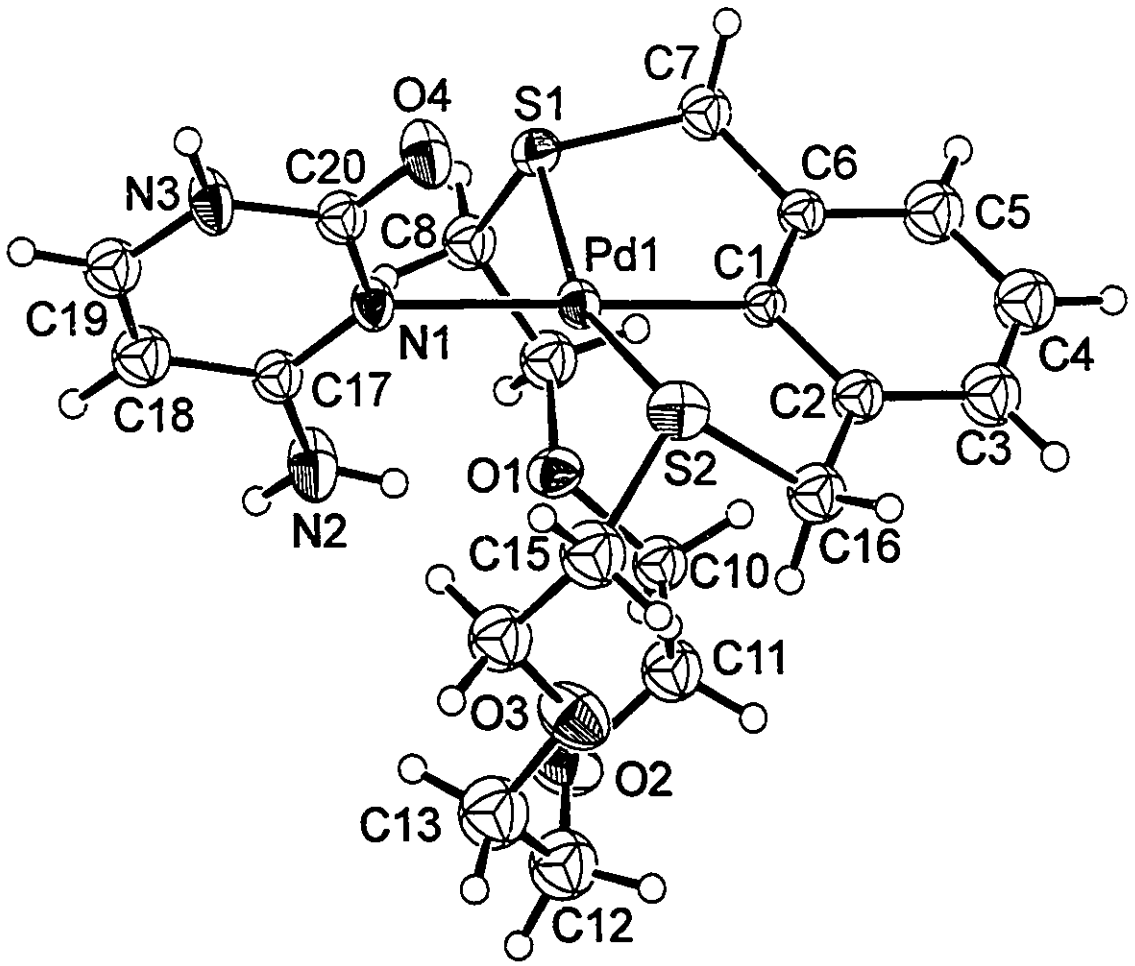

Figure 4.19 Perspective ORTEP drawing of $[Pd(CYT)(TOMB\text{-}3)]^+$ cation (34) showing the atom numbering scheme with 30% thermal ellipsoids. Selected bond distances (Å) and angles are: Pd1-S1 = 2.309(3), Pd1-S2 = 2.299(3), Pd1-N1 = 2.164(6), Pd1-C1 = 1.992(7), N2...O1 = 3.06(1). S1-Pd1-C1 = 85.4(2)°, S2-Pd1-C1 = 81.8(2)°, S1-Pd1-N1 = 92.0(2)°, S2-Pd1-N1 = 101.2(2)°, S1-Pd1-S2 = 161.80(8)°, N1-Pd1-C1 = 176.6(3)°.

S1-Pd1-S2 = 161.80(8)° is substantially reduced from its value in the structure of the free receptor. The amino group is positioned on the same side of the square plane as the ether oxygen atoms and there is a hydrogen-bond between N4 and O1 at a distance of 3.06(1) Å. In order to form the hydrogen bond between N4 and O1, the S2 atom moves away from the substrate and the polyether chain reorients itself to bring the O1 atom closer to the N4 atom. This results in a decrease of the S1-Pd1-S1 bond angle from 171.27(7)° to 161.80(8)°. The angle C1-Pd1-N1 = 176.6(3)° is essentially linear.

The conformation of the $[Pd(TOMB\text{-}3)]^+$ receptor in the 2-amino-4-picoline and cytosine complexes is very similar. This can be seen by examining the bond angles about the palladium atom (Table 4.2). The same reorientation of the polyether chain results upon complex formation with cytosine or 4-aminopicoline which both contain a hydrogen-bond donor group.

Table 4.2 Comparison of Bond Angles around palladium for the four $[Pd(L)(TOMB\text{-}3)]^+$ complexes.

Angles around Pd.	$[Pd(CH_3CN)(TOMB\text{-}3)]^+$	$[Pd(PYR)(TOMB\text{-}3)]^+$	$[Pd(PIC)(TOMB\text{-}3)]^+$	$[Pd(CYT)(TOMB\text{-}3)]^+$
S1-Pd1-S2	171.27(7)°	163.7(1)°	159.93(7)°	161.80(8)°
S1-Pd1-C1	85.7(2)°	84.7(3)°	85.1(2)°	85.5(2)°
S2-Pd1-C1	85.8(2)°	85.6(3)°	81.1(2)°	81.7(2)°
S1-Pd1-N1	94.2(2)°	93.7(3)°	94.7(2)°	92.0(2)°
S2-Pd1-N1	94.4(2)°	96.8(3)°	99.7(2)°	101.2(2)°
N1-Pd1-C1	177.2(3)°	175.4(4)°	177.2(2)°	176.7(3)°

The S2-Pd1-C1 angles decrease to about 81.5°, the S2-Pd1-N1 angles simultaneously increases to about 100°, and the S1-Pd1-S1 angles decrease to

about 160°, all due to the reorientation of the polyether chain in forming the hydrogen bond between N2 and O1.

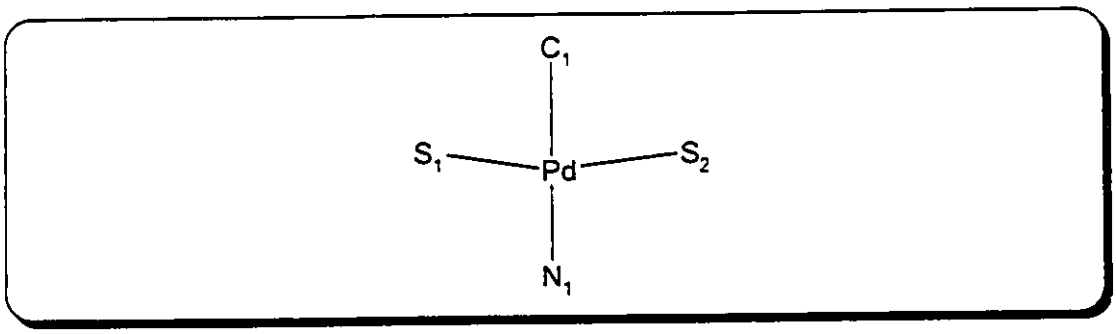

4.5 Conclusion

The three receptors $[Pd(CH_3CN)(TOMB\text{-}0)]^+$, $[Pd(CH_3CN)(TOMB\text{-}1)]^+$ and $[Pd(CH_3CN)(TOMB\text{-}3)]^+$ were reacted with pyridine and *o*-aminopyridine. Crystals of the receptor-substrate complexes $[Pd(OAP)(TOMB\text{-}1)][BF_4]$, $[Pd(PYR)(TOMB\text{-}3)][BF_4]$, $[Pd(PIC)(TOMB\text{-}3)][BF_4]$, and $[Pd(CYT)(TOMB\text{-}3)][BF_4]$ were isolated and the crystal structures were solved. In complexes in which the substrate contains an amino group, simultaneous interaction with the primary and secondary coordination sphere of the palladium atom occurs via σ-donation to the metal and hydrogen-bond formation with an oxygen atom in the polyether chain.

Competition experiments were performed between each of the three receptors and a mixture of pyridine and *o*-aminopyridine in a 1:1:1 ratio in $CDCl_3$. The NMR spectra were recorded at various temperatures and the percentage of coordinated *o*-aminopyridine was determined. It was observed that as the number of oxygen atoms in a receptor increases from 0 to 1 to 3 the ratio of coordinated OAP to coordinated PYR increases. The hydrogen-bonding

receptors are better able to select *o*-aminopyridine over pyridine than the model receptor [Pd(CH_3CN)(TOMB-0)][BF_4].

The concept of using simultaneous primary and secondary coordination to distinguish between substrates of different shapes was applied by performing several extraction experiments with the biological substrates cytosine, guanine, adenine or thymine. It was observed that [Pd(CH_3CN)(TOMB-3)][BF_4] is selective for cytosine over the other three biological nucleobases and that only [Pd(CH_3CN)(TOMB-1)][BF_4] is able to extract adenine into solution in an appreciable amount.

Chapter 5

Multi-point Binding of Amines

Chapter 5

5.1 Introduction

(i) Thought Process. It was observed in the work with the *ortho*-aminopyridine substrates in Chapter 4, that no more than one second-sphere hydrogen-bond is formed in the solid state between the substrate and the receptor to which it is coordinatively bonded. This is due to two factors. (i) The orientation of the NH_2 group to the polyether chain prevents the formation of more than one intramolecular hydrogen-bond. (ii) The presence of only one hydrogen-bond donor group on the substrate does not facilitate the formation of multiple hydrogen-bonds.

The goal of the work outlined in this chapter was, therefore, to choose substrates that would maximize the number second-sphere hydrogen-bonding interactions that accompany primary coordination by the substrate. The receptors $[Pd(CH_3CN)(TOMB\text{-}3)][BF_4]$ and $[Pd(CH_3CN)(TOMB\text{-}5)][BF_4]$ were chosen for this investigation because they contain polyether chains capable of forming multiple hydrogen-bonds. The substrates that were chosen all contain non-aromatic amine donor groups for primary coordination to the metal centre.

Examination of CPK models indicated that upon formation of the palladium-amine bond, the N-H protons are ideally situated to form two hydrogen-bonds with the ether oxygen atoms adjacent to the sulfur atoms in the receptor (Figure 5.1). In addition, some R-groups were chosen that also contain hydrogen-bond donors (X= $-NH_2$ and $-NH_3^+$) for additional hydrogen-bonding.

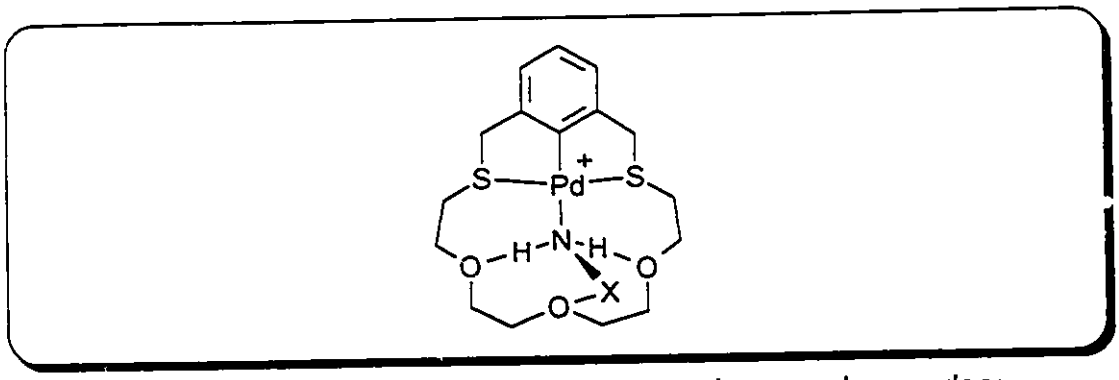

Figure 5.1 Schematic diagram of simultaneous primary and secondary coordination of amines. X=NH_2 or NH_3^+

(ii) Background Literature. Extensive work has been performed in binding ammonium cations using hydrogen-bonding interactions with several macrocyclic crown ethers. The research groups of McKervey[117], Stoddart[118], Izatt and Bradshaw[119] and Cram[120] have all performed studies on the thermodynamic and structural considerations involved in forming these complexes. Shown below (Figure 5.2) is a schematic diagram and a crystal structure of a complex isolated by Cram and coworkers[120f].

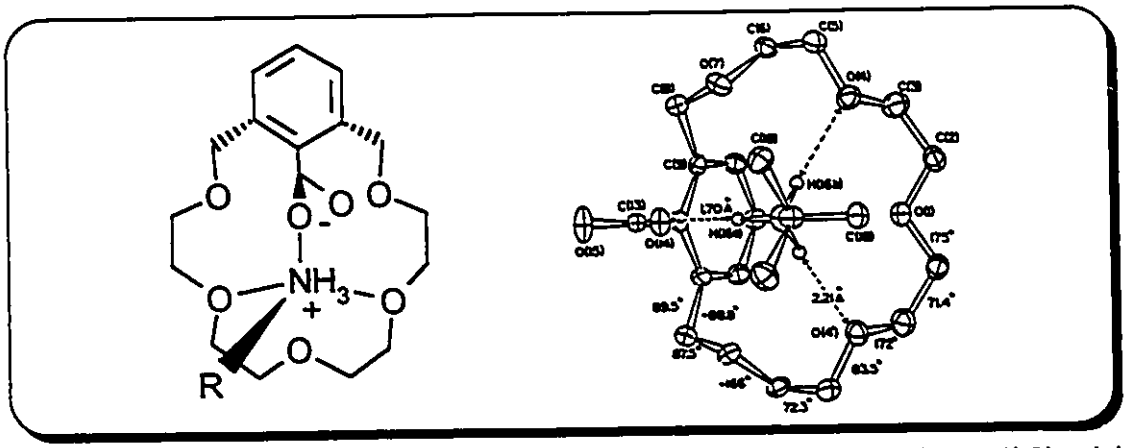

Figure 5.2 Schematic diagram and crystal structure of the 2'-carboxy-1',3'-xylyl-18-crown-5-(*t*-butylamine) complex.

Hydrogen-bonding interactions in the second-sphere between the Fe(III)

complex shown in Figure 5.3a and the hexa-aqua metal complexes $[M^{II}(OH_2)_6]^{2+}$ (M=Zn, Ni, Co, Mn) have been employed by Wieghardt *et al*[121] to effect selectivity of the Fe(III) complex for the Zn(II), Ni(II) and Co(II) complexes over the Mn(II) complex. The crystal structure of the hydrogen-bonded Zn(II) complex is shown in Figure 5.3b and shows the extensive hydrogen-bonding interactions.

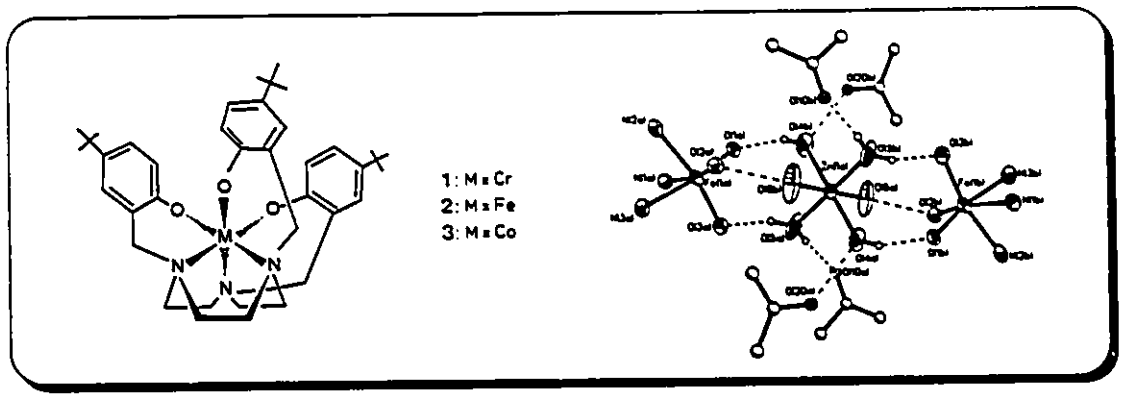

Figure 5.3 a) Schematic diagram of Fe(III) 'receptor' complex. b) Crystal structure of hydrogen-bonded Fe(III)-Zn(II) 'receptor-substrate' complex; receptor carbons are omitted for clarity.

Second-sphere interactions between crown ethers and the N-H hydrogens in metal-amine complexes have also been observed by Stoddart and coworkers[42] and others[122], as shown in Figure 5.4 for $\{[Cu(NH_3)_4(H_2O)][PF_6]_2\text{-}(C_{12}H_{24}O_6)\}_n$. A summary of Stoddart's work is found in the Introduction.

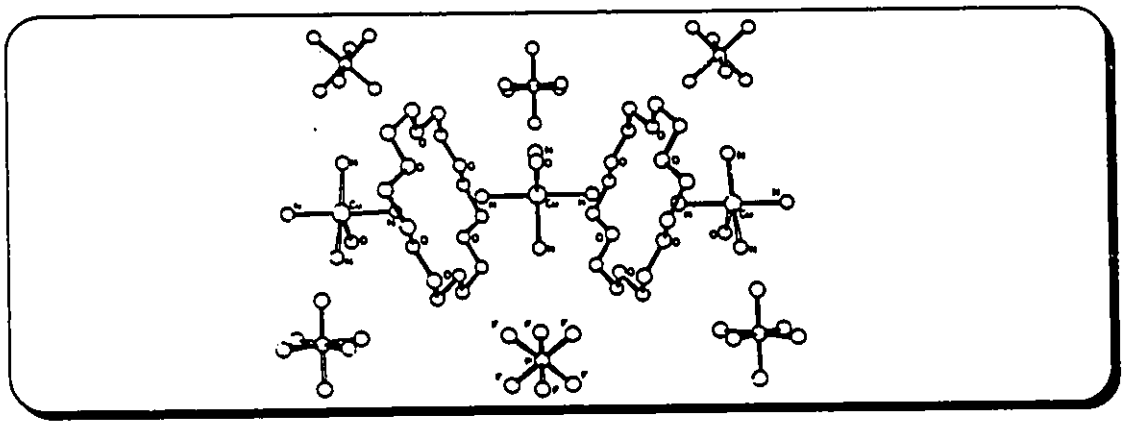

Figure 5.4 Crystal structure of $\{[Cu(NH_3)_4(H_2O)][PF_6]_2\text{-}(C_{12}H_{24}O_6)\}_n$.

There are several examples of simultaneous first- and second-sphere coordination to receptors containing Lewis acidic centres. Reetz and co-workers have also observed this phenomenon in which first-sphere coordination by a primary amine to a boron centre is accompanied by second-sphere coordination of the amine protons to a polyether chain[94] (Figure 5.5a). Stoddart and co-workers determined the crystal structure of a complex in which the two nitrogen atoms of N_2O_4 coordinate to two Rh (I) atoms and ammonia ligands bonded to the rhodium atoms simultaneously hydrogen-bond to the ether oxygen atoms of the macrocycle[123] (Figure 5.5b).

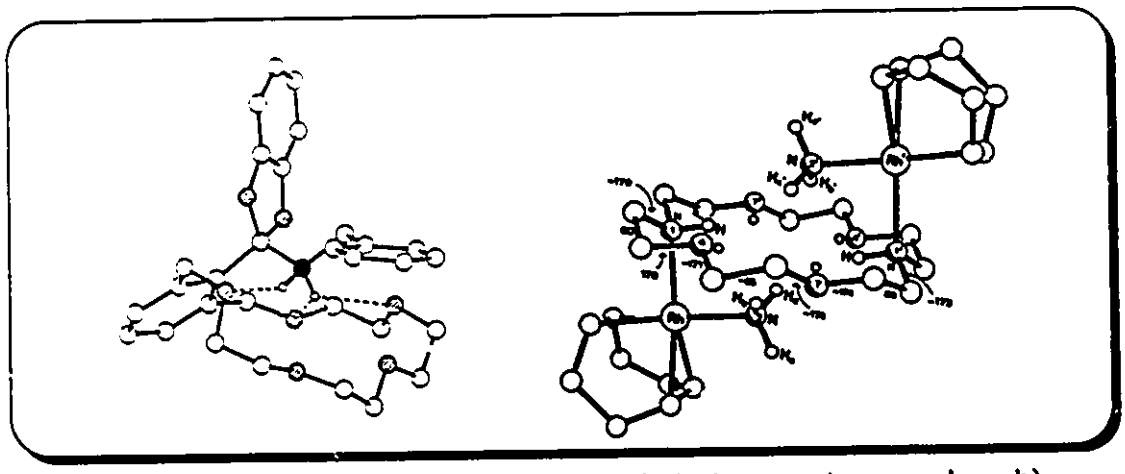

Figure 5.5 a) Crystal structure of Reetz's substrate-receptor complex. b) Crystal structure of Stoddart's $[(Rh(COD)(NH_3))_2N_2O_4][PF_6]_2$ complex.

In addition to the work done in this chapter on simultaneous first- and second-sphere coordination of amines, work in which the 'substrate' is a Ag^+ ion interacting with: the π-cloud of the aromatic ring; the polyether chain of the receptor; the palladium atom; and a $CF_3SO_3^-$ group, is also described. There is precedence for unusual interactions between silver atoms and aromatic rings[124]

(Figure 5.6) and several crystal structures have been determined.

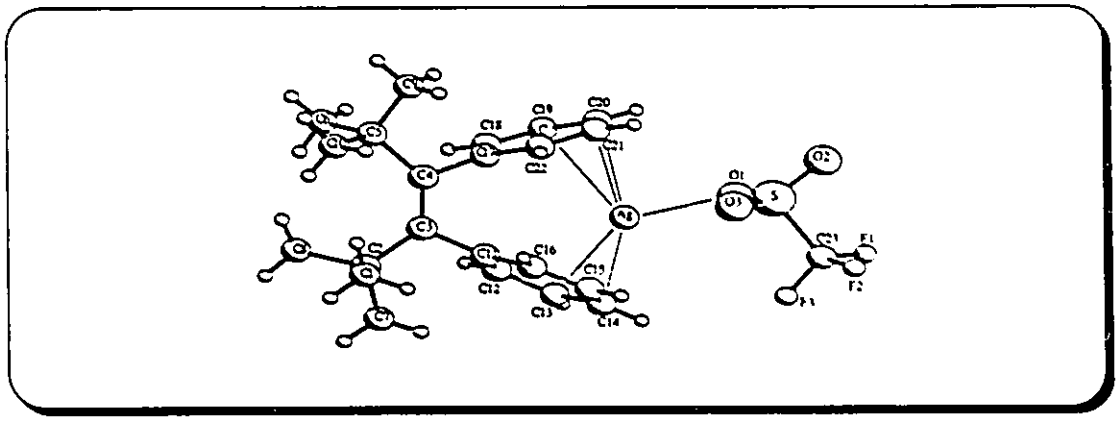

Figure 5.6 Crystal structure of the complex of Ag^+ with a *cis*-stilbene[124d].

The labs of Vrieze and Van Koten have both done research involving metal-metal bonds between d^8 *trans*ition metals and Ag and Cu[125, 126]. The silver atom is stabilized by the donor *trans*ition metal and a bridging ligand, as shown in Figure 5.7a. The aromatic ring was also shown to be electron rich enough to react with methyl iodide and form an sp^3 hybridized carbon atom (Figure 5.7b).

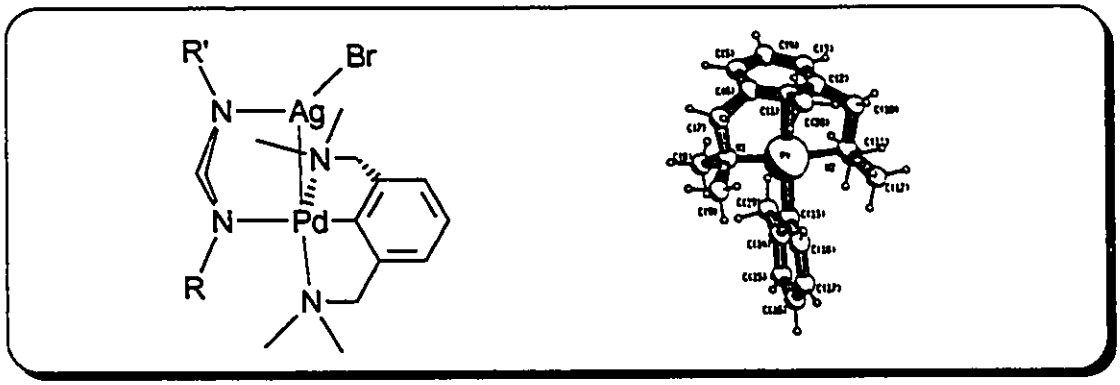

Figure 5.7 a) Schematic diagram of $[PtAg(C_6H_3(2,6\text{-}Me_2NCH_2)_2)(RNCHNR')Br]$ complex stabilized by a bridging ligand. R=*p*-tolyl, R'=alkyl.
b) Crystal Structure of $Pt((CH_3\text{-}C_6H_3(2,6\text{-}Me_2NCH_2)_2)(o\text{-tolyl})][I]$.

Part of the work described in this chapter has appeared as a preliminary communication[127].

5.2 Experimental

General Comments. All starting materials, hydrazine monohydrochloride, hydrazine monohydrate, *n*-butylamine, N-methylbutylamine, N,N-dimethyl-butylamine and allylamine (ALL), deuterated solvents and anhydrous N,N-dimethylformamide (DMF) were purchased from Aldrich Chemicals and used without further purification, except acetonitrile which was distilled from CaH_2 under N_2(g) and [Pd(CH_3CN)(TOMB-3)][BF_4] and [Pd(CH_3CN)(TOMB-5)][BF_4] which were prepared as per Chapter 3. All reactions were performed under an atmosphere of N_2(g) using standard Schlenk or dry-box techniques and all solvents and liquid starting materials were degassed prior to use. ^1H and $^{13}C\{^1H\}$ NMR spectra were recorded on a Brüker AC300 spectrometer locked to the deuterated solvent at 300.1 and 75.5 MHz respectively, and infrared spectra were recorded on a Nicolet 5DX FTIR spectrometer. Elemental analyses were performed by Canadian Microanalytical Service, Delta, British Columbia.

(i) Preparation of [Pd(NH_3)(TOMB-3)][BF_4], (38).

[Pd(CH_3CN)(TOMB-3)][BF_4] (0.031 g, 55 μmol) was dissolved in acetonitrile (5.0 mL) and NH_3 (g) was passed over the solution for 10 min. The solution was allowed to stir for 2 h at room temperature after which the solvent was removed *in vacuo*. The resulting paste was recrystallized from acetonitrile/diethyl ether. Yield of pale yellow powder: 0.021 g, (71%). ^1H NMR (CD_3CN, 298 K): δ (ppm) 7.13 (s br, 3H, aromatic), 4.49 (s br, 4H, benzylic), 4.01 (s br, 4H, OCH_2), 3.75 (s br, 4H, OCH_2), 3.69 (s br, 4H, OCH_2), 3.5-3.2 (m br, 4H, SCH_2), 2.54 (s br, 3H,

NH_3). $^{13}C\{^1H\}$ NMR (CD_3CN): δ (ppm) 148.56, 126.23, 123.36 (aromatic, Pd-C1 not observed), 71.06, 70.22, 68.86 (OCH_2), 47.07 (benzylic), 38.93 (SCH_2).

(ii) Preparation of [Pd(NH_2-*n*-Bu)(TOMB-3)][BF_4], (39).

[Pd(CH_3CN)(TOMB-3)][BF_4] (0.023 g, 41 μmol) was dissolved in acetonitrile (3.0 mL) and *n*-butylamine (7 μL, 71 μmol) was added by syringe. The solution was stirred at room temperature for 4 h, the solvent was removed and the resulting paste was triturated with diethyl ether overnight. The diethyl ether was decanted off, and the pale yellow powder was dried *in vacuo*. Yield: 0.023 g, (95%). ^1H NMR ($CDCl_3$): δ (ppm) 6.97 (m br, 3H, aromatic), 4.47 (d, 2H, ^2J = 14.8 Hz, benzylic), 4.33 (d, 2H, benzylic), 3.99 (s br, 4H, OCH_2), 3.7-3.2 (m, 12H, OCH_2; 2H, NH_2), 2.66 (m, 2H, N-(α)CH_2), 1.55 (m, 2H, N-(β)CH_2), 1.34 (m, 2H, N-(γ)CH_2), 0.92 (t, 3H, ^3J = 7.3 Hz, N-(δ)CH_3).

(iii) Preparation of [Pd(NH(Me)-*n*-Bu)(TOMB-3)][BF_4], (40).

[Pd(CH_3CN)(TOMB-3)][BF_4] (0.030 g, 53 μmol) was dissolved in acetonitrile (3.0 mL) and N-methylbutylamine (7 μL, 59 μmol) was added by syringe. The solution was stirred at room temperature for 4 h, the solvent was removed and the resulting paste was triturated with diethyl ether overnight. The diethyl ether was decanted off, and the pale yellow powder was dried *in vacuo*. Yield: 0.031 g, (96%). ^1H NMR ($CDCl_3$): δ (ppm) 6.94 (s br, 3H, aromatic), 4.47-4.36 (m, 4H, benzylic), 4.14-3.88 (m, 6H, OCH_2), 3.71-3.25 (m, 6H, OCH_2; 4H, SCH_2), 2.73 (m, 2H, N-(α)CH_2), 1.74 (m, 2H, N-(β)CH_2), 1.33 (m, 2H, N-(γ)CH_2), 0.92 (t, 3H, ^3J = 7.3 Hz, -N-(δ)CH_3).

(iv) Attempted Preparation of [Pd(NMe$_2$-*n*-Bu)(TOMB-3)][BF$_4$]. [Pd(CH$_3$CN)(TOMB-3)][BF$_4$] (0.030 g, 53 μmol) was dissolved in acetonitrile (3.0 mL) and N,N-dimethylbutylamine (8 μL, 57 μmol) was added by syringe. The solution was stirred at room temperature for 4 h, the solvent was removed and the resulting paste was triturated with diethyl ether overnight. The diethyl ether was decanted off, and the pale yellow powder was dried *in vacuo*. The powder was shown by ^{1}H NMR spectroscopy to be free [Pd(CH$_3$CN)(TOMB-3)][BF$_4$] receptor.

(v) Preparation of [Pd(ALL)(TOMB-3)][BF$_4$], (41). [Pd(CH$_3$CN)(TOMB-3)][BF$_4$] (0.045 g, 80 μmol) was dissolved in chloroform (15 mL) and allylamine (9 μL, 122 μmol) was added by syringe. The solution was stirred overnight and the solvent was then removed *in vacuo*. The resulting yellow paste was recrystallized from chloroform/diethyl ether. Yield: 0.042 g, (91%). ^{1}H NMR ($CDCl_3$): δ (ppm) 6.95 (m, 3H, aromatic), 5.96 (m, 1H, R-CH=R), 5.23 (m, 2H, R=CH$_2$), 4.45 (d, 2H, ^2J = 14.8 Hz, benzylic), 4.31 (d, 2H, benzylic), 3.97 (s br, 4H, OCH$_2$), 3.68-3.50 (m, 8H, OCH$_2$; 2H, NH$_2$), 3.32-3.24 (m, 4H, SCH$_2$; 2H, NCH$_2$). ^{13}C{^{1}H} NMR ($CDCl_3$): δ (ppm) 157.39, 147.36, 125.64, 122.74 (aromatic), 136.07 (olefinic CH), 117.82 (olefinic CH$_2$), 70.37, 69.17, 68.39 (OCH$_2$), 47.44 (NCH$_2$), 46.71 (benzylic), 38.87 (SCH$_2$).

(vi) Preparation of [Pd(H$_2$O)(TOMB-5)][BF$_4$], (42). Yellow crystals of [Pd(H$_2$O)(TOMB-5)][BF$_4$] were grown from a diffusion of diethyl ether into an acetonitrile solution of [Pd(CH$_3$CN)(TOMB-5)][BF$_4$]. Atmospheric moisture in the

acetonitrile/diethyl ether displaced the ancillary acetonitrile ligand. ^{1}H NMR (CD_3CN): δ (ppm) 6.99 (M, 3H, aromatic), 4.48 (m br, 4H, benzylic), 3.86 (s br, 4H, OCH_2), 3.54 (m br, 18H, OCH_2, H_2O), 3.26 (s br, 4H, SCH_2).

(vii) Preparation of [Pd(NH_2NH_2)(TOMB-3)][BF_4], (43). [Pd(CH_3CN)(TOMB-3)][BF_4] (0.061 g, 110 μmol) and excess hydrazine hydrate (NH_2NH_2-H_2O) were dissolved in acetonitrile (10 mL) and stirred overnight. The solvent was then removed *in vacuo* and the complex was recrystallized from acetonitrile/diethyl ether to give a pale yellow powder. Yield: 0.048 g (80%). ^{1}H NMR ($CDCl_3$): δ (ppm) 6.96 (m, 3H, aromatic), 5.57 (s, 2H, α-NH_2), 5.05 (s, 2H, β-NH_2), 4.39 (d, 2H, ^2J = 14.2 Hz, benzylic), 4.25 (d, 2H, benzylic), 4.03-3.57 (m, 12H, OCH_2; 2H, SCH_2), 3.22 (d br, 1H, ^2J = 14 Hz, SCH_2), 3.07 (d br, 1H, SCH_2).

(viii) Preparation of [Pd(NH_2NH_2)(TOMB-5)][BF_4], (44). [Pd(CH_3CN)(TOMB-5)][BF_4] (4.0 mL, 25 x mM, 100 μmol) and excess hydrazine monohydrate were dissolved in acetonitrile (10 mL) and stirred under N_2 overnight. The solution was filtered and the solvent was reduced to 1-2 mL. Diethyl ether was diffused into the solution which gave a pale yellow powder. Yield: 0.022 g (34%). ^{1}H NMR ($CDCl_3$): δ (ppm) 6.95 (m, 3H, aromatic), 5.6 (s br, NH_2NH_2), 4.6-3.9 (br, 8H, benzylic, OCH_2), 3.8-3.6 (m, 16H, OCH_2), 3.4-3.1 (s br, 4H, SCH_2).

(ix) Preparation of [Pd(NH_2NH_3)(TOMB-3)][CF_3SO_3]$_2$, (45). [$AgCF_3SO_3$] (0.062 g, 230 μmol), NH_2NH_2-HCl (0.009 g, 130 μmol) and [PdCl(TOMB-3)] (0.0534 g, 115 μmol) were stirred and warmed in acetonitrile . The AgCl was

filtered off and the solvent was removed *in vacuo* to give a yellow solid which was recrystallized from acetonitrile/diethyl ether. Yield: 0.053 g (60%). This compound was also prepared by the addition of one equivalent of $AgBF_4$ to hydrazine monohydrochloride and the receptor $[Pd(CH_3CN)(TOMB\text{-}3)][BF_4]$. The anions associated with the di-cationic species do not affect the ^1H NMR spectrum. ^1H NMR ($CDCl_3$): δ (ppm) 7.10-6.75 (d, t, d, 3H, aromatic), 4.65 (s br, 4H, benzylic), 4.21-3.61 (m, 12H, OCH_2; 5H, NH_2NH_3), 3.34 (s br, 4H, SCH_2).

(x) Preparation of $[Pd(NH_2NH_3)(TOMB\text{-}5)][BF_4]_2$, (46).

$[Pd(CH_3CN)(TOMB\text{-}5)][BF_4]$ (4.0 mL, 25 mM, μmol) and $[NH_2NH_3][BF_4]$ (2.0 mL, 52 mM, 100 μM) were stirred at room temperature for 1 h in acetonitrile (5 mL) after which time the solvent was reduced to 1 mL. Diethyl ether was diffused into the solution which yielded yellow crystals. Yield: 0.037 g (51%). A good quality NMR spectrum could not be obtained, however in CD_3COCD_3 the presence of the hydrazinium is indicated. ^1H NMR (CD_3COCD_3): δ (ppm) 7.00 (s br, 3H, aromatic), 4.57 (s vbr, 4H, benzylic), 4.2-3.9 (m br, 8H, OCH_2), 3.72- 3.31(m br, 21H, OCH_2, SCH_2, NH_2NH_3)

(xi) Preparation of $[PdAg(H_2O)(TOMB\text{-}3)(CF_3SO_3)][CF_3SO_3]$, (47).

$[Pd(TOMB\text{-}3)Cl]$ (0.075 g, 160 μmol), $AgCF_3SO_3$ (0.045 g, 345 μmol) and pyrazine (0.008 g, 81 μmol) were stirred in CH_2Cl_2 (7 mL) under N_2 and protected from light. The solution was filtered to remove AgCl and the solvent was reduced to 2 mL. The complex was recrystallized by vapour diffusion of diethyl ether into the CH_2Cl_2 solution leaving yellow crystals. Yield: 0.056 g, (41%). Solvation in

polar solvents resulted in decomposition of the complex so no solution spectra could be obtained. The compound was characterized by X-ray crystallography.

5.3 X-Ray Diffraction Data Collection, Solution, and Refinement.

(i) General Procedures. The general procedure for data collection and solution refinement is identical to that outlined in section 2.3 (i) and the reader is referred to it for the sake of brevity.

(ii) Structure Determination of [Pd(NH_3)(TOMB-3)][BF_4], (38). Yellow crystals of [Pd(NH_3)(TOMB-3)][BF_4] were grown by vapour diffusion of diethyl ether into an acetonitrile solution of the complex. A statistical analysis of the intensity distributions and a determination of observed extinctions were consistent with the *ortho*rhombic space group Pbca, and this was confirmed by a successful solution refinement. A total of 3863 reflections were collected, and 630 unique reflections with $F_o^2 > 3\sigma(F_o^2)$ were used in the refinement. The positions of the palladium and sulfur atoms were determined by direct methods from the *E*-map with the highest figure of merit. The remaining atoms were located from a difference Fourier map calculation. The tetraflouroborate anion and the aromatic ring were refined as a rigid groups. In the final cycles of refinement, the palladium, nitrogen and sulfur atoms were assigned anisotropic thermal parameters and the rigid group constraint was removed from the aromatic ring. This resulted in $R = 0.0662$ and $R_w = 0.0639$ at final convergence. The Δ/σ value for any parameter in the final cycle was less than 0.007. A final difference Fourier map calculation showed no peaks of chemical significance. Crystal data,

intensity collection and structure refinement details, as well as all atomic positional parameters, bond distances and angles are summarized in Appendix Table A15.

(iii) Structure Determination of [Pd(H_2O)(TOMB-5)][BF_4], (42).

Yellow crystals of [Pd(H_2O)(TOMB-5)][BF_4] were grown by vapour diffusion of diethyl ether into an acetonitrile solution of the complex. A statistical analysis of the intensity distributions was consistent with the triclinic space group $P\bar{1}$, and this was confirmed by a successful solution refinement. A total of 4521 reflections were collected, and 2277 unique reflections with $F_o^2 > 3\sigma(F_o^2)$ were used in the refinement. The positions of the palladium and sulfur atoms were determined by direct methods from the *E*-map with the highest figure of merit. The remaining atoms were located from a difference Fourier map calculation. In the final cycles of refinement, all atoms were assigned anisotropic thermal parameters. This resulted in $R = 0.0322$ and $R_w = 0.0412$ at final convergence. The Δ/σ value for any parameter in the final cycle was less than 0.0001. A final difference Fourier map calculation showed no peaks of chemical significance. Crystal data, intensity collection and structure refinement as well as all atomic positional parameters, bond distances and angles are summarized in Appendix Table A16.

(iv) Structure Determination of [Pd(NH_2NH_2)(TOMB-3)][BF_4], (43).

Pale yellow crystals of [Pd(NH_2NH_2)(TOMB-3)][BF_4] were grown by vapour diffusion of diethyl ether into an acetonitrile solution of the complex. A statistical analysis of the intensity distributions was consistent with the triclinic space group

$P\bar{1}$, and this was confirmed by a successful solution refinement. A total of 3817 reflections were collected, and 2713 unique reflections with $F_o^2 > 3\sigma(F_o^2)$ were used in the refinement. The positions of the palladium and sulfur atoms were determined by direct methods from the *E*-map with the highest figure of merit. The remaining atoms were located from a difference Fourier map calculation. In the final cycles of refinement, all atoms were assigned anisotropic thermal parameters. This resulted in $R = 0.0348$ and $R_w = 0.0286$ at final convergence. The Δ/σ value for any parameter in the final cycle was less than 0.0002. A final difference Fourier map calculation showed no peaks of chemical significance. Crystal Data, Intensity Collection and Structure Refinement as well as all atomic positional parameters, bond distances and angles are summarized in Appendix Table A17.

(v) Structure Determination of $[Pd(NH_2NH_3)(TOMB\text{-}3)][CF_3SO_3]_2$, (45). Yellow crystals of $[Pd(NH_2NH_3)(TOMB\text{-}3)][CF_3SO_3]_2$ were grown by vapour diffusion of diethyl ether into an acetonitrile solution of the complex. A statistical analysis of the intensity distributions and a determination of observed extinctions were consistent with the monoclinic space group $P2_1/c$, and this was confirmed by a successful solution refinement. A total of 5350 reflections were collected, and 2961 unique reflections with $F_o^2 > 3\sigma(F_o^2)$ were used in the refinement. The positions of the palladium and sulfur atoms were determined by direct methods from the *E*-map with the highest figure of merit. The remaining atoms including H1-H5, were located from a difference Fourier map calculation. In the final cycles of refinement, all non-hydrogen atoms were assigned anisotropic thermal

parameters. This resulted in R = 0.0430 and R_w = 0.0309 at final convergence. The Δ/σ value for any parameter in the final cycle was less than 0.03. A final difference Fourier map calculation showed no peaks of chemical significance. Crystal data, intensity collection and structure refinement details, as well as all atomic positional parameters, bond distances and angles are summarized in Appendix Table A18.

(vi) Structure Determination of $[Pd(NH_2NH_3)(TOMB\text{-}5)][BF_4]_2$, (46).

Yellow crystals of $[Pd(NH_2NH_3)(TOMB\text{-}5)][BF_4]_2$ were grown by vapour diffusion of diethyl ether into an acetonitrile solution of the complex. A statistical analysis of the intensity distributions was consistent with the triclinic space group $P\bar{1}$, and this was confirmed by a successful solution refinement. A total of 5195 reflections were collected, and 3070 unique reflections with $F_o^2 > 3\sigma(F_o^2)$ were used in the refinement. The positions of the palladium and sulfur atoms were determined by direct methods from the *E*-map with the highest figure of merit. The remaining atoms were located from a difference Fourier map calculation. In the final cycles of refinement, all atoms were assigned anisotropic thermal parameters. This resulted in R = 0.0405 and R_w = 0.0379 at final convergence. The Δ/σ value for any parameter in the final cycle was less than 0.0002. A final difference Fourier map calculation showed no peaks of chemical significance. Crystal data, intensity collection and structure refinement details, as well as all atomic positional parameters, bond distances and angles are summarized in Appendix Table A19.

(vii) Structure Determination of $[PdAg(H_2O)(TOMB\text{-}3)(CF_3SO_3)]^+$ $[CF_3SO_3]$, (47). Yellow X-ray quality crystals of the complex were grown from a vapour diffusion of diethyl ether into a CH_2Cl_2 solution of the complex. The crystal structure was determined by Dr. Stephen J. Loeb.

5.4 Results and Discussion

(i) Reaction of $[Pd(CH_3CN)(TOMB\text{-}3)][BF_4]$ with ammonia. Gaseous ammonia was passed over a solution of $[Pd(CH_3CN)(TOMB\text{-}3)][BF_4]$ in acetonitrile. The ^1H NMR spectrum of the product (Figure 5.8) in $CDCl_3$ indicates that the NH_3 is bonded to palladium by the presence of a peak for the substrate at 2.49 ppm. The broad resonances for the polyether chain are consistent with the

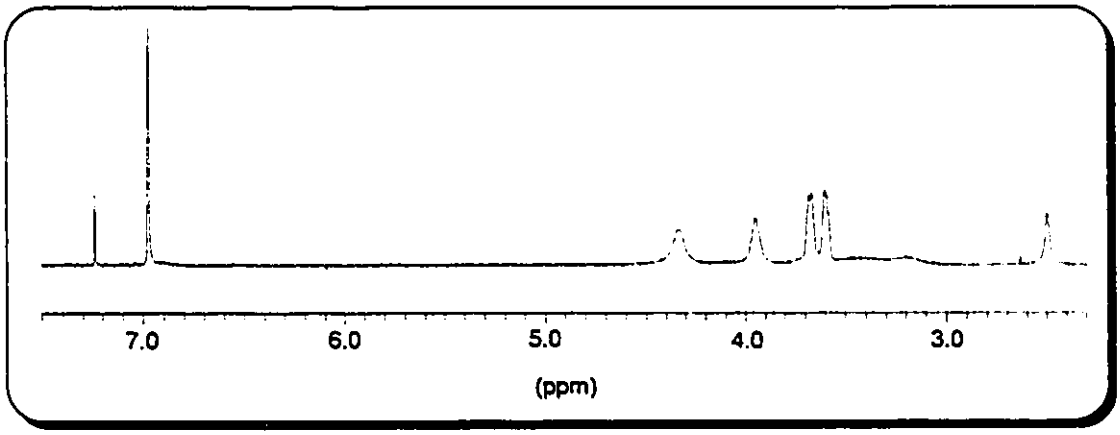

Figure 5.8 ^1H NMR spectrum of $[Pd(NH_3)(TOMB\text{-}3)][BF_4]$ in $CDCl_3$ at 298 K.

flipping process discussed in Chapter 3; the NH_3 substrate is small enough to remain inside the receptor's cavity during this process. The chemical shift of the resonance for the aromatic protons at 6.97 ppm remains essentially unchanged from that in the NMR spectrum of the free receptor.

The resonance for free ammonia appears at 0.42 ppm in CD_3CN[128]. Since acetonitrile is a hydrogen-bond acceptor[129] it would be expected that the resonance for ammonia in a *non*-hydrogen-bonding solvent, such as chloroform, would be upfield from where it appears in acetonitrile. The downfield shift of the resonance of more than 2 ppm for the ammonia substrate in $[Pd(NH_3)(TOMB\text{-}3)]^+[BF_4]$ in $CDCl_3$, in comparison to that for free ammonia in CD_3CN is consistent with the substrate being bonded to the palladium atom.

In order to determine to what extent hydrogen-bonding affects the chemical shift of the N-H protons, an NMR spectrum of the complex was also recorded at 218 K (Figure 5.9). As was indicated in Figure 5.2, two simultaneous hydrogen-bonds are possible at one instant leaving the third hydrogen atom in a non-hydrogen-bonding environment. Examination of the ^1H NMR spectrum

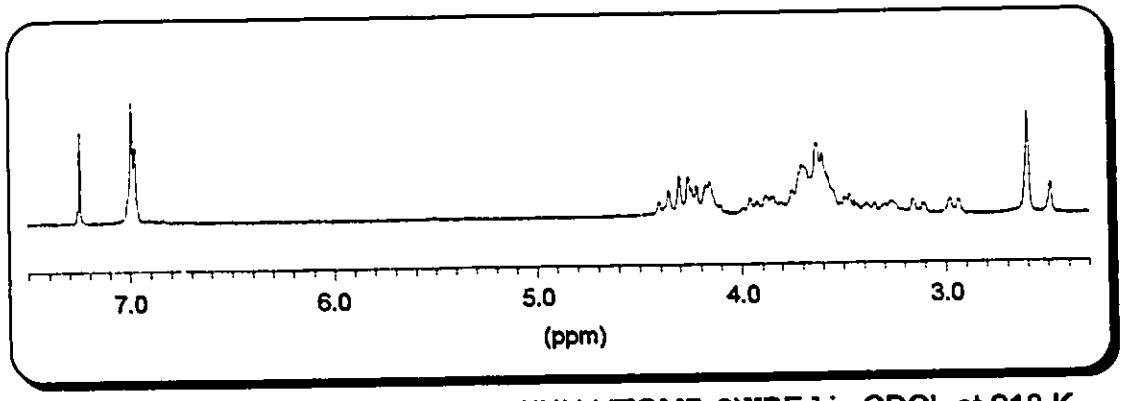

Figure 5.9 ^1H NMR spectrum of $[Pd(NH_3)(TOMB\text{-}3)][BF_4]$ in $CDCl_3$ at 218 K.

recorded at 218 K reveals that inversion of the sulfur atoms has slowed on the NMR time scale as indicated by the sharpened aliphatic resonances. More interestingly, the single resonance for NH_3 at 2.49 ppm has separated into two distinct resonances at 2.60 and 2.49 ppm which integrate to 2 and 1 hydrogens

respectively. The resonance further downfield at 2.60 ppm is assigned as the two hydrogen-bonded N-H protons and that at 2.49 ppm is assigned as the non-hydrogen-bonded N-H proton.

In addition to the NMR evidence for $[Pd(NH_3)(TOMB\text{-}3)][BF_4]$, X-ray quality crystals of the complex were isolated and the crystal structure was determined.

(ii) Crystal Structure of $[Pd(NH_3)(TOMB\text{-}3)][BF_4]$, (38). The unit cell is *ortho*rhombic and contains 8 cations and anions each of $[Pd(NH_3)(TOMB\text{-}3)]^+$ $[BF_4]$. A perspective view of the cation with the atom numbering scheme is shown in Figure 5.10. Listings of crystallographic parameters including atomic positions, bonding parameters and details of data collection are listed in Appendix Table A15. Selected bonding parameters are given in the figure caption.

The palladium atom is in a square planar environment with the S_2C bracket occupying three sites and the ammonia nitrogen atom occupying the fourth site on the metal atom. The Pd-S distances are Pd1-S1 = 2.27(1) Å and Pd1-S2 = 2.30(1) Å. Pd1-N1 = 2.15(3) Å and Pd1-C1 = 1.96(4) Å. The angles at the palladium atom are S1-Pd1-C1 = 83(1)° and S2-Pd1-C1 = 81(1)° at the 5-membered chelate rings and S1-Pd1-N1 = 99.9(8)° and S2-Pd1-N1 = 96.7(8) ° at the non-chelating substrate. S1-Pd1-S2 = 163.3(4)° and C1-Pd1-N1 = 176(1)° bonds both deviate from linearity, presumably due to the complex arranging itself in order to maximize hydrogen-bonding between the substrate and the receptor.

The aliphatic portion of the macrocycle is bent upwards towards the square plane of the palladium atom in order to form two hydrogen-bonds between O1 and O3 and the ammonia substrate, thus placing two of the ammonia

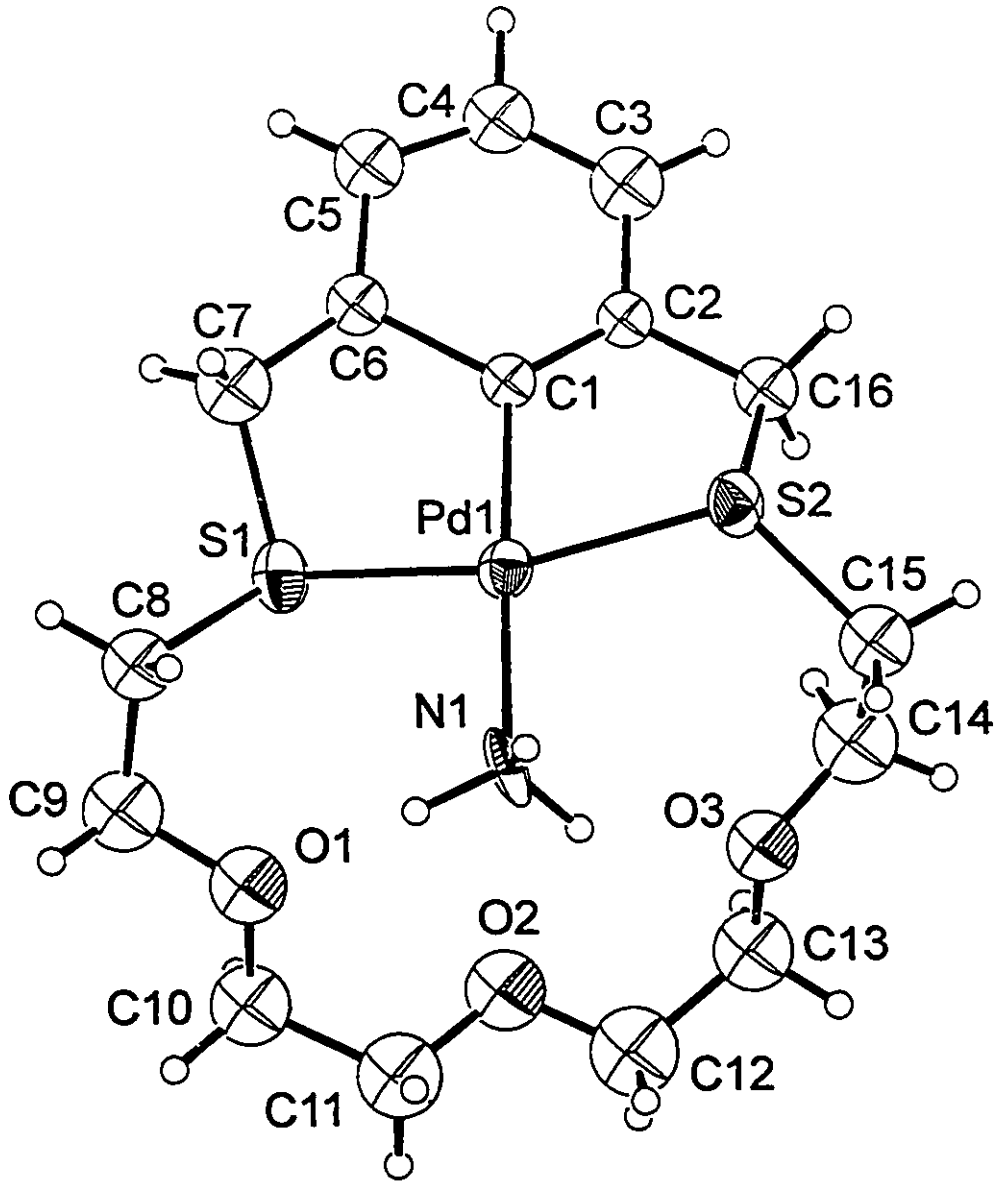

Figure 5.10 Perspective ORTEP drawing of the $[Pd(NH_3)(TOMB\text{-}3)]^+$ cation (38) showing the atom numbering scheme with 20% thermal ellipsoids. Selected bond distances (Å) and angles are: Pd1-S1 = 2.27(1), Pd1-S2 = 2.30(1), Pd1-N1 = 2.15(3), Pd1-C1 = 1.96(4). S1-Pd1-C1 = 83(1)°, S2-Pd1-C1 = 81(1)°, S1-Pd1-N1 = 99.9(8)°, S2-Pd1-N1 = 96.7(8) °, S1-Pd1-S2 = 163.3(4)°, C1-Pd1-N1 = 176(1)°.

hydrogen atoms in approximately equivalent environments. The hydrogen bonding distances are N1...O1 = 2.97(1) Å and N1...O3 = 3.04(1) Å[52, 98]. Note should be taken of the third hydrogen atom on ammonia which, as predicted by CPK models and observed by ^{1}H NMR spectroscopy, is directed away from the macrocyclic cavity in a non-hydrogen-bonding environment.

(iii) Reaction of [Pd(CH$_3$CN)(TOMB-3)][BF$_4$] with Amines: Formation of [Pd(NH$_2$-*n*-Bu)(TOMB-3)][BF$_4$] (39) and [Pd(NH(Me)-*n*-Bu)(TOMB-3)][BF$_4$] (40). In reactions with *n*-butylamine, N-methylbutylamine and N,N-dimethylbutylamine, [Pd(CH$_3$CN)(TOMB-3)][BF$_4$] formed 1:1 adducts with only the primary and secondary amines. The tertiary amine is expected to be more Lewis basic than the other two amines due to hyperconjugation from the aliphatic groups. Therefore, the receptor's reluctance to form a complex with N,N-dimethylbutylamine, as indicated by free amine and free receptor resonances in the ^{1}H NMR spectrum in CDCl$_3$, is most probably due to steric repulsion between the comparatively bulky amine and the receptor.

In the ^{1}H NMR spectra of [Pd(NH$_2$-*n*-Bu)(TOMB-3)][BF$_4$] and [Pd(NH(Me)-*n*-Bu)(TOMB-3)][BF$_4$] (Figure 5.11), the nitrogen-bonded CH$_2$ resonances of both substrates (and the CH$_3$ resonance for N-methylbutylamine) undergo additional coupling to the amino N-H proton(s) that is not observed in the 300 MHz spectra of the free substrates. The CH$_2$ resonances at 2.66 and 2.73 ppm for **39** and **40** respectively appear as complicated multiplets and the CH$_3$ resonance for N-methylbutylamine at 2.59 ppm is split into a doublet. The remaining resonances for the aliphatic chains are also consistent with

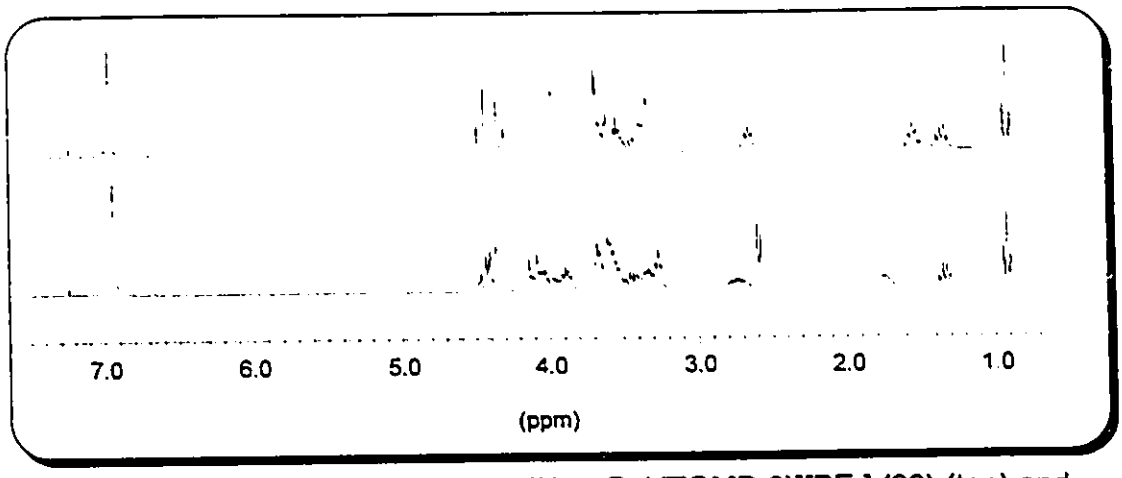

Figure 5.11 ^{1}H NMR spectra of [Pd(NH_2-*n*-Bu)(TOMB-3)][BF_4] (39) (top) and [Pd(NH(Me)-*n*-Bu)(TOMB-3)][BF_4] (40) (bottom) at 298K in $CDCl_3$.

coordination of the amines to the metal atom. The benzylic resonances for the receptor at about 4.4 ppm are split into the pattern of two sets of doublets and the aliphatic portion of the macrocycle exhibits sharpened resonances. Both these factors indicate that inversion of the sulfur atoms has stopped on the NMR time scale due to coordination by the substrate.

The NH_2 resonance for the [Pd(NH_2-*n*-Bu)(TOMB-3)][BF_4] and [Pd(NH(Me)-*n*-Bu)(TOMB-3)][BF_4] are shifted downfield and included in the group of resonances ranging from 3.7 ppm to 3.3 ppm.

(iv) Competition of NH_2-*n*-Bu and NH(Me)-*n*-Bu for [Pd(CH_3CN)(TOMB-3)][BF_4]. In a 1:1:1 competition experiment between NH_2-*n*-Bu and NH(Me)-*n*-Bu for [Pd(CH_3CN)(TOMB-3)][BF_4] in $CDCl_3$ (Figure 5.12), the *n*-butylamine formed a 1:1 complex with the receptor leaving the N-methylbutylamine as uncoordinated ligand. The CH_2 resonances for *n*-butylamine appear at the same chemical shifts and have the same splitting

pattern as is observed in the spectrum of [Pd(NH_2-*n*-Bu)(TOMB-3)][BF_4].

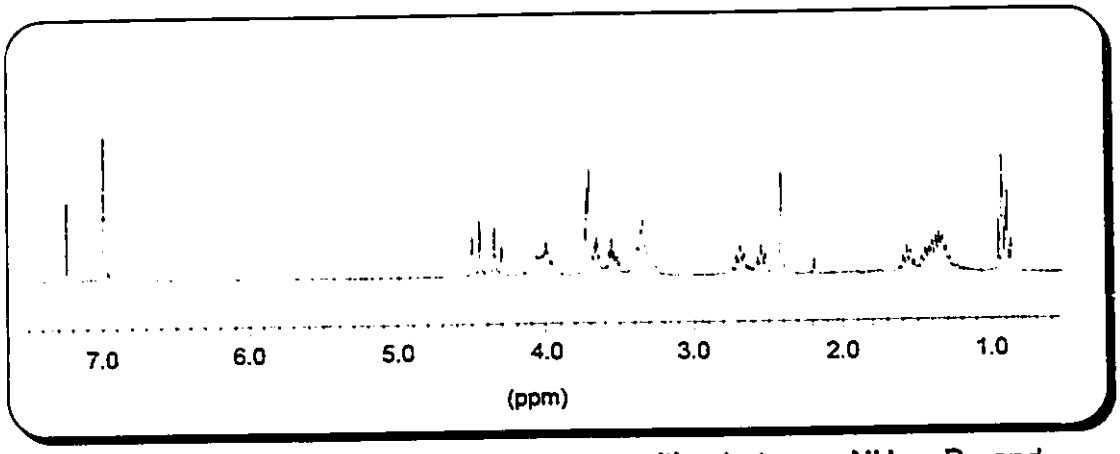

Figure 5.12 ^{1}H NMR spectrum of 1:1:1 competition between NH_2-*n*-Bu and NH(Me)-*n*-Bu for [Pd(CH_3CN)(TOMB-3)][BF_4] in $CDCl_3$ at 298 K.

The resonances for the N-methylbutylamine, by contrast, appear at the same chemical shifts and have the same splitting patterns observed in the spectrum of the uncoordinated substrate.

As the secondary amine would be expected to be a stronger Lewis base, the primary amine must compete successfully for the palladium coordination site as a result of two factors. (i) The primary amine is able to form one more hydrogen-bond with the receptor than N-methylbutylamine. (ii) *n*-Butylamine is sterically less bulky than the secondary amine.

(iv) Reaction of Allylamine with [Pd(CH_3CN)(TOMB-3)][BF_4]: Formation of [Pd(NH_2-CH_2CH=CH_2)(TOMB-3)][BF_4], (41) Allyl halides and allyl Grignard reagents are known to form η^3-complexes with *trans*ition metals. In the hope of using hydrogen-bonding to induce proton *trans*fer from the CH_2 group to the amine to form an organometallic receptor-substrate interaction (Figure 5.13), the receptor was reacted with allylamine in a 1:1 ratio. The substrate was

shown by ^{1}H and $^{13}C\{^{1}H\}$ NMR spectroscopy to be bonded to the palladium atom

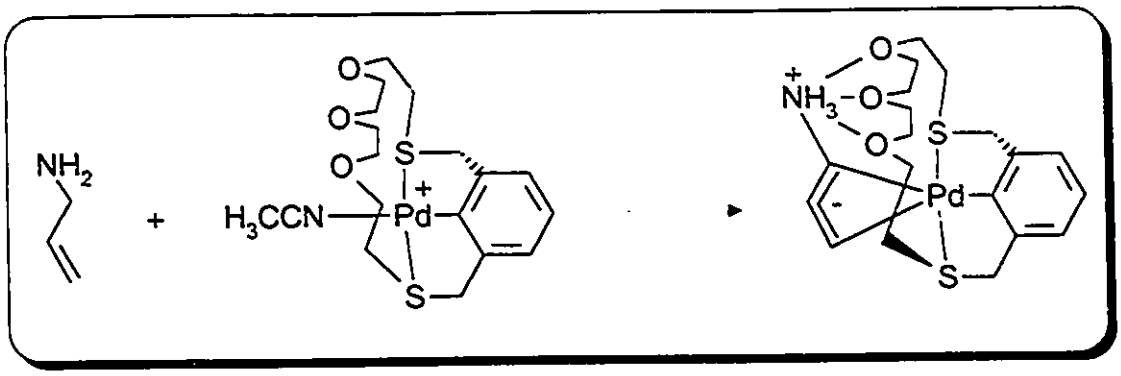

Figure 5.13 Intended geometry of organometallic receptor-substrate complex.

via the NH_2 group rather than a π-donor group.

Only minor changes in the chemical shifts and splitting patterns for the three olefinic hydrogen atoms are observed, and the aliphatic CH_2 group remains unchanged upon coordination to the metal. The NH_2 hydrogens are shifted downfield by 2.2 ppm. If proton transfer had occurred the aliphatic CH_2 resonance would have been replaced by an olefinic CH resonance integrating to 1 hydrogen and the amine resonance would have been replaced by an ammonium resonance integrating to 3 hydrogens. The metalated carbon resonance appears at 157.4 ppm, 2 ppm downfield from that observed in the free receptor.

(vi) Crystal Structure of [Pd(H_2O)(TOMB-5)][BF_4], (42). In an attempt to grow crystals of [Pd(CH_3CN)(TOMB-5)][BF_4] employing a vapour diffusion of diethyl ether into an acetonitrile solution of the complex, crystals of the aqua adduct were isolated and the crystal structure was solved.

The unit cell is triclinic and contains two cations and anions each of

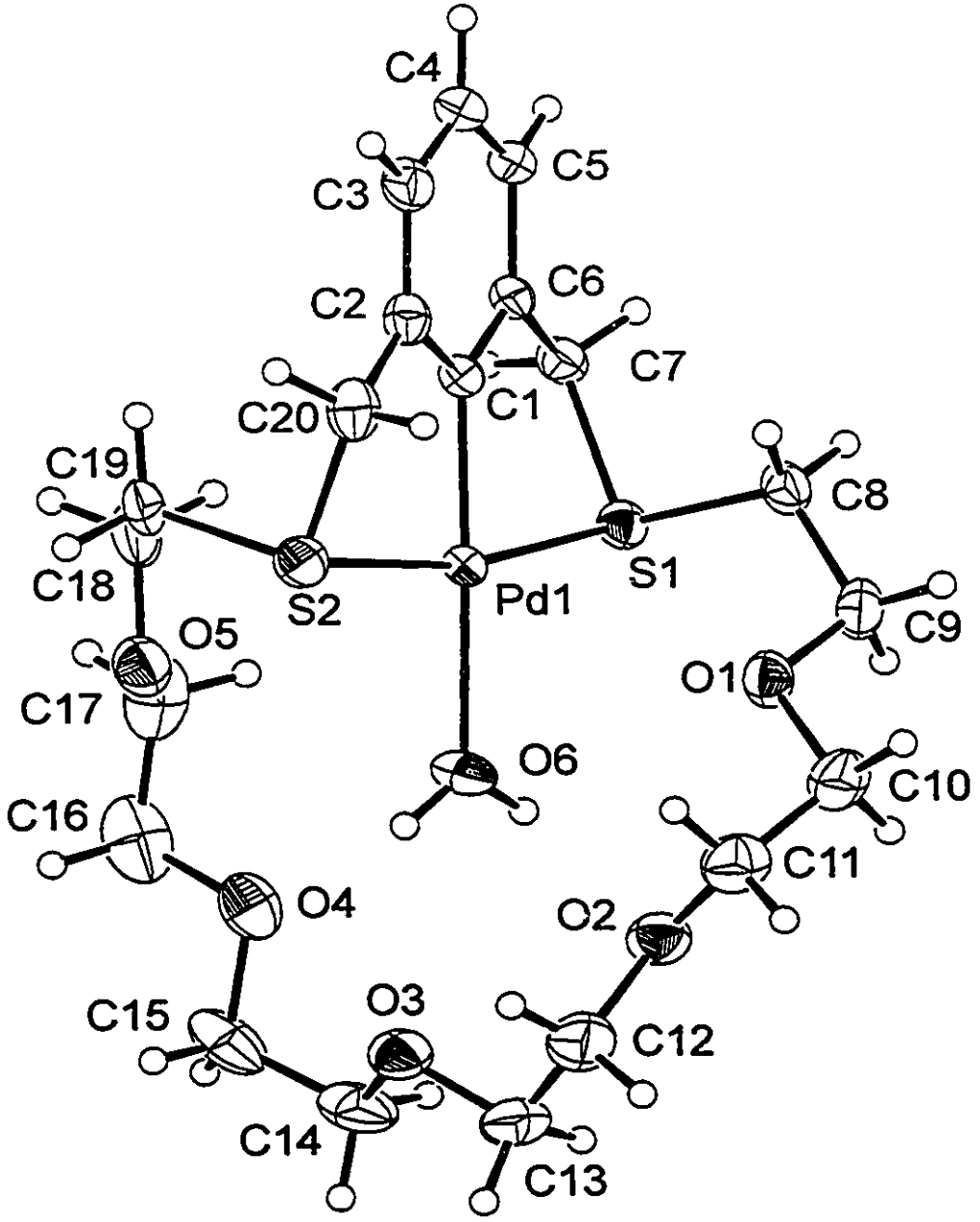

Figure 5.14 Perspective ORTEP drawing of the $[Pd(H_2O)(TOMB\text{-}5)]^+$ cation (42) showing the atom numbering scheme with 30% thermal ellipsoids. Selected bond distances (Å) and angles are: Pd1-S1 = 2.327(2), Pd1-S2 = 2.308(3), Pd1-O6 = 2.158(5), Pd1-C1 = 1.972(7), O6-O2 = 2.80(1), O6-O3 = 2.97(1), O6-O4 = 2.90(1), O6-O1 = 3.16(1), O6-O5 = 3.34(1) S1-Pd1-C1 = 84.9(2)°, S2-Pd1-C1 = 83.8(2)°, S1-Pd1-O6 = 94.8(2)°, S2-Pd1-O6 = 96.4(2)°, S1-Pd1-S2 = 168.36(8)°, C1-Pd1-O6 = 178.1(3)°.

$[Pd(H_2O)(TOMB\text{-}5)][BF_4]$. A perspective view of the cation witn the atom numbering scheme is shown in Figure 5.14. Complete listings of crystallographic parameters including atomic positions, bonding parameters and details of data collection are listed in Appendix Table A16. Selected bonding parameters are given in the figure caption.

The palladium atom is in a square planar environment with the S_2C bracket occupying three sites and the oxygen atom of the water molecule occupying the fourth site on the metal atom. The Pd-S distances are Pd1-S1 = 2.327(2) Å and Pd1-S2 = 2.308(3) Å. Pd1-O6 = 2.158(5) Å and Pd1-C1 = 1.972(7) Å. The angles at the palladium atom are S1-Pd1-C1 = 84.9(2)° and S2-Pd1-C1 = 83.8(2)° at the 5-membered chelate rings and S1-Pd1-O6 = 94.8(2)° and S2-Pd1-O6 = 96.4(2)° at the non-chelating substrate. The S1-Pd1-S2 = 168.36(8)° angle deviates from linearity presumably as a result of constraints imposed by the S_2C bracket, and of the receptor arranging itself in order to maximize hydrogen-bonding between the water molecule and the ether oxygen atoms. The C1-Pd1-O6 angle is almost linear at 178.1(3)°

The large aliphatic chain of the receptor loops around the water molecule with the S1-C8 and S2-C19 bonds directed away from each other on opposite sides of the aromatic ring. There are three strong hydrogen-bonds[5,6] with the substrate, with O6...O2 = 2.80(1) Å, O6...O3 = 2.97(1) Å, O6...O4 = 2.90(1) Å. There are also two weaker interactions, perhaps weak only as a result of crowding of the aliphatic chain, with O6...O1 = 3.16(1) Å and O6...O5 = 3.34(1) Å.

(vii) Reaction of $[Pd(CH_3CN)(TOMB\text{-}3)][BF_4]$ and $[Pd(CH_3CN)(TOMB\text{-}5)][BF_4]$ with Hydrazine: Formation of $[Pd(NH_2NH_2)(TOMB\text{-}3)][BF_4]$, (43) and $[Pd(NH_2NH_2)(TOMB\text{-}5)][BF_4]$, (44). The two receptor molecules were reacted with excess $NH_2NH_2{\cdot}H_2O$ in acetonitrile at room temperature and the complexes were isolated as hygroscopic pale yellow powders.

Upon examination of the ^1H NMR spectrum of $[Pd(NH_2NH_2)(TOMB\text{-}3)][BF_4]$ (Figure 5.15), the splitting of the benzylic resonances centred at 4.32 ppm into two slightly broad doublets and the sharpening of the remainder of the aliphatic resonances is consistent with coordination of the hydrazine substrate to the palladium (II) centre. In addition, resonances for the hydrazine substrate are observed at 5.59 ppm for the coordinating NH_2 and 5.07 ppm for the non-coordinating amine group. Both resonances integrate to 2 hydrogens each.

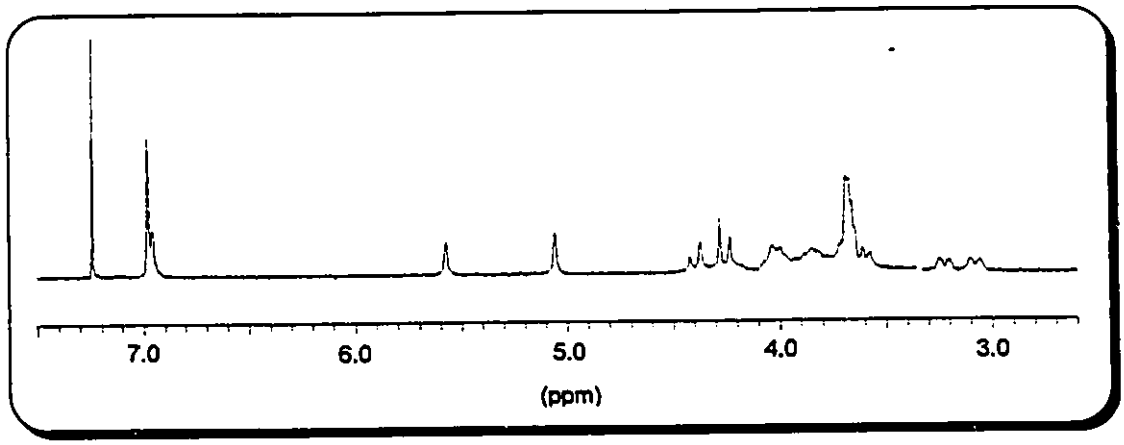

Figure 5.15 ^1H NMR spectrum of $[Pd(NH_2NH_2)(TOMB\text{-}3)][BF_4]$ in $CDCl_3$ at 298K.

The ^1H NMR spectrum of $[Pd(NH_2NH_2)(TOMB\text{-}5)][BF_4]$ ($CDCl_3$) is, as expected, broader and not quite as diagnostic as that for the smaller receptor. The only resonance observed for the hydrazine substrate appears as a broad

peak at 5.61 ppm, indicating that the nature of the receptor-substrate hydrogen-bonds are changing on the NMR time scale.

In addition to the NMR evidence observed for $[Pd(NH_2NH_2)(TOMB\text{-}3)][BF_4]$ X-ray quality crystals of the complex were isolated and the crystal structure was determined.

(viii) Crystal Structure of $[Pd(NH_2NH_2)(TOMB\text{-}3)][BF_4]$, (43). The unit cell is triclinic and contains two cations and anions each of $[Pd(NH_2NH_2)(TOMB\text{-}3)][BF_4]$. A perspective view of the cation with the atom numbering scheme is shown in Figure 5.16. Complete listings of crystallographic parameters including atomic positions, bonding parameters and details of data collection are listed in Appendix Table A17. Selected bonding parameters are given in the figure caption.

The palladium atom is in a square planar environment with the S_2C bracket occupying three sites and the nitrogen atom of hydrazine occupying the fourth site on the metal atom. The Pd-S distances are Pd1-S1 = 2.298(1) Å and Pd1-S2 = 2.289(1) Å. Pd1-N1 = 2.133(4) Å and Pd1-C1 = 1.986(5) Å. The angles at the palladium atom are S1-Pd1-C1 = 82.0(1)° and S2-Pd1-C1 = 83.2(2)° at the 5-membered chelate rings and S1-Pd1-N1 = 98.6(1)° and S2-Pd1-N1 = 96.1(1)° at the substrate. The C1-Pd1-N1 angle is essentially linear at 178.8(2)°. The S1-Pd1-S2 = 165.16(5)° angle deviates additionally from linearity due to the receptor arranging itself in order to maximize hydrogen-bonding interactions.

The aliphatic chain bends upwards towards the plane of the aromatic ring in order to form two hydrogen-bonds[5, 6] between the receptor and substrate.

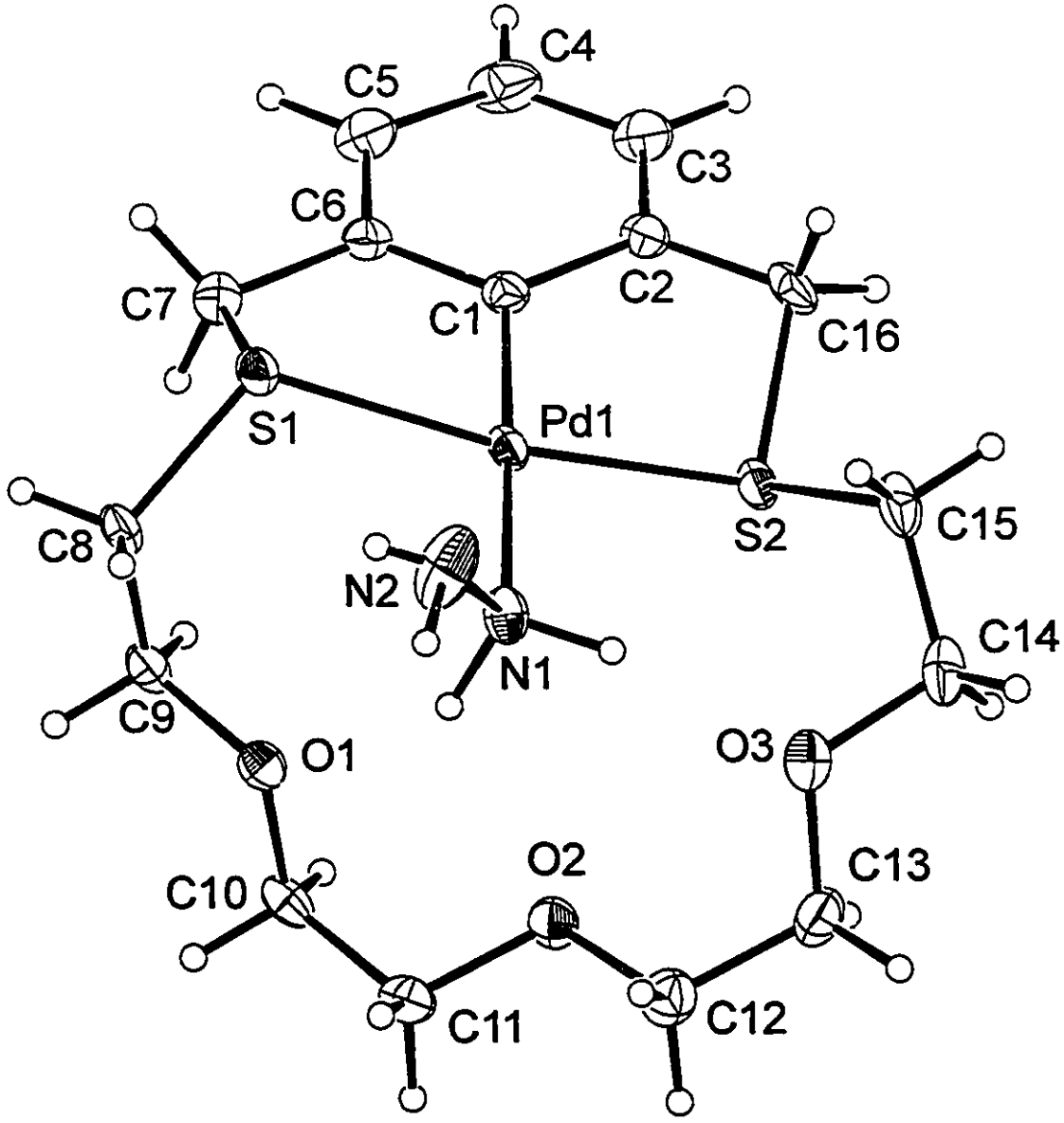

Figure 5.16 Perspective ORTEP drawing of the $[Pd(NH_2NH_2)(TOMB\text{-}3)]^+$ cation (43) showing the atom numbering scheme with 30% thermal ellipsoids. Selected bond distances (Å) and angles are: Pd1-S1 = 2.298(1), Pd1-S2 = 2.289(1), Pd1-N1 = 2.133(4), Pd1-C1 = 1.986(5), N1-O1 = 2.89(1), N1-O3 = 2.95(1), N2-O1 = 3.60(1). S1-Pd1-C1 = 82.0(1)°, S2-Pd1-C1 = 83.2(2)°, S1-Pd1-N1 = 98.6(1)°, S2-Pd1-N1 = 96.1(1)°, C1-Pd1-N1 = 178.8(2)°, S1-Pd1-S2 = 165.16(5)°.

The hydrogen-bonding distances are N1...O1 = 2.89(1) Å and N1...O3 = 2.95(1) Å and there is a weaker interaction between N2 and O1 at a distance of 3.60(1) Å. One can also envisage how partial rotation of the S1-Pd1-S2 vector around the C1-Pd1-N1 axis causes inversion of the sulfur atoms and renders the benzylic hydrogens partially equivalent, possibly explaining the slightly broadened set of doublets for the benzylic hydrogens observed in the ^{1}H NMR spectrum.

(ix) Reaction of [Pd(CH_3CN)(TOMB-3)][BF_4] and [Pd(CH_3CN)(TOMB-5)][BF_4] with the Hydrazinium cation: Formation of [Pd(NH_2NH_3)(TOMB-3)][CF_3SO_3]$_2$, (45) and [Pd(NH_2NH_3)(TOMB-5)][BF_4]$_2$, (46). The receptors were reacted with a previously prepared $CF_3SO_3^-$ or BF_4^- salt of the hydrazinium cation $NH_2NH_3^+$ in an approximately 1:1 ratio in acetonitrile to give the complexes in moderate yields. A fully diagnostic NMR spectrum of [Pd(NH_2NH_3)(TOMB-5)][BF_4]$_2$ could not be obtained in either CD_3CN and CD_3COCD_3 due to fluxional behaviour, however the spectrum recorded in CD_3COCD_3 is consistent with the formation of a 1:1 complex. The complex does not dissolve in less polar solvents such as chloroform or dichloromethane. The [Pd(NH_2NH_3)(TOMB-3)][CF_3SO_3]$_2$ complex was, however, soluble enough in $CDCl_3$ to obtain poorly resolved ^{1}H and ^{13}C{^{1}H} NMR spectra.

The resonances for the aromatic hydrogens, which normally appear as a set of overlapping peaks in the receptor-substrate complexes, appear as three separate resonances in the ^{1}H NMR spectrum at 7.10, 6.88 and 6.76 ppm. The benzylic hydrogens appear at 4.65 ppm as a broad peak. This is indicative of inversion of the sulfur atoms, possibly a result of electrostatic repulsion between

the cationic substrate and the cationic receptor allowing the oxygen atoms of the receptor to displace the hydrazinium cation. The remainder of the resonances for the aliphatic hydrogens are somewhat sharpened in comparison to the free receptor due to the presence of the substrate. Because of the broad nature of the spectrum it is difficult to identify the resonances for the hydrazinium substrate itself. It is likely, however, that they are very broad due to fluxional hydrogen-bonding with the ether oxygens and so are not observed.

In the $^{13}C\{^1H\}$ NMR spectrum, asymmetry is indicated in the receptor by the presence of six peaks in the aromatic region of the spectrum. This asymmetry must be a result of the presence of the hydrazinium cation as the free receptor is symmetrical in solution.

In addition to the spectroscopic evidence observed for $[Pd(NH_2NH_3)(TOMB\text{-}3)][CF_3SO_3]_2$ and $[Pd(NH_2NH_3)(TOMB\text{-}5)][BF_4]_2$, X-ray quality crystals of the complexes were isolated and the crystal structures were determined.

(x) Crystal Structure of $[Pd(NH_2NH_3)(TOMB\text{-}3)][CF_3SO_3]_2$, (45). The unit cell is monoclinic and contains four cations and anions each of $[Pd(NH_2NH_3)(TOMB\text{-}3)][CF_3SO_3]_2$. A perspective view of the cation with the atom numbering scheme is shown in Figure 5.17. Complete listings of crystallographic parameters including atomic positions, bonding parameters and details of data collection are listed in Appendix Table A18. Selected bonding parameters are in the figure caption.

The palladium atom is in a square planar environment with the S_2C bracket

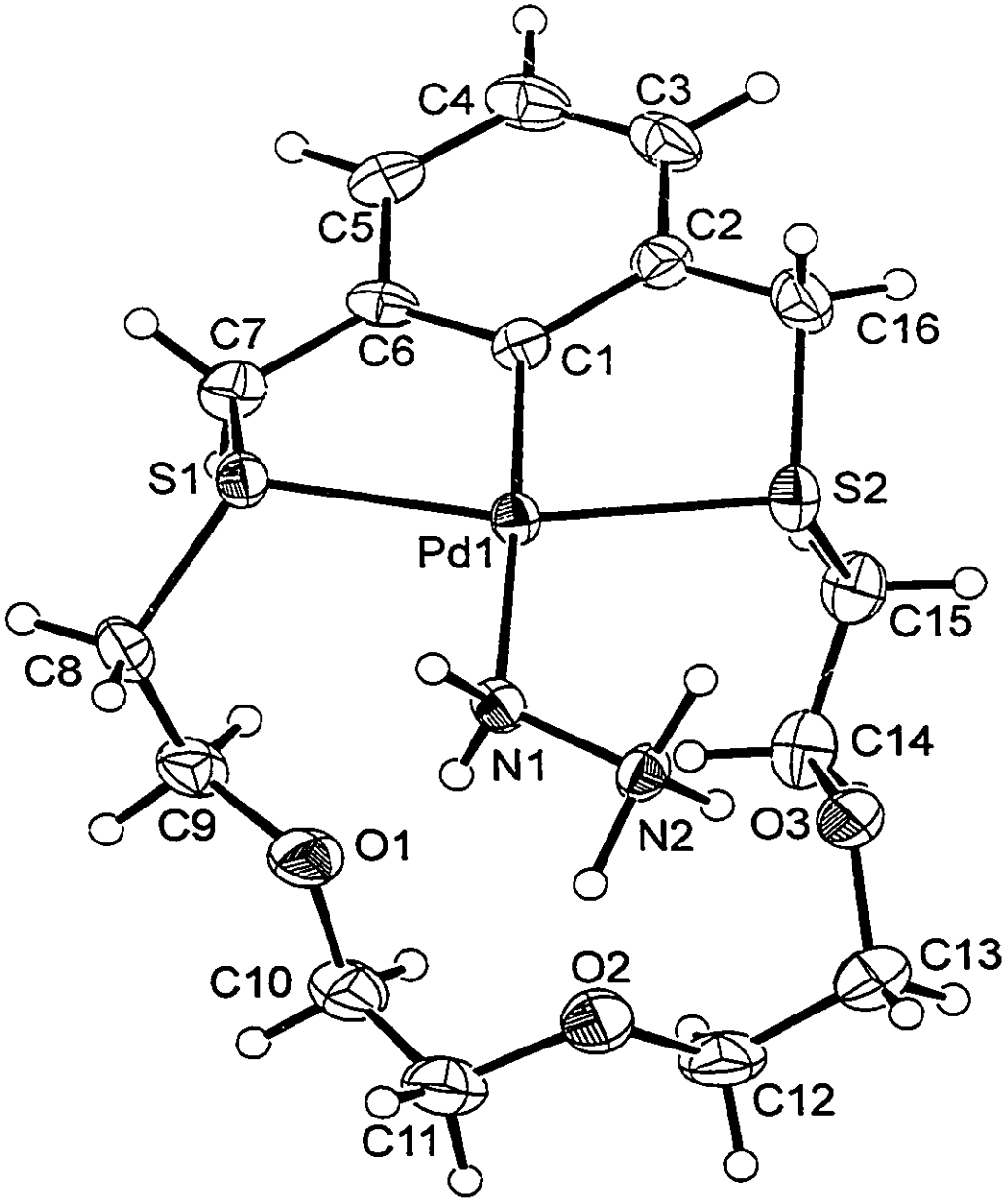

Figure 5.17 Perspective ORTEP drawing of the $[Pd(NH_2NH_3)(TOMB\text{-}3)]^{2+}$ dication (45) showing the atom numbering scheme with 30% thermal ellipsoids. Selected bond distances (Å) and angles are: Pd1-S1 = 2.290(2), Pd1-S2 = 2.314(2), Pd1-N1 = 2.172(6), Pd1-C1 = 1.987(5), N1-O1 = 2.885(8), N2-O2 = 2.956(9), N2-O3 = 2.952(8). Pd1-C1 = 83.1(2)°, S2-Pd1-C1 = 83.9(2)°, S1-Pd1-N1 = 94.5(2)°, S2-Pd1-N1 = 98.4(2)°, C1-Pd1-N1 = 177.4(3)°, S1-Pd1-S2 = 166.04(7)°.

occupying three sites and the NH_2 nitrogen atom of the substrate occupying the fourth site on the metal atom. The Pd-S distances are Pd1-S1 = 2.290(2) Å and Pd1-S2 = 2.314(2) Å. Pd1-N1 = 2.172(6) Å and Pd1-C1 = 1.987(6) Å. The angles at the palladium atom are S1-Pd1-C1 = 83.1(2)° and S2-Pd1-C1 = 83.9(2)° at the 5-membered chelate rings and S1-Pd1-N1 = 94.5(2)° and S2-Pd1-N1 = 98.4(2)° at the non-chelating substrate. The C1-Pd1-N1 angle is essentially linear at 177.4(3)°. The S1-Pd1-S2 = 166.04(7)° angle further deviates from linearity in comparison to the free receptor as a result of the receptor arranging itself in order to place the oxygen atoms in hydrogen-bonding proximity to the N-H atoms on the substrate.

(xi) Crystal Structure of $[Pd(NH_2NH_3)(TOMB\text{-}5)][BF_4]_2$, (46). The unit cell is triclinic and contains two cations and anions each of $[Pd(NH_2NH_3)(TOMB\text{-}5)][BF_4]_2$. A perspective view of the cation with the atom numbering scheme is shown in Figure 5.18. Complete listings of crystallographic parameters including atomic positions, bonding parameters and details of data collection are listed in Appendix Table A19. Selected bonding parameters are given in the figure caption.

The palladium atom is in a square planar environment with the S_2C bracket occupying three sites and the NH_2 nitrogen atom of the substrate occupying the fourth site on the metal atom. The Pd-S distances are Pd1-S1 = 2.307(2) Å and Pd1-S2 = 2.311(2) Å. Pd1-N1 = 2.167(6) Å and Pd1-C1 = 1.972(7) Å. The angles at the palladium atom are S1-Pd1-C1 = 85.6(2)° and S2-Pd1-C1 = 85.2(2)° at the 5-membered chelate rings and S1-Pd1-N1 = 91.0(2)° and S2-Pd1-N1 =

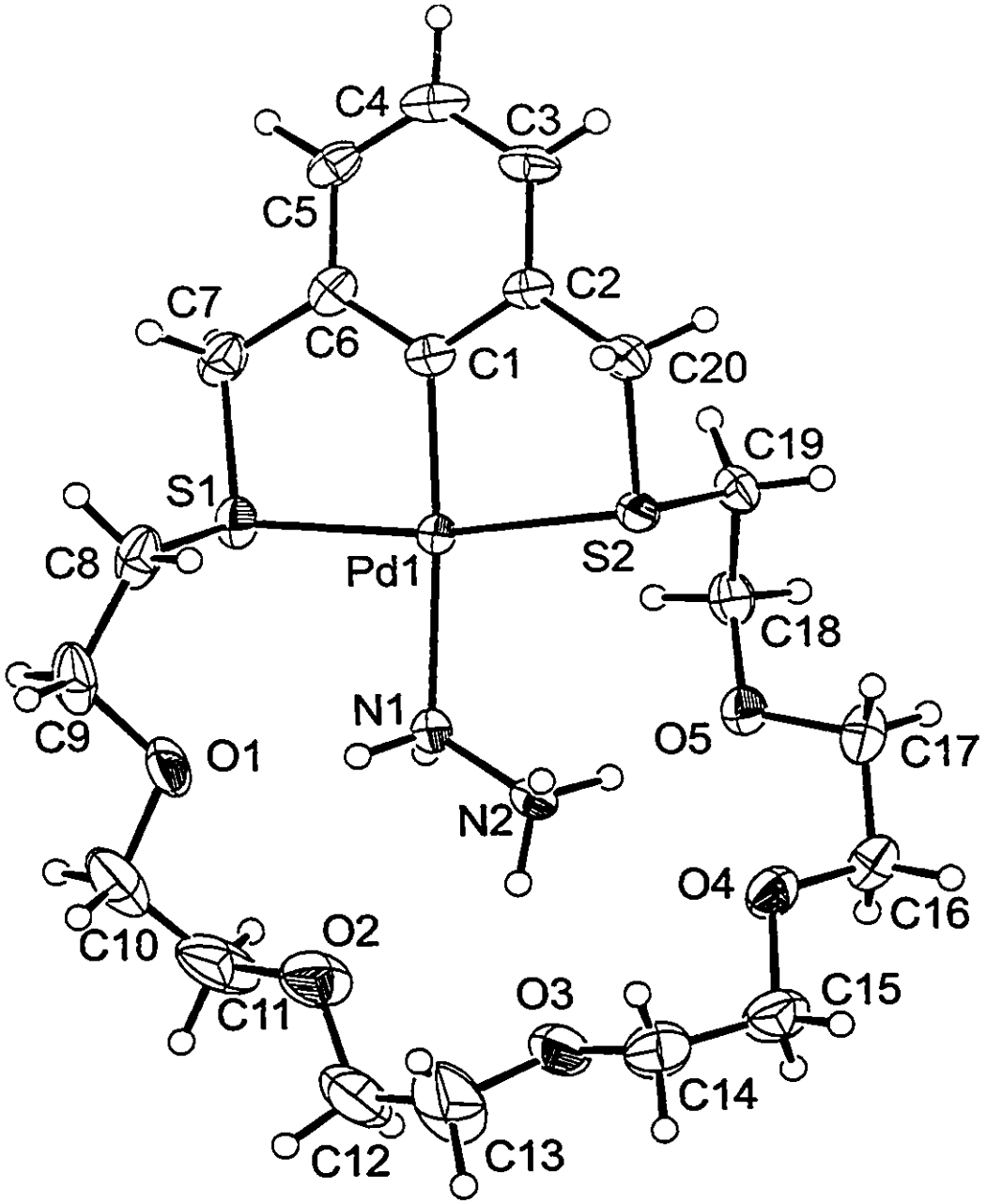

Figure 5.18 Perspective ORTEP drawing of the $[Pd(NH_2NH_3)(TOMB\text{-}5)]^{2+}$ dication (46) showing the atom numbering scheme with 30% thermal ellipsoids. Selected bond distances (Å) and angles are: Pd1-S1 = 2.307(2), Pd1-S2 = 2.311(2), Pd1-N1 = 2.167(6), Pd1-C1 = 1.972(7). N1-O1 = 2.853(7), N1-O2 = 3.005(8), N2-O2 = 3.053(8), N2-O3 = 2.834(8), N2-O4 = 2.782(7), N2-O5 = 2.773(8). S1-Pd1-C1 = 85.6(2)°, S2-Pd1-C1 = 85.2(2)°, S1-Pd1-N1 = 91.0(2)°, S2-Pd1-N1 = 98.1(2)°, C1-Pd1-N1 = 176.7(3)°, S1-Pd1-S2 = 170.79(7)°.

98.1(2)° at the non-chelating substrate. The C1-Pd1-N1 angle is essentially linear at 176.7(3)°. The S1-Pd1-S2 = 170.79(7)° angle is similar to that observed for $[Pd(H_2O)(TOMB\text{-}5)][BF_4]$ as a result of constraints imposed by the S_2C bracket, and the receptor arranging itself in order to place the oxygen atoms in hydrogen-bonding proximity to the N-H atoms on the substrate.

(xii) Comparative Structural Analysis for the $[Pd(NH_2NH_3)(TOMB\text{-}3)]^{2+}$ (45) and $[Pd(NH_2NH_3)(TOMB\text{-}5)]^{2+}$ (46) dications. In both compounds, the primary interaction is coordination of the amino nitrogen atom to the palladium atom. The degree of second-sphere coordination depends on the ability of the $NH_2NH_3^+$ cation to penetrate the different sized crown ether cavities and the number of ether oxygen atoms that can potentially act as hydrogen-bond acceptors. For $[Pd(NH_2NH_3)(TOMB\text{-}3)]^{2+}$, the polyether chain bends upwards towards the hydrazinium ion which perches over the crown ether ring. There is one hydrogen-bond from the NH_2 group to O1, N1...O1 = 2.885(8) Å, while another hydrogen atom of the NH_3^+ group forms a hydrogen-bond in a bifurcated fashion to O2 and O3; N2...O2 = 2.956(9) Å and N2...O3 = 2.952(8) Å. This results in a four point interaction between the receptor and the cationic substrate.

For $[Pd(NH_2NH_3)(TOMB\text{-}5)]^{2+}$, the fit of receptor and substrate is quite remarkable. The polyether chain wraps around the $NH_2NH_3^+$ ion which is nested within the larger crown ether cavity. Six hydrogen-bonding interactions accompany the Pd-N σ-bond, two to the NH_2 group: N1..O1 = 2.853(7) Å; N1...O2 = 3.005(8) Å, and four to the NH_3^+ group: N2...O2 = 3.053(8) Å; N2...O3 = 2.834(8) Å; N2-O4 = 2.782(7) Å; N2-O5 = 2.773(8) Å. This results in a seven

point interaction between the receptor and substrate.

It is noteworthy that the receptor and the substrate are both cationic, and despite the electrostatic repulsion that must be present between the two entities, the formation of stable complexes in the solid state, and to some extent in solution, is possible. This interaction is no doubt due in part to the formation of hydrogen-bonds between the receptor and the substrate as well as the formation of a σ-bond between the NH_2 group and the palladium (II) centre.

(xiii) Interaction of $AgCF_3SO_3$ with $[Pd(CH_3CN)(TOMB\text{-}3)][BF_4]$: Formation and Crystal Structure of $[PdAg(H_2O)(TOMB\text{-}3)(CF_3SO_3)][CF_3SO_3]$, (47). Another interesting application of $[Pd(CH_3CN)(TOMB\text{-}3)][BF_4]$ is that second-sphere coordination could be used to stabilize otherwise weak bonding interactions in the primary coordination sphere of the palladium (II) centre. The reaction of [Pd(TOMB-3)Cl] with two equivalents of $AgCF_3SO_3$ in CH_2Cl_2 resulted

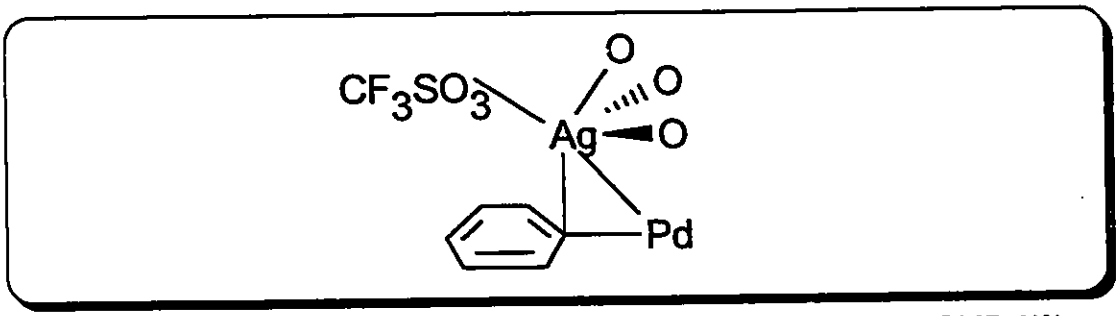

Figure 5.19 Schematic diagram of the interaction of Ag^+ with $[Pd(TOMB\text{-}3)]^+$.

in the formation of the bimetallic complex $[PdAg(H_2O)(TOMB\text{-}3)(CF_3SO_3)][CF_3SO_3]$ as identified by an X-ray crystal structure (Figure 5.20).

The complex crystallizes as the CH_2Cl_2 solvate and the water source is presumably atmospheric moisture or incomplete drying of the solvent. The

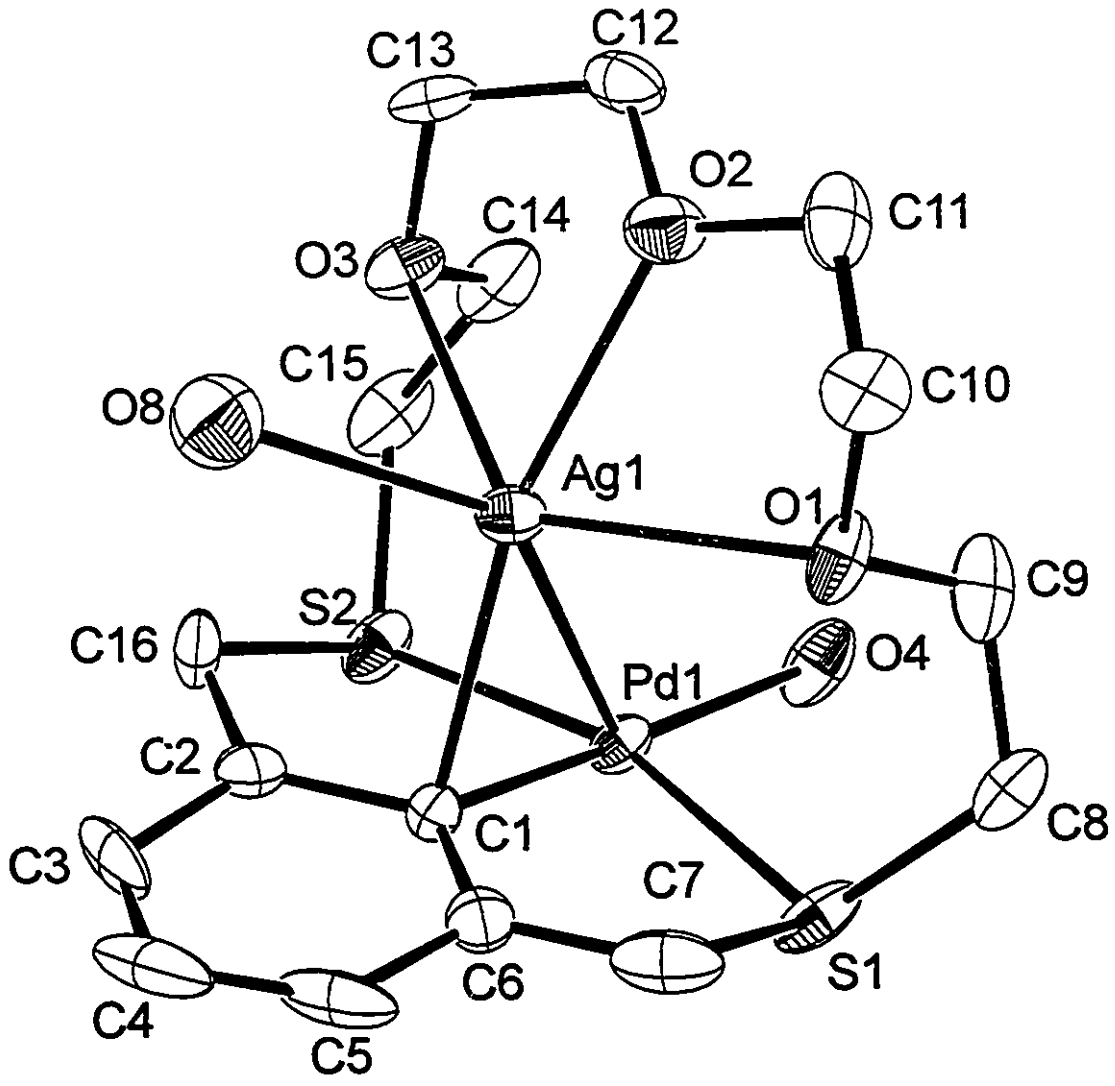

Figure 5.20 Perspective ORTEP drawing of $[PdAg(H_2O)(TOMB\text{-}3)(CF_3SO_3)]^+$, (47) showing the atom numbering scheme with 30% thermal ellipsoids; only O8 of the CF_3SO_3 ligand is shown. Selected bond distances (Å) and angles are: Pd-S1 = 2.296(5), Pd-S2 = 2.298(5), Pd-O4 = 2.14(1), Pd-C1 = 1.98(2), Ag-C1 = 2.40(2), Ag-Pd = 2.884(2), Ag-O1 = 2.60(1), Ag-O2 = 2.38(1), Ag-O3 = 2.66(1), Ag-O8 = 2.54(2). C1-Ag-O2 = 160.5(6)°, O1-Ag-O3 = 126.6(4)°, Pd-Ag-O9 = 137.6(5)°

palladium atom is in a square planar environment with the S_2C bracket occupying three sites and the water molecule occupying the fourth site on the metal atom. The Pd-S distances are Pd-S1 = 2.296(5), Pd-S2 = 2.298(5) Å, and Pd-O4 = 2.14(1) Å and Pd-C1 = 1.98(2) Å. The Ag^+ 'substrate' is situated directly over the Pd-C bond and is bonded to the metalated carbon atom at 2.40(2) Å and the palladium atom at a distance of 2.884(2) Å. The oxygen atoms of the polyether chain stabilize the receptor/substrate interaction in the second sphere of the Pd with Ag-O1 = 2.60(1), Ag-O2 = 2.38(1), Ag-O3 = 2.66(1) Å. A single oxygen atom from one of the $CF_3SO_3^-$ groups, Ag-O8 = 2.54(2) Å, completes the coordination sphere of the silver. The geometry around the silver(I) ion can best be described as a very distorted octahedron with the C1 *trans* to O2, C1-Ag-O2 = 160.5(6)°, O1 *trans* to O3, O1-Ag-O3 = 126.6(4)° and Pd *trans* to O9, Pd-Ag-O9 = 137.6(5)°.

The X-ray structure of $[PdAg(H_2O)(TOMB\text{-}3)(CF_3SO_3)][CF_3SO_3]$ demonstrates that the Ag^+ ion is bound inside a unique cavity stabilized by a set of four relatively weak interactions; (i) an Ag^+-C(π-arene) interaction (ii) a Pd-Ag donor-acceptor interaction, (iii) Ag^+ ion-ether oxygen dipolar interactions and (iv) electrostatic interaction between Ag^+ and $CF_3SO_3^-$. Molecular orbital calculations (performed by Dr. Stephen J. Loeb) suggest that the major interaction is that between the electrophilic Ag^+ centre and the electron rich Pd-C bond, which is then stabilized by peripheral coordination of the polyether oxygens and the counterion in the second-sphere of the palladium. Although each type of bonding interaction with the Ag^+ ion has precedence (see Ch. 5, Introduction), none is

substantial enough alone to stabilize the complex. It is only the sum of these weak secondary interactions that allows isolation of this unique compound and identification of the Ag-(Pd-C) interaction.

Attempts to record NMR spectra of this compound were thwarted by the need for polar solvents such as acetonitrile, which resulted in decomposition of the complex and formation of $[Pd(CH_3CN)(TOMB\text{-}3)][CF_3SO_3]$. A similar reaction of $[Pd(CH_3CN)(TOMB\text{-}3)][BF_4]$ with one equivalent of $AgCF_3SO_3$ in $CDCl_3$ was performed and the ^1H NMR was recorded (Figure 5.21). It shows a separation and downfield shift of the overlapping resonances observed for the aromatic protons of the free receptor to a triplet at 7.29 ppm for the hydrogen atom *para* to the metal, and a doublet at 7.08 ppm for the hydrogen atoms *meta* to the metal atom, indicative of a Ag^+-aromatic ring interaction. A sharpening of the aliphatic resonances into seven broad peaks rather than 5 peaks for the free receptor,

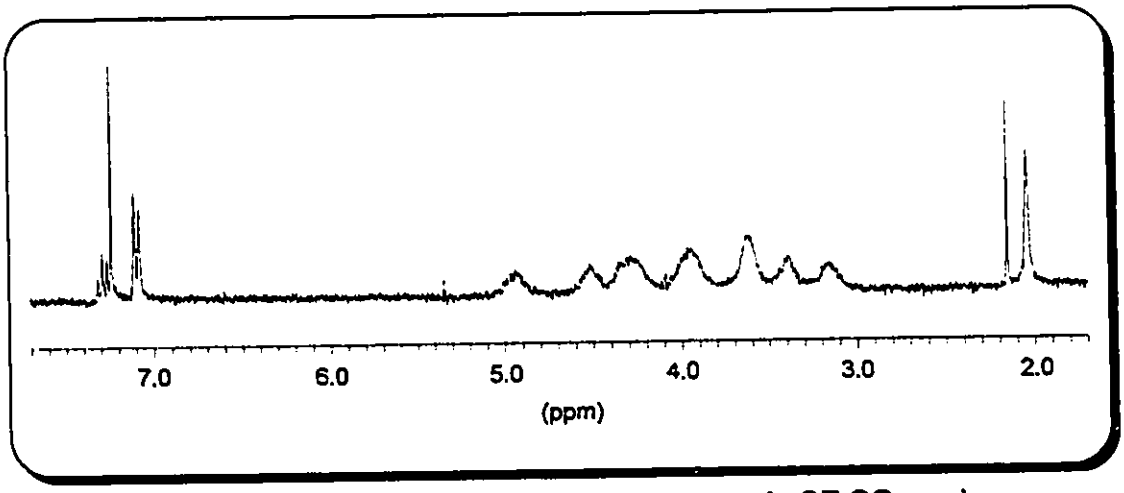

Figure 5.21 ^1H NMR spectrum of interaction between $AgCF_3SO_3$ and $[Pd(CH_3CN)(TOMB\text{-}3)][BF_4]$ in $CDCl_3$ at 298 K.

consistent with coordination of the ether oxygen atoms to the silver atom, is also

observed. The resonances at 4.9 and 4.5 ppm are assigned as the benzylic hydrogens and those at 3.4 and 3.15 ppm are assigned as the SCH_2 hydrogen atoms based on their integration to only 2 hydrogens each and their chemical shifts. The remainder of the resonances at 4.3, 3.9 and 3.6 ppm are assigned as the OCH_2 hydrogen atoms.

5.5 Conclusion

It was observed, both by low temperature NMR spectroscopy and X-ray crystallography, that the ammonia substrate in $[Pd(NH_3)(TOMB\text{-}3)][BF_4]$ exhibits simultaneous first- and second-sphere coordination to the receptor with the formation of two hydrogen-bonds between the amino hydrogens and two ether oxygen atoms.

In reactions of *n*-butylamine, N-methylbutylamine and N,N-dimethylbutylamine with $[Pd(CH_3CN)(TOMB\text{-}3)][BF_4]$ the formation of a 1:1 complex with the N,N-dimethylbutylamine was precluded due to steric interference between the methyl groups on the amine and the receptor. However, 1:1 complexes with the primary and secondary amines were formed quantitatively. In a 1:1:1 competition between $[Pd(CH_3CN)(TOMB\text{-}3)][BF_4]$, *n*-butylamine and N-methylbutylamine, the receptor forms a complex with the primary amine exclusively.

The reaction of amines containing additional hydrogen-bonding groups ($-NH_2$, $-NH_3^+$) with $[Pd(CH_3CN)(TOMB\text{-}3)][BF_4]$ and $[Pd(CH_3CN)(TOMB\text{-}5)][BF_4]$ yielded complexes with multipoint substrate-receptor interactions. X-ray crystallographic studies of $[Pd(NH_2NH_2)(TOMB\text{-}3)][BF_4]$,

$[Pd(NH_2NH_3)(TOMB\text{-}3)][BF_4]_2$ and $[Pd(NH_2NH_3)(TOMB\text{-}5)][BF_4]_2$ showed first-sphere coordination by the amine and 2, 3 and 6 second-sphere hydrogen-bonding interactions to the receptors respectively.

The reaction of $[Pd(L)(TOMB\text{-}3)][BF_4]$ ($L = H_2O$, CH_3CN) with $[Ag][CF_3SO_3]$ yielded the interesting bimetallic complex in which the Ag^+ atom is stabilized by Ag-C(arene), Pd-Ag, Ag-O(ether) and Ag-CF_3SO_3 bonding.

Chapter 6

Receptors Containing Ferrocene

Chapter 6

6.1 Introduction

(i) Thought Process. In Chapters 4 and 5, the application of the receptor molecules to simultaneous first- and second-sphere coordination was observed by ^{1}H NMR spectroscopy and X-ray crystallography. However, using these two methods of characterization demands that the substrate-receptor complexes have well resolved and well separated NMR resonances, and that crystals of the complexes can be isolated. In the case where NMR resonances are not well resolved or separated and/or crystals of the complex cannot be isolated, another method of characterization becomes a necessity. A good example of this scenario is $[Pd(NH_2NH_2)(TOMB\text{-}5)][BF_4]$ (44), which exhibits broad ^{1}H NMR resonances for the receptor-substrate complex, and for which crystals could not be isolated.

The approach taken to making another form of characterization available was to include a redox active molecule within the receptor's framework (Figure 6.1). Ferrocene is well known as an electrochemical standard, exhibiting a

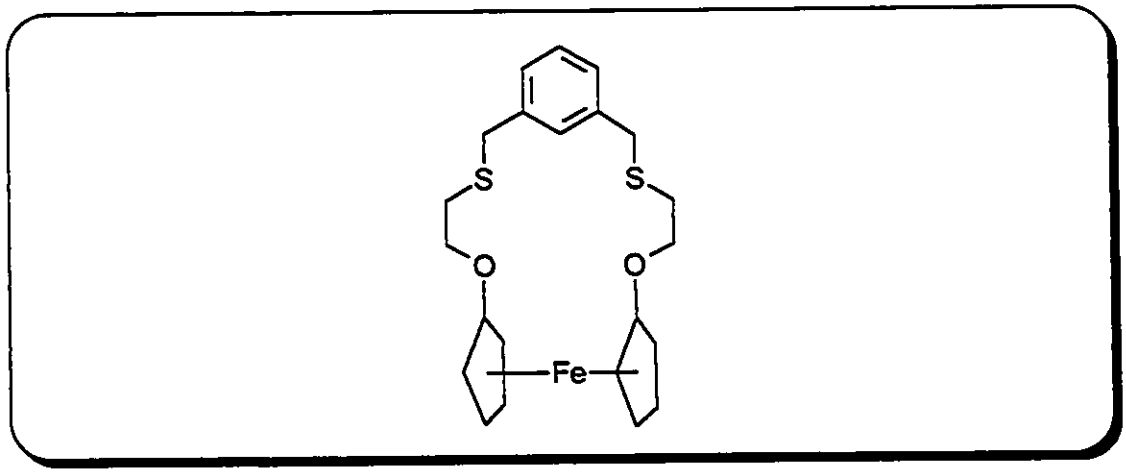

Figure 6.1 Schematic drawing of ligand TOMB-F2, containing ferrocene.

reversible one electron oxidation in most common organic solvents[131]. Attaching oxygen atoms to the cyclopentadienyl (Cp) rings would no doubt affect the oxidation-reduction potential of the ferrocene moiety; oxygen atoms are well known to affect the electronics of aromatic rings[132].

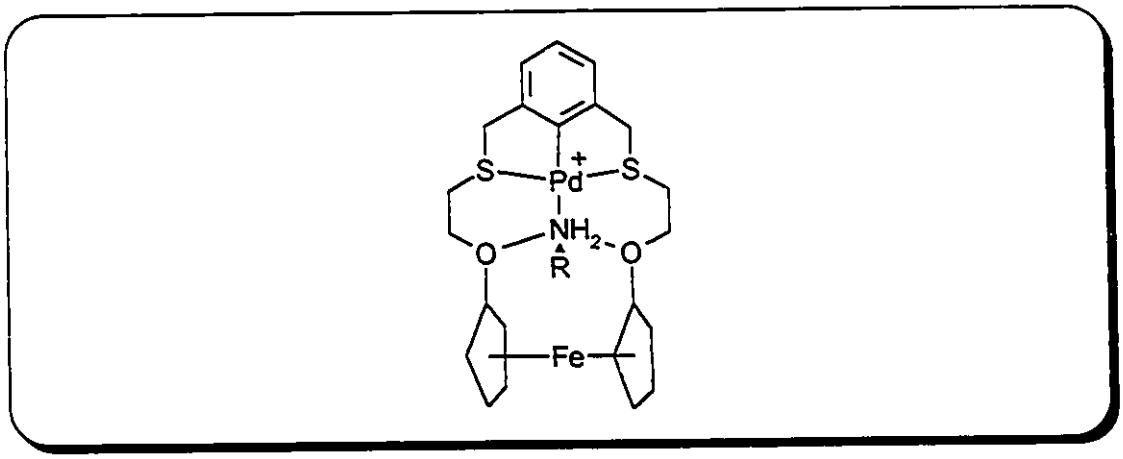

Figure 6.2 A primary amine hydrogen-bonding with the receptor induces a change in ferrocene moiety redox potential.

Therefore, the formation of hydrogen-bonds between the oxygen atoms and a substrate (Figure 6.2) would result in a change in the electron density on the oxygen atoms which would be communicated to the Cp rings. This would result in a change in the redox potentials of the ferrocene, measurable by cyclic voltammetry. In effect, the receptor would be an electrochemical sensor for hydrogen-bond formation.

(ii) Background Literature. The concept of including a ferrocene moiety within a macrocyclic framework has been used extensively in past years to provide an electrochemical handle on the binding of cationic guests by a macrocycle. This large volume of work available for comparison made ferrocene an obvious choice for the redox active moiety to be included within the

macrocycle.

The first group of crown ethers containing ferrocene, or 'ferrocenophanes' (Figure 6.3), were reported by Biernat and Wilczewski[133] and shortly thereafter pentaoxa[13]-ferrocenophane was shown by Saji *et al*[134] to exhibit anodic shifts in the oxidation potential resulting from the addition of alkali metal salts.

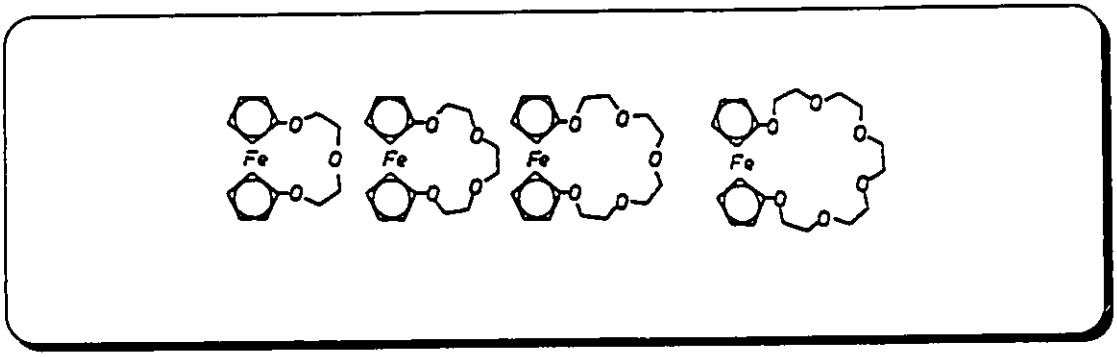

Figure 6.3 Selection of 'ferrocenophanes' initially reported by Biernat and Wilczewski.

Paul Beer and co-workers have done extensive work with macrocycles containing ferrocene both as a pendant arm redox centre, as a link joining two macrocycles and as part of the primary macrocyclic framework[135] (Figure 6.4).

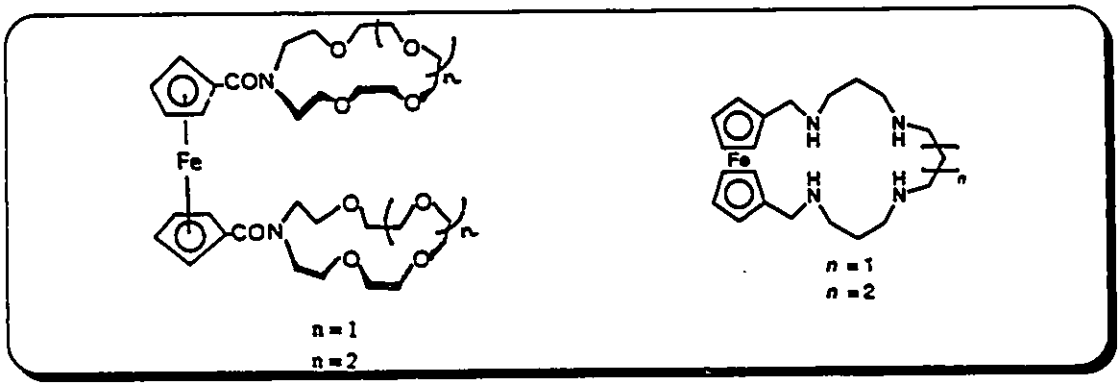

Figure 6.4 Selected macrocycles containing ferrocene synthesized by Beer's group.

Hall *et al*[136] and others[137] have synthesized ferrocene-cryptand molecules

in which the ferrocene moiety is part of the cryptand framework. These cryptands were shown to exhibit anodic shifted redox couples upon addition of alkali and lanthanide metal cations, consistent with inclusion of the cations in the macrocyclic environments.

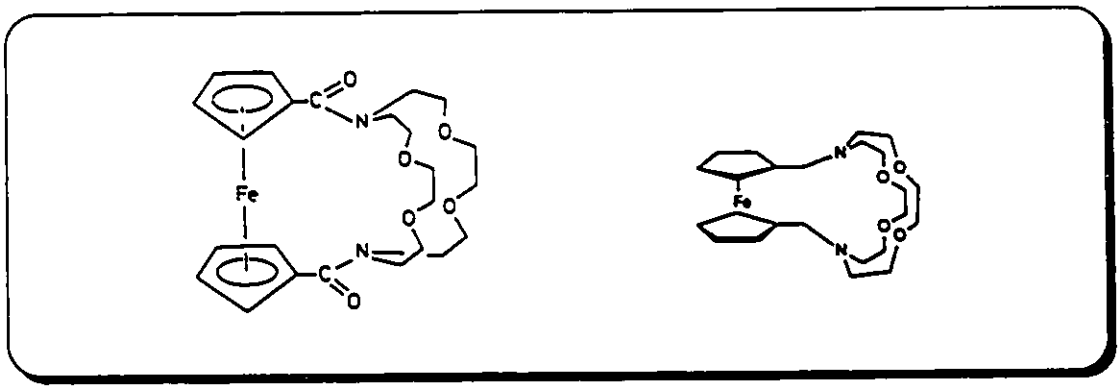

Figure 6.5 Cryptand molecules containing ferrocene.

In addition to molecules containing oxygen and nitrogen heteroatoms in the macrocycle, ferrocenophanes with sulfur atoms as the primary donors, designed to encapsulate transition metal atoms, have also been prepared by a number of groups[138]. Of particular interest is work done by Sato and coworkers[139] (Figure 6.6) which describes the spontaneous reduction of Cu(II) to Cu(I) by the ferrocene moiety, which is simultaneously oxidized to the ferricinium

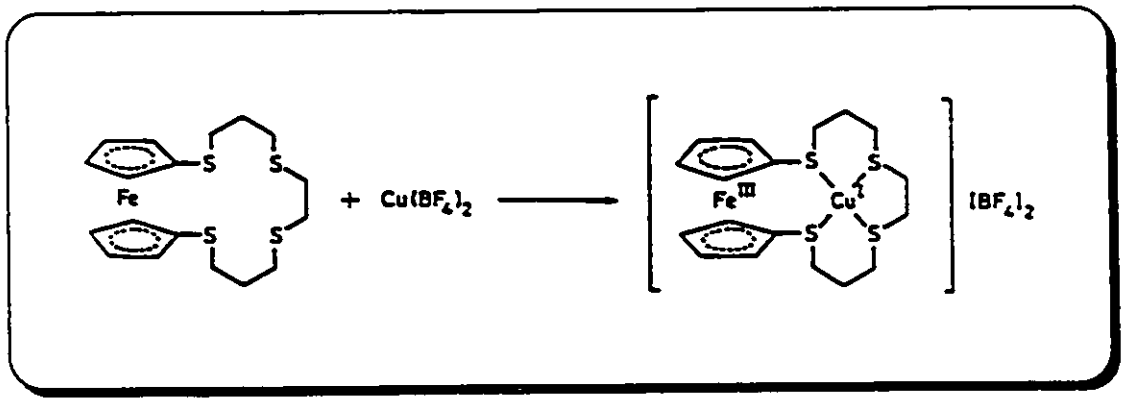

Figure 6.6 Spontaneous reduction of Cu(II) by ferrocene.

cation. Other work by the same authors[140] describes the inclusion of metal cations such as Pt(II), Cu(I), Ag(I), Hg(II), and Pd(II). Of particular interest within this series is the palladium complex of 1,5,9-trithia[9](1,1')-ferrocenophane in which there is a direct Fe(II)-Pd(II) bond.

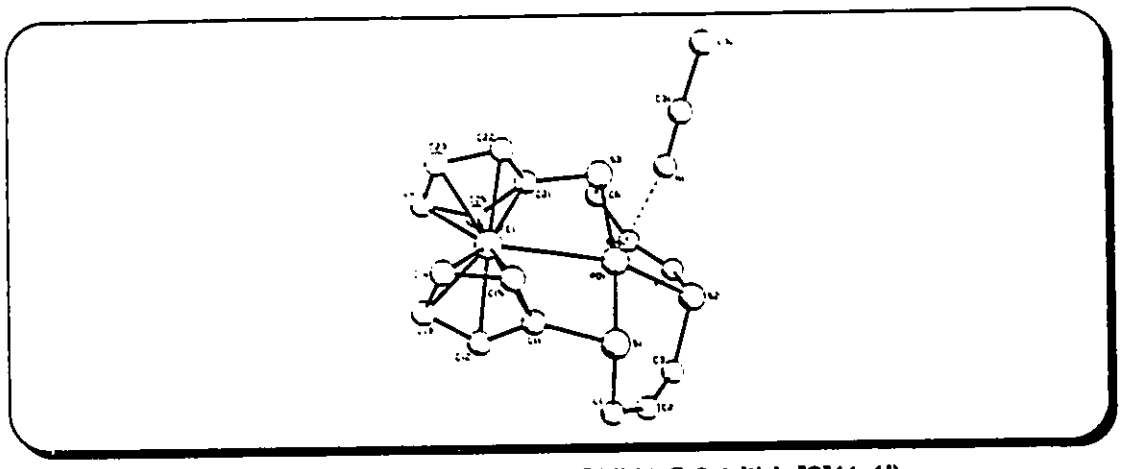

Figure 6.7 Crystal Structure of [Pd(CH_3CN)(1,5,9-trithia[9](1,1')-ferrocenophane)][BF_4]$_2$.

These and many other macrocycles, in which ferrocene is either a pendant arm or an integral part of the macrocyclic framework and the heteroatoms are either homogeneous or mixed, are described in reviews by Beer[135a] and by Reinhoudt[141].

6.2 Experimental.

General Comments. All starting materials, deuterated solvents and anhydrous *N,N*-dimethylformamide, (DMF), were purchased from Aldrich Chemicals or Strem Chemicals (copper(I) acetate) and used without further purification. Acetonitrile was distilled from CaH_2 under N_2(g). All reactions were performed under an atmosphere of N_2(g) using standard Schlenk techniques and

all solvents and liquid starting materials were degassed prior to use. ^{1}H and $^{13}C\{^{1}H\}$ NMR spectra were recorded on a Brüker AC300 spectrometer locked to the deuterated solvent at 300.1 and 75.5 MHz respectively, and infrared spectra were recorded on a Nicolet 5DX FTIR spectrometer.

(i) Preparation of 1,1'-Dibromoferrocene, (48)[142]. All solvents and reagents were distilled and/or dried under N_2 immediately prior to use. Ferrocene (6.000 g, 32.25 mmol) was dissolved in hexane (200 mL) and cannulaed into a slow addition funnel mounted on a 500 mL 3-neck flask. N,N,N',N'-tetramethyl-ethylenediamine (TMEDA) (12.0 mL, 79.5 mmol) followed by *n*-butyllithium (51 mL, 1.6 M in hexane, 81.6 mmol) were syringed into the flask under N_2 and stirred for 10 min. The ferrocene solution was added over 60 min. and then stirred at room temperature for 6 h during which time an orange precipitate formed. The solution was cooled to -78° C and 1,2-dibromotetrafluoroethane (8.6 mL, 72 mmol) was added *via* syringe over 15 min. The solution was warmed to room temperature, filtered through a pad of silica gel on celite and the solvent was removed *in vacuo*. The resulting solid was recrystallized from methanol twice and dried to give an orange solid. Yield: 7.140 g (64%). ^{1}H NMR ($CDCl_3$): δ (ppm) 4.40 (t, 4H, α-CH: Cp), 4.15 (t, 4H, β-CH: Cp), 4.14 (s, 3H, CH, 23% ferrocene impurity). $^{13}C\{^{1}H\}$ NMR ($CDCl_3$): δ (ppm) 78.3 (C-Br), 72.7 (α-C: Cp), 69.9 (β-C: Cp), 67.9 (ferrocene impurity).

(ii) Preparation of 1,1'-diacetoxyferrocene, (49)[143a]. 1,1'-dibromoferrocene (2.995 g, 6.54 mmol) and copper(I) acetate (7.502, 61.2 mmol) were dissolved in 50% aqueous ethanol (250 mL) under N_2 and refluxed

for 40 min. Upon cooling the solution was filtered and the filtrate was added to water (300 mL). The aqueous solution was extracted 4 times with diethyl ether (50 mL), the combined extracts were dried over $MgSO_4$, and the solvent was removed *in vacuo*. The product was purified by column chromatography (~35 g of 70-230 mesh 60 Å silica gel) using petroleum ether (b.p. 35-60°C) as eluent to remove ferrocene and 1,1'-dibromo-ferrocene impurities. The product was then flushed off the silica gel with acetone. The acetone was removed *in vacuo* to give an orange liquid that solidified on standing. Yield: 1.769 g (89%). ^{1}H NMR ($CDCl_3$): δ (ppm) 4.45 (s br, 4H, α-CH: Cp), 3.99 (s br, 4H, β-CH: Cp), 2.16 (s, 6H, CH_3). $^{13}C\{^1H\}$ NMR ($CDCl_3$): δ (ppm) 169.1 (CO), 116.0 (C-$OCOCH_3$), 64.6 (α-C: Cp), 62.1 (β-C: Cp), 21.3 (CH_3).

(iii) Preparation of 1,1'-bis(2-chloroethoxy)ferrocene, (50)[143b].

1,1'-diacetoxyferrocene (0.805 g, 2.66 mmol) and 18-crown-6 (0.202 g, 0.764 mmol) were added to 10% aqueous potassium hydroxide (10 mL) under nitrogen and the solution was refluxed for 30 min. The heat was reduced and 1,2-dichloroethane (9.6 mL, 121 mmol) was syringed in at once; the mixture was heated at 80° C for 6 h. The solution was cooled and extracted three time with diethyl ether (25 mL); the extracts were combined, washed with water, dried over $MgSO_4$ and the solvent was removed *in vacuo*. The remaining oil was purified by column chromatography (40 g of 70-230 mesh 60 Å silica gel) using 9:1 petroleum ether-acetone as eluent. The second band was collected and the solvent removed to give an orange solid. Yield: 0.402 g, (44%). ^{1}H NMR ($CDCl_3$): δ (ppm) 4.12 (t, ^3J = 1.9 Hz, 4H, α-CH: Cp), 4.06 (t, ^3J = 5.5 Hz, 4H,

OCH_2), 3.88 (t, ^3J = 1.9 Hz, 4H, β-CH: Cp), 3.74 (t, ^3J = 5.5 Hz, 4H, CH_2Cl). $^{13}C\{^1H\}$ NMR ($CDCl_3$): δ (ppm) 126.2 (O-C: quaternary), 70.5 (OCH_2), 62.7 (α-C: Cp), 56.5 (β-C: Cp), 42.4 (CH_2Cl).

(iv) Preparation of 1,1'-bis(5-chloro-3-oxapentoxy)ferrocene, (51)[143b]. This preparation follows that for compound 50 except bis(2-chloroethyl)ether was substituted for 1,2-dichloroethane. 1,1'-diacetoxyferrocene (0.576 g, 1.91 mmol), 18-crown-6 (0.146 g, 0.552 mmol), 10% aqueous potassium hydroxide (7.2 mL), bis(2-chloroethyl)ether (8.467 g, 60.5 mmol). The crude oil was purified by column chromatography (40 g of 70-230 mesh 60 Å silica gel) using 9:1 petroleum ether-acetone as eluent. The second band was collected and the solvent removed to give an orange solid. Yield: 0.301 g, (36%). ^1H NMR ($CDCl_3$): δ (ppm) 4.13 (s br, 4H, α-CH: Cp), 3.97 (t, ^3J = 4.4 Hz, 4H, OCH_2), 3.88 (s br, 4H, β-CH: Cp), 3.76 (m, 8H, OCH_2), 3.63 (t, ^3J = 5.8 Hz, 4H, CH_2Cl). $^{13}C\{^1H\}$ NMR ($CDCl_3$): δ (ppm) 126.9 (O-C: Cp quaternary), 71.6 ($CpOCH_2$), 70.0 (OCH_2), 69.9 (OCH_2), 62.6 (α-C: Cp), 56.1 (β-C: Cp), 42.8 (CH_2Cl).

(v) Preparation of 5,9-dioxa-2,12-dithia-6,8-ferrocenyl[13]-*m*-cyclophane, (TOMB-F2) (52). To a stirred suspension of Cs_2CO_3 (0.590 g, 1.81 mmol) in DMF (250 mL) at 57 °C was added a solution of 1,1'-bis(2-chloroethoxy)-ferrocene (0.206 g, 0.600 mmol) and *meta*-xylene-α,α'-dithiol (0.102 g, 0.599 mmol) in DMF (150 mL) over 72 h. The DMF was then removed *in vacuo* leaving a brown oil and cesium salts. The residue was dissolved in CH_2Cl_2 (100 mL), filtered, and washed with 0.1 M NaOH

(2 x 25 mL) and distilled water (25 mL). The solution was dried over anhydrous $MgSO_4$ for 12 h, filtered, the solvent evaporated, and the orange paste dried *in vacuo*. Recrystallization from hot hexane yielded a pale orange solid. Yield: 0.069 g (26%). ^1H NMR ($CDCl_3$): δ (ppm) 7.29 (m, 4H, aromatic), 4.07 (t, ^3J = 1.9 Hz, 4H, α-CH: Cp), 3.90 (t, ^3J = 6.2 Hz, 4H, OCH_2), 3.81 (t, ^3J = 1.9 Hz, 4H, β-CH: Cp), 3.77 (s, 4H, benzylic), 2.62 (t, ^3J = 6.8 Hz, 4H, SCH_2). $^{13}C\{^1H\}$ NMR ($CDCl_3$): δ (ppm) 138.4, 131.1, 129.6, 127.8 (aromatic), 126.2 (O-C: Cp quaternary), 71.2 (-OCH_2), 61.9 (α-CH), 55.8 (β-CH), 35.9 (benzylic), 28.4 (SCH_2).

(vi) Attempted preparation of 2,18-dithia-5,8,12,15-tetraoxa-9,11-ferrocenyl[19]-*m*-cyclophane, (TOMB-F4) (53). To a stirred suspension of Cs_2CO_3 (0.510 g, 1.56 mmol) in DMF (100 mL) at 57 °C was added a solution of 1,1'-bis(5-chloro-3-oxapentoxy)ferrocene (0.301 g, 0.698 mmol) and *meta*-xylene-α,α'-dithiol (0.102 g, 0.716 mmol) in DMF (50 mL) over 24 h. The DMF was then removed *in vacuo* leaving a brown oil and cesium salts. The residue was dissolved in CH_2Cl_2 (100 mL), filtered, and washed with 0.1 M NaOH (2 x 25 mL) and distilled water (25 mL). The solution was dried over anhydrous $MgSO_4$ for 12 h, filtered, the solvent evaporated, and the orange paste dried *in vacuo*. Yield (based on 1,1'-bis(5-chloro-3-oxapentoxy)ferrocene): 0.215 g (64%). ^1H NMR ($CDCl_3$): δ (ppm) 7.25 (m, 4H, aromatic), 4.18 (m br, 8H, α-CH: Cp), 3.95 (m, 16H, OCH_2), 3.77 (m, 8H, β-CH: Cp; 4H, benzylic), 3.62 (m, 8H, -OCH_2), 3.52 (t, ^3J = 7 Hz, 4H, CH_2Cl), 2.59 (t, ^3J = 7 Hz, 4H, SCH_2). $^{13}C\{^1H\}$

NMR ($CDCl_3$): δ (ppm) 138.8, 129.6, 129.0, 127.7 (aromatic), 71.5, 71.0, 70.0, 69.8, 69.7, 69.6 (OCH_2), 62.7, 62.3 (α-CH: Cp), 56.0, 53.4 (β-CH: Cp), 42.7 (CH_2Cl), 36.6 (benzylic), 30.3 (SCH_2).

6.3 X-Ray Diffraction Data Collection, Solution, and Refinement.

(i) General Procedures. The general procedure for data collection and solution refinement is identical to that outlined in section 2.3 (i) and the reader is referred to it for the sake of brevity.

(ii) Structure Determination of 5,9-dioxa-2,12-dithia-6,8-ferrocenyl [13]-*m*-cyclophane, (TOMB-F2) (52). Orange crystals of TOMB-F2 were grown by slow evaporation of an acetone solution of the macrocycle. A statistical analysis of the intensity distributions and a determination of observed extinctions were consistent with the monoclinic space group $P2_1/n$, and this was confirmed by a successful solution refinement. A total of 3947 reflections were collected, and 1732 unique reflections with $F_o^2 > 3\sigma(F_o^2)$ were used in the refinement. The positions of the iron and sulfur atoms were determined by direct methods from the *E*-map with the highest figure of merit. The remaining atoms were located from a difference Fourier map calculation. In the final cycles of refinement, all atoms were assigned anisotropic thermal parameters. This resulted in $R = 0.0440$ and $R_w = 0.0393$ at final convergence. The Δ/σ value for any parameter in the final cycle was less than 0.0006. A final difference Fourier map calculation showed no peaks of chemical significance. Crystal data, intensity collection and structure

refinement details, as well as all atomic positional parameters, bond distances and angles are summarized in Appendix Table A20.

6.4 Results and Discussion

(i) Synthesis of TOMB-F2, (52). The ligand TOMB-F2 was prepared by the reaction of 1,1'-bis(2-chloroethoxy)ferrocene with *meta*-xylene-α,α'-dithiol using the cesium ion mediated ring closure method of Buter and Kellogg[28] as is shown in Figure 6.8 below. 1,1'-bis(2-chloroethoxy)ferrocene was prepared according to the literature[142, 143].

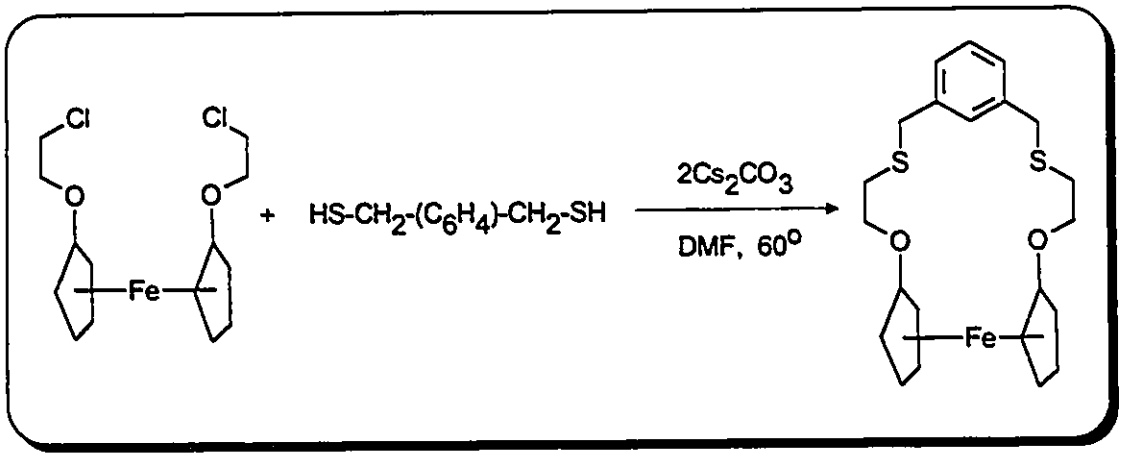

Figure 6.8 Preparation of TOMB-F2 from 1,1'-bis(2-chloroethoxy)ferrocene and *meta*-xylene-α,α'-dithiol.

The ^{1}H NMR spectrum (Figure 6.9) is consistent with the formation of the macrocycle with a multiplet centred at 7.25 ppm integrating to 4 aromatic hydrogens. Two triplets at 4.07 and 3.81 ppm are present for the hydrogens on the α and β positions of the Cp rings and are identified by their small coupling constants of 1.9 Hz. Two more triplets at 3.91 and 2.62 ppm for the OCH_2 and

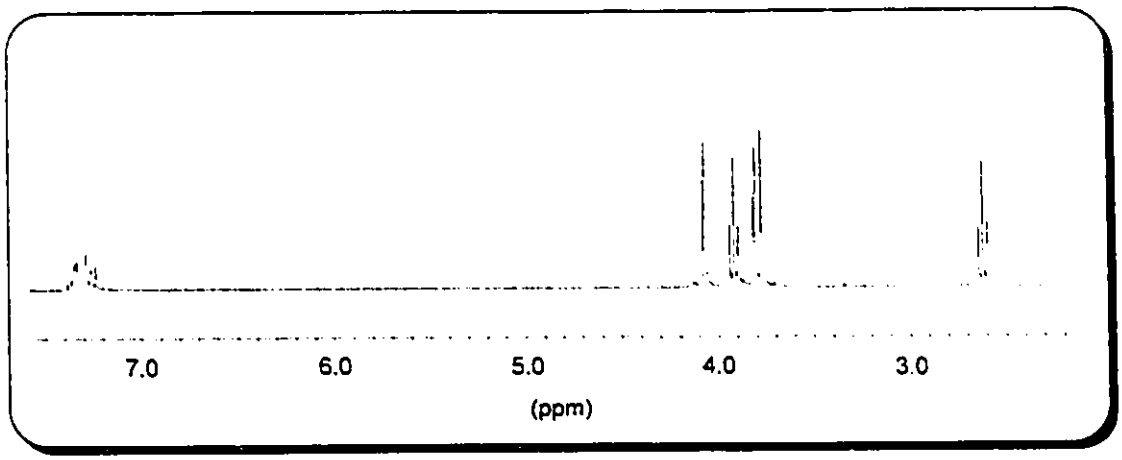

Figure 6.9 ^{1}H NMR spectrum of TOMB-F2 in $CDCl_3$.

SCH_2 ethylene hydrogens respectively, and a singlet at 3.77 ppm (benzylic) are consistent with the ^{1}H NMR spectra of other TOMB-X ligands (*vide supra*).

The $^{13}C\{^1H\}$ NMR spectrum is also consistent with the formation of the ligand with the expected *meta*-substitution pattern observed in the aromatic region along with a weak peak at 126.2 ppm for the quaternary O-C carbon atom of the Cp rings. Further upfield, resonances at 71.2 ppm for the OCH_2 carbon atoms, at 61.9 and 55.8 ppm for the carbon atoms on the α and β positions of the Cp rings, at 35.9 for the benzylic carbon atoms and at 28.4 ppm for the -SCH_2 carbon atoms are consistent with the macrocyclic structure drawn in Figure 6.8.

In addition to the spectroscopic evidence for the formation of the macrocycle, X-ray quality crystals were grown by slow evaporation of an acetone solution of TOMB-F2 and the crystal structure was determined.

(ii) Crystal Structure of TOMB-F2 (52). The unit cell is monoclinic and contains four molecules of TOMB-F2. A perspective view of the macrocycle with the atom numbering scheme is shown in Figure 6.10.

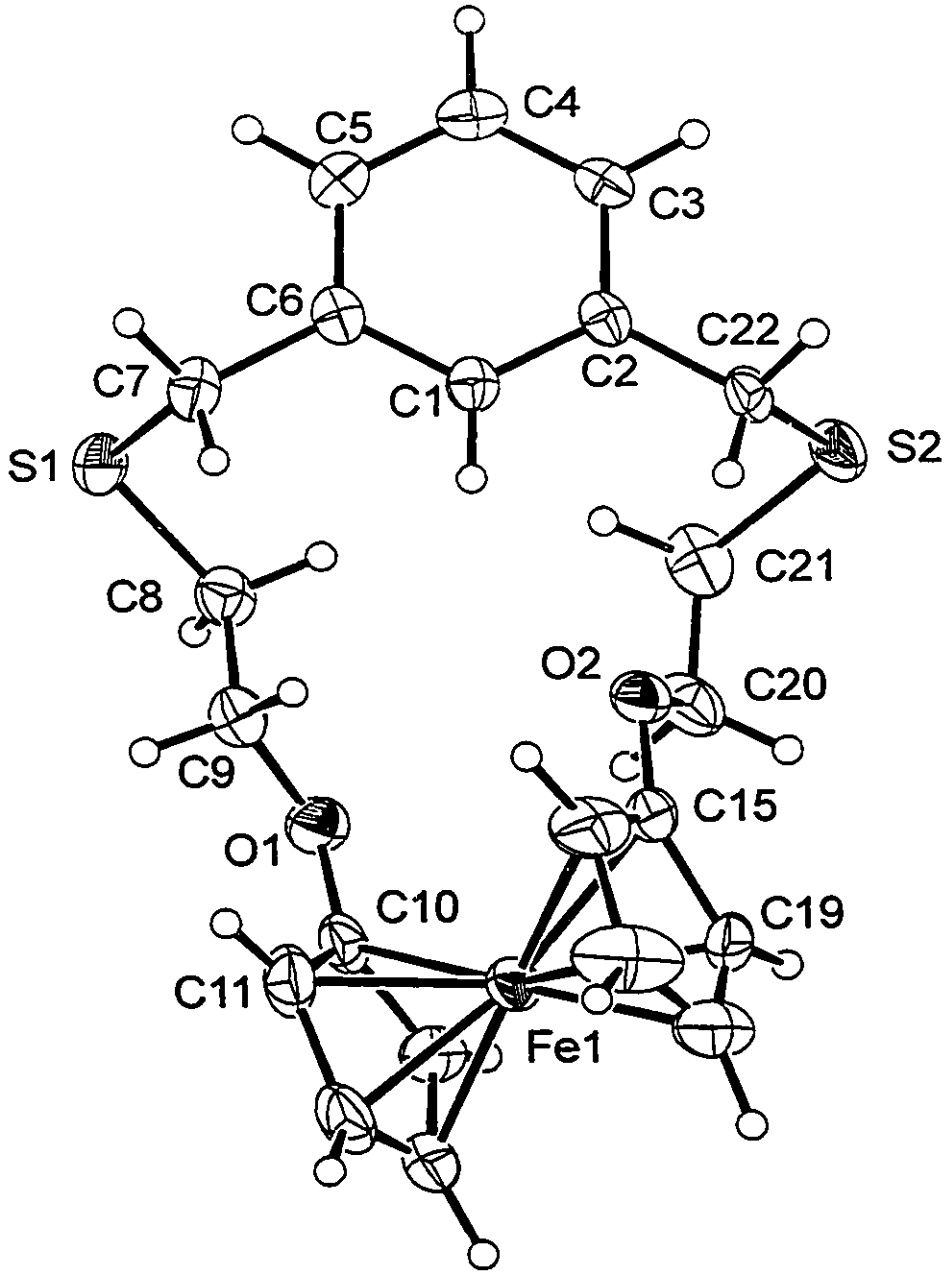

Figure 6.10 Perspective ORTEP drawing of TOMB-F2 (52) showing the atom numbering scheme with 30% thermal ellipsoids. Selected bond distances (Å) and angles are: S1-C7 = 1.813(6), S1-C8 = 1.797(7), S2-C21 = 1.799(7), S2-C22 = 1.811(6), average C(Cp)-O = 1.352(7), average $C(sp^3)$-O = 1.442(7), average $C(sp^2)$-$C(sp^2)$ = 1.386(7), average $C(sp^3)$-$C(sp^3)$ = 1.488(8), average $C(sp^2)$-$C(sp^3)$ = 1.505(8). Average C-C (Cp) = 1.408(9), average Fe-C(Cp) = 2.032(7) Å. C7-S1-C8 and C21-S2-C22 = 102.5(3)°.

crystallographic parameters including atomic positions, bonding parameters and details of data collection are listed in Appendix Table A20. Selected bonding parameters are given in the figure caption.

Sulfur-carbon distances range from 1.797(7) to 1.813(6) Å and $C(sp^2)$-$C(sp^2)$ distances range 1.376(8) to 1.406(7) Å. The two $C(sp^2)$-$C(sp^3)$ bonds are 1.509(8) and 1.501(7) Å and the $C(sp^3)$-$C(sp^3)$ bonds average 1.488(8) Å. The C(Cp)-O distances average 1.352(7) Å and the $C(sp^3)$-O distances average 1.442(7) Å. The C-C (Cp) distances average 1.408(9) and the Fe-C(Cp) distances average 2.032(7) Å. These distances compare well with those found for other thiacyclophanes, macrocyclic ethers and ferrocenyl complexes[31, 61, 85, 140b chapter 3].

In examining the structure of TOMB-F2, the main feature to note is the placement of the ferrocene moiety with respect to the aromatic ring. As observed for TT[11]MC[61], the two C(benzylic)-S bonds are approximately perpendicular to the plane of the aromatic ring with C7-S1-C8 and C21-S2-C22 angles both at 102.5(3)°. The two C(benzylic)-S bonds are oriented away from the aryl ring and the chain bends back as the backbone is traced away from the sulfur atoms, such that the plane of the aryl ring partially cuts the ferrocene moiety.

The two sulfur atoms are exodentate with torsional angles ranging from -58.8(5)° to -80.4(6)°, consistent with the range found for other thiacyclophanes[31, 61]. The torsional angles about the oxygen atoms are consistent with the endodentate conformation observed for other crown ethers; torsional angles involving the Cp carbon atoms of 7.3° and 13.3° (rather than values close to 180°)

are a result of Cp carbon atoms in the same plane as those with torsional angles close to 180° (Table 6.1 and Figure 6.10).

It is also noteworthy that although one would expect the low energy conformation of a 1,1' disubstituted ferrocene to have the substituents staggered, the two oxygen atoms bonded to the Cp rings are almost eclipsed, with a dihedral

Table 6.1 Torsional angles around sulfur and oxygen atoms for TOMB-F2.

linkage	angle (°)	linkage	angle (°)
C6-C7-S1-C8	64.9(5)	C20-C21-S2-C22	-80.4(6)
C7-S1-C8-C9	69.3(5)	C2-C22-S2-C21	-58.8(5)
C8-C9-O1-C10	178.6(4)	C15-O2-C20-C21	-168.5(5)
C9-O1-C10-C11	7.3(9)	C19-C15-O2-C20	13.3(9)
C9-O1-C10-C14	-173.3(6)	C16-C15-O2-C20	-171.2(6)

angle of 4.42° between the planes defined by O1-C10-Fe and Fe-C15-O2. This is perhaps due to energetic requirements placed on the ferrocene moiety in accommodating the low energy conformation of the remaining part of the macrocycle.

(iii) Attempted Preparation of (TOMB-F4) (53). In order to further explore the potential of a series of macrocyclic ligands containing ferrocene, the synthesis of a second macrocycle containing four oxygen atoms, TOMB-F4, was undertaken (Figure 6.11). The synthesis involved the reaction of *meta*-xylene-α,α'-dithiol with the appropriate dichloro starting material moiety, (1,1'-bis-(5-chloro-3-oxapentoxy)-ferrocene)[142, 143], using Buter and Kellogg's

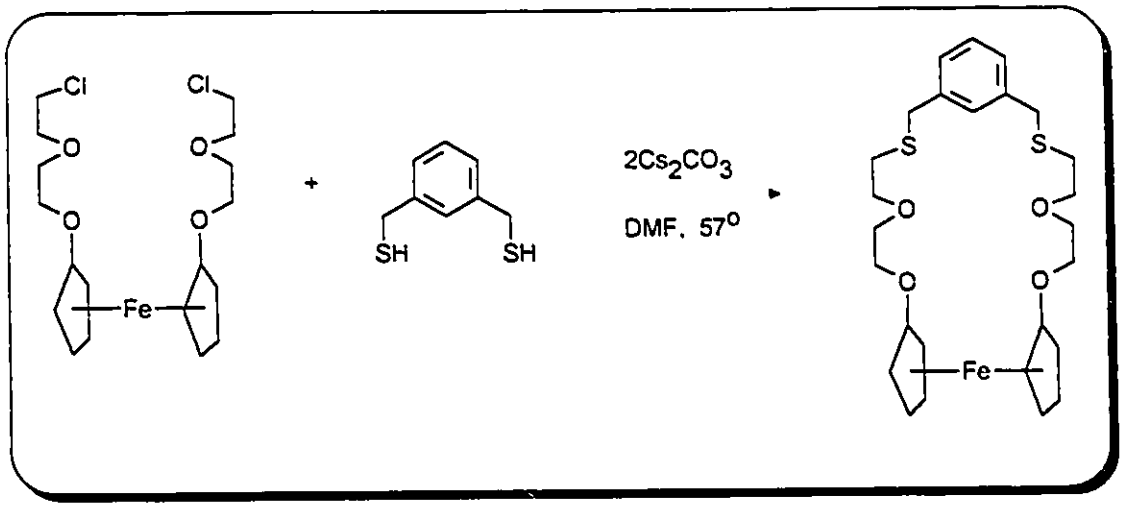

Figure 6.11 Intended preparation of TOMB-F4.

cesium ion technique[28]. However, upon analysis by ^{1}H and $^{13}C\{^{1}H\}$ NMR spectroscopy the product was determined to be a 2:1 substitution product as shown below in Figure 6.12. In the ^{1}H NMR spectrum a multiplet at 7.25 ppm with integration = 4 was assigned as the aromatic hydrogens. A broad multiplet with

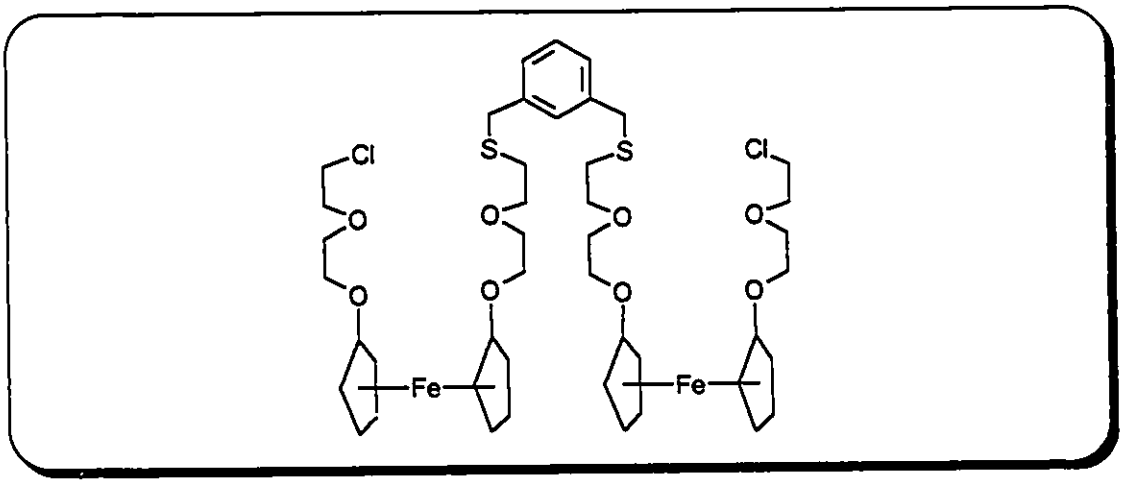

Figure 6.12 Actual product formed during preparation of TOMB-F4.

integration = 8 at 4.18 ppm was assigned as α-CH (Cp) hydrogen atoms and a multiplet at 3.77 ppm with integration = 12 was assigned as the 8 β-CH (Cp)

hydrogen atoms overlapping with the benzylic hydrogen atoms' resonance. A broad multiplet at 3.95 ppm with integration = 16 was assigned as OCH_2 resonances as was another multiplet at 3.62 ppm with integration = 8 hydrogens. A well defined triplet at 3.52 ppm with integration = 4 was assigned as CH_2Cl hydrogen atoms and an additional triplet at 2.59 ppm, also with integration = 4, was assigned as the SCH_2 resonance.

The $^{13}C\{^1H\}$ NMR spectrum is even more diagnostic with the expected *meta*-substitution pattern observed in the aromatic region of the spectrum, and six separate resonances for the OCH_2 carbon atoms at 71.5, 71.0, 70.0, 69.8, 69.7, 69.6 ppm indicating asymmetry within the ferrocene moiety. Each Cp carbon atom exhibits two resonances, appearing at 62.7 and 62.3 ppm (α-C: Cp), and 56.0 and 53.4 ppm (β-C: Cp) (the quaternary O-C carbon atoms were not observed). Finally, resonances at 42.7 ppm (CH_2Cl), 36.6 ppm (benzylic), and 30.3 ppm (SCH_2) all indicate that only one of two chlorine leaving groups on two separate 1,1'-bis(5-chloro-3-oxapentoxy)ferrocene molecules reacted with *meta*-xylene-α,α'-dithiol.

(iv) Attempted Metalation of TOMB-F2; Oxidation of Ferrocene. With TOMB-F2 synthesized, the next step was to metalate the ligand. Upon addition of acetonitrile (20 mL) to TOMB-F2 and $[Pd(CH_3CN)_4][BF_4]_2$ (1:1), the solution turned dark brown and was accompanied by the formation of a dark precipitate. The ^1H NMR spectrum (CD_3CN) of the reaction product consisted of a series of very broad and weak peaks and could not be interpreted. With the idea that the product might have been fluxional in acetonitrile, ^1H NMR spectra were also

recorded in $CDCl_3$ and DMSO-d_6. In both cases the result was the same: the spectra contained broad, uninterpretable resonances. An attempt to record $^{13}C\{^1H\}$ NMR spectra was also made but only solvent peaks were observed.

These results indicated that the product may have been paramagnetic. If one examines the redox potentials for ferrocene and Pd^{2+} in aqueous solution[144] (Scheme 6.1), the potential for the two combined half reactions is positive meaning that the reaction is spontaneous. In order to test if the same reaction is

2 Ferrocene	$\longrightarrow$ 2 Ferrocene$^+$ + 2e$^-$	E^O= -0.400 V
Pd^{2+} + 2e$^-$	$\longrightarrow$ Pd^O	E^O= 0.915 V
2 Ferrocene + Pd^{2+}	$\longrightarrow$ 2 Ferrocene$^+$ + Pd^O	E^O= +0.515 V

Scheme 6.1 The redox potential for 2 ferrocene + Pd^{2+} is positive; the reaction is spontaneous.

spontaneous in acetonitrile (the solvent in which the metalation was attempted), ferrocene and $[Pd(CH_3CN)_4][BF_4]_2$ were mixed in a 2:1 ratio and the solution turned deep green almost immediately, indicating oxidation from Fe(II) to Fe(III). The same test was then performed using TOMB-F2 and $[Pd(CH_3CN)_4]^{2+}$ in a 2:1 ratio. After refluxing, the solution turned green with precipitation of Pd°, consistent with the formation of the ferricinium cation of TOMB-F2 (Figure 6.13). The brown colour of the attempted metalation was therefore most probably due to the presence of the additional equivalent of $[Pd(CH_3CN)_4][BF_4]_2$.

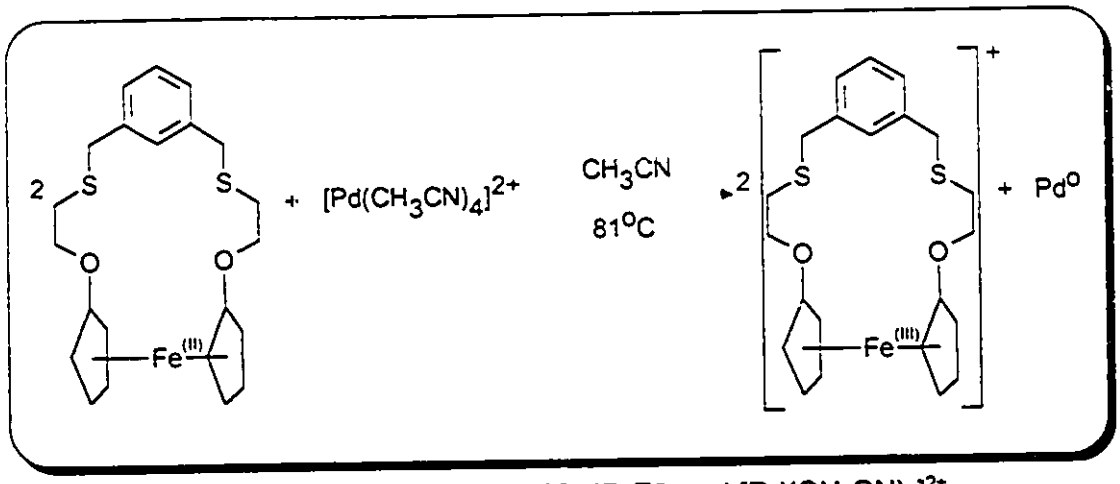

Figure 6.13 Redox reaction between TOMB-F2 and $[Pd(CH_3CN)_4]^{2+}$.

6.5 Conclusion

In this chapter the synthetic route towards a new series of TOMB-FX ligands was developed. The synthesis of TOMB-F2 was performed and the ligand was isolated in moderate yield. The crystal structure of the ligand was determined and shows typical bond distances and torsional angles, and the oxygen atoms bonded to the ferrocene moiety are in an eclipsed conformation. The attempted synthesis of TOMB-F4 resulted in the formation of a 2:1 substitution product and was not pursued further. It is the opinion of the author, however, that TOMB-F4 can be synthesized under carefully controlled conditions.

The attempted metalation of TOMB-F2 did not result in insertion of the palladium atom into the S_2C bracket as was expected. The palladium starting material instead oxidizes the ferrocene to the ferricinium cation precipitating palladium metal in the process. Attempts are now being made to overcome this problem. Chemical oxidation of the ferrocene moiety prior to the metalation reaction will be performed to prevent decomposition of $[Pd(CH_3CN)_4][BF_4]_2$ by

ferrocene (Figure 6.14). Upon metalation of [TOMB-F2]$^{+}$[X]$^{-}$, the ferricinium moiety will be reduced back to ferrocene so that NMR spectroscopy and cyclic voltammetry can be used to characterize the receptor and its receptor- substrate complexes. Preliminary electrochemical tests on the potential required to reduce [Pd(CH_3CN)(TOMB-3)][BF_4] will also be performed in order to

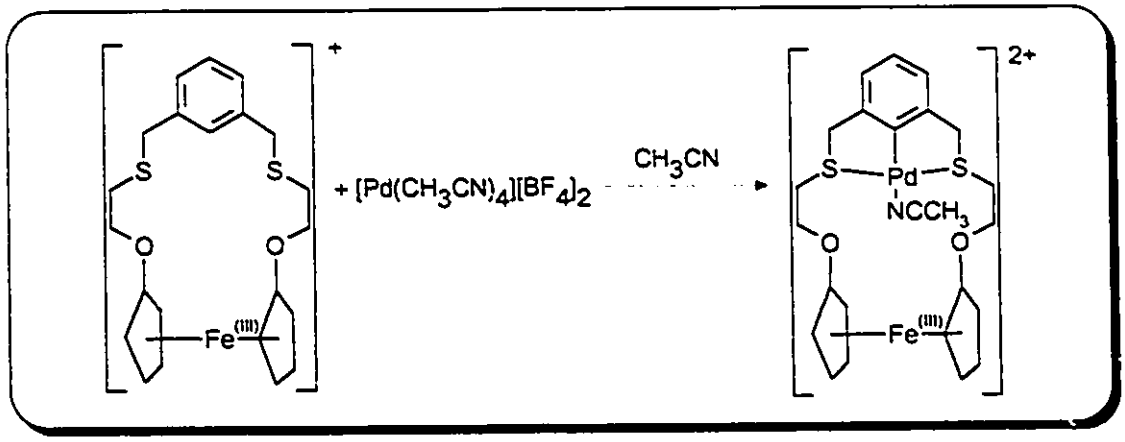

Figure 6.14 Proposed method of metalation of TOMB-F2.

determine the potential required to reduce the palladium atom inside the S_2C bracket. Hopefully this potential will be less than the absolute value of the oxidation potential of the ferrocene moiety, which will make the potential of the combined half reactions negative.

Appendix A

Supplementary Material for X-ray Structural Determinations

Table A1.1 Summary of Crystal Data, Intensity Collection and Structure Refinement for *pr*-TOMB-1, (13).

formula	$C_{14}H_{20}OS_2$
fw	268.43 $gmol^{-1}$
colour/form	colourless block
a, Å	10.592(4)
b, Å	16.601(6)
c, Å	7.944(2)
α, β, γ, deg	90
V (Å^3)	1396.9(1.5)
crystal system	orthorhombic
space group	*P*nma (#62)
ρ (gmL^{-1})	1.28
Z	4
μ, cm^{-1}	3.63
diffractometer	Rigaku AFC6S
λ, (Å)	0.71O69
T (°C)	23
scan type	ω–2θ
speed, deg min^{-1}	32
scan width (deg)	1.05 +0.30 tan
2θ range (deg)	4.5-50
# data collected	1461 (+h,+k,+l)
# unique data with $F_o^2>3\sigma(F_o^2)$	712
# variables	83
data/var ratio	8.6
goodness of fit	1.66
$R(F_o)$, %	3.85
$R_w(F_o)$, %	2.33

Table A1.2 Positional parameters and β(eq) for *pr*-TOMB-1, (13).

atom	x	y	z	β(eq)
S1	0.17383(9)	0.45510(5)	0.05127(13)	4.47(5)
O1	0.4409(3)	1/4	0.0377(4)	3.8(2)
C1	0.1268(4)	1/4	-0.1352(5)	2.9(2)
C2	0.0649(3)	0.3225(2)	-0.1121(4)	2.9(2)
C3	-0.0604(3)	0.3221(2)	-0.0629(4)	3.5(2)
C4	-0.1222(4)	1/4	-0.0361(6)	3.8(3)
C5	0.1311(3)	0.4021(2)	-0.1412(4)	4.3(2)
C6	0.2919(3)	0.3883(2)	0.1365(4)	3.6(2)
C7	0.4183(3)	0.3910(2)	0.0445(4)	4.2(2)
C8	0.5023(3)	0.3212(2)	0.0890(4)	4.2(2)

Table A1.3 Intramolecular Distances (Å) Involving the Nonhydrogen Atoms for *pr*-TOMB-1, (13).

atom-atom	distance	atom-atom	distance
S1-C5	1.822(3)	C2-C5	1.513(4)
S1-C6	1.803(3)	C3-C4	1.381(4)
O1-C8	1.409(3)	C6-C7	1.527(4)
C1-C2	1.382(3)	C7-C8	1.504(4)
C2-C3	1.385(4)		

Table A1.4 Intramolecular Bond Angles Involving the Nonhydrogen Atoms for *pr*-TOMB-1, (13).

linkage	angle (°)	linkage	angle (°)
C5-S1-C6	101.0(1)	C2-C3-C4	120.1(3)
C8-O1-C8	113.9(3)	C3-C4-C3	120.2(4)
C2-C1-C2	121.1(4)	S1-C5-C2	114.2(2)
C1-C2-C3	119.2(3)	S1-C6-C7	114.3(2)
C1-C2-C5	121.4(3)	C6-C7-C8	112.6(3)
C3-C2-C5	119.4(3)	O1-C8-C7	107.8(3)

Table A1.5 Torsional Angles for *pr*-TOMB-1, (13).

linkage	angle (°)	linkage	angle (°)
S1-C5-C2-C1	-104.9(4)	C2-C1-C2-C5	178.5(3)
S1-C5-C2-C3	75.6(3)	C2-C3-C4-C3	-1.9(8)
S1-C6-C7-C8	-165.5(2)	C2-C5-S1-C6	66.9(3)
O1-C8-C7-C6	62.3(4)	C4-C3-C2-C5	179.9(4)
C2-C1-C2-C3	-0.9(7)	C7-C8-O1-C8	-173.1(2)
C1-C2-C3-C4	0.5(6)	C5-S1-C6-C7	73.9(3)

Table A2.1 Summary of Crystal Data, Intensity Collection, and Structure Refinement for [Pd(*pr*-TOMB-1)][BF_4], (14).

formula	$C_{15}H_{20}BF_4OS_2Cl_3Pd$
fw	580.01 $gmol^{-1}$
colour/form	yellow block
a, Å	10.728(4)
b, Å	12.723(4)
c, Å	8.425(2)
α, deg	92.38(3)
β, deg	106.12(2)
γ, deg	105.18(3)
V ($Å^3$)	1058.2(1.4)
crystal system	triclinic
space group	$P\bar{1}$ (#2)
ρ (gmL^{-1})	1.82
Z	2
μ, cm^{-1}	14.75
diffractometer	Rigaku AFC6S
λ, (Å)	0.71
T (°C)	23
scan type	ω–2θ
speed, deg min^{-1}	8
scan width (deg)	1.05 +0.30 tan
2θ range (deg)	4.5-50
# data collected	3721(h,±k,±l)
# unique data with $F_o^2>3\sigma(F_o^2)$	2116
# variables	245
data/var ratio	8.6
goodness of fit	1.34
$R(F_o)$, %	4.62
$R_w(F_o)$, %	3.67

Table A2.2 Positional Parameters and β(eq) for [Pd(*pr*-TOMB-1)][BF_4], (14).

atom	x	y	z	β(eq)
Pd1	0.94773(8)	0.87780(6)	0.27012(9)	2.93(2)
Cl1	0.4178(3)	0.4553(2)	0.1748(3)	5.5(1)
Cl2	0.3555(3)	0.5911(2)	0.4044(3)	6.4(1)
Cl3	0.1400(3)	0.4466(2)	0.1415(3)	5.9(1)
S1	0.8720(2)	1.0280(2)	0.2938(3)	3.54(9)
S2	1.0605(2)	0.7545(2)	0.2296(3)	3.58(9)
F1	0.8486(9)	0.357(1)	1.223(1)	16.8(6)
F2	0.694(1)	0.2306(6)	1.264(1)	13.4(5)
F3	0.7041(8)	0.2533(6)	1.0117(8)	9.5(4)
F4	0.650(1)	0.3666(8)	1.151(1)	15.5(7)
O1	0.7690(6)	0.7649(5)	0.2873(7)	4.1(3)
C1	1.114(1)	0.9857(7)	0.267(1)	3.2(3)
C2	1.2344(9)	0.9583(7)	0.309(1)	3.3(3)
C3	1.355(1)	1.0365(8)	0.314(1)	4.4(4)
C4	1.351(1)	1.1417(8)	0.286(1)	5.7(5)
C5	1.232(1)	1.1682(7)	0.243(1)	5.0(4)
C6	1.113(1)	1.0917(7)	0.234(1)	3.4(3)
C7	0.976(1)	1.1128(7)	0.182(1)	4.4(4)
C8	0.701(1)	0.9801(8)	0.149(1)	5.2(4)
C9	0.619(1)	0.884(1)	0.209(1)	6.0(5)
C10	0.640(1)	0.7722(9)	0.182(1)	5.8(5)
C11	0.772(1)	0.6574(8)	0.321(1)	5.7(5)
C12	0.903(1)	0.6531(8)	0.431(1)	4.9(4)
C13	1.014(1)	0.6474(7)	0.357(1)	5.0(4)
C14	1.2293(8)	0.8418(7)	0.344(1)	4.0(4)
C15	0.306(1)	0.5299(7)	0.197(1)	4.1(4)

Table A2.3 Intramolecular Distances (Å) Involving the Nonhydrogen Atoms for [Pd(*pr*-TOMB-1)][BF_4], (14).

atom-atom	distance	atom-atom	distance
Pd1-S1	2.286(2)	O1-C10	1.45(1)
Pd1-S2	2.284(3)	O1-C11	1.42(1)
Pd1-O1	2.119(5)	C1-C2	1.38(1)
Pd1-C1	1.951(8)	C1-C6	1.39(1)
Cl1-C15	1.758(9)	C2-C3	1.40(1)
Cl2-C15	1.758(9)	C2-C14	1.51(1)
Cl3-C15	1.736(9)	C3-C4	1.38(1)
S1-C7	1.826(9)	C4-C5	1.37(1)
S1-C8	1.83(1)	C5-C6	1.37(1)
S2-C13	1.825(9)	C6-C7	1.51(1)
S2-C14	1.826(9)	C8-C9	1.31(1)
F1-B1	1.30(1)	C9-C10	1.51(1)
F2-B1	1.29(1)	C11-C12	1.47(1)
F3-B1	1.33(1)	C12-C13	1.50(1)
F4-B1	1.28(1)		

Table A2.4 Intramolecular Bond Angles Involving the Nonhydrogen Atoms for [Pd(*pr*-TOMB-1)][BF_4], (14).

linkage	angle (°)	linkage	angle (°)
S1-Pd1-S2	167.20(8)	C3-C4-C5	121.0(9)
S1-Pd1-O1	94.3(2)	C4-C5-C6	120.8(9)
S1-Pd1-C1	84.1(3)	C1-C6-C5	119.3(9)
S2-Pd1-O1	98.2(2)	C1-C6-C7	116.4(8)
S2-Pd1-C1	83.5(3)	C5-C6-C7	124.2(9)
O1-Pd1-C1	176.7(3)	S1-C7-C6	107.1(6)
Pd1-S1-C7	96.0(3)	S1-C8-C9	109.7(7)
Pd1-S1-C8	101.1(3)	C8-C9-C10	119(1)
C7-S1-C8	106.1(5)	O1-C10-C9	112.8(8)
Pd1-S2-C13	104.3(3)	O1-C11-C12	113.1(8)
Pd1-S2-C14	96.0(3)	C11-C12-C13	119.6(9)
C13-S2-C14	107.3(4)	S2-C13-C12	116.5(6)
Pd1-O1-C10	118.2(5)	S2-C14-C2	107.4(6)
Pd1-O1-C11	118.9(6)	Cl1-C15-Cl2	109.3(5)
C10-O1-C11	114.6(7)	Cl1-C15-Cl3	111.4(5)
Pd1-C1-C2	119.5(6)	Cl2-C15-Cl3	110.4(5)
Pd1-C1-C6	120.3(7)	F1-B1-F2	109(1)
C2-C1-C6	120.1(8)	F1-B1-F3	108(1)
C1-C2-C3	119.9(8)	F1-B1-F4	107(1)
C1-C2-C14	117.7(8)	F2-B1-F3	114(1)
C3-C2-C14	122.3(9)	F2-B1-F4	110(1)
C2-C3-C4	118.7(9)	F3-B1-F4	108(1)

Table A3.1 Summary of Crystal Data, Intensity Collection and Structure Refinement for TOMB-3, (18).

formula	$C_{16}H_{24}O_3S_2$
fw	328.48 $gmol^{-1}$
colour/form	colourless block
a, Å	11.280(3)
b, Å	14.085(2)
c, Å	12.166(7)
α, deg	90
β, deg	115.62(3)
γ, deg	90
V ($Å^3$)	1743(1)
crystal system	monoclinic
space group	$P2_1/a$(#14)
ρ (gmL^{-1})	1.25
Z	4
μ, cm^{-1}	3.12
diffractometer	Rigaku AFC6S
λ, (Å)	0.71069
T (°C)	23
scan type	ω–2θ
scan width (deg)	1.05 +0.30 tan
2θ range (deg)	4.5-50
# data collected	3214
# unique data with $F_o^2>3\sigma(F_o^2)$	853
# variables	110
data/var ratio	7.8
largest +/- peaks ($e/Å^3$)	0.292/-0.260
max shift/error	0.00016
goodness of fit	1.84
$R(F_o)$, %	6.28
$R_w(F_o)$, %	4.41

Table A3.2 Positional parameters and β(eq) for TOMB-3, (18).

atom	x	y	z	β(eq)
S1	0.0678(2)	0.7302(2)	0.0822(2)	6.6(1)
S2	-0.4897(2)	0.7028(2)	-0.5547(2)	6.3(1)
O1	-0.1636(6)	0.8983(5)	-0.0200(6)	6.3(4)
O2	-0.2308(6)	0.9975(4)	-0.2419(7)	6.2(3)
O3	-0.3162(6)	0.8903(5)	-0.4621(6)	6.9(4)
C1	-0.2201(9)	0.7253(6)	-0.2358(8)	4.2(2)
C2	-0.3294(8)	0.6706(6)	-0.3079(8)	4.2(2)
C3	-0.3183(8)	0.5729(6)	-0.2988(8)	4.9(2)
C4	-0.202(1)	0.5325(6)	-0.2214(9)	5.0(2)
C5	-0.0972(8)	0.5849(7)	-0.1528(8)	4.8(2)
C6	-0.1015(8)	0.6835(7)	-0.1563(8)	4.1(2)
C7	0.0137(8)	0.7444(6)	-0.0807(8)	5.5(2)
C8	-0.0761(8)	0.7616(7)	0.1010(8)	5.3(2)
C9	-0.1045(9)	0.8642(7)	0.100(1)	6.2(3)
C10	-0.186(1)	0.9984(8)	-0.032(1)	7.0(3)
C11	-0.277(1)	1.0204(8)	-0.156(1)	7.4(3)
C12	-0.318(1)	1.0289(8)	-0.359(1)	7.8(3)
C13	-0.284(1)	0.9869(9)	-0.452(1)	7.1(3)
C14	-0.327(1)	0.8462(7)	-0.569(1)	5.7(3)
C15	-0.3421(8)	0.7437(7)	-0.5616(8)	5.6(2)
C16	-0.4523(8)	0.7199(6)	-0.3943(8)	5.2(2)

Table A3.3 Intramolecular Distances (Å) Involving the Nonhydrogen Atoms for TOMB-3, (18).

atom-atom	distance	atom-atom	distance
S1-C7	1.815(9)	C1-C6	1.398(9)
S1-C8	1.791(8)	C2-C3	1.38(1)
S2-C15	1.799(9)	C2-C16	1.50(1)
S2-C16	1.825(9)	C3-C4	1.36(1)
O1-C9	1.40(1)	C4-C5	1.34(1)
O1-C10	1.43(1)	C5-C6	1.39(1)
O2-C11	1.39(1)	C6-C7	1.50(1)
O2-C12	1.41(1)	C8-C9	1.48(1)
O3-C13	1.40(1)	C10-C11	1.45(1)
O3-C14	1.40(1)	C12-C13	1.46(1)
C1-C2	1.40(1)	C14-C15	1.46(1)

Table A3.4 Intramolecular Bond Angles Involving the Nonhydrogen Atoms for TOMB-3, (18).

linkage	angle (°)	linkage	angle (°)
C7-S1-C8	102.5(4)	C1-C6-C7	120.1(9)
C15-S2-C16	102.5(4)	C5-C6-C7	123.0(9)
C9-O1-C10	115.3(8)	S1-C7-C6	113.6(6)
C11-O2-C12	111.2(8)	S1-C8-C9	116.3(7)
C13-O3-C14	115.6(8)	O1-C9-C8	110.6(8)
C2-C1-C6	121.6(8)	O1-C10-C11	109.3(9)
C1-C2-C3	118.3(8)	O2-C11-C10	113.9(9)
C1-C2-C16	118.9(8)	O2-C12-C13	110.7(9)
C3-C2-C16	122.8(9)	O3-C13-C12	108.6(9)
C2-C3-C4	119.8(9)	O3-C14-C15	110.5(9)
C3-C4-C5	121.8(9)	S2-C15-C14	116.9(7)
C4-C5-C6	121.5(9)	S2-C16-C2	113.9(6)
C1-C6-C5	116.9(8)		

Table A3.5 Torsional Angles for TOMB-3, (18).

linkage	angle (°)	linkage	angle (°)
S1-C7-C6-C1	117.9(8)	C1-C6-C5-C4	-1(1)
S1-C7-C6-C5	-63(1)	C2-C3-C4-C5	0(2)
S1-C8-C9-O1	79.5(9)	C2-C3-C4-C5	0(2)
S2-C15-C14-O3	65(1)	C14-C15-S2-C16	-80.5(9)
C2-C1-C6-C5	0(1)	C2-C16-S2-C15	-55.9(8)
C2-C1-C6-C7	179.9(8)	C6-C7-S1-C8	-59.0(8)
S2-C16-C2-C1	110.6(9)	C7-S1-C8-C9	-77.7(8)
S2-C16-C2-C3	-67(1)	C8-C9-O1-C10	-175.3(7)
C6-C1-C2-C16	-177.9(8)	C9-O1-C10-C11	-164.9(8)
C3-C2-C1-C6	0(1)	C10-C11-O2-C12	-174.2(9)
O1-C10-C11-O2	-63(1)	C11-O2-C12-C13	-167.4(9)
C3-C4-C5-C6	0(2)	C12-C13-O3-C14	161.7(8)
O2-C12-C13-O3	71(1)	C13-O3-C14-C15	171.8(8)
C4-C5-C6-C7	179.9(8)		

Table A4.1 Summary of Crystal Data, Intensity Collection and Structure Refinement for [Pd(CH_3CN)(TOMB-0)][BF_4], (21).

formula	$C_{23}H_{35}N_2BF_4S_2Pd$
fw	596.87 $gmol^{-1}$
colour/form	yellow block
a, Å	13.273(4)
b, Å	19.206(2)
c, Å	20.323(2)
α, deg	90
β, deg	93.98(2)
γ, deg	90
V (Å^3)	5168(3)
crystal system	monoclinic
space group	C2/c (#5)
ρ (gmL^{-1})	1.481
Z	8
μ, cm^{-1}	9.02
diffractometer	Rigaku AFC6S
λ, (Å)	0.71
T (°C)	23
scan type	ω–2θ
scan width (deg)	1.05 +0.30 tan
2θ range (deg)	4.5-50
# data collected	4703
# unique data with $F_o^2>3\sigma(F_o^2)$	2959
# variables	287
data/var ratio	10.3
largest +/- peaks (e/Å^3)	0.711/ -0.772
max shift/error	0.04
goodness of fit	2.38
$R(F_o)$, %	5.62
$R_w(F_o)$, %	5.28

Table A4.2 Positional Parameters and β(eq) for [Pd(CH_3CN)(TOMB-0)][BF_4], (21).

Atom	x	y	z	β(eq)
Pd1	0.77425(4)	0.16126(3)	0.50639(3)	3.32(3)
S1	0.8932(2)	0.1938(1)	0.5882(1)	4.4(1)
S2	0.6780(2)	0.1259(1)	0.4122(1)	4.4(1)
F1	0.3153(6)	0.1512(6)	0.6920(4)	17.2(8)
F2	0.211(1)	0.2129(5)	0.6467(6)	21(1)
F3	0.1625(7)	0.1297(6)	0.6896(5)	22(1)
F4	0.2327(9)	0.2033(6)	0.7518(5)	20.7(9)
N1	0.6649(5)	0.1392(3)	0.5751(3)	4.2(3)
N2	1/2	0.0591(8)	1/4	11(1)
C1	0.8810(6)	0.1816(3)	0.4452(4)	3.3(4)
C2	0.8590(6)	0.1782(4)	0.3768(4)	3.6(4)
C3	0.9334(7)	0.1957(4)	0.3344(4)	4.9(5)
C4	1.0283(7)	0.2150(4)	0.3596(5)	5.4(5)
C5	1.0504(6)	0.2174(4)	0.4259(5)	4.9(5)
C6	0.9788(6)	0.2005(4)	0.4700(4)	4.0(4)
C7	1.0050(6)	0.2035(5)	0.5427(5)	6.3(6)
C8	0.9213(6)	0.1166(5)	0.6376(4)	5.3(5)
C9	0.9308(7)	0.0507(5)	0.5993(5)	6.1(5)
C10	0.9549(8)	-0.0125(6)	0.6431(6)	8.2(7)
C11	0.880(1)	-0.0296(6)	0.6926(6)	8.7(8)
C12	0.770(1)	-0.0368(6)	0.6668(6)	8.4(8)
C13	0.746(1)	-0.0912(6)	0.6181(6)	8.3(8)
C14	(0.6398(8)	-0.0905(6)	0.5867(6)	7.4(7)
C15	0.6307(9)	-0.1190(6)	0.5181(6)	8.5(7)
C16	0.685(1)	-0.0799(6)	0.4669(6)	8.6(8)
C17	0.6553(9)	-0.0063(6)	0.4606(5)	7.4(7)
C18	0.7091(8)	0.0330(5)	0.4065(5)	6.8(6)
C19	0.7544(6)	0.1621(5)	0.3500(4)	5.0(4)
C20	0.6132(6)	0.1270(4)	0.6162(4)	4.0(4)
C21	0.5525(6)	0.1101(5)	0.6701(4)	5.6(5)
C22	1/2	0.116(1)	1/4	7(1)
C23	1/2	0.191(1)	1/4	9(1)

B1	0.228(1)	0.166(2)	0.6984(7)	12(1)

Table A4.3 Intramolecular Distances (Å) Involving the Nonhydrogen Atoms for [Pd(CH_3CN)(TOMB-0)][BF_4], (21).

atom-atom	distance	atom-atom	distance
Pd1-S1	2.299(2)	C2-C19	1.49(1)
Pd1-S2	2.327(2)	C3-C4	1.38(1)
Pd1-N1	2.125(6)	C4C5	1.36(1)
Pd1-C1	1.987(7)	C5-C6	1.39(1)
S1-C7	1.811(9)	C6-C7	1.49(1)
S1-C8	1.814(9)	C8-C9	1.50(1)
S2-C18	1.84(1)	C9-C10	1.53(1)
S2-C19	1.814(8)	C10-C11	1.50(1)
F1-B1	1.27(2)	C11-C12	1.52(1)
F2-B1	1.27(2)	C12-C13	1.46(1)
F3-B1	1.19(2)	C13-C14	1.50(1)
F4-B1	1.26(2)	C14-C15	1.49(1)
N1-C20	1.124(8)	C15-C16	1.51(1)
N2-C22	1.09(2)	C16-C17	1.47(1)
C1-C2	1.404(9)	C17-C18	1.55(1)
C1-C6	1.41(1)	C20-C21	1.46(1)
C2-C3	1.39(1)	C22-C23	1.43(2)

Table A4.4 Intramolecular Bond Angles Involving the Nonhydrogen Atoms for [Pd(CH_3CN)(TOMB-0)][BF_4], (21).

linkage	angle (°)	linkage	angle (°)
S1-Pd1-S2	169.86(8)	C1-C6-C7	120.6(7)
S1-Pd1-N1	92.6(2)	C5-C6-C7	120.4(8)
S1-Pd1-C1	85.1(2)	S1-C7-C6	111.0(6)
S2-Pd1-N1	97.0(2)	S1-C8-C9	115.1(6)
S2-Pd1-C1	85.3(2)	C8-C9-C10	113.0(9)
N1-Pd1-C1	177.6(3)	C9-C10-C11	116.4(9)
Pd1-S1-C7	101.8(3)	C10-C11-C12	117(1)
Pd1-S1-C8	106.4(3)	C11-C12-C13	118(1)
C7-S1-C8	102.9(4)	C12-C13-C14	116(1)
Pd1-S2-C18	102.8(3)	C13-C14-C15	114(1)
Pd1-S2-C19	99.2(3)	C14-C15-C16	116.7(9)
C18-S2-C19	100.9(4)	C15-C16-C17	114(1)
Pd1-N1-C20	172.8(7)	C16-C17-C18	113(1)
Pd1-C1-C2	120.2(6)	S2-C18-C17	108.2(7)
Pd1-C1-C6	120.5(6)	S2-C19-C2	112.2(5)
C2-C1-C6	119.3(7)	N1-C20-C21	178.7(9)
C1-C2-C3	119.5(8)	N2-C22-C23	180.00
C1-C2-C19	119.8(7)	F1-B1-F2	104(1)
C3-C2-C19	120.4(7)	F1-B1-F3	114(2)
C2-C3-C4	120.3(8)	F1-B1-F4	102(1)
C3-C4-C5	120.5(8)	F2-B1-F3	105(2)
C4-C5-C6	121.4(8)	F2-B1-F4	116(2)
C1-C6-C5	119.0(8)	F3-B1-F4	115(2)

Table A5.1 Summary of Crystal Data, Intensity Collection and Structure Refinement for [Pd(CH_3CN)(TOMB-1)][CF_3SO_3], (23).

formula	$C_{15}H_{18}O_4NF_3S_3Pd$
fw	535.89 $gmol^{-1}$
colour/form	orange block
a, Å	8.639(4)
b, Å	17.165(2)
c, Å	13.099(2)
α, deg	90
β, deg	91.85(2)
γ, deg	90
V ($Å^3$)	1941.3(5)
crystal system	monoclinic
space group	$P2_1/c$ (#14)
ρ (gmL^{-1})	1.833
Z	4
μ, cm^{-1}	13.282
diffractometer	Rigaku AFC6S
λ, (Å)	0.71069
T (°C)	23
scan type	ω–2θ
scan width (deg)	1.05 +0.30 tan
2θ range (deg)	4.5-50
# data collected	3558
# unique data with $F_o^2>3\sigma(F_o^2)$	1333
# variables	179
data/var ratio	7.4
max +/- peaks ($e/Å^3$)	0.566/-0.507
max shift/error	0.000135
goodness of fit	1.36
$R(F_o)$, %	4.69
$R_w(F_o)$, %	4.07

Table A5.2 Positional Parameters and β(eq) for [Pd(CH_3CN)(TOMB-1)] [CF_3SO_3], (23).

atom	x	y	z	β(eq)
Pd1	0.4927(1)	0.03704(6)	0.11411(8)	2.49(4)
S1	0.7544(4)	0.0204(2)	0.1511(3)	3.5(2)
S2	0.2272(4)	0.0396(3)	0.1336(3)	3.7(2)
S3	-0.0035(5)	-0.3592(2)	-0.0505(3)	4.1(2)
F1	0.115(1)	-0.2252(7)	-0.096(1)	12(1)
F2	-0.079(2)	-0.2178(8)	-0.015(1)	15(1)
F3	-0.099(2)	-0.2454(7)	-0.163(1)	14(1)
O1	0.492(1)	0.0657(5)	0.3178(6)	3.4(5)
O2	-0.152(1)	-0.3827(8)	-0.040(1)	11(1)
O3	0.061(2)	-0.3922(7)	-0.134(1)	12(1)
O4	0.093(2)	-0.3582(8)	0.033(1)	14(1)
N1	0.507(1)	0.1596(6)	0.0916(8)	3.3(6)
C1	0.475(1)	-0.0760(7)	0.1405(8)	2.3(6)
C2	0.328(1)	-0.1117(7)	0.146(1)	2.8(3)
C3	0.320(2)	-0.1936(9)	0.161(1)	4.1(3)
C4	0.450(2)	-0.2368(8)	0.173(1)	3.4(3)
C5	0.596(2)	-0.2035(8)	0.171(1)	4.0(3)
C6	0.609(1)	-0.1228(7)	0.155(1)	2.7(3)
C7	0.765(2)	-0.0850(9)	0.153(1)	3.8(3)
C8	0.762(1)	0.046(1)	0.288(1)	4.1(3)
C9	0.624(1)	0.0233(8)	0.348(1)	3.6(3)
C10	0.343(1)	0.0315(9)	0.339(1)	3.7(3)
C11	0.221(2)	0.0657(9)	0.270(1)	4.4(3)
C12	0.184(2)	-0.0636(8)	0.133(1)	4.0(3)
C13	0.512(2)	0.2249(8)	0.081(1)	3.3(3)
C14	0.520(2)	0.3091(8)	0.067(1)	3.9(3)
C15	-0.016(2)	-0.256(1)	-0.083(2)	5(1)

Table A5.3 Intramolecular Distances (Å) Involving the Nonhydrogen Atoms for $[Pd(CH_3CN)(TOMB\text{-}1)][CF_3SO_3]$, (23).

atom-atom	distance	atom-atom	distance
Pd1-S1	2.315(4)	O1-C9	1.40(1)
Pd1-S2	2.318(4)	O1-C10	1.45(1)
Pd1-N1	2.13(1)	N1-C13	1.13(1)
Pd1-C1	1.98(1)	C1-C2	1.42(2)
S1-C7	1.81(1)	C1-C6	1.41(2)
S1-C8	1.85(1)	C2-C3	1.42(2)
S2-C11	1.84(1)	C2-C12	1.50(2)
S2-C12	1.81(1)	C3-C4	1.35(2)
S3-O2	1.36(1)	C4-C5	1.38(2)
S3-O3	1.37(1)	C5-C6	1.41(2)
S3-O4	1.36(1)	C6-C7	1.50(2)
S3-C15	1.82(2)	C8-C9	1.50(2)
F1-C15	1.27(2)	C10-C11	1.49(2)
F2-C15	1.25(2)	C13-C14	1.46(2)
F3-C15	1.26(2)	Pd1...O1	2.714(8)

Table A5.4 Intramolecular Bond Angles Involving the Nonhydrogen Atoms for [Pd(CH_3CN)(TOMB-1)][CF_3SO_3], (23).

linkage	angle (°)	linkage	angle (°)
S1-Pd1-S2	160.6(1)	C1-C2-C3	119(1)
S1-Pd1-N1	95.3(3)	C1-C2-C12	120(1)
S1-Pd1-C1	85.4(4)	C3-C2-C12	121(1)
S2-Pd1-N1	93.3(3)	C2-C3-C4	121(1)
S2-Pd1-C1	85.4(4)	C3-C4-C5	122(1)
N1Pd1-C1	177.6(5)	C4-C5-C6	119(1)
Pd1-S1-C7	100.1(5)	C1-C6-C5	121(1)
Pd1-S1-C8	100.3(4)	C1-C6-C7	119(1)
C7-S1-C8	103.0(7)	C5-C6-C7	121(1)
Pd1-S2-C11	100.0(5)	S1-C7-C6	113(1)
Pd1-S2-C12	100.8(5)	S1-C8-C9	116.2(9)
C11-S2-C12	103.3(7)	O1-C9-C8	112(1)
O2-S3-O3	112(1)	O1-C10-C11	110(1)
O2-S3-O4	119(1)	S2-C11-C10	117(1)
O2-S3-C15	105.4(9)	S2-C12-C2	111(1)
O3-S3-O4	113(1)	N1-C13-C14	180(2)
O3-S3-C15	103.8(9)	S3-C15-F1	113(1)
O4-S3-C15	102.0(9)	S3-C15-F2	112(2)
C9-O1-C10	117(1)	S3-C15-F3	111(1)
Pd1-N1-C13	179(1)	F1-C15-F2	107(2)
Pd1-C1-C2	120.4(9)	F1-C15-F3	108(2)
Pd1-C1-C6	121.0(9)	F2-C15-F3	105(2)
C2-C1-C6	119(1)		

Table A6.1 Summary of Crystal Data, Intensity Collection and Structure Refinement for [Pd(TOMB-3)Cl], (24).

formula	$C_{16}H_{23}O_3S_2ClPd$
fw	469.33 $gmol^{-1}$
colour/form	yellow block
a, Å	10.276(5)
b, Å	10.343(5)
c, Å	8.875(3)
α, deg	94.04(4)
β, deg	94.34(4)
γ, deg	100.22(4)
V (Å^3)	922.3(7)
crystal system	triclinic
space group	$P\bar{1}$ (#2)
ρ (gmL^{-1})	1.690
Z	2
μ, cm^{-1}	13.88
diffractometer	Rigaku AFC6S
λ, (Å)	0.71069
T (°C)	23
scan type	ω–2θ
scan width (deg)	1.05 +0.30 tan
2θ range (deg)	4.5-50
# data collected	3261
# unique data with $F_o^2>3\sigma(F_o^2)$	2647
# variables	208
data/var ratio	12.7
largest +/- peaks (e/Å^3)	1.489/-1.598
max shift/error	0.00076
goodness of fit	2.93
$R(F_o)$, %	5.15
$R_w(F_o)$, %	4.10

Table A6.2 Positional parameters and β(eq) for [Pd(TOMB-3)Cl], (24).

atom	x	y	z	β(eq)
Pd1	0.68850(6)	0.61461(6)	0.16299(6)	2.91(2)
Cl1	0.8072(2)	0.5788(2)	-0.0550(2)	4.6(1)
S1	0.5221(2)	0.6910(2)	0.0317(2)	3.15(8)
S2	0.8307(2)	0.5312(2)	0.3238(2)	3.55(8)
O2	0.9786(5)	1.0604(5)	0.2541(6)	4.4(2)
O3	0.7133(5)	1.0649(5)	0.0669(6)	4.2(2)
O4	1.1322(6)	0.8353(6)	0.3175(8)	6.5(3)
C1	0.5991(7)	0.6574(6)	0.3462(7)	2.6(3)
C2	0.6526(7)	0.6380(6)	0.4912(7)	3.0(3)
C3	0.5895(8)	0.6636(7)	0.6178(7)	3.5(3)
C4	0.4737(8)	0.7113(8)	0.6033(8)	4.5(4)
C5	0.4188(8)	0.7353(8)	0.4632(8)	4.2(4)
C6	0.4818(7)	0.7080(7)	0.3337(7)	3.0(3)
C7	0.4173(7)	0.7225(7)	0.1788(8)	3.9(3)
C8	0.5974(7)	0.8544(7)	-0.0094(8)	3.5(3)
C9	0.6830(7)	0.9396(7)	0.1175(8)	3.8(3)
C10	0.7966(9)	1.1622(7)	0.169(1)	4.7(4)
C11	0.939(1)	1.1618(8)	0.171(1)	5.0(4)
C12	1.1136(9)	1.0575(8)	0.253(1)	5.2(4)
C13	1.1610(8)	0.9706(9)	0.363(1)	5.7(4)
C14	0.9994(8)	0.7745(8)	0.314(1)	4.8(4)
C15	0.9955(8)	0.6289(8)	0.3174(8)	4.3(4)
C16	0.7819(8)	0.5869(8)	0.5068(8)	4.0(3)

Table A6.3 Interatomic distances (Å) Involving the Nonhydrogen atoms for [Pd(TOMB-3)Cl], (24).

atom-atom	distance	atom-atom	distance
Pd1-Cl1	2.405(2)	O3-C14	1.385(9)
Pd1-S1	2.284(2)	C1-C2	1.402(8)
Pd1-S2	2.285(2)	C1-C6	1.399(9)
Pd1-C1	1.982(7)	C2-C3	1.380(9)
S1-C7	1.794(8)	C2-C16	1.516(9)
S1-C8	1.796(7)	C3-C4	1.36(1)
S2-C15	1.816(8)	C4-C5	1.385(9)
S2-C16	1.814(7)	C5-C6	1.407(9)
O1-C9	1.405(8)	C6-C7	1.508(8)
O1-C10	1.410(8)	C8-C9	1.503(9)
O2-C11	1.416(9)	C10-C11	1.48(1)
O2-C12	1.406(9)	C12-C13	1.47(1)
O3-C13	1.415(9)	C14-C15	1.51(1)

Table A6.4 Intramolecular Bond Angles Involving the Nonhydrogen Atoms for [Pd(TOMB-3)Cl], (24).

linkage	angle	linkage	angle
Cl1-Pd1-S1	94.96(7)	C1-C2-C16	118.9(6)
Cl1-Pd1-S2	93.91(8)	C3-C2-C16	119.9(6)
Cl1-Pd1-C1	175.7(2)	C2C3C4	119.6(7)
S1-Pd1-S2	170.54(8)	C3-C4-C5	121.4(7)
S1-Pd1-C1	85.4(2)	C4-C5-C6	119.2(7)
S2-Pd1-C1	86.0(2)	C1-C6-C5	120.1(6)
Pd1-S1-C7	102.0(2)	C1-C6-C7	119.7(6)
Pd1-S1-C8	104.3(2)	C5-C6-C7	120.0(7)
C7-S1-C8	103.1(3)	S1-C7-C6	111.4(5)
Pd1-S2-C15	107.3(2)	S1-C8-C9	116.8(5)
Pd1-S2-C16	100.8(2)	O3-C9-C8	106.3(6)
C15-S2-C16	103.4(4)	O3-C10-C11	115.8(7)
C11-O2-C12	112.9(7)	O2-C11-C10	112.7(7)
C9-O3-C10	116.1(6)	O2-C12-C13	113.5(8)
C13-O4-C14	116.1(7)	O4-C13-C12	115.8(7)
Pd1-C1-C2	120.8(5)	O4-C14-C15	107.5(7)
Pd1-C1-C6	120.8(5)	S2-C15-C14	114.7(5)
C2-C1-C6	118.4(6)	S2-C16-C2	112.0(5)
C1-C2-C3	121.2(7)		

Table A7.1 Summary of Crystal Data, Intensity Collection and Structure Refinement for $[Pd(CH_3CN)(TOMB\text{-}3)][BF_4]$, (25).

formula	$C_{18}H_{20}BNO_3F_4S_2Pd$
fw	561.73 $gmol^{-1}$
colour/form	yellow block
a, Å	10.838(5)
b, Å	11.295(4)
c, Å	10.219(6)
α, deg	98.31(4)
β, deg	108.86(4)
γ, deg	102.78(4)
V (Å^3)	1122(2)
crystal system	triclinic
space group	$P\bar{1}$ (#2)
ρ (gmL^{-1})	1.66
Z	2
μ, cm^{-1}	10.66
diffractometer	Rigaku AFC6S
λ, (Å)	0.71069
T (°C)	23
scan type	ω–2θ
scan width (deg)	1.05 +0.30 tan
2θ range (deg)	4.5-50
# data collected	3957
# unique data with $F_o^2>3\sigma(F_o^2)$	2226
# variables	267
data/var ratio	8.3
largest +/- peaks (e/Å^3)	0.612/-0.404
max shift/error	0.00044
goodness of fit	1.45
$R(F_o)$, %	4.59
$R_w(F_o)$, %	3.67

Table A7.2 Positional parameters and β(eq) for [Pd(CH_3CN)(TOMB-3)][BF_4], (25).

atom	x	y	z	β(eq)
Pd1	0.54145(6)	0.87465(6)	0.42239(7)	3.85(2)
S1	0.5122(2)	0.9565(2)	0.2240(2)	4.54(7)
S2	0.6004(2)	0.8180(2)	0.6364(2)	4.36(8)
F1	1.0259(8)	0.7124(6)	0.7734(7)	12.1(4)
F2	1.126(1)	0.8933(7)	0.9163(8)	14.1(4)
F3	1.1737(8)	0.7336(9)	0.9775(8)	14.9(5)
F4	0.986(1)	0.759(1)	0.961(1)	17.8(6)
O1	0.6113(6)	0.7006(5)	-0.0045(6)	5.9(2)
O2	0.7389(6)	0.5627(5)	0.2162(6)	5.4(2)
O3	0.7065(6)	0.5201(5)	0.4976(6)	5.1(2)
N1	0.3467(6)	0.7420(6)	0.3344(7)	4.9(3)
C1	0.7272(7)	0.9927(6)	0.5005(8)	3.6(2)
C2	0.8174(7)	0.9960(6)	0.6363(8)	3.8(3)
C3	0.9495(8)	1.0730(8)	0.6869(9)	5.2(3)
C4	0.9921(8)	1.1483(8)	0.607(1)	6.1(4)
C5	0.9048(9)	1.1465(8)	0.473(1)	5.2(3)
C6	0.7727(7)	1.0690(6)	0.4196(8)	3.6(3)
C7	0.6747(8)	1.0733(7)	0.2795(9)	5.0(3)
C8	0.5147(9)	0.8420(8)	0.081(1)	5.8(3)
C9	0.6207(9)	0.7777(8)	0.123(1)	5.8(4)
C10	0.722(1)	0.648(1)	0.014(1)	6.2(4)
C11	0.708(1)	0.533(1)	0.068(1)	5.9(4)
C12	0.734(1)	0.4534(8)	0.271(1)	6.1(4)
C13	0.7938(9)	0.4886(8)	0.430(1)	5.5(4)
C14	0.6974(8)	0.6444(7)	0.5037(8)	4.4(3)
C15	0.6255(8)	0.6655(7)	0.6033(8)	4.5(3)
C16	0.7720(8)	0.9212(7)	0.7304(8)	4.8(3)
C17	0.2432(8)	0.6762(7)	0.2855(8)	4.5(3)
C18	0.1055(8)	0.5886(8)	0.224(1)	6.2(4)
B1	1.080(1)	0.773(1)	0.909(1)	4.7(4)

Table A7.3 Intramolecular Distances (Å) Involving the Nonhydrogen Atoms for $[Pd(CH_3CN)(TOMB\text{-}3)][BF_4]$, (25).

atom-atom	distance	atom-atom	distance
Pd1-S1	2.307(3)	O3-C13	1.42(1)
Pd1-S2	2.299(3)	O3-C14	1.42(1)
Pd1-N1	2.120(6)	N1-C17	1.106(9)
Pd1-C1	1.984(6)	C1-C2	1.41(1)
S1-C7	1.810(8)	C1-C6	1.40(1)
S1-C8	1.82(1)	C2-C3	1.38(1)
S2-C15	1.804(9)	C2-C16	1.50(1)
S2-C16	1.818(7)	C3-C4	1.37(1)
F1-B1	1.33(1)	C4-C5	1.38(1)
F2-B1	1.32(1)	C5-C6	1.38(1)
F3-B1	1.25(1)	C6-C7	1.50(1)
F4-B1	1.28(2)	C8-C9	1.47(1)
O1-C9	1.42(1)	C10-C11	1.47(2)
O1-C10	1.43(1)	C12-C13	1.49(1)
O2-C11	1.41(1)	C14-C15	1.49(1)
O2-C12	1.42(1)	C17-C18	1.47(1)

Table A7.4 Intramolecular Bond Angles Involving the Nonhydrogen Atoms for $[Pd(CH_3CN)(TOMB\text{-}3)][BF_4]$, (25).

linkage	angle (°)	linkage	angle (°)
S1-Pd1-S2	171.27(7)	C3-C4-C5	120.6(7)
S1-Pd1-N1	94.2(2)	C4-C5-C6	120.1(9)
S1-Pd1-C1	85.7(2)	C1-C6-C5	120.1(7)
S2-Pd1-N1	94.4(2)	C1-C6-C7	119.4(6)
S2-Pd1-C1	85.8(2)	C5-C6-C7	120.3(8)
N1-Pd1-C1	177.2(3)	S1-C7-C6	112.8(6)
Pd1-S1-C7	100.6(3)	S1-C8-C9	115.0(6)
Pd1-S1-C8	108.8(3)	O1-C9-C8	105.8(7)
C7-S1-C8	103.7(4)	O1-C10-C11	115.2(9)
Pd1-S2-C15	106.9(3)	O2-C11-C10	110.9(7)
Pd1-S2-C16	101.7(3)	O2-C12-C13	110.1(7)
C15-S2-C16	103.6(4)	O3-C13-C12	115.5(8)
C9-O1-C10	113.2(6)	O3-C14-C15	105.3(7)
C11-O2-C12	111.2(7)	S2-C15-C14	116.2(6)
C13-O3-C14	114.5(7)	S2-C16-C2	111.0(5)
Pd1-N1-C17	177.1(7)	N1-C17-C18	179(1)
Pd1-C1-C2	120.0(6)	F1-B1-F2	108(1)
Pd1-C1-C6	121.0(5)	F1-B1-F3	111(1)
C2-C1-C6	119.0(6)	F1-B1-F4	108.9(8)
C1-C2-C3	119.8(8)	F2-B1-F3	110.3(9)
C1-C2-C16	121.2(6)	F2-B1-F4	108(1)
C3-C2-C16	118.9(7)	F3-B1-F4	110(1)
C2-C3-C4	120.4(7)		

Table A8.1 Summary of Crystal Data, Intensity Collection and Structure Refinement for [Pd(CH_3CN)(TOMB-P4)][BF_4], (27).

formula	$C_{30}H_{34}BNO_4F_4S_2Pd$
fw	729.93 $gmol^{-1}$
colour/form	yellow block
a, Å	12.076(2)
b, Å	12.314(2)
c, Å	11.730(2)
α, deg	109.59(1)
β, deg	106.18(1)
γ, deg	75.73(1)
V ($Å^3$)	1555.3(4)
crystal system	triclinic
space group	$P\bar{1}$ (#2)
ρ (gmL^{-1})	1.56
Z	2
μ, cm^{-1}	7.91
diffractometer	Rigaku AFC6S
λ, (Å)	0.71069
T (°C)	23
scan type	ω–2θ
scan width (deg)	1.05 +0.30 tan
2θ range (deg)	4.5-50
# data collected	5480
# unique data with $F_o^2>3\sigma(F_o^2)$	3818
# variables	388
data/var ratio	9.8
max shift/error	0.01
goodness of fit	1.98
$R(F_o)$, %	4.18
$R_w(F_o)$, %	4.23

Table A8.2 Positional Parameters and β(eq) for $[Pd(CH_3CN)(TOMB\text{-}P4)]^+$ $[BF_4]$, (27).

atom	x	y	z	β(eq)
Pd1	0.73065(4)	0.38840(4)	0.43701(4)	2.53(2)
S1	0.7571(1)	0.2235(1)	0.2723(1)	2.97(7)
S2	0.7126(1)	0.5729(1)	0.5752(1)	3.19(7)
O1	0.7711(4)	-0.0625(3)	0.6398(4)	4.0(2)
O2	0.5729(4)	-0.0267(4)	0.7326(4)	4.4(2)
O3	0.3918(4)	0.1525(4)	0.8226(4)	4.3(2)
O4	0.5178(3)	0.3337(4)	0.8945(4)	4.1(2)
N1	0.6308(4)	0.3099(4)	0.5025(4)	3.1(2)
C1	0.8166(5)	0.4575(5)	0.3632(5)	2.7(2)
C2	0.8498(5)	0.5679(5)	0.4260(6)	3.2(3)
C3	0.8984(5)	0.6202(5)	0.3678(6)	3.9(3)
C4	0.9164(5)	0.5658(6)	0.2510(7)	4.3(3)
C5	0.8872(5)	0.4561(6)	0.1884(6)	3.7(3)
C6	0.8368(5)	0.4013(5)	0.2439(5)	3.1(3)
C7	0.7987(6)	0.2844(5)	0.1721(6)	3.9(3)
C8	0.8952(5)	0.1374(5)	0.3323(5)	3.2(3)
C9	0.8702(5)	0.0846(5)	0.4188(5)	2.7(2)
C10	0.8894(5)	0.1349(5)	0.5455(6)	3.1(3)
C11	0.8601(5)	0.0881(5)	0.6237(5)	3.2(3)
C12	0.8083(5)	-0.0108(5)	0.5727(5)	2.8(2)
C13	0.7878(5)	-0.0625(5)	0.4460(6)	3.4(3)
C14	0.8199(5)	-0.0170(5)	0.3693(5)	3.1(3)
C15	0.7678(5)	-0.0012(6)	0.7671(6)	4.0(3)
C16	0.6860(6)	-0.0488(6)	0.8047(6)	4.6(3)
C17	0.4834(6)	-0.0449(6)	0.7780(7)	4.8(4)
C18	0.4412(6)	0.0598(6)	0.8750(6)	4.7(4)
C19	0.3619(6)	0.2606(6)	0.9098(6)	4.6(3)
C20	0.3930(5)	0.3542(5)	0.8739(6)	3.9(3)
C21	0.5696(5)	0.3955(5)	0.8519(5)	3.0(3)
C22	0.5105(5)	0.4880(5)	0.8025(6)	3.6(3)
C23	0.5737(5)	0.5442(5)	0.7646(5)	3.6(3)
C24	0.6929(5)	0.5128(5)	0.7757(5)	3.2(3)

C25	0.7509(5)	0.4190(5)	0.8240(5)	3.3(3)
C26	0.6889(5)	0.3614(5)	0.8618(5)	3.3(3)
C27	0.7621(6)	0.5753(6)	0.7384(6)	4.2(3)
C28	0.8340(5)	0.6250(5)	0.5567(6)	3.7(3)
C29	0.5806(5)	0.2581(5)	0.5265(5)	3.1(3)
C30	0.5141(6)	0.1901(5)	0.5563(6)	4.1(3)
F1	0.0804(5)	0.2168(4)	0.1019(5)	10.2(3)
F2	-0.0522(5)	0.1890(6)	-0.0606(5)	11.8(4)
F3	0.1260(6)	0.0940(6)	-0.0695(5)	14.1(5)
F4	0.0713(8)	0.2743(8)	-0.056(1)	23.1(9)
B1	0.062(1)	0.189(1)	-0.023(1)	5.9(5)

Table A8.3 Intramolecular Distances (Å) Involving the Nonhydrogen Atoms for [Pd(CH_3CN)(TOMB-P4)][BF_4], (27).

atom-atom	distance	atom-atom	distance
Pd1-S1	2.313(2)	C6-C7	1.513(8)
Pd1-S2	2.307(2)	C8-C9	1.501(7)
Pd1-N1	2.137(5)	C9-C10	1.381(8)
Pd1-C1	1.995(5)	C9-C14	1.401(7)
S1-C7	1.818(6)	C10-C11	1.391(7)
S1-C8	1.837(6)	C11-C12	1.382(7)
S2-C27	1.831(6)	C12-C13	1.383(8)
S2-C28	1.827(6)	C13-C14	1.383(7)
O1-C12	1.379(6)	C15-C16	1.489(8)
O1-C15	1.437(7)	C17-C18	1.494(9)
O2-C16	1.408(7)	C19-C20	1.508(8)
O2-C17	1.421(7)	C21-C22	1.398(8)
O3-C18	1.402(7)	C21-C26	1.380(8)
O3-C19	1.416(7)	C22-C23	1.383(8)
O4-C20	1.430(7)	C23-C24	1.376(8)
O4-C21	1.373(6)	C24-C25	1.402(8)
N1-C29	1.122(6)	C24-C27	1.493(8)
C1-C2	1.409(7)	C25-C26	1.385(8)
C1-C6	1.398(7)	C29-C30	1.468(8)

C2-C3	1.390(7)	F1-B1	1.35(1)
C2-C28	1.502(8)	F2-B1	1.33(1)
C3-C4	1.361(9)	F3-B1	1.28(1)
C4-C5	1.383(9)	F4-B1	1.27(1)
C5-C6	1.403(7)		

Table A8.4 Intramolecular Bond Angles Involving the Nonhydrogen Atoms for [Pd(CH_3CN)(TOMB-P4)][BF_4], (27).

linkage	angle (°)	linkage (°)	angle
S1-Pd1-S2	167.70(5)	C1-C6-C5	119.9(6)
S1-Pd1-N1	92.3(1)	C1-C6-C7	120.1(5)
S1-Pd1-C1	84.8(2)	C5-C6-C7	119.9(6)
S2-Pd1-N1	99.1(1)	S1-C7-C6	110.7(4)
S2-Pd1-C1	83.6(2)	S1-C8-C9	107.1(4)
N1-Pd1-C1	175.7(2)	C8-C9-C10	122.9(5)
Pd1-S1-C7	100.6(2)	C8-C9-C14	119.0(5)
Pd1-S1-C8	104.1(2)	C10-C9-C14	118.1(5)
C7-S1-C8	103.1(3)	C9-C10-C11	122.1(5)
Pd1-S2-C27	114.4(2)	C10-C11-C12	118.9(5)
Pd1-S2-C28	99.7(2)	O1-C12-C11	124.3(5)
C27-S2-C28	99.8(3)	O1-C12-C13	115.6(5)
C12-O1-C15	118.7(5)	C11-C12-C13	120.0(5)
C16-O2-C17	113.7(5)	C12-C13-C14	120.6(5)
C18-O3-C19	113.8(5)	C9-C14-C13	120.2(5)
C20-O4-C21	118.5(5)	O1-C15-C16	108.4(5)
Pd1-N1-C29	172.4(5)	O2-C16-C15	108.9(5)
Pd1-C1-C2	120.7(4)	O2-C17-C18	112.9(6)
Pd1-C1-C6	120.4(4)	O3-C18-C17	108.9(5)
C2-C1-C6	118.7(5)	O3-C19-C20	107.3(5)
C1-C2-C3	120.0(6)	O4-C20-C19	106.2(5)
C1-C2-C28	118.5(5)	O4-C21-C22	124.7(5)
C3-C2-C28	121.5(6)	O4-C21-C26	115.3(5)
C2-C3-C4	121.1(6)	C22-C21-C26	120.1(6)
C3-C4-C5	120.1(6)	C21-C22-C23	118.8(6)

C4-C5-C6	120.2(6)	C22-C23-C24	122.0(6)
C23-C24-C25	118.6(5)	N1-C29-C30	179.3(7)
C23-C24-C27	122.3(6)	F1-B1-F2	103.6(8)
C25-C24-C27	119.2(6)	F1-B1-F3	113.0(9)
C24-C25-C26	120.2(5)	F1-B1-F4	111(1)
C21-C26-C25	120.4(5)	F2-B1-F3	115(1)
S2-C27-C24	112.8(4)	F2-B1-F4	100.8(9)
S2-C28-C2	108.1(4)	F3-B1-F4	113(1)

Table A9.1 Summary of Crystal Data, Intensity Collection and Structure Refinement for [Pd(OAP)(TOMB-1)][BF_4], (31).

formula	$C_{17}H_{21}ON_2BF_4S_2Pd$
fw	526.69 $gmol^{-1}$
colour/form	orange block
a, Å	10.056(2)
b, Å	18.889(2)
c, Å	11.294(7)
α, deg	90
β, deg	112.32(4)
γ, deg	90
V (Å^3)	1976(2)
crystal system	monoclinic
space group	$P2_1/c$ (#14)
ρ (gmL^{-1})	1.770
Z	4
μ, cm^{-1}	11.75
diffractometer	Rigaku AFC6S
λ, (Å)	0.71069
T (°C)	23
scan type	ω–2θ
scan width (deg)	1.05 +0.30 tan
2θ range (deg)	4.5-50
# data collected	3915
# unique data with $F_c^2>3\sigma(F_o^2)$	2326
# variables	254
data/var ratio	9.2
max shift/error	0.001
goodness of fit	2.54
$R(F_o)$, %	6.95
$R_w(F_o)$, %	6.14

Table A9.2 Positional Parameters and β(eq) for [Pd(OAP)(TOMB-1)][BF_4], (31).

atom	x	y	z	β(eq)
Pd1	0.2441(1)	0.09334(5)	0.2570(1)	2.00(3)
S1	0.3920(3)	0.0933(2)	0.4700(3)	3.2(1)
S2	0.0392(3)	0.1003(2)	0.0726(3)	2.7(1)
F1	0.172(1)	0.0920(5)	0.789(1)	6.5(5)
F2	0.241(1)	0.1919(5)	0.729(1)	7.9(6)
F3	0.040(1)	0.1911(5)	0.772(1)	6.5(5)
F4	0.255(1)	0.1813(7)	0.9287(9)	8.3(6)
O1	0.047(1)	0.0502(5)	0.3566(7)	3.0(4)
N1	0.311(1)	-0.0077(6)	0.213(1)	2.7(4)
N2	0.177(1)	-0.0765(6)	0.291(1)	4.5(6)
C1	0.199(1)	0.1933(6)	0.287(1)	2.1(5)
C2	0.089(1)	0.2301(7)	0.193(1)	2.6(5)
C3	0.054(1)	0.2991(7)	0.215(1)	3.5(6)
C4	0.132(2)	0.3317(7)	0.330(1)	3.6(6)
C5	0.241(2)	0.2961(7)	0.427(1)	3.3(6)
C6	0.276(1)	0.2260(7)	0.404(1)	2.4(5)
C7	0.393(1)	0.1872(8)	0.508(1)	3.0(5)
C8	0.268(2)	0.0573(8)	0.540(1)	4.0(6)
C9	0.111(1)	0.0798(8)	0.480(1)	3.5(6)
C10	-0.077(1)	0.0845(8)	0.266(1)	3.4(6)
C11	-0.093(1)	0.0650(7)	0.132(1)	3.3(5)
C12	0.005(2)	0.1945(7)	0.067(1)	3.4(6)
C13	0.266(2)	-0.0728(6)	0.233(1)	3.1(6)
C14	0.323(2)	-0.1358(8)	0.201(1)	4.3(7)
C15	0.426(2)	-0.127(1)	0.149(1)	4.8(8)
C16	0.473(2)	-0.064(1)	0.126(1)	4.8(8)
C17	0.414(2)	-0.0058(8)	0.162(1)	3.6(6)
B1	0.179(2)	0.164(1)	0.805(2)	4.1(8)

Table A9.3 Intramolecular Distances Involving the Nonhydrogen Atoms for [Pd(OAP)(TOMB-1)][BF_4], (31).

atom-atom	distance	atom-atom	distance
Pd1-S1	2.298(4)	N2-C13	1.29(2)
Pd1-S2	2.312(4)	C1-C2	1.39(2)
Pd1-N1	2.14(1)	C1-C6	1.39(2)
Pd1-C1	1.99(1)	C2-C3	1.39(2)
S1-C7	1.82(1)	C2-C12	1.51(2)
S1-C8	1.84(1)	C3-C4	1.38(2)
S2-C11	1.83(1)	C4-C5	1.39(2)
S2-C12	1.80(1)	C5-C6	1.41(2)
F1-B1	1.37(2)	C6-C7	1.50(2)
F2-B1	1.34(2)	C8-C9	1.53(2)
F3-B1	1.39(2)	C10-C11	1.50(2)
F4-B1	1.35(2)	C13-C14	1.42(2)
O1-C9	1.41(1)	C14-C15	1.37(2)
O1-C10	1.43(1)	C15-C16	1.33(2)
N1-C13	1.35(1)	C16-C17	1.37(2)
N1-C17	1.36(2)		

Table A9.4 Intramolecular Bond Angles Involving the Nonhydrogen Atoms for [Pd(OAP)(TOMB-1)][BF_4], (31).

linkage	angle	linkage	angle
S1-Pd1-S2	160.8(1)	C4-C5-C6	119(1)
S1-Pd1-N1	96.1(3)	C1-C6-C5	120(1)
S1-Pd1-C1	85.5(4)	C1-C6-C7	121(1)
S2-Pd1-N1	95.4(3)	C5-C6-C7	119(1)
S2-Pd1-C1	85.3(4)	S1-C7-C6	110.8(9)
N1-Pd1-C1	172.0(4)	S1-C8-C9	117.6(9)
Pd1-S1-C7	100.9(4)	O1-C9-C8	110(1)
Pd1-S1-C8	100.3(4)	O1-C10-C11	110(1)
C7-S1-C8	101.7(7)	S2-C11-C10	117.7(9)
Pd1-S2-C11	99.8(4)	S2-C12-C2	112.0(9)
Pd1-S2-C12	100.3(4)	N1-C13-N2	118(1)
C11-S2-C12	102.4(7)	N1-C13-C14	121(1)
C9-O1-C10	118(1)	N2-C13-C14	120(1)
Pd1-N1-C13	127.6(9)	C13-C14-C15	116(1)
Pd1-N1-C17	115.6(9)	C14-C15-C16	125(2)
C13-N1-C17	117(1)	C15-C16-C17	115(2)
Pd1-C1-C21	20.5(9)	N1-C17-C16	126(1)
Pd1-C1-C6	119.9(9)	F1-B1-F2	108(1)
C2-C1-C6	120(1)	F1-B1-F3	109(1)
C1-C2-C3	121(1)	F1-B1-F4	111(2)
C1-C2-C12	120(1)	F2-B1-F3	110(2)
C3-C2-C12	120(1)	F2-B1-F4	111(1)
C2-C3-C4	119(1)	F3-B1-F4	108(1)
C3-C4-C5	122(1)		

Table A10.1 Summary of Crystal Data, Intensity Collection and Structure Refinement for [Pd(PYR)(TOMB-3)][BF_4], (32).

formula	$C_{22}H_{29}O_3NBF_4S_2Cl_3Pd$
fw	719.16 $gmol^{-1}$
colour/form	yellow block
a, Å	11.982(3)
b, Å	12.858(3)
c, Å	10.048(2)
α, deg	103.59(2)
β, deg	99.63(2)
γ, deg	77.56(2)
V ($Å^3$)	1458.2(6)
crystal system	triclinic
space group	$P\bar{1}$ (#2)
ρ (gmL^{-1})	1.64
Z	2
μ, cm^{-1}	11.05
diffractometer	Rigaku AFC6S
λ, (Å)	0.71069
T (°C)	23
scan type	ω–2θ
scan width (deg)	1.05 +0.30 tan
2θ range (deg)	4.5-50
# data collected	3304
# unique data with $F_o^2>3\sigma(F_o^2)$	2079
# variables	220
data/var ratio	9.4
max shift/error	0.001
goodness of fit	1.87
$R(F_o)$, %	5.14
$R_w(F_o)$, %	4.62

Table A10.2 Positional Parameters and β(eq) for [Pd(PYR)(TOMB-3)][BF_4], (32).

atom	x	y	z	β(eq)
Pd1	0.13430(8)	-0.09833(8)	-0.1230(1)	2.90(5)
Cl1	0.7690(4)	0.6349(4)	0.8445(6)	12.1(4)
Cl2	0.9292(4)	0.4409(4)	0.8302(5)	10.9(3)
Cl3	0.7048(5)	0.4523(4)	0.8948(6)	12.4(4)
S1	0.1873(3)	0.0690(2)	-0.0500(3)	3.8(2)
S2	0.0321(3)	-0.2368(3)	-0.1791(3)	3.8(2)
F1	0.1200(8)	0.3556(8)	0.614(1)	13.6(8)
F2	0.232(1)	0.369(1)	0.798(1)	14.3(9)
F3	0.288(1)	0.3905(9)	0.625(2)	16(1)
F4	0.2769(7)	0.2298(6)	0.6325(9)	7.6(5)
O1	0.4853(6)	-0.0214(7)	-0.2095(8)	5.1(5)
O2	0.4297(7)	-0.2225(7)	-0.4171(8)	4.9(5)
O3	0.2540(7)	-0.3280(6)	-0.3764(8)	4.9(5)
N1	0.2768(7)	-0.1768(7)	-0.000(1)	3.3(5)
C1	0.0115(9)	-0.0247(9)	-0.246(1)	2.9(2)
C2	-0.076(1)	-0.0780(9)	-0.322(1)	3.4(2)
C3	-0.156(1)	-0.030(1)	-0.419(1)	4.0(3)
C4	-0.147(1)	0.071(1)	-0.437(1)	4.4(3)
C5	-0.067(1)	0.127(1)	-0.358(1)	3.8(3)
C6	0.015(1)	0.0792(9)	-0.262(1)	3.3(2)
C7	0.102(1)	0.141(1)	-0.181(1)	4.3(3)
C8	0.333(1)	0.0600(9)	-0.078(1)	3.9(3)
C9	0.365(1)	-0.008(1)	-0.215(1)	4.1(3)
C10	0.529(1)	-0.073(1)	-0.335(1)	6.2(4)
C11	0.538(1)	-0.192(1)	-0.371(1)	6.6(4)
C12	0.435(1)	-0.335(1)	-0.449(1)	5.6(3)
C13	0.316(1)	-0.361(1)	-0.490(1)	5.5(3)
C14	0.147(1)	-0.363(1)	-0.408(1)	4.9(3)
C15	0.102(1)	-0.364(1)	-0.279(1)	4.4(3)
C16	-0.085(1)	-0.188(1)	-0.304(1)	4.4(3)
C17	0.282(1)	-0.152(1)	0.138(1)	3.8(3)
C18	0.377(1)	-0.195(1)	0.220(1)	5.1(3)

C19	0.465(1)	-0.260(1)	0.162(1)	5.4(3)
C20	0.462(1)	-0.287(1)	0.024(2)	6.4(4)
C21	0.365(1)	-0.244(1)	-0.058(1)	5.2(3)
C22	0.813(1)	0.521(1)	0.911(1)	5.6(8)
B1	0.227(2)	0.335(1)	0.665(2)	5(1)

Table A10.3 Intramolecular Distances (Å) Involving the Nonhydrogen Atoms for [Pd(PYR)(TOMB-3)][BF_4], (32).

atom-atom	distance	atom-atom	distance
Pd1-S1	2.294(3)	C2-C16	1.50(1)
Pd1-S2	2.285(3)	C3-C4	1.39(1)
Pd1-N1	2.144(8)	C4-C5	1.35(1)
Pd1-C1	1.98(1)	C5-C6	1.41(1)
Cl1-C22	1.69(1)	C6-C7	1.47(1)
Cl2-C22	1.74(1)	C8-C9	1.51(1)
Cl3-C22	1.69(1)	C10-C11	1.47(2)
S1-C7	1.83(1)	C12-C13	1.50(2)
S1-C8	1.79(1)	C14-C15	1.49(2)
S2-C15	1.82(1)	O3-C14	1.41(1)
S2-C16	1.83(1)	N1-C17	1.34(1)
F1-B1	1.30(2)	N1-C21	1.33(1)
F2-B1	1.30(2)	C1-C2	1.40(1)
F3-B1	1.28(2)	C1-C6	1.39(1)
F4-B1	1.35(2)	C2-C3	1.40(1)
O1-C9	1.40(1)	C17-C18	1.38(2)
O1-C10	1.41(1)	C18-C19	1.32(2)
O2-C11	1.41(1)	C19-C20	1.34(2)
O2-C12	1.39(1)	C20-C21	1.41(2)
O3-C13	1.40(1)		

Table A10.4 Intramolecular Bond Angles Involving the Nonhydrogen Atoms for [Pd(PYR)(TOMB-3)][BF_4], (32).

linkage	angle (°)	linkage	angle (°)
S1-Pd1-S2	163.7(1)	C3-C4-C5	122(1)
S1-Pd1-N1	93.7(3)	C4-C5-C6	120(1)
S1-Pd1-C1	84.7(3)	C1-C6-C5	120(1)
S2-Pd1-N1	96.8(3)	C1-C6-C7	121(1)
S2-Pd1-C1	85.6(3)	C5-C6-C7	119(1)
N1-Pd1-C1	175.4(4)	S1-C7-C6	110.9(8)
Pd1-S1-C7	100.8(4)	S1-C8-C9	115.3(9)
Pd1-S1-C8	110.3(4)	O1-C9-C8	107(1)
C7-S1-C8	104.1(5)	S2-C15-C14	119.0(9)
Pd1-S2-C15	115.8(4)	O2-C11-C10	112(1)
Pd1-S2-C16	101.9(4)	S2-C16-C2	110.8(8)
C15-S2-C16	102.7(5)	O2-C12-C13	111(1)
C9-O1-C10	114.8(9)	N1-C17-C18	121(1)
C11-O2-C12	114(1)	O3-C13-C12	110(1)
C13-O3-C14	111.3(9)	C17-C18-C19	119(1)
Pd1-N1-C17	119.9(7)	C18-C19-C20	121(1)
Pd1-N1-C21	120.9(8)	C19-C20-C21	119(1)
C17-N1-C21	119(1)	N1-C21-C20	120(1)
Pd1-C1-C2	120.6(8)	Cl1-C22-Cl2	108.6(8)
Pd1-C1-C6	120.2(8)	Cl1-C22-Cl3	111.4(8)
C2-C1-C6	119(1)	Cl2-C22-Cl3	111.4(8)
C1-C2-C3	121(1)	F1-B1-F2	107(2)
C1-C2-C16	121(1)	F1-B1-F3	112(2)
C3-C2-C16	119(1)	F1-B1-F4	114(2)
C2-C3-C4	118(1)	F2-B1-F3	106(2)
O3-C14-C15	111(1)	F2-B1-F4	110(2)
O1-C10-C11	115(1)	F3-B1-F4	108(2)

Table A11.1 Summary of Crystal Data, Intensity Collection and Structure Refinement for [Pd(PIC)(TOMB-3)][BF_4], (34).

formula	$C_{22}H_{31}O_3N_2BF_4S_2Pd$
fw	628.82 $gmol^{-1}$
colour/form	yellow chunk
a, Å	12.588(4)
b, Å	14.249(6)
c, Å	8.206(2)
α, deg	95.65(3)
β, deg	104.26(2)
γ, deg	66.07(3)
V (Å^3)	1304(2)
crystal system	triclinic
space group	$P\bar{1}$ (#2)
ρ (gmL^{-1})	1.60
Z	2
μ, cm^{-1}	9.09
diffractometer	Rigaku AFC6S
λ, (Å)	0.71069
T (°C)	23
scan type	ω–2θ
scan width (deg)	1.05 +0.30 tan
2θ range (deg)	4.5-50
# data collected	4929
# unique data with $F_o^2>3\sigma(F_o^2)$	3084
# variables	316
data/var ratio	9.8
max shift/error	0.001
goodness of fit	1.24
$R(F_o)$, %	4.38
$R_w(F_o)$, %	4.72

Table A11.2 Positional Parameters and β(eq) for [Pd(PIC)(TOMB-3)][BF_4], (34).

atom	x	y	z	β(eq)
Pd(1)	0.16963(5)	0.35027(4)	0.49493(7)	2.49(3)
S(1)	0.2733(2)	0.3829(2)	0.7511(2)	3.6(1)
S(2)	0.0426(1)	0.3789(1)	0.2325(2)	3.1(1)
F(1)	0.6705(5)	0.1643(4)	0.1040(8)	8.3(5)
F(2)	0.7695(8)	0.218(1)	-0.003(1)	16(1)
F(3)	0.7935(6)	0.2302(6)	0.2665(8)	12.3(6)
F(4)	0.6264(8)	0.3262(6)	0.107(1)	17.4(8)
O(1)	0.4560(4)	0.2169(4)	0.5422(6)	3.8(3)
O(2)	0.4694(4)	0.0676(4)	0.2722(7)	4.6(3)
O(3)	0.2022(4)	0.1506(4)	0.1436(7)	4.6(3)
N(1)	0.1195(5)	0.2446(4)	0.5930(7)	2.9(3)
N(2)	0.3078(5)	0.1164(4)	0.6204(9)	4.4(4)
C(1)	0.2234(6)	0.4427(5)	0.4030(8)	2.7(4)
C(2)	0.2051(6)	0.4522(5)	0.2285(8)	2.8(4)
C(3)	0.2475(7)	0.5136(6)	0.1671(9)	3.9(5)
C(4)	0.3089(8)	0.5646(6)	0.273(1)	4.8(6)
C(5)	0.3268(7)	0.5575(6)	0.445(1)	4.3(5)
C(6)	0.2846(6)	0.4969(5)	0.5124(9)	3.2(4)
C(7)	0.2958(7)	0.4926(6)	0.697(1)	4.2(5)
C(8)	0.4248(7)	0.2887(6)	0.810(1)	4.9(5)
C(9)	0.4996(7)	0.2663(6)	0.682(1)	4.5(5)
C(10)	0.5110(7)	0.2088(6)	0.407(1)	4.3(5)
C(11)	0.4453(7)	0.1725(6)	0.254(1)	4.4(5)
C(12)	0.3981(8)	0.0302(6)	0.140(1)	5.5(6)
C(13)	0.2809(8)	0.0456(6)	0.172(1)	4.8(5)
C(14)	0.0897(7)	0.1690(6)	0.170(1)	4.3(5)
C(15)	0.0050(7)	0.2758(6)	0.123(1)	4.2(5)
C(16)	0.1399(6)	0.3938(5)	0.1168(8)	3.3(4)
C(17)	0.1929(6)	0.1466(5)	0.6333(8)	3.2(4)
C(18)	0.1533(7)	0.0780(6)	0.684(1)	3.8(5)
C(19)	0.0374(7)	0.1093(6)	0.696(1)	4.0(5)
C(20)	-0.0385(7)	0.2124(7)	0.655(1)	4.6(6)

C(21)	0.0054(7)	0.2748(6)	0.607(1)	3.8(5)
C(22)	-0.009(1)	0.0361(8)	0.741(1)	6.5(8)
B(1)	0.715(1)	0.235(1)	0.126(2)	5.4(7)

Table A11.3 Intramolecular Distances (Å) Involving the Nonhydrogen Atoms for [Pd(PIC)(TOMB-3)][BF_4], (34).

atom-atom	distance	atom-atom	distance
Pd1-S1	2.299(2)	N1-C21	1.353(8)
Pd1-S2	2.304(2)	N2-C17	1.361(9)
Pd1-N1	2.139(5)	C1-C2	1.405(9)
Pd1-C1	1.983(6)	C1-C6	1.414(9)
S1-C7	1.812(8)	C2-C3	1.380(9)
S1-C8	1.809(8)	C2-C16	1.496(9)
S2-C15	1.814(8)	C3-C4	1.37(1)
S2-C16	1.809(7)	C4-C5	1.37(1)
F1-B1	1.32(1)	C5-C6	1.40(1)
F2-B1	1.35(1)	C6-C7	1.49(1)
F3-B1	1.31(1)	C8-C9	1.50(1)
F4-B1	1.32(1)	C10-C11	1.49(1)
O1-C9	1.400(9)	C12-C13	1.49(1)
O1-C10	1.421(9)	C14-C15	1.48(1)
O2-C11	1.415(9)	C17-C18	1.398(9)
O2-C12	1.434(9)	C18-C19	1.37(1)
O3-C13	1.423(9)	C19-C20	1.41(1)
O3-C14	1.400(9)	C19-C22	1.50(1)
N1-C17	1.344(8)	C20-C21	1.35(1)

Table A11.4 Intramolecular Bond Angles Involving the Nonhydrogen Atoms for [Pd(PIC)(TOMB-3)][BF_4], (34).

linkage	angle (°)	linkage	angle (°)
S1-Pd1-S2	159.93(7)	C4-C5-C6	120.4(7)
S1-Pd1-N1	94.7(2)	C1-C6-C5	119.3(6)
S1-Pd1-C1	85.1(2)	C1-C6-C7	118.8(6)
S2-Pd1-N1	99.7(2)	C5-C6-C7	121.7(6)
S2-Pd1-C1	81.1(2)	S1-C7-C6	111.1(5)
N1-Pd1-C1	177.2(2)	S1-C8-C9	116.7(5)
Pd1-S1-C7	100.2(2)	O1-C9-C8	110.3(6)
Pd1-S1-C8	113.2(3)	O1-C10-C11	108.9(6)
C7-S1-C8	101.9(4)	O2-C11-C10	110.1(6)
Pd1-S2-C15	120.1(3)	O2-C12-C13	114.0(7)
Pd1-S2-C16	98.2(2)	O3-C13-C12	109.1(7)
C15-S2-C16	103.5(3)	O3-C14-C15	110.8(6)
C9-O1-C10	112.6(6)	S2-C15-C14	117.4(5)
C11-O2-C12	113.4(6)	S2-C16-C2	106.6(5)
C13-O3-C14	111.4(6)	N1-C17-N2	116.9(6)
Pd1-N1-C17	124.0(5)	N1-C17-C18	121.9(7)
Pd1-N1-C21	119.0(4)	N2-C17-C18	121.2(7)
C17-N1-C21	116.9(6)	C17-C18-C19	120.5(7)
Pd1-C1-C21	20.4(5)	C18-C19-C20	117.2(7)
Pd1-C1-C6	120.4(5)	C18-C19-C22	121.7(8)
C2-C1-C6	119.2(6)	C20-C19-C22	121.1(8)
C1-C2-C3	119.5(6)	C19-C20-C21	119.4(7)
C1-C2-C16	117.7(6)	N1-C21-C20	124.1(7)
C3-C2-C16	122.8(6)	F1-B1-F2	103(1)
C2-C3-C4	121.3(7)	F1-B1-F3	116(1)
C3-C4-C5	120.3(7)	F1-B1-F4	109(1)
F2-B1-F3	109(1)	F2-B1-F4	109(1)
F3-B1-F4	111(1)		

Table A12.1 Summary of Crystal Data, Intensity Collection and Structure Refinement for [Pd(CYT)(TOMB-3)][BF_4], (35).

formula	$C_{22}H_{31}BN_4O_4F_4S_2Pd$
fw	672.83 $gmol^{-1}$
colour/form	colourless block
a, Å	12.877(4)
b, Å	16.567(3)
c, Å	13.714(5)
α, deg	90
β, deg	101.53(2)
γ, deg	90
V ($Å^3$)	2866.5(2.6)
crystal system	monoclinic
space group	$P2_1/n$ (#14)
ρ (gmL^{-1})	1.56
Z	4
μ, cm^{-1}	8.36
diffractometer	Rigaku AFC6S
λ, (Å)	0.71069
T (°C)	23
scan type	ω–2θ
scan width (deg)	1.05 +0.30 tan
2θ range (deg)	4.5-50
# data collected	5258
# unique data with $F_o^2>3\sigma(F_o^2)$	2335
# variables	242
data/var ratio	9.6
max shift/error	0
goodness of fit	21.52
$R(F_o)$, %	4.61
$R_w(F_o)$, %	3.54

Table A12.2 Positional parameters and β(eq) for [Pd(CYT)(TOMB-3)][BF_4], (35).

atom	x	y	z	β(eq)
Pd1	0.14166(5)	0.06126(5)	0.34342(5)	2.87(3)
S1	0.0886(2)	-0.0708(2)	0.3108(1)	3.3(1)
S2	0.1696(2)	0.1857(2)	0.4182(2)	4.3(1)
F1	0.4359(6)	0.1017(5)	0.9285(6)	11.6(6)
F2	0.3121(6)	0.0164(5)	0.9385(7)	11.5(6)
F3	0.2771(7)	0.1371(5)	0.9485(7)	13.8(7)
F4	0.3030(7)	0.092(1)	0.8093(5)	18.5(9)
O1	-0.0102(4)	0.0466(4)	0.1228(4)	3.7(3)
O2	-0.0096(5)	0.2039(4)	0.0290(4)	5.2(3)
O3	0.1482(5)	0.2734(4)	0.1990(4)	5.8(4)
O4	0.3658(4)	0.0307(4)	0.4712(4)	4.8(3)
N1	0.2947(5)	0.0382(4)	0.3067(4)	3.2(3)
N2	0.2302(6)	0.0500(7)	0.1375(5)	5.1(4)
N3	0.4720(5)	-0.0014(5)	0.3649(5)	4.3(4)
N4	0.505(1)	0.2091(8)	0.271(1)	12.0(9)
C1	-0.0030(6)	0.0784(5)	0.3705(5)	2.5(2)
C2	-0.0378(7)	0.1563(5)	0.3871(6)	3.4(2)
C3	-0.1401(8)	0.1673(6)	0.4067(7)	5.0(2)
C4	-0.2057(8)	0.1014(7)	0.4092(7)	5.2(2)
C5	-0.1721(8)	0.0242(6)	0.3916(7)	4.9(2)
C6	-0.0712(6)	0.0128(5)	0.3723(6)	2.8(2)
C7	-0.0344(6)	-0.0704(6)	0.3577(6)	3.9(2)
C8	0.0426(7)	-0.0872(5)	0.1785(6)	4.0(2)
C9	-0.0451(7)	-0.0343(6)	0.1246(6)	4.4(2)
C10	-0.0975(7)	0.1002(6)	0.1007(6)	4.0(2)
C11	-0.0568(8)	0.1848(6)	0.1108(7)	5.0(2)
C12	0.0381(9)	0.2797(7)	0.0364(8)	6.2(3)
C13	0.1485(9)	0.2796(7)	0.0961(8)	6.7(3)
C14	0.2483(9)	0.2523(7)	0.2558(8)	5.6(3)
C15	0.2475(8)	0.2576(7)	0.3651(7)	5.9(3)
C16	0.0344(7)	0.2251(6)	0.3848(6)	4.5(2)
C17	0.3108(7)	0.0321(5)	0.2122(6)	3.4(2)

C18	0.4095(8)	0.0044(6)	0.1921(7)	4.6(2)
C19	0.4876(7)	-0.0119(6)	0.2707(7)	4.3(2)
C20	0.3766(7)	0.0231(6)	0.3847(6)	3.5(2)
C21	0.558(1)	0.196(1)	0.218(1)	8.9(4)
C22	0.625(1)	0.167(1)	0.155(1)	13.1(5)
B1	0.333(1)	0.091(1)	0.898(2)	8(1)

Table A12.3 Intramolecular Distances (Å) Involving the Nonhydrogen Atoms for [Pd(CYT)(TOMB-3)][BF_4], (35).

atom-atom	distance	atom-atom	distance
Pd1-S1	2.309(3)	N1-C20	1.366(9)
Pd1-S2	2.299(3)	N2-C17	1.34(1)
Pd1-N1	2.164(6)	N3-C19	1.36(1)
Pd1-C1	1.992(7)	N3-C20	1.37(1)
S1-C7	1.824(8)	N4-C21	1.11(2)
S1-C8	1.814(8)	C1-C2	1.40(1)
S2-C15	1.80(1)	C1-C6	1.40(1)
S2-C16	1.829(9)	C2-C3	1.41(1)
F1-B1	1.32(2)	C2-C16	1.48(1)
F2-B1	1.39(2)	C3-C4	1.39(1)
F3-B1	1.33(2)	C4-C5	1.39(1)
F4-B1	1.21(2)	C5-C6	1.39(1)
O1-C9	1.42(1)	C6-C7	1.48(1)
O1-C10	1.42(1)	C8-C9	1.50(1)
O2-C11	1.42(1)	C10-C11	1.49(1)
O2-C12	1.39(1)	C12-C13	1.49(1)
O3-C13	1.42(1)	C14-C15	1.50(1)
O3-C14	1.41(1)	C17-C18	1.43(1)
O4-C20	1.228(9)	C18-C19	1.35(1)
N1-C17	1.356(9)	C21-C22	1.42(2)

Table A12.4 Intramolecular Bond Angles Involving the Nonhydrogen Atoms for [Pd(CYT)(TOMB-3)][BF_4], (35).

linkage	angle (°)	linkage (°)	angle
S1-Pd1-S2	161.80(8)	C3-C4-C5	120.7(9)
S1-Pd1-N1	92.0(2)	C4-C5-C6	119.6(9)
S1-Pd1-C1	85.4(2)	C1-C6-C5	120.7(8)
S2-Pd1-N1	101.2(2)	C1-C6-C7	120.0(7)
S2-Pd1-C1	81.8(2)	C5-C6-C7	119.2(8)
N1-Pd1-C1	176.6(3)	S1-C7-C6	112.0(6)
Pd1-S1-C7	99.9(3)	S1-C8-C9	118.0(6)
Pd1-S1-C8	111.1(3)	O1-C9-C8	110.5(7)
C7-S1-C8	102.7(4)	O1-C10-C11	108.6(7)
Pd1-S2-C15	117.5(4)	O2-C11-C10	109.5(8)
Pd1-S2-C16	98.8(3)	O2-C12-C13	113(1)
C15-S2-C16	104.0(5)	O3-C13-C12	110.8(9)
C9-O1-C10	110.8(6)	O3-C14-C15	110.5(9)
C11-O2-C12	113.4(8)	S2-C15-C14	118.7(8)
C13-O3-C14	112.6(8)	S2-C16-C2	106.9(7)
Pd1-N1-C17	123.7(5)	N1-C17-N2	118.2(8)
Pd1-N1-C20	116.5(5)	N1-C17-C18	121.3(8)
C17-N1-C20	119.6(7)	N2-C17-C18	120.5(8)
C19-N3-C20	122.3(8)	C17-C18-C19	17.5(9)
Pd1-C1-C2	120.3(6)	N3-C19-C18	120.5(9)
Pd1-C1-C6	120.3(6)	O4-C20-N1	121.3(8)
C2-C1-C6	119.4(7)	O4-C20-N3	120.0(8)
C1-C2-C3	119.5(9)	N1-C20-N3	118.7(8)
C1-C2-C16	119.0(8)	N4-C21-C22	172(2)
C3-C2-C16	121.5(9)	F1-B1-F2	105(2)
C2-C3-C4	120(1)	F1-B1-F3	112(2)
F1-B1-F4	114(2)	F2-B1-F4	112(2)
F2-B1-F3	98(1)	F3-B1-F4	115(2)

Table A13.1 Summary of Crystal Data, Intensity Collection and Structure Refinement for [Pd(PAP)(TOMB-P4)][BF_4], (36).

formula	$C_{33}H_{37}BN_2O_4F_4S_2Pd$
fw	782.99 $gmol^{-1}$
colour/form	yellow block
a, Å	14.329(3)
b, Å	15.123(2)
c, Å	8.832(1)
α, deg	99.04(1)
β, deg	97.22(2)
γ, deg	114.83(2)
V ($Å^3$)	1675.8(6)
crystal system	triclinic
space group	$P\bar{1}$ (#2)
ρ (gmL^{-1})	1.76
Z	2
μ, cm^{-1}	12.62
diffractometer	Rigaku AFC6S
λ, (Å)	0.71069
T (°C)	23
scan type	ω–2θ
scan width (deg)	1.05 +0.30 tan
2θ range (deg)	4.5-50
# data collected	5902
# unique data with $F_o^2>3\sigma(F_o^2)$	3241
# variables	425
data/var ratio	7.6
max shift/error	0.0002
goodness of fit	1.35
$R(F_o)$, %	4.00
$R_w(F_o)$, %	3.48

Table A13.2 Positional Parameters and β(eq) for [Pd(PAP)(TOMB-P4)][BF_4], (36).

atom	x	y	z	β(eq)
Pd1	0.15212(4)	0.20221(4)	0.44192(6)	2.57(2)
S1	0.3157(1)	0.2273(1)	0.3963(2)	3.35(6)
S2	-0.0234(1)	0.1655(1)	0.3935(2)	3.02(6)
F1	0.4087(4)	0.2363(4)	0.8642(6)	8.6(3)
F2	0.3522(4)	0.0883(4)	0.6988(5)	8.6(2)
F3	0.4876(5)	0.1460(5)	0.8949(8)	11.0(3)
F4	0.3289(5)	0.0940(4)	0.9410(6)	10.1(3)
O1	0.3229(4)	0.6527(4)	0.3248(6)	5.0(2)
O2	0.3337(4)	0.8246(4)	0.5581(6)	5.2(2)
O3	0.2719(4)	0.7590(3)	0.8345(5)	4.4(2)
O4	0.0689(4)	0.5876(3)	0.8218(6)	4.4(2)
N1	0.2196(4)	0.3460(4)	0.6032(6)	2.8(2)
N2	0.3965(5)	0.6350(4)	0.8828(8)	5.7(3)
C1	0.1011(5)	0.0684(4)	0.2976(7)	2.8(2)
C2	-0.0067(5)	0.0036(4)	0.2446(7)	2.7(2)
C3	-0.0413(5)	-0.0840(5)	0.1271(7)	3.6(2)
C4	0.0304(6)	-0.1072(5)	0.0645(8)	3.9(3)
C5	0.1371(6)	-0.0479(5)	0.1213(8)	3.4(3)
C6	0.1727(5)	0.0381(5)	0.2408(7)	3.0(2)
C7	0.2876(5)	0.0983(5)	0.3136(8)	3.9(3)
C8	0.3182(5)	0.2719(5)	0.2138(8)	4.3(3)
C9	0.3203(6)	0.3740(5)	0.2362(8)	3.7(3)
C10	0.4147(5)	0.4581(5)	0.3032(8)	4.0(3)
C11	0.4185(5)	0.5530(5)	0.3320(8)	3.9(3)
C12	0.3283(6)	0.5634(5)	0.2951(8)	3.8(3)
C13	0.2348(5)	0.4791(6)	0.2246(8)	3.7(3)
C14	0.2310(5)	0.3858(5)	0.1972(7)	3.6(3)
C15	0.4181(6)	0.7407(6)	0.411(1)	5.4(3)
C16	0.3908(7)	0.8266(6)	0.440(1)	6.1(4)
C17	0.3960(6)	0.8690(6)	0.710(1)	5.2(3)
C18	0.3272(6)	0.8609(5)	0.8254(9)	4.8(3)
C19	0.2076(6)	0.7472(5)	0.948(1)	4.9(3)

C20	0.1550(6)	0.6407(5)	0.9538(8)	4.3(3)
C21	0.0315(5)	0.4862(5)	0.7731(8)	3.4(3)
C22	-0.0467(5)	0.4426(5)	0.6371(8)	3.9(3)
C23	-0.0852(5)	0.3415(5)	0.5708(8)	3.8(3)
C24	-0.0489(5)	0.2823(5)	0.6399(8)	3.1(2)
C25	0.0258(5)	0.3270(5)	0.7773(8)	3.4(3)
C26	0.0660(5)	0.4279(5)	0.8458(8)	3.7(3)
C27	-0.0851(5)	0.1740(5)	0.5614(8)	3.8(3)
C28	-0.0851(5)	0.0292(5)	0.3147(8)	3.7(3)
C29	0.2892(5)	0.3643(5)	0.7346(8)	3.4(3)
C30	0.3480(5)	0.4586(5)	0.8325(8)	3.9(3)
C31	0.3357(5)	0.5390(5)	0.7946(8)	3.8(3)
C32	0.2629(5)	0.5205(5)	0.6596(8)	3.5(3)
C33	0.2073(5)	0.4248(5)	0.5698(7)	2.9(2)
B1	0.3896(8)	0.1402(8)	0.848(1)	5.4(4)

Table A13.3 Intramolecular Distances (Å) Involving the Nonhydrogen Atoms for [Pd(PAP)(TOMB-P4)][BF_4], (36).

atom-atom	distance	atom-atom	distance
Pd1-S1	2.311(2)	C2-C28	1.502(8)
Pd1-S2	2.301(2)	C3-C4	1.367(9)
Pd1-N1	2.147(5)	C4-C5	1.382(9)
Pd1-C1	1.992(6)	C5-C6	1.393(8)
S1-C7	1.822(6)	C6-C7	1.498(9)
S1-C8	1.841(7)	C8-C9	1.513(9)
S2-C27	1.833(7)	C9-C10	1.383(9)
S2-C28	1.839(6)	C9-C14	1.374(9)
F1-B1	1.34(1)	C10-C11	1.393(9)
F2-B1	1.34(1)	C11-C12	1.372(9)
F3-B1	1.37(1)	C12-C13	1.384(9)
F4-B1	1.33(1)	C13-C14	1.369(9)
O1-C12	1.372(8)	C15-C16	1.50(1)
O1-C15	1.452(8)	C17-C18	1.49(1)

O2-C16	1.402(9)	C19-C20	1.476(9)
O2-C17	1.402(9)	C21-C22	1.388(9)
O3-C18	1.427(8)	C21-C26	1.378(9)
O3-C19	1.427(8)	C22-C23	1.384(9)
O4-C20	1.428(8)	C23-C24	1.389(8)
O4-C21	1.367(7)	C24-C25	1.372(8)
N1-C29	1.339(8)	C24-C27	1.507(9)
N1-C33	1.347(7)	C25-C26	1.382(8)
N2-C31	1.374(8)	C29-C30	1.383(8)
C1-C2	1.403(8)	C30-C31	1.383(9)
C1-C6	1.402(8)	C31-C32	1.387(9)
C2-C3	1.402(8)	C32-C33	1.367(8)

Table A13.4 Intramolecular Bond Angles Involving the Nonhydrogen Atoms for [Pd(PAP)(TOMB-P4)][BF_4], (36).

linkage	angle (°)	linkage	angle (°)
S1-Pd1-S2	159.98(6)	C3-C4-C5	120.7(6)
S1-Pd1-N1	91.1(1)	C4-C5-C6	120.0(6)
S1-Pd1-C1	84.7(2)	C1-C6-C5	120.4(6)
S2-Pd1-N1	101.1(1)	C1-C6-C7	118.8(6)
S2-Pd1-C1	83.6(2)	C5-C6-C7	120.7(6)
N1-Pd1-C1	175.1(2)	S1-C7-C6	109.7(5)
Pd1-S1-C7	99.7(2)	S1-C8-C9	112.6(5)
Pd1-S1-C8	102.7(2)	C8-C9-C10	118.9(7)
C7-S1-C8	98.7(3)	C8-C9-C14	122.2(6)
Pd1-S2-C27	118.4(2)	C10-C9-C14	118.9(7)
Pd1-S2-C28	101.1(2)	C9-C10-C11	120.4(7)
C27-S2-C28	101.1(3)	C10-C11-C12	120.1(6)
C12-O1-C15	117.1(6)	O1-C12-C11	124.6(6)
C16-O2-C17	114.4(6)	O1-C12-C13	116.3(6)
C18-O3-C19	112.7(5)	C11-C12-C13	119.1(7)
C20-O4-C21	118.7(5)	C12-C13-C14	120.7(7)
Pd1-N1-C29	119.6(4)	C9-C14-C13	120.8(6)

Pd1-N1-C33	123.1(4)	O1-C15-C16	107.3(7)
C29-N1-C33	116.6(5)	O2-C16-C15	113.8(7)
Pd1-C1-C2	121.4(5)	O2-C17-C18	109.6(6)
Pd1-C1-C6	120.5(5)	O3-C18-C17	110.2(6)
C2-C1-C6	118.0(6)	O3-C19-C20	109.7(6)
C1-C2-C3	120.5(6)	O4-C20-C19	108.9(6)
C1-C2-C28	119.4(5)	O4-C21-C22	114.3(6)
C3-C2-C28	120.1(6)	O4-C21-C26	125.6(6)
C2-C3-C4	119.9(6)	C22-C21-C26	120.0(6)
C21-C22-C23	119.4(6)	N2-C31-C30	121.6(7)
C22-C23-C24	121.2(6)	N2-C31-C32	120.5(7)
C23-C24-C25	117.9(6)	C30-C31-C32	117.9(6)
C23-C24-C27	121.1(6)	C31-C32-C33	119.2(6)
C25-C24-C27	120.9(6)	N1-C33-C32	123.8(6)
C24-C25-C26	122.2(6)	F1-B1-F2	112.4(9)
C21-C26-C25	119.2(6)	F1-B1-F3	103.6(7)
S2-C27-C24	110.0(4)	F1-B1-F4	113.5(9)
S2-C28-C2	107.9(4)	F2-B1-F3	107.5(9)
N1-C29-C30	123.2(6)	F2-B1-F4	111.3(8)
C29-C30-C31	119.3(6)	F3-B1-F4	108.1(9)

Table A14.1 Summary of Crystal Data, Intensity Collection and Structure Refinement for [Pd(PAP)(TOMB-M4)][BF_4], (37).

formula	$C_{33}H_{37}BN_2O_4F_4S_2Pd$
fw	782.99 $gmol^{-1}$
colour/form	yellow block
a, Å	9.310(5)
b, Å	24.201(5)
c, Å	15.518(4)
α, deg	90
β, deg	105.93(3)
γ, deg	90
V (Å^3)	3362(2)
crystal system	monoclinic
space group	$P2_1/c$(#14)
ρ (gmL^{-1})	1.55
Z	4
μ, cm^{-1}	7.39
diffractometer	Rigaku AFC6S
λ, (Å)	0.71069
T (°C)	23
scan type	ω–2θ
scan width (deg)	1.05 +0.30 tan
2θ range (deg)	4.5-50
# data collected	5047
# unique data with $F_o^2>3\sigma(F_o^2)$	1404
# variables	260
data/var ratio	5.4
max shift/error	0.000648
goodness of fit	1.67
$R(F_o)$, %	5.47
$R_w(F_o)$, %	4.82

Table A14.2 Positional parameters and β(eq) for [Pd(PAP)(TOMB-M4)][BF_4], (37).

atom	x	y	z	β(eq)
Pd(1)	0.2124(2)	0.04541(7)	0.4789(1)	4.22(7)
S(1)	0.2064(5)	-0.0463(2)	0.4369(3)	4.8(2)
S(2)	0.2587(6)	0.1270(2)	0.5586(4)	5.9(3)
F(1)	0.789(2)	0.1982(6)	0.554(1)	11(1)
F(2)	0.576(2)	0.2053(7)	0.584(1)	14(1)
F(3)	0.669(2)	0.2751(6)	0.543(1)	16(1)
F(4)	0.580(2)	0.2116(7)	0.451(1)	14(1)
O(1)	-0.109(1)	0.0031(6)	0.0768(9)	6.3(8)
O(2)	-0.374(1)	0.0754(5)	0.009(1)	6.8(8)
O(3)	-0.395(2)	0.1720(6)	0.111(1)	7.4(8)
O(4)	-0.210(2)	0.2421(5)	0.246(1)	5.8(8)
N(1)	0.116(2)	0.0800(6)	0.351(1)	4.3(8)
N(2)	-0.064(2)	0.1588(7)	0.108(1)	6(1)
C(1)	0.309(2)	0.0139(7)	0.600(1)	4.1(4)
C(2)	0.312(2)	0.0431(9)	0.679(1)	5.0(4)
C(3)	0.372(2)	0.0204(8)	0.765(1)	5.2(5)
C(4)	0.428(2)	-0.0318(8)	0.768(1)	5.6(5)
C(5)	0.426(2)	-0.0612(7)	0.692(1)	5.1(5)
C(6)	0.368(2)	-0.0381(8)	0.609(1)	4.6(4)
C(7)	0.366(2)	-0.0693(7)	0.525(1)	5.3(5)
C(8)	0.272(2)	-0.0587(7)	0.338(1)	5.4(5)
C(9)	0.142(2)	-0.0705(8)	0.255(1)	4.2(4)
C(10)	0.091(2)	-0.1253(8)	0.241(1)	5.7(5)
C(11)	-0.027(2)	-0.1355(8)	0.165(1)	6.1(5)
C(12)	-0.092(2)	-0.096(1)	0.108(2)	7.0(6)
C(13)	-0.048(2)	-0.041(1)	0.125(1)	6.0(5)
C(14)	0.074(2)	-0.0307(7)	0.199(1)	4.6(5)
C(15)	-0.232(2)	-0.0055(8)	-0.001(1)	5.9(5)
C(16)	-0.284(2)	0.050(1)	-0.039(1)	7.2(6)
C(17)	-0.437(2)	0.126(1)	-0.027(1)	7.3(6)
C(18)	-0.510(2)	0.1551(9)	0.032(2)	7.0(6)
C(19)	-0.448(2)	0.203(1)	0.175(2)	7.1(6)

C(20)	-0.326(3)	0.2087(9)	0.259(1)	6.4(6)
C(21)	-0.080(3)	0.239(1)	0.308(2)	6.0(6)
C(22)	0.040(2)	0.2660(8)	0.286(1)	5.7(5)
C(23)	0.179(2)	0.2631(8)	0.348(1)	6.4(5)
C(24)	0.209(2)	0.2356(9)	0.428(1)	6.7(6)
C(25)	0.091(2)	0.2095(8)	0.448(1)	5.0(5)
C(26)	-0.051(2)	0.2103(8)	0.388(1)	5.0(5)
C(27)	0.110(2)	0.1734(9)	0.535(1)	7.6(6)
C(28)	0.246(2)	0.1005(8)	0.667(1)	5.8(5)
C(29)	0.203(2)	0.1101(8)	0.313(1)	5.4(5)
C(30)	0.147(2)	0.1359(8)	0.231(1)	5.3(5)
C(31)	-0.004(2)	0.1334(7)	0.185(1)	3.9(4)
C(32)	-0.088(2)	0.0975(7)	0.225(1)	4.3(4)
C(33)	-0.022(2)	0.0740(8)	0.307(1)	4.4(4)
B(1)	0.662(4)	0.224(1)	0.536(2)	7(2)

Table A14.3 Intramolecular Distances (Å) Involving the Nonhydrogen Atoms for [Pd(PAP)(TOMB-M4)][BF_4], (37).

atom-atom	distance	atom-atom	distance
Pd1-S1	2.310(6)	C2-C28	1.51(2)
Pd1-S2	2.306(6)	C3-C4	1.36(2)
Pd1-N1	2.11(1)	C4-C5	1.38(2)
Pd1-C1	2.00(2)	C5-C6	1.37(2)
S1-C7	1.80(2)	C6-C7	1.50(2)
S1-C8	1.83(2)	C8-C9	1.53(2)
S2-C27	1.74(2)	C9-C10	1.41(2)
S2-C28	1.83(2)	C9-C14	1.33(2)
F1-B1	1.29(3)	C10-C11	1.40(2)
F2-B1	1.31(3)	C11-C12	1.33(2)
F3-B1	1.25(3)	C12-C13	1.39(3)
F4-B1	1.37(3)	C13-C14	1.40(2)
O1-C13	1.34(2)	C15-C16	1.50(3)
O1-C15	1.43(2)	C17-C18	1.46(3)

O2-C16	1.41(2)	C19-C20	1.48(3)
O2-C17	1.41(2)	C21-C22	1.41(2)
O3-C18	1.44(2)	C21-C26	1.39(2)
O3-C19	1.43(2)	C22-C23	1.39(2)
O4-C20	1.41(2)	C23-C24	1.37(2)
O4-C21	1.32(2)	C24-C25	1.37(2)
N1-C29	1.35(2)	C25-C26	1.39(2)
N1-C33	1.29(2)	C25-C27	1.58(2)
N2-C31	1.33(2)	C29-C30	1.38(2)
C1-C2	1.41(2)	C30-C31	1.39(2)
C1-C6	1.36(2)	C31-C32	1.42(2)
C2-C3	1.41(2)	C32-C33	1.38(2)

Table A14.4 Intramolecular Bond Angles Involving the Nonhydrogen Atoms for [Pd(PAP)(TOMB-M4)][BF_4], (37).

linkage	angle (°)	linkage	angle (°)
S1-Pd1-S2	163.8(2)	C3-C4-C5	122(2)
S1-Pd1-N1	98.4(4)	C4-C5-C6	120(2)
S1-Pd1-C1	82.5(5)	C1-C6-C5	121(2)
S2-Pd1-N1	97.6(4)	C1-C6-C7	118(2)
S2-Pd1-C1	81.5(5)	C5-C6-C7	121(2)
N1-Pd1-C1	178.3(6)	S1-C7-C6	108(1)
Pd1-S1-C7	97.6(6)	S1-C8-C9	112(1)
Pd1-S1-C8	114.1(6)	C8-C9-C10	117(2)
C7-S1-C8	100.7(8)	C8-C9-C14	123(2)
Pd1-S2-C27	114.7(8)	C10-C9-C14	120(2)
Pd1-S2-C28	98.2(7)	C9-C10-C11	117(2)
C27-S2-C28	100(1)	C10-C11-C12	123(2)
C13-O1-C15	118(2)	C11-C12-C13	120(2)
C16-O2-C17	115(2)	O1-C13-C12	127(2)
C18-O3-C19	115(2)	O1-C13-C14	116(2)
C20-O4-C21	117(2)	C12-C13-C14	117(2)
Pd1-N1-C29	119(1)	C9-C14-C13	122(2)

Pd1-N1-C33	124(1)	O1-C15-C16	107(2)
C29-N1-C33	118(2)	O2-C16-C15	111(2)
Pd1-C1-C2	121(1)	O2-C17-C18	113(2)
Pd1-C1-C6	120(1)	O3-C18-C17	108(2)
C2-C1-C6	118(2)	O3-C19-C20	109(2)
C1-C2-C3	122(2)	O4-C20-C19	112(2)
C1-C2-C28	116(2)	O4-C21-C22	116(2)
C3-C2-C28	122(2)	O4-C21-C26	126(2)
C2-C3-C4	116(2)	C22-C21-C26	118(2)
C21-C22-C23	118(2)	N2-C31-C30	124(2)
C22-C23-C24	125(2)	N2-C31-C32	122(2)
C23-C24-C25	117(2)	C30-C31-C32	114(2)
C24-C25-C26	121(2)	C31-C32-C33	120(2)
C24-C25-C27	123(2)	N1-C33-C32	125(2)
C26-C25-C27	116(2)	F1-B1-F2	113(3)
C21-C26-C25	122(2)	F1-B1-F3	115(3)
S2-C27-C25	116(2)	F1-B1-F4	110(2)
S2-C28-C2	108(1)	F2-B1-F3	109(3)
N1-C29-C30	122(2)	F2-B1-F4	102(3)
C29-C30-C31	122(2)	F3-B1-F4	107(3)

Table A15.1 Summary of Crystal Data, Intensity Collection and Structure Refinement for $[Pd(NH_3)(TOMB\text{-}3)][BF_4]$, (38).

formula	$C_{16}H_{26}NO_3BF_4S_2Pd$
fw	537.71 $gmol^{-1}$
colour/form	yellow block
a, Å	21.376(4)
b, Å	21.656(5)
c, Å	9.437(6)
α, deg	90
β, deg	90
γ, deg	90
V ($Å^3$)	4368(3)
crystal system	orthorhombic
space group	Pbca (#61)
ρ (gmL^{-1})	1.63
Z	8
μ, cm^{-1}	10.91
diffractometer	Rigaku AFC6S
λ, (Å)	0.71069
T (°C)	23
scan type	ω–2θ
scan width (deg)	1.05 +0.30 tan
2θ range (deg)	4.5-50
# data collected	3863
# unique data with $F_o^2>3\sigma(F_o^2)$	630
# variables	125
data/var ratio	5.0
max shift/error	0.006611
goodness of fit	2.04
$R(F_o)$, %	6.62
$R_w(F_o)$, %	6.39

Table A15.2 Positional parameters and β(eq) for [Pd(NH_3)(TOMB-3)][BF_4], (38).

atom	x	y	z	β(eq)
Pd1	0.2124(1)	0.3958(1)	-0.0134(3)	4.3(1)
S1	0.2901(6)	0.4647(5)	-0.056(1)	5.9(6)
S2	0.1510(4)	0.3089(4)	-0.014(1)	5.3(6)
O1	0.212(2)	0.571(1)	0.031(3)	8.2(7)
O2	0.106(1)	0.548(1)	-0.147(3)	9(1)
O3	0.055(1)	0.425(1)	-0.123(3)	7.0(8)
N1	0.150(1)	0.453(1)	0.108(3)	5(2)
C1	0.269(2)	0.339(2)	-0.115(4)	4(1)
C2	0.250(2)	0.291(2)	-0.182(4)	4(1)
C3	0.290(2)	0.250(3)	-0.258(5)	7.6(9)
C4	0.352(2)	0.264(2)	-0.256(5)	7(1)
C5	0.381(2)	0.311(2)	-0.193(4)	7(1)
C6	0.342(2)	0.357(2)	-0.124(5)	5(1)
C7	0.358(2)	0.413(2)	-0.046(5)	8(1)
C8	0.306(2)	0.523(2)	0.090(4)	7(1)
C9	0.274(2)	0.580(2)	0.045(5)	9(1)
C10	0.184(2)	0.617(2)	-0.057(5)	9(1)
C11	0.114(2)	0.600(2)	-0.067(5)	10(1)
C12	0.046(3)	0.534(3)	-0.171(6)	11(1)
C13	0.035(2)	0.470(2)	-0.215(5)	9(1)
C14	0.055(2)	0.368(2)	-0.174(5)	10(1)
C15	0.068(2)	0.319(2)	-0.058(4)	7(1)
C16	0.182(2)	0.274(2)	-0.183(4)	6(1)
B1	0.5565(7)	0.1332(7)	0.595(2)	14.7
F1	0.593(1)	0.163(1)	0.500(2)	10.7
F2	0.574(1)	0.0728(7)	0.601(3)	16.2
F3	0.4956(7)	0.137(1)	0.554(3)	19.1
F4	0.563(1)	0.159(1)	0.725(2)	17.4

Table A15.3 Intramolecular Distances (Å) Involving the Nonhydrogen Atoms for $[Pd(NH_3)(TOMB\text{-}3)][BF_4]$, (38).

atom-atom	distance	atom-atom	distance
Pd1-S1	2.27(1)	C1-C6	1.62(5)
Pd1-S2	2.30(1)	C2-C3	1.43(6)
Pd1-N1	2.15(3)	C2-C16	1.49(5)
Pd1-C1	1.96(4)	C3-C4	1.36(6)
S1-C7	1.83(5)	C4-C5	1.33(6)
S1-C8	1.91(4)	C5-C6	1.44(6)
S2-C15	1.84(4)	C6-C7	1.46(6)
S2-C16	1.88(4)	C8-C9	1.47(6)
O1-C9	1.36(6)	C10-C11	1.54(7)
O1-C10	1.43(5)	C12-C13	1.47(7)
O2-C11	1.37(6)	C14-C15	1.54(7)
O2-C12	1.33(7)	B1-F1	1.36(3)
O3-C13	1.37(6)	B1-F2	1.36(2)
O3-C14	1.34(6)	B1-F3	1.36(2)
C1-C2	1.29(5)	B1-F4	1.36(3)

Table A15.4 Intramolecular Bond Angles Involving the Nonhydrogen Atoms for $[Pd(NH_3)(TOMB\text{-}3)][BF_4]$, (38).

linkage	angle (°)	linkage	angle (°)
S1-Pd1-S2	163.3(4)	C3-C4-C5	128(4)
S1-Pd1-N1	99.9(8)	C4-C5-C6	118(4)
S1-Pd1-C1	83(1)	C1-C6-C5	115(3)
S2-Pd1-N1	96.7(8)	C1-C6-C7	113(3)
S2-Pd1-C1	81(1)	C5-C6-C7	132(4)
N1-Pd1-C1	176(1)	S1-C7-C6	108(3)
Pd1-S1-C7	100(1)	S1-C8-C9	105(3)
Pd1-S1-C8	116(1)	O1-C9-C8	111(3)
C7-S1-C8	103(2)	O1-C10-C11	106(4)
Pd1-S2-C15	117(1)	O2-C11-C10	111(4)
Pd1-S2-C16	97(1)	O2-C12-C13	115(5)
C15-S2-C16	101(2)	O3-C13-C12	116(4)
C9-O1-C10	112(3)	O3-C14-C15	112(4)
C11-O2-C12	114(4)	S2-C15-C14	115(3)
C13-O3-C14	115(4)	S2-C16-C2	104(3)
Pd1-C1-C2	123(3)	F1-B1-F2	110(2)
Pd1-C1-C6	118(2)	F1-B1-F3	110(2)
C2-C1-C6	118(3)	F1-B1-F4	110(2)
C1-C2-C3	123(4)	F2-B1-F3	109(2)
C1-C2-C16	120(4)	F2-B1-F4	109(2)
C3-C2-C16	116(4)	F5-B1-F4	109(2)
C2-C3-C4	117(5)		

Table A16.1 Summary of Crystal Data, Intensity Collection and Structure Refinement for [Pd(H_2O)(TOMB-5)][BF_4], (42).

formula	$C_{20}H_{33}O_6BF_4S_2Pd$
fw	626.80 $gmol^{-1}$
colour/form	yellow block
a, Å	11.076(3)
b, Å	15.147(4)
c, Å	8.586(2)
α, deg	92.42(2)
β, deg	112.12(2)
γ, deg	74.58(2)
V (Å^3)	1284(1)
crystal system	triclinic
space group	$P\bar{1}$ (#2)
ρ (gmL^{-1})	1.62
Z	2
μ, cm^{-1}	9.48
diffractometer	Rigaku AFC6S
λ, (Å)	0.71069
T (°C)	23
scan type	ω–2θ
scan width (deg)	1.05 +0.30 tan
2θ range (deg)	4.5-50
# data collected	4521
# unique data with $F_o^2>3\sigma(F_o^2)$	2277
# variables	307
data/var ratio	7.4
max shift/error	0.00009
goodness of fit	1.31
$R(F_o)$, %	3.22
$R_w(F_o)$, %	4.12

Table A16.2 Positional Parametersand β(eq) for [Pd(H_2O)(TOMB-5)][BF_4], (42).

atom	x	y	z	β(eq)
Pd1	0.22963(7)	0.18080(5)	0.23883(8)	2.98(3)
S1	0.1205(2)	0.2412(1)	0.4198(2)	3.3(1)
S2	0.3334(3)	0.0930(2)	0.0747(3)	5.0(2)
F1	0.6522(6)	0.2953(4)	0.9470(7)	8.5(4)
F2	0.7283(7)	0.2770(5)	1.2245(8)	9.9(5)
F3	0.8032(6)	0.1671(4)	1.0849(8)	8.7(4)
F4	0.5907(7)	0.1992(5)	1.065(1)	11.5(6)
O1	0.3682(5)	0.3117(4)	0.5038(6)	4.1(3)
O2	0.3654(6)	0.4263(4)	0.2367(7)	4.9(4)
O3	0.1828(6)	0.4565(4)	-0.1161(7)	4.9(4)
O4	-0.0260(6)	0.3776(4)	-0.2060(7)	5.3(4)
O5	0.0381(6)	0.1827(4)	-0.1762(7)	5.0(4)
O6	0.1933(6)	0.3118(4)	0.1152(7)	5.0(4)
C1	0.2567(8)	0.0610(5)	0.3469(9)	3.2(4)
C2	0.3524(8)	-0.0176(5)	0.3295(9)	3.4(4)
C3	0.3697(8)	-0.1011(6)	0.409(1)	4.2(5)
C4	0.294(1)	-0.1061(6)	0.503(1)	4.4(5)
C5	0.1998(8)	-0.0306(5)	0.5188(9)	3.7(5)
C6	0.1795(7)	0.0541(5)	0.4398(8)	2.9(4)
C7	0.0723(8)	0.1381(5)	0.4469(9)	3.4(4)
C8	0.2559(8)	0.2379(5)	0.6240(9)	3.8(5)
C9	0.3206(8)	0.3149(6)	0.636(1)	4.4(5)
C10	0.452(1)	0.3708(6)	0.526(1)	5.5(6)
C11	0.4822(9)	0.3760(6)	0.371(1)	5.5(6)
C12	0.394(1)	0.4517(7)	0.097(1)	6.3(7)
C13	0.270(1)	0.5107(7)	-0.027(1)	6.6(7)
C14	0.050(1)	0.5100(6)	-0.202(1)	6.4(7)
C15	-0.036(1)	0.4516(7)	-0.309(1)	6.3(6)
C16	-0.118(1)	0.3262(9)	-0.293(1)	7.3(8)
C17	-0.090(1)	0.2418(9)	-0.189(1)	6.8(8)
C18	0.062(1)	0.0967(9)	-0.103(1)	7.2(8)
C19	0.204(1)	0.0437(7)	-0.069(1)	7.2(7)

C20	0.4299(8)	-0.0049(6)	0.226(1)	4.6(5)
B1	0.692(1)	0.2339(8)	1.076(1)	5.0(7)

Table A16.3 Intramolecular Distances Involving the Nonhydrogen Atoms for $[Pd(H_2O)(TOMB\text{-}5)][BF_4]$, (42).

atom-atom	distance	atom-atom	distance
Pd1-S1	2.327(2)	O4-C15	1.41(1)
Pd1-S2	2.308(3)	O4-C16	1.41(1)
Pd1-O6	2.158(5)	O5-C17	1.43(1)
Pd1-C1	1.972(7)	O5-C18	1.38(1)
S1-C7	1.829(7)	C1-C2	1.41(1)
S1-C8	1.819(8)	C1-C6	1.39(1)
S2-C19	1.82(1)	C2-C3	1.40(1)
S2-C20	1.816(9)	C2-C20	1.50(1)
F1-B1	1.34(1)	C3-C4	1.38(1)
F2-B1	1.38(1)	C4-C5	1.37(1)
F3-B1	1.35(1)	C5-C6	1.402(9)
F4-B1	1.33(1)	C6-C7	1.51(1)
O1-C9	1.418(9)	C8-C9	1.51(1)
O1-C10	1.411(9)	C10-C11	1.50(1)
O2-C11	1.42(1)	C12-C13	1.46(1)
O2-C12	1.44(1)	C14-C15	1.50(1)
O3-C13	1.41(1)	C16-C17	1.49(1)
O3-C14	1.40(1)	C18-C19	1.48(1)

Table A16.4 Intramolecular Bond Angles Involving the Nonhydrogen Atoms for $[Pd(H_2O)(TOMB\text{-}5)][BF_4]$, (42).

linkage	angle (°)	linkage	angle (°)
S1-Pd1-S2	168.36(8)	C4-C5-C6	119.9(7)
S1-Pd1-O6	94.8(2)	C1-C6-C5	119.6(7)
S1-Pd1-C1	84.9(2)	C1-C6-C7	118.7(6)
S2-Pd1-O6	96.4(2)	C5-C6-C7	121.7(7)
S2-Pd1-C1	83.8(2)	S1-C7-C6	109.4(5)
O6-Pd1-C1	178.1(3)	S1-C8-C9	112.3(5)
Pd1-S1-C7	96.2(3)	O1-C9-C8	109.0(6)
Pd1-S1-C8	105.1(3)	O1-C10-C11	110.0(7)
C7-S1-C8	100.2(3)	O2-C11-C10	110.5(8)
Pd1-S2-C19	104.0(4)	O2-C12-C13	109.6(8)
Pd1-S2-C20	97.3(3)	O3-C13-C12	109.2(8)
C19-S2-C20	98.9(4)	O3-C14-C15	110.3(8)
C9-O1-C10	111.9(6)	O4-C15-C14	108.8(7)
C11-O2-C12	113.5(7)	O4-C16-C17	109.7(9)
C13-O3-C14	112.0(8)	O5-C17-C16	108.4(8)
C15-O4-C16	111.9(8)	O5-C18-C19	109.7(9)
C17-O5-C18	112.1(8)	S2-C19-C18	115.8(7)
Pd1-C1-C2	120.5(6)	S2-C20-C2	110.1(6)
Pd1-C1-C6	119.4(6)	F1-B1-F2	109(1)
C2-C1-C6	120.1(7)	F1-B1-F3	111.8(9)
C1-C2-C3	118.9(7)	F1-B1-F4	110(1)
C1-C2-C20	116.9(7)	F2-B1-F3	106.0(9)
C3-C2-C20	124.2(8)	F2-B1-F4	108.6(9)
C2-C3-C4	120.1(8)	F3-B1-F4	111(1)
C3-C4-C5	121.4(8)		

Table A17.1 Summary of Crystal Data, Intensity Collection and Structure Refinement for $[Pd(NH_2NH_2)(TOMB\text{-}3)][BF_4]$, (43).

formula	$C_{16}H_{27}N_2O_3BF_4S_2Pd$
fw	552.72 $gmol^{-1}$
colour/form	yellow block
a, Å	11.652(2)
b, Å	12.669(4)
c, Å	8.356(1)
α, deg	94.12(2)
β, deg	92.34(2)
γ, deg	117.21(1)
V (Å^3)	1090.3(4)
crystal system	triclinic
space group	$P\bar{1}$ (#2)
ρ (gmL^{-1})	1.68
Z	2
μ, cm^{-1}	10.96
diffractometer	Rigaku AFC6S
λ, (Å)	0.71069
T (°C)	23
scan type	ω–2θ
scan width (deg)	1.05 +0.30 tan
2θ range (deg)	4.5-50
# data collected	3817
# unique data with $F_o^2>3\sigma(F_o^2)$	2,713
# variables	263
data/var ratio	10.3
max shift/error	0.0066
goodness of fit	1.58
$R(F_o)$, %	3.48
$R_w(F_o)$, %	2.86

Table A17.2 Positional Parameters and β(eq) for [Pd(NH_2NH_2)(TOMB-3)] [BF_4], (43).

atom	x	y	z	β(eq)
Pd1	0.03233(5)	0.21618(4)	0.39616(5)	2.81(2)
S1	0.1302(1)	0.2652(1)	0.6542(2)	3.23(5)
S2	-0.1111(2)	0.1369(1)	0.1723(2)	3.68(6)
F1	0.5864(5)	0.3682(4)	-0.0389(5)	9.8(3)
F2	0.5181(4)	0.1955(4)	-0.1781(4)	8.8(2)
F3	0.5817(4)	0.2167(3)	0.0842(5)	6.9(2)
F4	0.3982(4)	0.2143(6)	0.0057(5)	12.1(3)
O1	0.0166(3)	0.4400(3)	0.1924(4)	3.5(2)
O2	0.2117(3)	0.5840(3)	0.4462(4)	3.8(2)
O3	0.3577(4)	0.4776(4)	0.5708(4)	4.3(2)
N1	0.1882(4)	0.3414(4)	0.2775(5)	3.6(2)
N2	0.2193(5)	0.2981(5)	0.1345(6)	6.8(3)
C1	-0.1163(5)	0.0999(4)	0.5045(6)	3.0(2)
C2	-0.0958(6)	0.0683(5)	0.6566(6)	3.4(2)
C3	-0.1993(7)	-0.0063(5)	0.7350(7)	4.9(3)
C4	-0.3230(7)	-0.0546(6)	0.6636(8)	5.7(3)
C5	-0.3452(6)	-0.0296(5)	0.5091(8)	4.9(3)
C6	-0.2412(6)	0.0486(5)	0.4309(7)	3.5(2)
C7	-0.2631(6)	0.0813(5)	0.2662(7)	4.6(3)
C8	-0.1204(6)	0.2473(5)	0.0539(6)	3.9(2)
C9	-0.1141(5)	0.3576(5)	0.1441(6)	3.5(2)
C10	0.0274(6)	0.5475(5)	0.2737(6)	3.6(2)
C11	0.1672(6)	0.6309(5)	0.3211(7)	4.0(2)
C12	0.3465(6)	0.6484(5)	0.4815(7)	4.7(3)
C13	0.3828(6)	0.4208(6)	0.6984(7)	5.0(3)
C14	0.2962(6)	0.2899(6)	0.6686(7)	4.6(3)
C15	0.0414(6)	0.1191(5)	0.7289(6)	4.0(2)
C16	0.3878(6)	0.5993(6)	0.6164(7)	4.7(3)
B1	0.5198(8)	0.2478(8)	-0.031(1)	4.9(4)

Table A17.3 Intramolecular Distances (Å) Involving the Nonhydrogen Atoms for $[Pd(NH_2NH_2)(TOMB\text{-}3)][BF_4]$, (43).

atom-atom	distance	atom-atom	distance
Pd1-S1	2.298(1)	O3-C13	1.412(6)
Pd1-S2	2.289(1)	O3-C16	1.425(6)
Pd1-N1	2.133(4)	N1-N2	1.423(5)
Pd1-C1	1.986(5)	C1-C2	1.396(6)
S1-C14	1.818(6)	C1-C6	1.396(7)
S1-C15	1.835(5)	C2-C3	1.372(7)
S2-C7	1.823(6)	C2-C15	1.498(7)
S2-C8	1.810(5)	C3-C4	1.365(8)
F1-B1	1.366(9)	C4-C5	1.392(8)
F2-B1	1.336(7)	C5-C6	1.394(7)
F3-B1	1.363(7)	C6-C7	1.497(7)
F4-B1	1.342(8)	C8-C9	1.512(7)
O1-C9	1.416(6)	C10-C11	1.491(7)
O1-C10	1.427(6)	C12-C16	1.494(7)
O2-C11	1.425(6)	C13-C14	1.498(8)
O2-C12	1.413(6)		

Table A17.4 Intramolecular Bond Angles Involving the Nonhydrogen Atoms for [Pd(NH_2NH_2)(TOMB-3)][BF_4], (43).

linkage	angle (°)	linkage	angle (°)
S1-Pd1-S2	165.16(5)	C2-C3-C4	120.3(5)
S1-Pd1-N1	98.6(1)	C3-C4-C5	120.3(6)
S1-Pd1-C1	82.0(1)	C4-C5-C6	119.5(6)
S2-Pd1-N1	96.1(1)	C1-C6-C5	120.4(5)
S2-Pd1-C1	83.2(2)	C1-C6-C7	119.0(5)
N1-Pd1-C1	178.8(2)	C5-C6-C7	120.7(5)
Pd1-S1-C14	114.5(2)	S2-C7-C6	108.4(4)
Pd1-S1-C15	98.0(2)	S2-C8-C9	117.3(4)
C14-S1-C15	103.9(3)	O1-C9-C8	109.6(4)
Pd1-S2-C7	99.8(2)	O1-C10-C11	109.0(4)
Pd1-S2-C8	113.9(2)	O2-C11-C10	109.1(4)
C7-S2-C8	102.0(3)	O2-C12-C16	110.1(5)
C9-O1-C10	111.5(4)	O3-C13-C14	108.6(5)
C11-O2-C12	112.2(4)	S1-C14-C13	108.2(4)
C13-O3-C16	112.4(4)	S1-C15-C2	106.7(3)
Pd1-N1-N2	116.8(3)	O3-C16-C12	109.7(5)
Pd1-C1-C2	121.2(4)	F1-B1-F2	107.0(6)
Pd1-C1-C6	120.7(4)	F1-B1-F3	108.9(6)
C2-C1-C6	118.1(5)	F1-B1-F4	111.3(7)
C1-C2-C3	121.3(5)	F2-B1-F3	112.0(7)
C1-C2-C15	117.2(5)	F2-B1-F4	109.2(6)
C3-C2-C15	121.5(5)	F3-B1-F4	108.4(6)

Table A18.1 Summary of Crystal Data, Intensity Collection and Structure Refinement for $[Pd(NH_2NH_3)(TOMB\text{-}3)][CF_3SO_3]_2$, (45).

formula	$C_{18}H_{28}N_2O_9F_6S_4Pd$
fw	765.06 $gmol^{-1}$
colour/form	yellow block
a, Å	11.906(4)
b, Å	17.19(1)
c, Å	15.313(4)
α, deg	90
β, deg	111.18(2)
γ, deg	90
V ($Å^3$)	2923(4)
crystal system	monoclinic
space group	$P2_1/c$ (#14)
ρ (gmL^{-1})	1.74
Z	4
μ, cm^{-1}	10.07
diffractometer	Rigaku AFC6S
λ, (Å)	0.71069
T (°C)	23
scan type	ω–2θ
scan width (deg)	1.05 +0.30 tan
2θ range (deg)	4.5-50
# data collected	5350
# unique data with $F_o^2>3\sigma(F_o^2)$	2961
# variables	382
data/var ratio	7.8
max shift/error	0.03
goodness of fit	1.62
$R(F_o)$, %	4.30
$R_w(F_o)$, %	3.09

Table A18.2 Positional Parameters and β(eq) for $[Pd(NH_2NH_3)(TOMB\text{-}3)][CF_3SO_3]_2$ (45).

atom	x	y	z	β(eq)
Pd1	0.65811(5)	0.00195(4)	0.31915(4)	2.57(2)
S1	0.7448(2)	-0.1188(1)	0.3365(1)	3.12(8)
S2	0.6151(2)	0.1322(1)	0.3288(1)	3.58(9)
S3	0.6830(2)	0.1326(1)	0.0607(2)	4.0(1)
S4	0.2890(2)	0.3241(1)	0.4402(1)	3.31(9)
F1	0.8619(7)	0.0694(5)	0.1883(5)	13.8(5)
F2	0.9025(6)	0.1108(7)	0.0766(6)	17.6(7)
F3	0.8805(7)	0.1850(5)	0.1757(7)	16.4(6)
F4	0.0706(4)	0.2909(3)	0.4259(4)	9.2(4)
F5	0.0889(6)	0.3193(5)	0.2996(5)	13.7(5)
F6	0.0949(6)	0.4056(4)	0.3958(7)	15.0(6)
O1	0.4412(5)	-0.1470(3)	0.2660(4)	4.9(3)
O2	0.2586(5)	-0.0323(3)	0.1850(4)	5.1(3)
O3	0.3575(4)	0.1094(3)	0.2667(4)	4.2(3)
O4	0.6321(6)	0.1450(4)	0.1282(4)	7.5(4)
O5	0.6516(6)	0.0609(4)	0.0187(5)	10.8(5)
O6	0.6763(6)	0.1917(5)	0.0001(6)	13.2(6)
O7	0.3112(5)	0.3393(3)	0.5360(4)	5.6(3)
O8	0.3074(5)	0.2468(3)	0.4188(4)	6.1(3)
O9	0.3356(5)	0.3810(3)	0.3943(4)	6.1(3)
N1	0.5269(6)	-0.0217(4)	0.1805(5)	3.2(3)
N2	0.4482(6)	0.0391(4)	0.1280(5)	3.3(3)
C1	0.7829(6)	0.0198(4)	0.4451(4)	2.8(3)
C2	0.8164(7)	0.0949(5)	0.4777(6)	3.7(4)
C3	0.9030(7)	0.1068(5)	0.5672(6)	4.6(4)
C4	0.9580(7)	0.0444(6)	0.6200(6)	4.6(4)
C5	0.9299(7)	-0.0298(5)	0.5877(5)	4.0(4)
C6	0.8396(6)	-0.0431(5)	0.5007(5)	3.2(3)
C7	0.8070(6)	-0.1230(4)	0.4641(5)	3.7(3)
C8	0.6387(7)	-0.1984(4)	0.3089(5)	4.2(4)
C9	0.5298(7)	-0.1916(5)	0.3357(5)	4.4(4)
C10	0.3276(8)	-0.1517(5)	0.2757(7)	5.6(5)

C11	0.2393(8)	-0.1140(6)	0.1918(7)	6.0(5)
C12	0.1989(7)	0.0133(6)	0.2311(6)	6.1(5)
C13	0.2309(8)	0.0962(6)	0.2288(6)	5.5(5)
C14	0.4135(7)	0.0885(5)	0.3638(5)	4.5(4)
C15	0.5264(7)	0.1350(5)	0.4023(5)	4.5(4)
C16	0.7610(7)	0.1598(4)	0.4138(6)	4.5(4)
C17	0.841(1)	0.1231(9)	0.127(1)	8.3(8)
C18	0.1280(9)	0.3363(7)	0.3898(8)	6.4(6)
H1	0.481(4)	-0.053(3)	0.181(4)	0(1)
H2	0.573(6)	-0.040(4)	0.138(4)	5(1)
H3	0.38(1)	0.002(8)	0.072(9)	20.6(9)
H4	0.509(7)	0.082(5)	0.127(5)	8(1)
H5	0.405(6)	0.064(4)	0.158(5)	5(1)

Table A18.3 Intramolecular Distances (Å) Involving the Nonhydrogen Atoms $[Pd(NH_2NH_3)(TOMB\text{-}3)][CF_3SO_3]_2$ (45).

atom-atom	distance	atom-atom	distance
Pd1-S1	2.290(2)	F6-C18	1.27(1)
Pd1-S2	2.314(2)	O1-C9	1.424(8)
Pd1-N1	2.172(6)	O1-C10	1.416(9)
Pd1-C1	1.987(6)	O2-C11	1.43(1)
S1-C7	1.824(7)	O2-C12	1.409(9)
S1-C8	1.806(7)	O3-C13	1.423(9)
S2-C15	1.801(7)	O3-C14	1.439(8)
S2-C16	1.817(8)	N1-N2	1.439(8)
S3-O4	1.390(6)	C1-C2	1.390(9)
S3-O5	1.379(7)	C1-C6	1.391(9)
S3-O6	1.359(6)	C2-C3	1.40(1)
S3-C17	1.79(1)	C2-C16	1.47(1)
S4-O7	1.418(5)	C3-C4	1.36(1)
S4-O8	1.405(5)	C4-C5	1.37(1)
S4-O9	1.428(5)	C5-C6	1.396(9)
S4-C18	1.802(9)	C6-C7	1.48(1)
F1-C17	1.28(1)	C8-C9	1.50(1)
F2-C17	1.26(1)	C10-C11	1.48(1)
F3-C17	1.29(1)	C12-C13	1.48(1)
F4-C18	1.29(1)	C14-C15	1.49(1)
F5-C18	1.32(1)		

Table A18.4 Intramolecular Bond Angles Involving the Nonhydrogen Atoms for $[Pd(NH_2NH_3)(TOMB\text{-}3)][CF_3SO_3]_2$ (45).

linkage	angle(°)	linkage	angle (°)
S1-Pd1-S2	166.04(7)	C13-O3-C14	114.1(6)
S1-Pd1-N1	94.5(2)	Pd1-N1-N2	120.2(5)
S1-Pd1-C1	83.1(2)	Pd1-C1-C2	120.6(6)
S2-Pd1-N1	98.4(2)	Pd1-C1-C6	120 1(5)
S2-Pd1-C1	83.9(2)	C2-C1-C6	119.3(7)
N1-Pd1-C1	177.4(3)	C1-C2-C3	120.1(8)
Pd1-S1-C7	98.8(3)	C1-C2-C16	117.6(7)
Pd1-S1-C8	114.4(3)	C3-C2-C16	122.3(8)
C7-S1-C8	101.5(4)	C2-C3-C4	119.5(8)
Pd1-S2-C15	105.0(3)	C3-C4-C5	121.3(8)
Pd1-S2-C16	97.0(3)	C4-C5-C6	120.1(7)
C15-S2-C16	99.8(4)	C1-C6-C5	119.5(7)
O4-S3-O5	111.5(5)	C1-C6-C7	119.1(6)
O4-S3-O6	117.3(5)	C5-C6-C7	121.3(7)
O4-S3-C17	104.1(6)	S1-C7-C6	108.5(5)
O5-S3-O6	114.3(5)	S1-C8-C9	118.5(5)
O5-S3-C17	103.6(6)	O1-C9-C8	108.5(6)
O6-S3-C17	104.2(6)	O1-C10-C11	106.8(7)
O7-S4-O8	115.4(4)	O2-C11-C10	114.1(7)
O7-S4-O9	115.0(4)	O2-C12-C13	110.1(7)
O7-S4-C18	101.2(5)	O3-C13-C12	112.8(7)
O8-S4-O9	114.4(4)	O3-C14-C15	106.8(6)
O8-S4-C18	104.0(5)	S2-C15-C14	112.8(5)
O9-S4-C18	104.5(4)	S2-C16-C21	11.1(5)
C9-O1-C10	111.5(6)	S3-C17-F1	112(1)
C11-O2-C12	112.7(7)	S3-C17-F2	113(1)
S3-C17-F3	110(1)	S4-C18-F5	109.9(9)
F1-C17-F2	109(1)	S4-C18-F6	112.9(9)
F1-C17-F3	104(1)	F4-C18-F5	106(1)
F2-C17-F3	109(1)	F4-C18-F6	108(1)
S4-C18-F4	113.2(7)	F5-C18-F6	106.4(9)

Table A19.1 Summary of Crystal Data, Intensity Collection and Structure Refinement for $[Pd(NH_2NH_3)(TOMB\text{-}5)][BF_4]_2$, (46).

formula	$C_{20}H_{36}N_2O_5B_2F_8S_2Pd$
fw	728.64 $gmol^{-1}$
colour/form	yellow block
a, Å	9.390(3)
b, Å	18.292(5)
c, Å	9.107(2)
α, deg	94.46(3)
β, deg	102.02(2)
γ, deg	103.51(1)
V ($Å^3$)	1474.4(8)
crystal system	triclinic
space group	$P\bar{1}$ (#2)
ρ (gmL^{-1})	1.64
Z	2
μ, cm^{-1}	8.55
diffractometer	Rigaku AFC6S
λ, (Å)	0.71069
T (°C)	23
scan type	ω–2θ
scan width (deg)	1.05 +0.30 tan
2θ range (deg)	4.5-50
# data collected	5195
# unique data with $F_o^2>3\sigma(F_o^2)$	3070
# variables	362
data/var ratio	8.5
max shift/error	0.007
goodness of fit	1.56
$R(F_o)$, %	4.65
$R_w(F_o)$, %	3.79

Table A19.2 Positional parameters and β(eq) for [Pd(NH_2NH_3)(TOMB-5)] $[BF_4]_2$, (46).

atom	x	y	z	β(eq)
Pd1	0.47148(7)	0.18260(4)	0.11483(7)	2.64(2)
S1	0.5471(2)	0.1684(1)	-0.1087(2)	3.47(8)
S2	0.4155(2)	0.1821(1)	0.3502(2)	2.95(8)
F1	0.8708(6)	-0.1597(3)	0.2811(7)	7.9(3)
F2	0.9756(6)	-0.1942(4)	0.1047(6)	9.2(3)
F3	1.1059(6)	-0.1718(4)	0.3336(6)	9.5(3)
F4	1.0529(8)	-0.0780(4)	0.217(1)	12.0(4)
F5	0.6877(6)	0.3300(4)	0.4294(7)	9.1(3)
F6	0.5057(6)	0.3864(3)	0.3612(6)	7.6(3)
F7	0.6516(6)	0.3700(3)	0.2059(6)	7.8(3)
F8	0.7471(6)	0.4529(3)	0.4152(6)	8.0(3)
O1	0.5133(7)	0.3194(3)	-0.1820(6)	5.4(3)
O2	0.2887(8)	0.3913(4)	-0.1390(7)	7.1(3)
O3	0.1458(8)	0.4233(4)	0.0947(7)	6.3(3)
O4	0.0965(6)	0.3272(3)	0.3212(6)	4.8(3)
O5	0.0931(5)	0.1812(3)	0.2300(5)	3.9(2)
N1	0.3447(7)	0.2612(3)	0.0278(6)	3.5(3)
N2	0.2757(7)	0.2987(3)	0.1260(7)	3.9(3)
C1	0.5917(8)	0.1113(4)	0.1834(8)	3.0(3)
C2	0.6133(7)	0.0951(4)	0.3334(8)	2.9(3)
C3	0.6862(8)	0.0412(4)	0.3787(9)	3.9(3)
C4	0.7397(9)	0.0011(5)	0.276(1)	4.6(4)
C5	0.7277(8)	0.0186(4)	0.131(1)	3.7(3)
C6	0.6542(8)	0.0736(4)	0.0844(9)	3.3(3)
C7	0.6421(9)	0.0935(4)	-0.073(1)	4.4(4)
C8	0.696(1)	0.2534(5)	-0.093(1)	5.1(4)
C9	0.648(1)	0.3039(5)	-0.206(1)	6.0(5)
C10	0.448(1)	0.3595(6)	-0.294(1)	7.4(6)
C11	0.296(1)	0.3610(6)	-0.281(1)	8.5(6)
C12	0.204(2)	0.4421(8)	-0.138(1)	12.3(9)
C13	0.217(2)	0.4764(6)	0.017(2)	13(1)
C14	0.152(1)	0.4498(6)	0.246(1)	6.9(5)

C15	0.051(1)	0.3963(6)	0.311(1)	6.0(5)
C16	-0.017(1)	0.2665(5)	0.347(1)	4.9(4)
C17	0.044(1)	0.2000(5)	0.363(1)	4.9(4)
C18	0.1226(8)	0.1094(4)	0.2137(8)	3.7(3)
C19	0.2558(9)	0.1011(4)	0.3301(8)	3.7(3)
C20	0.5639(8)	0.1432(4)	0.4455(8)	3.4(3)
B1	1.003(1)	-0.1479(7)	0.241(1)	4.7(5)
B2	0.647(1)	0.3857(7)	0.351(1)	4.5(5)

Table A19.3 Intramolecular Distances (Å) Involving the Nonhydrogen Atoms for $[Pd(NH_2NH_3)(TOMB\text{-}5)]\ [BF_4]_2$, (46).

atom-atom	distance	atom-atom	distance
Pd1-S1	2.307(2)	O3-C14	1.41(1)
Pd1-S2	2.311(2)	O4-C15	1.43(1)
Pd1-N1	2.167(6)	O4-C16	1.420(9)
Pd1-C1	1.972(7)	O5-C17	1.425(8)
S1-C7	1.817(8)	O5-C18	1.407(8)
S1-C8	1.807(8)	N1-N2	1.430(7)
S2-C19	1.812(8)	C1-C2	1.403(9)
S2-C20	1.805(7)	C1-C6	1.394(9)
F1-B1	1.34(1)	C2-C3	1.369(9)
F2-B1	1.39(1)	C2-C20	1.509(9)
F3-B1	1.32(1)	C3-C4	1.39(1)
F4-B1	1.31(1)	C4-C5	1.38(1)
F5-B2	1.37(1)	C5-C6	1.39(1)
F6-B2	1.36(1)	C6-C7	1.50(1)
F7-B2	1.34(1)	C8-C9	1.51(1)
F8-B2	1.36(1)	C10-C11	1.47(1)
O1-C9	1.41(1)	C12-C13	1.46(2)
O1-C10	1.42(1)	C14-C15	1.45(1)
O2-C11	1.39(1)	C16-C17	1.47(1)
O2-C12	1.36(1)	C18-C19	1.51(1)
O3-C13	1.37(1)		

Table A19.4 Intramolecular Bond Angles Involving the Nonhydrogen Atoms for $[Pd(NH_2NH_3)(TOMB\text{-}5)]\ [BF_4]_2$, (46).

linkage	angle (°)	linkage (°)	angle
S1-Pd1-S2	170.79(7)	C4-C5-C6	119.7(7)
S1-Pd1-N1	91.0(2)	C1-C6-C5	121.0(7)
S1-Pd1-C1	85.6(2)	C1-C6-C7	119.0(7)
S2-Pd1-N1	98.1(2)	C5-C6-C7	120.0(7)
S2-Pd1-C1	85.2(2)	S1-C7-C6	113.0(5)
N1-Pd1-C1	176.7(3)	S1-C8-C9	110.2(7)
Pd1-S1-C7	100.1(3)	O1-C9-C8	108.4(7)
Pd1-S1-C8	103.2(3)	O1-C10-C11	110.3(8)
C7-S1-C8	105.1(4)	O2-C11-C10	114(1)
Pd1-S2-C19	105.5(2)	O2-C12-C13	111(1)
Pd1-S2-C20	98.9(2)	O3-C13-C12	110(1)
C19-S2-C20	99.7(3)	O3-C14-C15	111.7(9)
C9-O1-C10	112.8(7)	O4-C15-C14	110.5(8)
C11-O2-C12	115.9(9)	O4-C16-C17	108.4(7)
C13-O3-C14	115.0(9)	O5-C17-C16	109.8(7)
C15-O4-C16	113.0(7)	O5-C18-C19	114.1(6)
C17-O5-C18	116.0(6)	S2-C19-C18	110.8(5)
Pd1-N1-N2	119.3(4)	S2-C20-C2	110.7(5)
Pd1-C1-C2	120.7(5)	F1-B1-F2	105.7(9)
Pd1-C1-C6	121.5(6)	F1-B1-F3	113.6(9)
C2-C1-C6	117.8(7)	F1-B1-F4	112.7(9)
C1-C2-C3	121.0(7)	F2-B1-F3	104.3(9)
C1-C2-C20	117.8(6)	F2-B1-F4	107.1(9)
C3-C2-C20	121.0(7)	F3-B1-F4	113(1)
C2-C3-C4	120.3(8)	F5-B2-F6	108.0(8)
C3-C4-C5	119.9(7)	F5-B2-F7	108.8(9)
F5-B2-F8	108.0(9)	F6-B2-F8	111.0(9)
F6-B2-F7	110.3(9)	F7-B2-F8	110.7(8)

Table A20.1 Summary of Crystal Data, Intensity Collection and Structure Refinement for TOMB-F2, (52).

formula	$C_{22}H_{24}O_2S_2Fe$
fw	440.39 $gmol^{-1}$
colour/form	orange chunk
a, Å	14.492(2)
b, Å	7.372(2)
c, Å	19.366(3)
α, deg	90
β, deg	95.31(1)
γ, deg	90
V (Å^3)	2059.9(6)
crystal system	monoclinic
space group	$P2_1/n$ (#14)
ρ (gmL^{-1})	1.42
Z	4
μ, cm^{-1}	9.39
diffractometer	Rigaku AFC6S
λ, (Å)	0.71069
T (°C)	23
scan type	ω–2θ
scan width (deg)	1.05 +0.30 tan
2θ range (deg)	4.5-50
# data collected	3947
# unique data with $F_o^2>3\sigma(F_o^2)$	1732
# variables	245
data/var ratio	7.1
max shift/error	0.0006
goodness of fit	1.62
$R(F_o)$, %	4.40
$R_w(F_o)$, %	3.93

Table A20.2 Positional parameters and β(eq) for TOMB-F2, (52).

atom	x	y	z	β(eq)
Fe1	0.76994(6)	0.0873(1)	0.91894(5)	3.61(4)
S1	0.9634(1)	0.5074(3)	1.18930(9)	4.65(9)
S2	0.5055(1)	0.3761(3)	1.1294(1)	4.9(1)
O1	0.8719(3)	0.0961(6)	1.0664(2)	4.3(2)
O2	0.6565(3)	0.2729(6)	1.0267(2)	4.6(2)
C1	0.7232(4)	0.6385(8)	1.1253(3)	3.3(3)
C2	0.6333(4)	0.6582(8)	1.1423(3)	3.1(3)
C3	0.6177(4)	0.7501(8)	1.2023(3)	3.4(3)
C4	0.6913(5)	0.8227(9)	1.2438(3)	4.5(4)
C5	0.7815(4)	0.8056(9)	1.2262(3)	3.8(3)
C6	0.7984(4)	0.7122(8)	1.1671(3)	3.3(3)
C7	0.8960(4)	0.6903(9)	1.1473(3)	4.2(3)
C8	0.9013(4)	0.3093(9)	1.1570(3)	4.2(3)
C9	0.9080(4)	0.274(1)	1.0815(3)	4.2(4)
C10	0.8701(4)	0.040(1)	0.9992(3)	4.0(4)
C11	0.9079(4)	0.126(1)	0.9427(4)	5.5(4)
C12	0.8900(4)	0.008(1)	0.8840(4)	6.1(4)
C13	0.8427(5)	-0.143(1)	0.9040(4)	5.6(4)
C14	0.8282(4)	-0.123(1)	0.9744(3)	4.4(4)
C15	0.6641(4)	0.221(1)	0.9610(4)	4.1(4)
C16	0.7040(5)	0.332(1)	0.9133(4)	5.7(4)
C17	0.6970(7)	0.246(1)	0.8478(4)	8.3(6)
C18	0.6522(6)	0.081(1)	0.8547(5)	8.0(6)
C19	0.6316(4)	0.063(1)	0.9238(5)	6.1(4)
C20	0.6263(5)	0.136(1)	1.0736(4)	5.5(4)
C21	0.6038(5)	0.226(1)	1.1382(4)	5.3(4)
C22	0.5538(4)	0.5807(9)	1.0956(3)	3.7(3)

Table A20.3 Intramolecular Distances Involving the Non-Hydrogen Atoms for TOMB-F2, (52).

atom-atom	distance (Å)	atom-atom	distance (Å)
Fe1-C10	2.056(6)	C5-C6	1.376(8)
Fe1-C11	2.030(6)	C6-C7	1.509(8)
Fe1-C12	2.012(6)	C8-C9	1.497(8)
Fe1-C13	2.030(7)	C10-C11	1.417(8)
Fe1-C14	2.026(6)	C10-C14	1.413(8)
Fe1-C15	2.055(7)	C11-C12	1.437(9)
Fe1-C16	2.038(7)	C12-C13	1.38(1)
Fe1-C17	2.029(8)	C13-C14	1.406(9)
Fe1-C18	2.017(7)	C15-C16	1.398(9)
Fe1-C19	2.024(6)	C15-C19	1.430(9)
S1-C7	1.813(6)	C16-C17	1.41(1)
S1-C8	1.797(7)	C17-C18	1.39(1)
S2-C21	1.799(7)	C1-C6	1.406(7)
S2-C22	1.811(6)	C2-C3	1.382(7)
O1-C9	1.432(7)	C2-C22	1.510(7)
O1-C10	1.363(7)	C3-C4	1.383(8)
O2-C15	1.342(7)	C4-C5	1.387(8)
O2-C20	1.452(8)	C18-C19	1.40(1)
C1-C2	1.381(7)	C20-C21	1.479(9)

Table A20.4 Intramolecular Bond Angles Involving the Non-Hydrogen Atoms for TOMB-F2, (52).

linkage	angle (°)	linkage	angle (°)
C10-Fe1-C11	40.6(2)	C13-Fe1-C16	167.8(4)
C10-Fe1-C12	68.5(3)	C13-Fe1-C17	129.0(3)
C10-Fe1-C13	68.1(3)	C13-Fe1-C18	108.2(3)
C10-Fe1-C14	40.5(2)	C13-Fe1-C19	117.5(3)
C10-Fe1-C15	106.4(3)	C14-Fe1-C15	116.6(3)
C10-Fe1-C16	119.0(3)	C14-Fe1-C16	151.1(3)
C10-Fe1-C17	153.8(4)	C14-Fe1-C17	165.3(4)
C10-Fe1-C18	163.8(4)	C14-Fe1-C18	126.6(4)
C10-Fe1-C19	125.7(3)	C14-Fe1-C19	105.8(3)
C11-Fe1-C12	41.6(3)	C15-Fe1-C16	39.9(3)
C11-Fe1-C13	68.7(3)	C15-Fe1-C17	68.4(3)
C11-Fe1-C14	68.5(3)	C15-Fe1-C18	68.7(3)
C11-Fe1-C15	126.7(3)	C15-Fe1-C19	41.0(3)
C11-Fe1-C16	109.5(3)	C16-Fe1-C17	40.6(3)
C11-Fe1-C17	120.9(4)	C16-Fe1-C18	67.8(3)
C11-Fe1-C18	154.5(4)	C16-Fe1-C19	67.7(3)
C11-Fe1-C19	164.0(3)	C17-Fe1-C18	40.3(4)
C12-Fe1-C13	39.9(3)	C17-Fe1-C19	68.1(4)
C12-Fe1-C14	68.0(3)	C18-Fe1-C19	40.7(3)
C12-Fe1-C15	166.8(3)	C7-S1-C8	102.5(3)
C12-Fe1-C16	130.9(4)	C21-S2-C22	102.5(3)
C12-Fe1-C17	110.6(4)	C9-O1-C10	116.4(5)
C12-Fe1-C18	119.6(3)	C15-O2-C20	116.8(6)
C12-Fe1-C19	151.8(3)	C2-C1-C6	121.4(6)
C13-Fe1-C14	40.6(2)	O1-C9-C8	107.6(5)
C13-Fe1-C15	150.9(3)	Fe1-C10-C14	68.6(3)
C1-C2-C3	118.9(5)	C11-C10-C14	107.6(6)
C1-C2-C22	120.2(5)	Fe1-C11-C10	70.7(3)
C3-C2-C22	120.9(5)	Fe1-C11-C12	68.5(4)
C2-C3-C4	120.0(6)	C16-C17-C18	107.5(9)
C3-C4-C5	121.1(6)	C17-C18-C19	108.5(8)
Fe1-C10-O1	128.4(4)	C15-C19-C18	108.3(8)

Fe1-C10-C11	68.7(4)	O2-C20-C21	108.6(6)
C4-C5-C6	119.6(6)	Fe1-C14-C13	69.9(4)
O1-C10-C11	128.9(7)	C10-C14-C13	108.6(6)
O1-C10-C14	123.4(6)	Fe1-C19-C15	70.7(4)
C1-C6-C5	119.0(5)	Fe1-C19-C18	69.4(4)
C1-C6-C7	120.4(6)	Fe1-C15-O2	129.9(4)
C5-C6-C7	120.6(6)	Fe1-C15-C16	69.4(4)
S1-C7-C6	116.3(4)	Fe1-C15-C19	68.3(4)
C10-C11-C12	106.7(7)	O2-C15-C16	122.4(7)
Fe1-C12-C11	69.9(4)	O2-C15-C19	131.2(8)
Fe1-C12-C13	70.8(4)	C16-C15-C19	106.3(7)
S1-C8-C9	113.9(5)	Fe1-C16-C15	70.7(4)
C11-C12-C13	108.8(6)	Fe1-C16-C17	69.3(4)
Fe1-C13-C12	69.3(4)	C15-C16-C17	109.5(8)
Fe1-C13-C14	69.6(4)	S2-C21-C20	115.5(5)
C12-C13-C14	108.3(7)	Fe1-C17-C16	70.1(4)
Fe1-C18-C17	70.3(5)	Fe1-C17-C18	69.4(5)
Fe1-C18-C19	69.9(4)	S2-C22-C2	113.4(4)
Fe1-C14-C10	70.9(4)		

References

1. C. J. Pederson, *J. Am. Chem. Soc.*, **1967**, 89, 7017.

2. a) N. F. Curtis, *J. Chem. Soc.*, 4409, (1960). b) N. F. Curtis, Y. M. Curtis, H. K. J. Powell, *J. Chem. Soc. A*, 1015, (1966). c) G. A. Melson, D. H. Busch, *J. Am. Chem. Soc.*, **1965**, 87, 1706. d) M. C. Thompson, D. H. Busch, *J. Am. Chem. Soc.*, **1964**, 86, 3651.

3. C. J. Pederesen, *Angew. Chem. Int. Ed. Engl.*, 27, 1021, **1988**.

4. D. J. Cram, *Angew. Chem. Int. Ed. Engl.*, 27, 1009, **1988**.

5. J. M. Lehn, *Angew. Chem. Int. Ed. Engl.*, 27, 89, **1988**.

6. George W. Gokel, *Crown Ethers and Cryptands*, The Royal Society of Chemistry, Cambridge, 1991, p6.

7. F. L. Cook, T. C. Caruso, M. P. Byrne, C. W. Bowers, D. H. Speck, C. L. Liotta, *Tetrahedron Lett.*, 4029, (1974).

8. R. N. Greene, *Tetrahedron Lett.*, **1972**, 1793.

9. L. Mandolini, B. Masci, *J. Am. Chem. Soc.*, **1984**, 106, 168

10. J. M. Lehn, S. H. Pine, E. Watanabe, A. K. Willard, *J. Am. Chem. Soc.*, **1977**, 99, 6766.

11. J. M. Lehn, *Acc. Chem. Res.*, **1978**, 11, 49.

12. L. F. Lindoy, *The Chemistry of Macrocyclic Complexes*, Cambridge University Press, Cambridge, 1989, pp 140-143.

13. J. M. Timko, S. S. Moore, D. M. Walba, P. C. Hiberty, D. J. Cram, *J. Am. Chem. Soc.*, **1977**, 99, 4207.

14. D. J. Cram, T. Kaneda, R. C. Helgeson, G. M. Lein, *J. Am. Chem. Soc.*, **1979**, 101, 4987.

15. J. R. Moran, S. Karbach, D. J. Cram, *J. Am. Chem. Soc.*, **1982**, 104, 5826.

16. D. J. Cram, I. B. Dicker, G. M. Lein, C. B. Knobler, K. N. Trueblood, *J. Am. Chem. Soc.*, **1982**, 104, 6827.

17. D. B. Gutsche, B. Dhawan, K. H. No, R. Muthukrishan, *J. Am. Chem. Soc.*, **1981**, 103, 3872.

18. D. B. Gutsche, J. A. Levine, *J. Am. Chem. Soc.*, **1982**, 104, 2652.

19. R. A. Schultz, D. M. Dishong, G. W. Gokel, *J. Am. Chem. Soc.*, **1982**, 104, 625.

20. G. W. Gokel, *Chem. Soc. Rev.*, **1992**, 21, 39.

21. (a) F. N. Diederich, in *Cyclophanes*, Royal Society of Chemistry, 1991. (b) K. Odashima, A. Itai, Y. Itaka, K. Koga, *J. Org. Chem.*, **1985**, 50, 4478. (c) C. Kreiger, F. N. Diederich, *Chem. Ber.*, **1985**, 118, 3620. (d) S. B. Smithrud, T. B. Wyman, F. N. Diederich, *J. Am. Chem. Soc.* **1991**, 113, 5420. (e) D. A. Dougherty, D. A. Stauffer, *Science*, **1990**, 250, 1558.

22. H. Stetter, E. E. Ross, *Chemische Berichte*, **1955**, 88, 1390.

23. G. Faust, M. Pallas, *Journal fur Praktische*, **1960**, 11, 146.

24. D. H. Busch, *Acc. Chem. Res.*, **1978**, 11, 392, and references therein.

25. W. Rosen, D. H. Busch, *J. Am. Chem. Soc.*, **1969**, 91, 4694.

26. K. Travis, D. H. Busch, *Inorganic Chenistry*, **1974**, 13, 2591.

27. D. Gerber, P. Chongsawangvirod, A. K. Leung, L. A. Ochrymowycz, *J. Org. Chem.*, **1977**, 42, 2644.

28. a) J. Buter, R. M. Kellog, *J. Org. Chem.*, **1981**, 46, 4481. b) J. Buter, R. M. Kellog, *Org. Synth.*, **1987**, 65, 150.

29. G. Dijkstra, W. H. Kruzinga, R. M. Kellog, *J. Org. Chem.*, **1987**, 52, 4230.

30. a) J. Dale, *Acta Chem. Scand.*, **1973**, 27, 1115. b) J. Dale, *Isr. J. Chem.*, **1980**, 20, 3, and references therein.

31. R. E. Wolf Jr., J. R. Hartman, J. M. E. Storey, B. M. Foxman, S. R. Cooper, *J. Am. Chem. Soc.*, **1987**, 109, 4328, and references therein.

32. R. E. DeSimmone, M. E. Glick, *J. Am. Chem. Soc.*, **1976**, 98, 762.

33. S. G. Murray, F. R. Hartley, *Chem. Rev.*, **1981**, 81, 365.

34. C. A. McAuliffe, W. Levason, *Phosphine, Arsine and Stibene Complexes of Transition Elements*, Elsevier, Amsterdam, 1979.

35. A. J. Blake, M. Schröder, *Advances in Inorganic Chemistry*, **1990**, 34, 1.

36. S. R. Cooper, S. C. Rawle, *Strucutre and Bonding*, **1990**, 72, 1.

37. a) H. Beinert, *Coord. Chem. Rev.*, **1980**, 33, 55. b) P. M. Colman, H. C. Freeman, J. M. Guss, M. Murata, V. A. Norris, J. A. M. Ramshaw, M. P. Venkatappa, *Nature*, **1978**, 272, 319. c) E. T. Adman, R. E. Stenkamp, L.

C. Sieker, L. H. Jensen, *J. Mol. Biol.*, **1978**, 123, 35. d) G. E. Norris, B. F. Anderson, E. N. Baker, *J. Mol. Biol.*, **1983**, 165, 501.

38. F. A. Cotton, G. Wilkinson, *Advanced Inorganic Chemistry, 4th Ed.*, Wiley-Interscience, Toronto, 1980, p71.

39. a) D. K. Cabbiness, D. W. Margerum, *J. Am. Chem. Soc.*, **1969**, 92, 2151. b) D. K. Cabbiness, D. W. Margerum, *J. Am. Chem. Soc.*, **1969**, 92, 6540.

40. a) L. L. Diaddario, L. L. Zimmer, T. E. Jones, L. S. W. L. Sokol, R. B. Cruz, E. L. Yee, L. A. Ochrymowycz, D. B. Rorabacher, *J. Am. Chem. Soc.*, **1979**, 101, 3511. b) L. S. W. L. Sokol, L. A. Ochrymowycz, D. B. Rorabacher, *Inorganic Chemistry*, **1981**, 20, 3189.

41. a) A. Z. Werner, *Anorg. Chemie.*, **1893**, 3, 267. b) G. B. Kauffman, *Classics in Coordination Chemistry, Part 1: The Selected Papers of Alfred Werner*, Dover, New York, 1968, p. 9-88. c) G. B. Kauffman, *Alfred Werner, Founder of Coordination Chemistry*, Springer Verlag, Berlin, 1966. d) J. Bjerrum, in *Werner Centennial , Advances in Chemistry Series No. 62*, ed. G. B. Kauffman, ACS, Washington D.C. 1967, pp. 178. e) M. T. Beck, *Coord. Chem. Rev.*, **1968**, 3, 91. f) Y. A. Makashev and V. E. Moronov, *Russ. Chem. Rev.*, **1980**, 49, 631.

42. H. M. Colquhoun, J. F. Stoddart, D. J. Williams, *Angew. Chem. Int. Ed. Engl.*, **1986**, 25, 487.

43. a) H. M. Colquhoun, J. F. Stoddart and D. J. Williams, *J. Chem. Soc., Chem. Commun.*, **1981**, 847. b) H. M. Colquhoun, D. F. Lewis, J. F. Stoddart and D. J. Williams, *J. Chem. Soc., Dalton Trans.*, **1983**, 607.

44. D. R. Alston, J. F. Stoddart and D. J. Williams, *J. Chem. Soc., Chem. Commun.*, **1985**, 532.

45. a) H. M. Colquhoun, S. M. Doughty, J. F. Stoddart and D. J. Williams, *Angew. Chem., Int. Ed. Engl.*, **1984**, 23, 235. b) H. M. Colquhoun, S. M. Doughty, J. F. Stoddart, A. M. Z. Slawin and D. J. Williams, *J. Chem. Soc., Dalton Trans.*, **1986**, 1639.

46. a) H. M. Colquhoun, J. F. Stoddart, D. J. Williams J. B. Westenholme and R. Zarzycki, *Angew. Chem., Int. Ed. Engl.*, **1981**, 20, 1051. b) H. M. Colquhoun, S. M. Doughty, J. M. Maud, J. F. Stoddart, D. J. Williams and J. B. Wolstenholme, *Isr. J. Chem.*, **1985**, 25, 15.

47. B. L. Allwood, H. M. Colquhoun, S. M. Doughty, F. H. Kohnke, A. M. Z. Slawin, J. F. Stoddart, D. J. Williams and R. Zarzycki, *J. Chem. Soc., Chem. Commun.*, **1987**, 1054.

48. D. R. Alston, A. M. Z. Slawin, J. F. Stoddart, D. J. Williams, *Angew. Chem., Int. Ed. Engl.*, **1984**, 23, 821.

49. a) D. R. Alston, Ph.D. thesis, The University of Sheffield, U.K. 1985. b) D. R. Alston, A. M. Z. Slawin, J. F. Stoddart and D. J. Williams, *Angew. Chem., Int. Ed. Engl.*, **1984**, 23, 821.

50. a) N. W. Alcock, J. M. Brown, J. C. Jeffery, *J. Chem. Soc., Chem Commun.*, **1974**, 829 b) N. W. Alcock, J. M. Brown, J. C. Jeffery, *J. Chem. Soc., Dalton Trans.*, **1976**, 583. c) N. W. Alcock, J. M. Brown, J. C. Jeffery, *J. Chem. Soc., Dalton Trans.*, **1977**, 888.

51. J. Rebek Jr., *Angew. Chem., Int. Ed. Engl.*, **1990**, 29, 245.

52. (a) Hamilton, A. D. *Advances in Supramolecular Chemistry, Vol1*, G. Gokel, Ed., Jai Press, Greenwich, 1990, 1. (b) B. J. Whitlock, W. H. Whitlock, *J. Am. Chem. Soc.*, **1990**, 112, 3910. (c) K. Chapman, W. C. Still, *J. Am. Chem. Soc.*, **1989**, 111, 3075. (d) Y. Tanaka, Y. Kato, Y. Aoyama, *J. Am. Chem. Soc.*, **1990**, 112, 2807. (e) F. Garcia-Tellado, S. Goswami, S. K. Chang, S. Geib, A. D. Hamilton, *J. Am. Chem. Soc.*, **1990**, 112, 7393. (f) T. R. Kelley, M. P. Maguire, *J. Am. Chem. Soc.*, **1987**, 109, 6549. (g) V. Hegde, J. D. Madhukar, R. P. Thimmel, *J. Am. Chem. Soc.*, **1990**, 112, 4549. (h) K. S. Jeong, T. Tjivikua, A. Muehldorf, G. Deslongchamps, M. Famulok, J. Rebek Jr., *J. Am. Chem. Soc.*, **1991**, 113, 201. (i) M. Gallent, M. T. P. Viet, J. D. Wuest, *J. Org. Chem.*, **1991**, 56, 2284. (j) T. W. Bell, J. Liu, *J. Am. Chem. Soc.*, **1988**, 110, 3673. (k) A. M. Kelly-Rowley, L. A. Cabell, E. V. Anslyn, *J. Am. Chem. Soc.*, **1991**, 113, 9687. (l) A. D. Hamilton, D. J. van Engen, *J. Am. Chem. Soc.*, **1987**, 109, 5035. (m) J. C. Medina, C. Li, S. G. Bott, J. L. Atwood, G. W. Gokel, *J. Am. Chem. Soc.*, **1991**, 113, 366. (n) G. Deslongchamps, A. Galan, J. de Mendoza, J. Rebek Jr., *Angew.Chem., Int. Ed. Engl.*, **1992**, 31, 61. (o) J. E. Cochran, T. J. Parrot, B. J. Whitlock, H. W. Whitlock, *J. Am. Chem. Soc.*, **1992**, 114, 2269. (p) C. S. Wilcox, J. C. Adrain Jr., T. H. Webb, F. J. Zawacki, *J. Am. Chem. Soc.*, **1992**, 114, 10189 and references therein.

53. S. K. Chang, A. D. Hamilton, *J. Am. Chem. Soc.*, **1988**, 110, 1318.

54. J. E. Cochran, T. J. Parrot, B. J. Whitlock, H. W. Whitlock., *J. Am. Chem. Soc.*, **1992**, 114, 2269.

55. J. Rebek Jr., *Angew. Chem., Int. Ed. Engl.*, **1990**, 29, 245.

56. S. Goswami, A. D. Hamilton, D. J. van Engen, *J. Am. Chem. Soc.*, **1989**, 111, 3425.

57. R. P. Sijbesma, S. S. Wijmenga, R. J. M. Nolte, *J. Am. Chem. Soc.*, **1992**, 114, 9807.

58. (a) R. E. Sheridan, H. W. Whitlock, *J. Am. Chem. Soc.*, **1986**, 108, 7120. (b) K. M. Neder, H. W. Whitlock, *J. Am. Chem. Soc.*, **1990**, 112, 9412. (c) J. E. Cochran, T. J. Parrot, B. J. Whitlock, H. W. Whitlock, *J. Am. Chem. Soc.*, **1992**, 114, 2269.

59. (a) S. C. Zimmerman, Z. Zeng, W. Wu, D. E. Reichert, *J. Am. Chem. Soc.*, **1991**, 113, 183. (b) S. C. Zimmerman, Z. Zeng, W. Wu, *J. Am. Chem. Soc.*, **1991**, 113, 196.

60. B. de Groot, G. S. Hanan, S. J. Loeb, *Inorg. Chem.*, **1991**, 30, 4644.

61. G. R. Giesbrecht, G. S. Hanan, J. E. Kickham, S. J. Loeb, *Inorg. Chem.*, **1992**, 31, 3286.

62. a) P. R. Markies, T. Nomoto, G. Schat, O. S. Akkerman, F. Bickelhaupt, *Organometallics*, **1991**, 10, 3826. b) P. R. Markies, O. S. Akkerman, F. Bickelhaupt, W. J. J. Smeets, A. L. Spek, *J. Am. Chem. Soc.*, **1988**, 110, 4284.

63. P. R. Markies, A. Villena, O. S. Akkerman, F. Bickelhaupt, W. J. J. Smeets, A. L. Spek, *J. Organomet. Chem.*, **1993**, 463, 7.

64. a) J. A. M. van Beek, G. van Koten, W. J, J, Smeets, A. L. Spek, *J. Am Chem. Soc.*, **1986**, 108, 5010. b) J. Terheijden, G. van Koten, W. P. Mul, D. J. Stufkens, *Organometallics*, **1986**, 5, 519. c) D. M. Grove, G. van Koten, H. J. C. Ubbels, R. Zoet, *Organometallics*, **1984**, 3, 1003. d) J. A. M. van Beek, G. van Koten, M. J. Ramp, N. C. Coenjaarts, D. M. Grove, K. Goubitz, M. C. Zoutberg, C. H. Stam, W. J. J. Smeets, A. L. Spek, *Inorg. Chem.*, **1991**, 30, 3059. e) A. F. M. J. van der Ploeg, G. van Koten, K. Vrieze, *Inorg. Chim. Acta.*, **1982**, 58, 35.

65. J. Terheijden, G van Koten, J. A. M. van Beek, B. K. Vriesema, R. M. Kellogg, M. C. Zoutberg, C. H. Stam, *Organometallics*, **1987**, 6, 89.

66. A. de Koster, J. A. Kanters, A. L. Spek, A. A. H. van der Zeijden, G. van Koten, K. Vrieze, *Acta. Cryst.*, **1985**, C41, 893.

67. G. van Koten, J. T. B. H. Jastrzebski, J. G. Noltes, A. L. Spek, J. C. Schoone, *J. Organomet. Chem.*, **1978**, 148, 233.

68. a) A. F. M. J. van der Ploeg, G. van Koten, K. Vrieze, *J. Organomet. Chem.*, **1981**, 222, 155 b) D. M. Grove, G. van Koten, J. N. Louwen, J. G. Noltes, A. L. Spek, H. J. C. Ubbels, *J. Am. Chem. Soc.*, **1982**, 104, 6609.

69. G. van Koten, *Pure & Appl. Chem.*, **1989**, 61, 1681.

70. C. J. Moulton, B. L. Shaw, *J. Chem. Soc., Dalton Trans.*, **1976**, 1020.

71. a) H. Rimml, L. M. Venanzi, *J. Organomet. Chem.*, **1983**, C6, 259. b) H. Rimml, L. M. Venanzi, *J. Organomet. Chem.*, **1984**, C52, 260.

72. A. Jouaiti, M. Geoffroy, G. Terron, G. Bernardinelli, *J. Chem. Soc., Chem. Commun.*, **1992**, 155.

73. J. Dupont, N. Beydoun, M. Pfeffer, *J. Chem. Soc., Dalton Trans.*, **1989**, 1715.

74. J. Dupont, M. Pfeffer, *J. Chem. Soc., Dalton Trans.*, **1990**, 3193.

75. J. Errington, W. S. McDonald, B. L. Shaw, *J. Chem. Soc., Dalton Trans.*, **1980**, 2312.

76. a) G. S. Hanan, J. E. Kickham, and S. J. Loeb. *J. Chem. Soc., Chem. Commun.*, **1991**, 893-895. b) G. S. Hanan, J. E. Kickham, S. J. Loeb, *Organometallics*, **1992**, 11, 3063.

77. J. A. M. van Beek, G. van Koten. I. C. M. Wehman-Ooyevaar, W. J. J. Smeets, P. van der Sluis, A. L. Spek, *J. Chem. Soc., Dalton Trans.*, **1991**, 883.

78. S. Chattopadhyay, C. Sinha, P. Basu, A. Chakravorty, *Organometallics*, **1991**, 10, 1135, and references therein.

79. H. C. Clark, L. E. Manzer, *J. Organomet. Chem.*, **1973**, 59, 411.

80. a) W. Rosen. D. H. Busch, *Inorg. Chem.*, **1970**, 9, 262. b) J. R. Mansfield, *M.Sc. Thesis*, University of Manitoba, 1990.

81. S. C. Rawle, G. A. Admans, S. R. Cooper, *J. Chem. Soc., Dalton Trans.*, **1988**, 93

82. TEXSAN-TEXRAY Structure Analysis Package, Molecular Structure Corp., 1985.

83. D. T. Cromer, J. T. Waber, *International Tables for X-ray Crystallography, Vol 4*, Kynock Press, Birmingham, U. K., 1974, Table 2.2a.

84. a) J. A. Ibers, W. C. Hamilton, *Acta Crystallogr., Sect. A*, **1974**, 17, 781. b) D. T. Cromer, J. T. Waber, *International Tables for X-ray Crystallography, Vol 4*, Kynock Press, Birmingham, U. K., 1974, Table 2.3.1.

85. a) B. D. Groot, S. J. Loeb, *Inorg. Chem.*, **1990**, 29, 4084. b) J. M. Desper, D. R. Powell, S. H. Gellman, *J. Am. Chem. Soc.*, **1990**, 112, 4321. c) E. Jurasti, *J. Chem. Ed.*, **1978**, 56, 438, and references therein.

86. S. R. Cooper, Acc. Chem. Res. **1988**, 21, 141.

87. H. Günther, *NMR Spectroscopy*, Wiley, New York, **1985**.

88. G. W. Parshall, S. D. Ittel, *Homogeneous Catalysis, 2nd Ed.*, Wiley-Interscience, New York, **1992**, p166-168.

89. F. A. Cotton, G. Wilkinson, *Advanced Inorganic Chemistry, 4th Ed.*, Wilet-Interscience, Toronto, **1980**, pp87-88.

90. a) N. K. Dalley, J. S. Smith, S. B. Larson, K. L. Matheson, J. J. Chistensen, R. M. Izatt, *J. Chem. Soc., Chem. Commun.*, **1975**, 85. b) N. K. Dalley, J. S. Smith, S. B. Larson, K. L. Matheson, J. J. Chistensen, R. M. Izatt, *J. Heterocycli Chem.*, **1981**, 18, 463. c) C8* is related to C8 by a mirror plane, the * indicates symmetry related atoms.

91. a) C. Crawford, J. Matonic, W. Strieb, J. Huffman, K. Dunbar, G. Christou, *Inorg. Chem.*, **1993**, 32, 3125, and references therein. b) K. Aoki, M. Inaba, S. Teratani, H. Yamazaki, Y. Miyashita, *Inorg. Chem.*, **1994**, 33, 3018, and references therein.

92. a) Y. Aoyama, A. Yamagishi, M. Asagawa, H. Toj, H. Ogoshi, J. Am. Chem. Soc., 1988, 110, 4076. b) T. Mizutani, T. Ema, T. Yoshida, Y. Kuroda, H. Ogoshi, *Inorg. Chem.*, **1993**, 32, 2072, and references therein. c) Y. Kuroda, Y. Kato, T. Higashoiji, H. Ogoshi, *Angew. Chem., Int. Ed. Engl.*, **1993**, 32, 723, and references therein.

93. M. Shionoya, T. Ikeda, E. Kimura, M. Shiro, *J. Am. Chem. Soc.*, **1994**, 116, 3848, and references therein.

94. a) M. Reetz, C. Niemeyer, M. Hermes, R. Goddard, *Angew. Chem., Int. Ed. Engl.*, **1992**, 31, 1017. b) M. Reetz, C. Niemeyer, K. Harms, *Angew. Chem. Int. Ed. Engl.*, **1991**, 30, 1472. c) M. Reetz, C. Niemeyer, K. Harms, *Angew. Chem., Int. Ed. Engl.*, **1991**, 30, 1474.

95. a) C. van Staveren, J. van Eerden, F. van Veggel, S. Harkema and D. Reinhoudt, *J. Am. Chem. Soc.*, 1988, 110, 4995. b) D. Rudkevich, Z. Brzozka, M. Palys, H. Visser, W. Verboom, D. Reinhoudt, *Angew. Chem., Int. Ed. Engl.*, **1994**, 33, 467. c) F. van Veggel, M. Bos, S. Harkema, W. Verboom, D. Reinhoudt, *Angew. Chem., Int. Ed. Engl.*, **1989**, 29, 746. d) C.van Staveren, D. Reinhoudt, J. van Eerden, S. Harkema, *J. Chem. Soc., Chem. Commun.*, **1987**, 974. e) C. van Staveren, D. Reinhoudt, D. Fenton, J. van Eerden, S. Harkema, *J. Am. Chem. Soc.*, **1987**, 109, 3456. f) D. Rudkevich, W. Stauthamer, W. Verboom, J. Engbersen, S. Harkema, D. Reinhoudt, *J. Am. Chem. Soc.*, **1992**, 114, 9671.

96. a) A. Carroy, J. M. Lehn, *J. Chem. Soc., Chem Commun.*, **1986**, 1232. b) D. Parker, *J. Chem. Soc., Chem. Commun.*, **1985**, 1129.

97. a) W. Wieder, R. Nätscher, F. Vögtle, *Liebigs Ann. Chem.*, **1976**, 924. b) F. Vögtle, J. Grütze, R. Nätscher, W. Wieder, E. Weber, R. Grun, *Chem. Ber.*, **1975**, 108, 1694. c) E. Weber, F. Vögtle, *Chem. Ber.*, **1976**, 109, 1803. d) F. Vögtle, E. Weber, *Angew. Chem., Int. Ed. Engl.*, **1974**, 13, 149. e) E. Weber, W. Wieder, F. Vögtle, *Chem. Ber.*, **1976**, 109, 1002.

98. J. E. Kickham, S. J. Loeb, S. L. Murphy, *J. Am. Chem. Soc.*, **1993**, 115, 7031.

99. J. E. Kickham, S. J. Loeb, S. L. Murphy, *Inorg. Chem.*, **1995**, manuscript in preparation.

100. Y. Angus, M. Gross, M. Labarelle, R. Louis, B. Metz, *J. Chem. Soc., Chem. Commun.*, **1994**, 939.

101. J. E. Kickham, S. J. Loeb, *Inorg. Chem.*, **1994**, 33, 4351.

102. M. Sato, K. Suzuki, H. Asano, M. Sekino, Y. Kawata, Y. Habata, S. Akabori, *J. Organomet. Chem.*, **1994**, 470, 263.

103. H. Murakami, S. Shinkai, *J. Chem. Soc., Chem. Commun.*, **1993**, 1533.

104. M. W. Hosseini, A. J. Blacker, J. M. Lehn, *J. Am. Chem. Soc.*, **1990**, 112, 3896.

105. S. Mallik, R. D. Johnson, F. H. Arnold, *J. Am. Chem. Soc.*, **1993**, 115, 2518.

106. K. Hamasaki, H. Ikeda, A. Nakamura, A. Veno, F. Toda, I. Suzuki, T. Osa, *J. Am. Chem. Soc.*, **1993**, 115, 5035.

107. C. Y. Hung, T. Hopfner, R. P. Thummel, *J. Am. Chem. Soc.*, **1993**, 115, 12601.

108. J. Rosengaus, I. Willner, *J. Chem. Soc., Chem. Commun.*, **1993**, 1044.

109. a) B. T. Khan, S. Shamsuddin, K. Venkatasubramanian, *Polyhedron*, **1992**, 11, 6, 671. b) M. Krumm, E. Zangrando, L. Randaccio, S. Menzer, B. Lippert, *Inorg. Chem.*, **1993**, 32, 700. c) U. Frey, J. D. Ranford, P. J. Saddler, *Inorg. Chem.*, **1993**, 32, 1333. d) S. E. Sherman, D. Gibson, A. H. J. Wang, S. J. Lippard, *J. Am. Chem. Soc.*, **1988**, 110, 7368.

110. a) V. M. L. J. Aarts, C. J. van Staveren, P. D. J. Grootenhuis, J. van Eerden, L. Kruise, S. Harkema, D. N. Reinhoudt, *J. Am. Chem. Soc.*, **1986**, 108, 5035. b) A. R. van Dorn, M. Bos, S. Harkema, J. van Eerden, W. Verboom, D. N. Reinhoudt, *J. Org. Chem.*, **1991**, 56, 2371.

111. D. N. Reinhoudt, A. R. van Doorn, W. Verboom, *J. Coord. Chem.*, **1992**, 27, 91.

112. T. Mizutani, T. Ema, T. Yoshida, T. Renne, H. Ogoshi, *Inorg. Chem.*, **1994**, 33, 3358.

113. a) J. R. Rubin, T. P. Harmony, M. Sundaralingam, *Acta. Cryst.*, **1991**, C47, 1712. b) K. Aoki, H. Yamazaki, *J. Chem. Soc., Chem. Commun.*, **1980**, 186. c) K. Aoki, M. Hoshino, T. Okada, H. Yamazaki, H Sekizawa, *J. Chem. Soc., Chem. Commun.*, **1986**, 314.

114. K. Aoki, H. Yamazaki, *J. Am. Chem. Soc.*, **1984**, 100, 3691.

115. T. Sorrel, L. Epps, T. J. Kistenmacher, L. Marzilli, *J. Am Chem. Soc.*, **1977**, 97, 2173.

116. O. F. Schall, G. W. Gokel, *J. Am. Chem. Soc.*, **1994**, 116, 6089.

117. C. M. Browne, G. Ferguson, M. A. McKervey, D. L. Mullholland, T. O'Connor, M. Parvez, *J. Am. Chem. Soc.*, **1985**, 107, 2703.

118. L. Mendez, R. Singleton, A. M. Z. Slawin, J. F. Stoddart, D. J. Williams, M. K. Williams, *Angew. Chem., Int. Ed. Engl.*, **1992**, 31, 478.

119. a) J. S. Bradshaw, P. Huszthy, C. W. McDaniel, M. Oue, C. Y. Zhu, R. M. Izatt, *J. Coord. Chem.*, **1992**, 27, 105. b) I.-H. Chu, D. V. Dearden, J. S. Bradshaw, P. Huszthy, R. M. Izatt, *J. Am. Chem. Soc.*, **1993**, 115, 4318.

120. a) R. B. Silverman, D. Dolphin, T. J. Carty, E. K. Krodel, R. H. Abeles, *J. Am. Chem. Soc.*, **1974**, 99, 7097. b) E. P. Kyba, R. C. Helgeson, K. Madam, G. W. Gokel, T. L. Tarnowski, S. S. Moore, D. J. Cram, *J. Am. Chem. Soc.*, **1977**, 99, 2564. c) J. M. Timko, S. S. Moore, D. M. Walba, P. C. Hiberty, D. J. Cram, *J. Am. Chem. Soc.*, **1977**, 99, 4207. d) M. Newcomb, J. M. Timko, D. M. Walba, D. J. Cram., *J. Am. Chem. Soc.*, **1977**, 99, 6392. e) S. S. Moore, T. L. Tarnowski, M. Newcomb, D. J. Cram., *J. Am. Chem. Soc.*, **1977**, 99, 6398. f) M. Newcomb, S. S. Moore, D. J. Cram., *J. Am. Chem. Soc.*, **1977**, 99, 6405.

121. U. ayerbach, C. Stokheim, T. Weyhermuller, K. Wieghardt, *Angew. Chem., Int. Ed. Engl.*, **1993**, 32, 5, 714.

122. M. D. Todd, Y. Dong, J. Horney, D. I. Yoon, J. T. Hupp, *Inorg. Chem.*, **1993**, 32, 2001, and references therein.

123. H. M. Colquhoun, S. M. Doughty, D. J. Williams, *Angew. Chem., Int. Ed. Engl.*, **1985**, 24, 2, 135.

124. a) E. A. Griffith, E. L. Amma, *J. Am. Chem. Soc.*, **1971**, 93, 3169. b) J. L. Pierre, P. Baret, P. Chautemps, M. Armand, *J. Am. Chem. Soc.*, **1981**, 103, 2986. c) H. C. Kang, A. W. Hanson, B. Eaton, V. Boekelheide, *J. Am. Chem. Soc.*, **1985**, 107, 1979. d) J. E. Gano, G. Subramaniam, R. Burnbaum, *J. Org. Chem.*, **1990**, 55, 4760. e) W. Xu, R. J. Puddephatt, K. W. Muir, A. A. Torabi, *Organometallics*, **1994**, 13, 3054.

125. a) J. Kuyper, P. I. van Vliet, K. Vrieze, *J. Organomet. Chem.*, **1975**, 96, 289. b) J. Kuyper, P. I. van Vliet, K. Vrieze, *J. Organomet. Chem.*, **1976**, 105, 379. c) J. Kuyper, K. Vrieze, *J. Organomet. Chem.*, **1976**, 107, 129. d) P. I. van Vliet, K. Vrieze, *J. Organomet. Chem.*, **1977**, 139, 337.

126. a) P. I. van Vliet, G. van Koten, K. Vrieze, *J. Organomet. Chem.*, **1979**, 182, 105. b) A. F. M. J. van der Ploeg, G. van Koten, K. Vrieze, *Inorg. Chem.*, **1982**, 21, 2026. c) J. Terheijden, G. van Koten, I. C. Vinke, A. L. Spek, *J. Am. Chem. Soc.*, **1985**, 107, 2891.

127. J. E. Kickham, S. J. Loeb, *J. Chem. Soc., Chem. Commun.*, **1993**, 1848.

128. The ^{1}H NMR of NH_3 in CD_3CN was recorded at room temperature as a reference.

129. R. T. Morrison, R. N. Boyd, *Organic Chemistry, 5th Ed.*, Allyn & Bacon Inc., Toronto, **1987**, pp 229-232.

130. F. A. Cotton, G. Wilkinson, *Advanced Inorganic Chemistry, 4th Ed.*, Wiley-Interscience, Toronto, **1980**, pp 1152-1156.

131. a) M. Rosenblum, *Chemistry of the Iron Group Metallocenes*, Part 1, Wiley-Interscience, New York, 1965. b) D. E. Bublitz, K. -L. Rinehard, *Org. React.*, **1969**, 17, 1. c) W. E. Watts, in *Comprehensive Organometallic Chemistry*, G. Wilkinson, F. G. A. Stone, E. W. Abel, eds. Permagon, Oxford, **1982**, Vol 8, p 1013.

132. R. T. Morrison, R. N. Boyd, *Organic Chemistry, 5th Ed.*, Allyn & Bacon Inc., Toronto, **1987**, pp 501-504

133. J. F. Biernat, T. Wilczewski, *Tetrahedron*, **1980**, 36, 2521.

134. T. Saji, *Chem. Lett.*, **1986**, 275.

135. a) P. D. Beer, *Adv. Inorg. Chem.*, **1992**, 39, 79 and references therein. b) P. D. Beer, H. Sikanyika, A. M. Z. Slaivin, D. J. Williams, *Polyhedron*, **1989**, 8, 879. c) P. D. Beer, H. Sikanyika, *Polyhedron*, **1990**, 9, 1091. d) P. D. Beer, Z. Chen, M. Drew, J. Kingston, M. Ogden, P. Spencer, *J. Chem. Soc., Chem. Commun.*, **1993**, 1046.

136. C. D. Hall, N. W. Sharpe, I. P. Danks, Y. P. Sang, *J. Chem. Soc., Chem. Commun.*, **1989**, 419.

137. a) J. C. Medina, T. T. Goodnow, S. Bott, J. L. Atwood, A. E. Kaifer, G. W. Gokel, *J. Chem. Soc., Chem. Commun.*, **1992**, 602. b) J. C. Medina, T. T. Goodnow, M. T. Rojas, J. L. Atwood, B. C. Lynn, A. E. Kaifer, G. W. Gokel, *J. Am. Chem. Soc.*, **1992**, 114, 10583.

138. a) M. Sato, H. Watanabe, S. Abine, S. Akabori, *Bull. Chem. Soc. Jpn.*, **1984**, 57, 1929. b) P. D. Beer, J. E. Nation, S. L. Brown, *J. Organomet. Chem.*, **1989**, 377, C23. c) C. D. Hall, I. P. Danks, N. W. Sharpe, *J. Organomet. Chem.*, **1990**, 390, 227. d) I. Bernal, G. M. Reisner, R. A. Bartsch, R. A. Holwerda, B. P. Czech, *Organometallics*, **1988**, 7, 247. e) R. A. Holwerda, T. W. Robison, R. A. Bartsch, B. P. Czech, *Organometallics*, **1991**, 10, 2652. f) B. Czech, A. Ratajczak, *Pol. J. Chem.* **1980**, 54, 767.

139. M. Sato, M. Katada, S. Nakashima, H. Sano, S Akabori, *J. Chem. Soc., Dalton Trans.*, **1990**, 1979.

140. a) M. Sato, M. Sekino, S. Akabori, *J. Organomet. Chem.*, **1988**, 344, C31-C34. b) M. Sato, K. Suzuki, H. Asano, M. Sekino, Y. Kawata, Y. Habata, S. Akabori, *J. Organomet. Chem.*, **1994**, 470, 263. c) M. Sato, M. Sekino, M. Katada, S. Akabori, *J. Organomet. Chem.*, **1989**, 377, 327. d) M. Sato, H. Asano, K. Suzuki, M. Katada, S. Akabori, *Bull. Chem. Soc. Jpn.*, **1989**, 62, 3828. e) M. Sato, K. Suzuki, S. Akabori, *Bull. Chem. Soc. Jpn.*, **1986**, 59, 3611.

141. F. C. J. M. van Veggel, W. Verboom, D. N. Reinhoudt, *Chemical Reviews.*, **1994**, 94, 279.

142. a) M. D. Rausch, D. J. Ciappenelli, *J. Organomet. Chem.*, **1967**, 10, 127. b) R. F. Kovar, M. D. Rausch, H. Rosenberg, *Organomet. in Chem. Syn.*, **1970/1971**, 1, 173.

143. a) S. Akabori, Y. Habata, Y. Sakamoto, M. Sato, *Bull. Chem. Soc. Jpn.*, **1983**, 56, 537. b) S. Akabori, Y. Habata, M. Sato, S. Ebine, *Bull. Chem. Soc. Jpn.*, **1983**, 56, 1461.

144. D. C. Harris, *Quantitative Chemical Analysis, 3rd Ed.*, W. H. Freeman & Co., New York, **1991**, AP34-AP43.

Curriculum Vitae: James Edward Kickham

Address:	9631 Ridge Rd., Windsor Ont. N8R-1G5
Birthplace:	Halifax, N. S.
Birthdate:	March 14, 1967
Citizenship:	Canadian
Marital Status:	Single
Education:	B. Sc., 1990, Honours Chemistry University of Windsor, Windsor, Ont., Canada, N9B-3P4
	Ph.D., 1994, Inorganic Chemistry University of Windsor, Windsor, Ont., Canada, N9B-3P4

Scholarships and Awards

University of Windsor Summer Research Scholarship, 04-94 to 08-94

Ontario Graduate Scholarship, 05-93 to 04-94

University of Windsor Tuition Scholarship, 05-93 to 04-94

University of Windsor Travel Grant, 09-92

Experience

Graduate Student, Inorganic Chemistry (Supervisor: Dr. S. J. Loeb), Dept. of Chemistry and Biochemistry, University of Windsor, Windsor, Ont., Canada. (1990-1994)

Teaching Assistant (Supervisor: David Hill), Introductory Chemistry, Introductory Organic Chemistry, Advanced Organic Chemistry. Dept of Chemistry and Biochemistry, University of Windsor, Windsor, Ont., Canada. (1990-1994)

4th year Research Project Student (Supervisor: Dr. Dennis G. Tuck), Inorganic Chemistry, University of Windsor, Windsor, Ont., Canada. (1989-1990)

Teaching Assistant (Supervisor: Dr. Keith Taylor), Introductory Organic Chemistry, (1989)

Journal Publications

1. James E. Kickham and Stephen J. Loeb "Simultaneous First and Second Sphere Coordination. Organopalladium Complexes as Receptors for o-Aminopyridine Derivatives." *Inorganic Chemistry*, **1994**, 33, 4351-4359

2. James E. Kickham and Stephen J. Loeb "Receptors For the Hydrazinium Ion. Simultaneous First and Second Sphere Coordination Inside Organopalladium Crownether Complexes." *Journal of the Chemical Society, Chemical Communications*, **1993**, 1848-1850.

3. James E. Kickham, Stephen J. Loeb, and Shannon L. Murphy "Molecular Recognition of Nucleobases Via Simultaneous First and Second Sphere Coordination." *Journal of the American Chemical Society*, **1993**, 115, 7031-7032

4. Garry S. Hanan, James E. Kickham, and Stephen J. Loeb "Metalation of the Crown Thioether Ligand 2,6,10-Trithia[11]-m-cyclophane, TT[11]MC. Synthesis, Structure and Reactivity of [Pt(TT[11]MC)][BF_4] and Structures of [Pt(PPh_2Me)(TT[11]MC)][BF_4] and [PtI_2(TT[11]MC)][BF_4]." *Organometallics*, **1992**, 11, 3063-3068.

5. Garth R. Giesbrecht, Garry S. Hanan, James E. Kickham, and Stephen J. Loeb "Thiacyclophanes Containing the -$S(CH_2)_3S(CH_2)_3S$- Linkage. Synthesis and Structures of 2,6,10-Triathia[11]-o-cyclophane, TT[11]OC, 2,6,10-Triathia[11]-m-cyclophane, TT[11]MC and the Palladation Product [Pd(TT[11]MC)][BF_4]." *Inorganic Chemistry*, **1992**, 31, 3286-3291.

6. Garry S. Hanan, James E. Kickham, and Stephen J. Loeb "Metallation of a Crown Thioether Ligand. Synthesis, Structure and Reactivity of [Pt(L1)][BF_4] and Structure of [PtI_2(L1)][BF_4], (L1 =2,6,10-Trithia[11]-m-benzenophane)." *Journal of the Chemical Society, Chemical Communications*, **1991**, 893-895.

7. Theodore A. Annan, James E. Kickham, and Dennis G. Tuck "The Direct Electrochemical Synthesis of the Novel Copper(I) Complex $Cu_2[OC_6Cl_4(OH)]_2[(C_6H_5)_2PCH_2P(C_6H_5)_2]_2$." *Canadian Journal of Chemistry*, 69, 2, **1991**, 251-256

8. A. A. El-Hadad, J. E. Kickham, S. J. Loeb, L. Taricani, D. G. Tuck "The Properties of Some Thallium(I) Derivatives of Aromatic Diols" *Inorganic Chemistry* **1995**, 34, (in press).

9. James E. Kickham and Stephen J. Loeb "The Unusual Interaction of Ag^+ with an Organopalladium Complex. Synthesis and Structures of [PdCl(L)] and

$[Pd(H_2O)(L)(Ag)][CF_3SO_3]_2$ (L=5,8,11-trioxa-2,14-Dithia-[15]-*m*-cyclophane)." *Organometallics*, **1995**. (submitted)

10. James E. Kickham, Stephen J. Loeb, and Shannon L. Murphy "Simultaneous First and Second Sphere Coordination. Organopalladium Receptors Employing Hydrogen Bonding and π-Stacking Interactions." *Inorganic Chemistry*. (in preparation)

11. J. E. Kickham, S. J. Loeb "Simultaneous First and Second-Sphere Coordination of Water, Ammonia, Amines and Hydrazines Employing Organopalladium Crown Ether Complexes" *Inorganic Chemistry*. (in preparation)

Conference Presentations (*=presenter)

1. James E. Kickham*, Stephen J. Loeb, and Shannon L. Murphy, "Macrocyclic Organopalladium Receptors Containing the 1,3-Xylyldithioether Fragment." XXVIth Inorganic Discussion Weekend, Guelph, Ontario, 1993

2. James E. Kickham, Stephen J. Loeb*, and Shannon L. Murphy, "Molecular Recognition Via Simultaneous First and Second Sphere Coordination." 76th Canadian Chemical Conference and Exhibition, Sherbrooke, Quebec, 1993

3. James E. Kickham and Stephen J. Loeb*, "Molecular Recognition Via Simultaneous First and Second-Sphere Coordination." 2nd International Summer School on Supramolecular Chemistry, Strasbourg, France, 1992.

4. James E. Kickham and Stephen J. Loeb*, "Molecular Recognition Via Simultaneous First and Second-Sphere Coordination." XVIIth International Symposium on Macrocyclic Chemistry, Provo, USA, 1992.

5. James E. Kickham*, Stephen J. Loeb, and Shannon L. Murphy, "Organopalladium Thioether Complexes as Metalloreceptors." XVIIth International Symposium on Macrocyclic Chemistry, Provo, USA, 1992.

6. James E. Kickham and Stephen J. Loeb*, "Molecular Recognition Via Second Sphere Coordination. Organopalladium Thioether Complexes as Metalloreceptors." 75th Canadian Chemical Conference and Exhibition, Edmonton, Alberta, 1992.

7. Garry S. Hanan, James E. Kickham*, and Stephen J. Loeb, "Metallated Thioether Macrocycles." XXIVth Inorganic Discussion Weekend, Kingston, Ontario, 1991.

8. Garry S. Hanan, James E. Kickham, and Stephen J. Loeb*, "Metallated Thioether Macrocycles." XVIth International Symposium on Macrocyclic Chemistry, Sheffield, England, 1991.

9. Garry S. Hanan, James E. Kickham*, and Stephen J. Loeb, "Metallated Thioether Macrocycles. Complexation and Reaction Chemistry." 74th Canadian Chemical Conference and Exhibition, Hamilton, Ontario, 1991.

10. James E. Kickham*, Garry S. Hanan, and Stephen J. Loeb "Metallated Thioether Macrocycles, Complexation and Reaction Chemistry." Ninth Annual Graduate Students' Symposium, State University of New York at Buffalo, 1991

11. Garry S. Hanan, James E. Kickham, and Stephen J. Loeb*, "Complexes of the Platinum Group Metals with Trithia Macrocycles Containing Xylyl Units." XXIIIth Inorganic Discussion Weekend, Waterloo, Ontario, 1990.

12. Theodore A. Annan*, James E. Kickham, and Dennis G. Tuck "The Direct Electrochemical Synthesis of the Novel Copper(I) Complex $Cu_2[OC_6Cl_4(OH)]_2[(C_6H_5)_2PCH_2P(C_6H_5)_2]_2$." XXIIth Inorganic Discussion Weekend, St. Catherines, Ontario, 1989.